Studies on Energetic Polynitro Containing Materials and on Organomercury Tetrazoles

Richard Moll

2013

Dissertation zur Erlangung des Doktorgrades
der Fakultät für Chemie und Pharmazie
der Ludwig-Maximilians-Universität München

Studies on Energetic Polynitro Containing Materials and on Organomercury Tetrazoles

Richard Moll

aus

München

2013

Danksagung

Mein Dank gilt an vorderster Stelle meinem Doktorvater Prof. Dr. Thomas M. Klapötke für die Aufnahme in den Arbeitskreis, die interessante Themenstellung sowie für die lückenlose finanzielle Unterstützung. Sehr geschätzt habe ich die gute Betreuung, wobei er sich für wirklich alle Belange immer die nötige Zeit genommen hatte. Erwähnenswert waren vor allem die extrem kurzen E-Mail Reaktionszeiten (auch Nachts, an Wochenenden oder Feiertagen), die offenbar auch nicht von irgendwelchen Zeitzonen zu beeinflussen waren.

Herrn Prof. Dr. Konstantin Karaghiosoff danke ich nicht nur für die freundliche Übernahme des Zweitgutachtens dieser Dissertation, sondern auch für seine Unterstützung vor allem im übersetzen russischer Originalliteratur (meistens an Wochenenden oder Feiertagen).

Der Prüfungskommission, bestehend aus Prof. Dr. Thomas. M. Klapötke, Prof. Dr. Konstantin Karaghiosoff, Prof. Dr. Jürgen Evers, Prof. Dr. Wolfgang Beck, Prof. Dr. Ingo-Peter Lorenz und Prof. Dr. Paul Knochel, danke ich für Ihre Zeit und der Bereitschaft zur Bildung derselbigen.

Herrn Dr. Burkhard Krumm danke ich für die sehr gute Betreuung, den zahllosen Anregungen, Diskussionen und Hilfestellungen, der immer sehr akribischen Korrektur jeglicher Schriftstücke sowie für die Aufnahme zahlreicher NMR Spektren. Des weiteren möchte ich Ihm danken für die Erkenntnis, dass 11:18 Uhr (in Worten: „elf-Uhr-achtzehn") nicht nur eine Uhrzeit, sondern auch eine absolut(!) unverrückbare Institution sein kann.

Dr. Jörg Stierstorfer danke ich für Hilfestellungen und Anregungen aller Art, sowie (wenn auch unwissentlich seinerseits) für das erweitern meines sportlichen Repertoires um den Laufsport.

Frau Irene Scheckenbach danke ich für Ihr sehr großes organisatorisches Talent, Ihr Engagement in der Überwindung verschiedenster bürokratischer Hürden sowie für das bereitstellen einer geeigneten und gekühlten Schokoladen-Auswahl.

Table of Contents

List of Schemes

List of Figures

Hexanitrohexyne and Trinitroethane

Halogenotrinitromethanes

Nitrilotriacetyl Chloride

Organomercury(II) Azides

Organomercury(II) Tetrazoles

Summary

Appendix

List of Tables

Organomercury(II) Tetrazoles

Summary

Appendix

1. Introduction

1.1. Classification of Energetic Materials

An energetic material is defined as a compound or mixture of substances, which derives their energy from a chemical reaction. It usually contains both a fuel and an oxidizer in a metastable state, and reacts readily with the release of energy and gaseous products, and does not need atmospheric oxygen to maintain the exothermic reaction. [1,2] Energetic materials can be initiated using thermal, mechanical or electrostatic ignition sources.

According to their use, nowadays energetic materials are best classified into *primary explosives*, *secondary/high explosives*, *propellants* and *pyrotechnics* (Figure 1). In some cases, also *polymers/binders* may show mentionable energetic properties and therefore an additional class could be discussed. Furthermore, often a general separation of the energetic materials into civil and military applications is made.
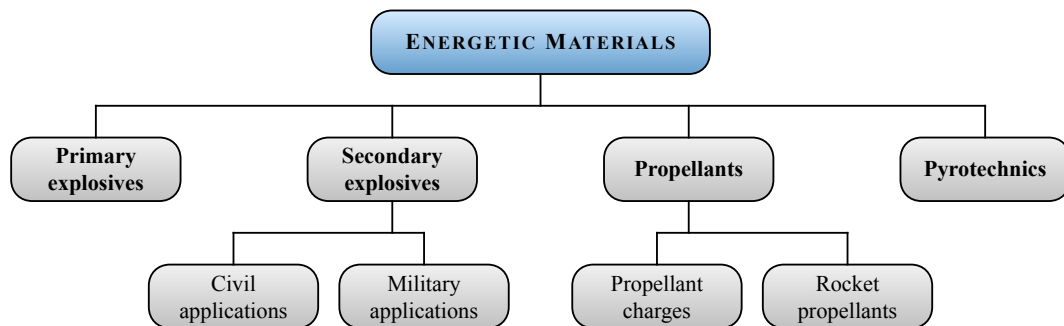
Figure 1.: Classification of energetic materials based on their use.

Propellants differ from primary and secondary explosives in such manner, that their prime objective is to deflagrate and not to detonate. Deflagration is a term describing combustion at subsonic speed propagating through heat transfer. Therefore, it distinguishes from detonation, which is supersonic and propagates through shock. [2] The desired property of propellants is the relatively high pressure produced over a longer period of time, enabling the potential to propel objects.

1.2. Propellants

The propellants can be further divided according to their use into gun propellant charges and rocket propellants. [1,5]

1.2.1. Gun Propellant Charges

Propellant charges can be either single-base propellants or multi-base propellant charges. The former consists of nitrocellulose (NC) and is used in all kinds of weapons from pistols to artillery guns. Double- and triple-base propellants contain further substances, such as nitroglycerine (NG) and nitroguanidine (NQ). [2] In case of the double-base propellant (NC + NG), mainly used in mortars, a higher performance is achieved compared to pure NC. But the better performing double-base formulations show disadvantages due to their high combustion temperatures. [5] This leads to enhanced erosion of the gun barrel, generally caused by the formation of iron carbide at these temperatures. [1] A further problem is the possible appearance of a muzzle flash after partial explosion of the combustion gases upon contact with the air. [3] To prevent these problems, triple-base propellants (NC + NG + NQ) were developed, containing additional NQ compared to double-base formulations. [2] Although the performance of the triple-base propellants does not reach that of the double-base compounds, they are particularly used in large caliber weapons. Also triple-base propellants with hexogen (RDX) instead of NQ have current applications, which increases the performance but also the erosion due to the again higher combustion temperature. Nitrogen-rich compounds can overcome the erosion problem, because the formation of N_2 instead of CO suppresses the formation of iron carbide. The formation of iron nitride instead, does not have the erosive properties of iron carbide.

The propellant charges burn considerably faster than rocket propellants (see Chapter 1.2.2). The pressure formed by gun propellant charges (up to 4000 bar) is much higher than that formed in the combustion chambers of rockets (around 70 bar). [1]

1.2.2. Rocket Propellants

Sir Isaac Newton (* January 4th, 1643; † March 31th, 1727) stated in his *Third Law of Motion* that "every action is accompanied by an equal and opposite reaction". This basic principle is also valid for every kind of rocket and jet engines. The continuous ejection of a steam of hot gases in one direction causes a steady motion of the rocket in the opposite direction. These high-temperature and high-pressure gases are produced by an exothermic chemical reaction of the rocket propellant.

Generally, two types of rocket propellants can be distinguished, liquid and solid rocket propellants (Figure 2). Also hybrid propellants, usually consisting of a solid fuel

and a liquid or gaseous oxidizer exist. These hybrid motors try to combine the advantages of both liquid and solid propellants, but suffer a major drawback. The difficulty is the mixing of the propellants during the combustion process resulting in quite a lot of unburned propellant. Therefore, hybrid propellants lack of current applications.[5]
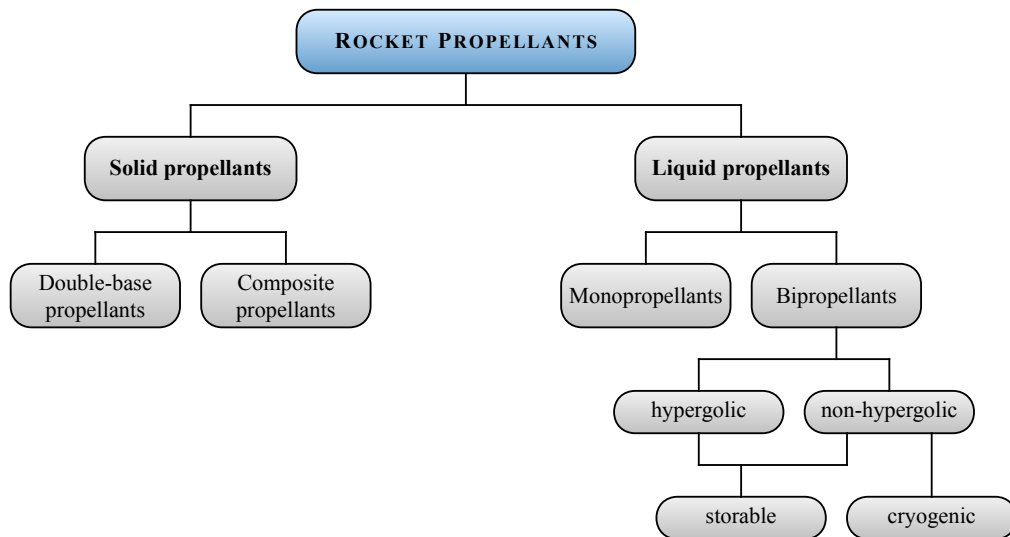
Figure 2.: Classification of rocket propellants.

Liquid Propellants

Depending on the number of ingredients, liquid propellants are categorized into mono- and bipropellants. The bipropellants can be further separated into two different classes, either in accordance with their ignition behavior into hypergolic or non-hypergolic mixtures or in accordance to their temperature behavior into storable and cryogenic formulations (Figure 2).[1,5]

The most commonly used monopropellant is hydrazine (N_2H_4), which decomposes exothermically, mainly due to a catalyst, into nitrogen and hydrogen.[3] Further examples are hydrogen peroxide (H_2O_2), isopropyl nitrate ((CH_3)$_2$HCONO$_2$), nitromethane (CH_3NO_2) and nitrous oxide (N_2O).[5] Monopropellants are necessarily endothermic compounds, which decompose in the absence of oxygen to deliver the required thrust. Although the energy content and performance of the monopropellants is relatively small, their long-term storability and simplicity of use favors them for attitude control and spacecraft orbital station-keeping, e. g. in the Orbital Maneuvering Subsystem of the Space Shuttle Orbiter Vehicle.

The bipropellants show better performances, which consist of a fuel and an oxidizer. The fuel and the oxidizer are stored in separate places, whereas they are combined in the combustion chamber. The propellant mixtures are called "hypergolic", if they spontaneously ignite (self-ignition in less than 20 milliseconds) when they come into contact with each other, whereas non-hypergolic mixtures need an external ignition source. Various hypergolic propellant combinations are known, such as hydrazine or its derivatives monomethyl hydrazine (MMH) and unsymmetrical dimethylhydrazine (UDMH) as fuel, and dinitrogen tetroxide (NTO, when used as a propellant usually referred to simply "nitrogen tetroxide") or nitric acid as oxidizer. [1,5] The most important and most used hypergolic mixture consists of MMH and NTO. [5] Moreover, NTO is often used with the addition of a small percentage of nitric oxide (NO), which inhibits stress-collision cracking of metal alloys. These solutions are referred to as "mixed oxides of nitrogen" (MON). A broad range of compositions is available, whereas often MON3 is preferred, containing 3% nitric oxide in dinitrogen tetroxide (MONi, i represents the percentage of nitric oxide in the mixture). A higher percentage of NO decreases the corrosiveness of the liquid, while the cost increase and the oxidation potential is decreased. The high vapor pressure of MON limits the concentration of nitric oxide in dinitrogen tetroxide to about 40% (by weight). Although hypergolic propellants tend to be difficult to handle because of their corrosiveness and extreme toxicity (see Chapter 1.3.2), hypergolic engines are inherently simple and easy to ignite reliably and repeatedly. Furthermore, both liquids are storable for long periods at reasonable temperatures and pressures. This results in a large variety of applications in outer space environment, such as upper stages of space launchers, for deep space rockets and particularly for spacecraft maneuvering. Relative to their mass, these hypergolic propellants are less energetic than some cryogenic propellant combinations, such as liquid hydrogen (LH2) and liquid oxygen (LOX). Beside the advantage of a high specific impulse of the propellant mixture, those chemicals require special handling and cryogenic storage technology such as special thermally insulated containers. Therefore, the practical use of cryogenics is limited to space launch application at ground level where they need to be stored only for a short time. Nevertheless, the Space Shuttle Main Engine (SSME) uses these cryogenic liquid fuels alongside the Solid Rocket Boosters (see Chapter 1.2.2) at liftoff, also because of the high specific impulse of $I_{\mathrm{sp}} = 363\,\mathrm{s}$ at sea level and $I_{\mathrm{sp}} = 452\,\mathrm{s}$ in a vacuum. Also fluorine or fluorine containing oxygen (FLOX) oxidizers as well as beryllium containing propellants were considered, but both have not found application because of serious technical, toxical and ecological reasons.

The liquid rocket propellants show the highest specific impulses, I_{sp} (definition of I_{sp} see Chapter 1.3.1) of all chemical rockets. In this context, the highest specific impulse ever test-fired in a rocket was lithium and fluorine, with hydrogen added to improve

the exhaust thermodynamics. This combination delivered a specific impulse in vacuum of remarkable $I_{sp} = 542\,s$ (for comparison: $LH2 + LOX$: $455\,s$; $N_2H_4 + NTO$: $344\,s$). But it has never been considered for practical application because of multiple serious drawbacks. All three components must be kept liquid, hydrogen and fluorine below $-252\,°C$ respectively $-188\,°C$ and lithium above $180\,°C$. Furthermore, lithium ignites on contact with air and fluorine ignites in contact with most fuels including hydrogen and is moreover very toxic.

Solid Propellants

Solid propellants are typically much easier to store and handle than liquid propellants. Their simplicity makes solid rockets a good choice whenever large amounts of thrust are needed and cost is an issue. For this reason, practically all orbital launch vehicles use solid-fueled rockets in their boost stage. But relative to liquid fuel rockets, solid fuel rockets have lower specific impulse, I_{sp} (definition of I_{sp} see Chapter 1.3.1), because of the solids' lower exhaust velocities. A further drawback in contrast especially to hypergolic liquid propellants is that solid rocket propellants cannot be throttled in real time, although a programmed thrust schedule can be created by adjusting the interior propellant geometry.

Solid rocket propellants are either homogeneous mixtures of one or more macroscopically indistinguishable ingredients, or heterogeneous, so called "composites propellants".[1] Homogeneous propellants are generally based on nitrocellulose (NC), often used together in formulations with nitroglycerine (NG) and nitroguanidine (NQ) (see Chapter 1.2.1). Heterogeneous composites typically consists for the most part of a mixture of solid oxidizer with a fuel.[2] If required, polymer binders, metallic additives, plasticizers, stabilizers and burn rate modifiers are added. Most solid propellants are based on ammonium perchlorate (AP), which is primarily used on a very large scale as an oxidizer for solid rocket and missile propellants. Furthermore, it has applications in munitions, fireworks and as an inflator in airbag systems in motor vehicles, various aircrafts and even employed in an airbag landing system for spacecrafts.[1] The most prominent use of AP was during the Space Shuttle program (1981–2011), officially called Space Transportation System (STS). It was used as an oxidizer in the solid rocket boosters, during lift-off for all 135 missions. The so called "Solid Rocket Boosters" (SRBs) were the largest solid-fuel rocket motors ever flown. Each SRB contained of about $500\,t$ of solid propellant by an inert weight of only approximately $91\,t$. The propellant mixture consisted of $69.6\,\%$ AP as oxidizer, $16\,\%$ aluminum as fuel, as well as $0.4\,\%$ iron oxide as catalyst, $12.04\,\%$ of a polymer binder and $1.96\,\%$ of an epoxy curing agent. The polymer, such as polybutadiene (acrylic acid) acrylonitrile (PBAN) or hydroxyl-terminated polybutadiene (HTPB) forms a solid body of the propellant ingredients and holds the mixture together.

Moreover, the rubbery binder is also used as a fuel, because it usually contains mainly carbon and hydrogen. This propellant mixture is commonly referred to as "Ammonium Perchlorate Composite Propellant" (APCP). It develops a specific impulse of $I_{sp} = 242\,s$ at sea level and $268\,s$ in a vacuum. The pair of these solid rockets provided about $83\,\%$ of the lift-off thrust, which had to accelerate the total mass of the Space Shuttle with over $2000\,t$ (Orbiter Vehicle + external tank + 2 SRBs) and burned during the first two minutes of the flight (Figure 3).
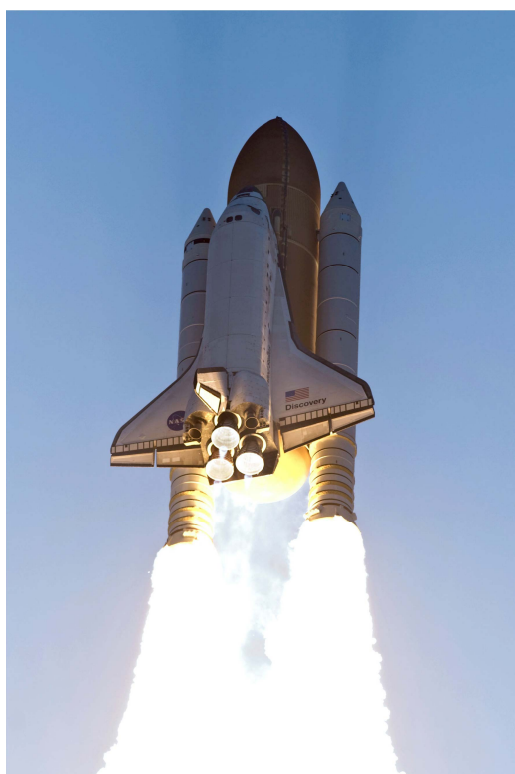
Figure 3.: Launch of the Space Shuttle Discovery (STS-124) on May 31st, 2008, showing the two Solid Rocket Boosters (solid-fuel rocket engines) and the Space Shuttle Main Engine (liquid-fuel cryogenic rocket engine). Picture taken from the official NASA homepage with courtesy of the NASA.

There are several reasons, why AP currently is the most important and most used oxidizer. Foremost, the very high oxygen balance (see Chapter 1.3.1), assuming that all the chlorine is consumed by hydrogen forming HCl, of $\Omega_{CO_2} = \Omega_{CO} = 34.0\,\%$. Further advantages imply the complete conversion to gaseous reaction products during combustion and the facile preparation method. The synthesis is easily performed by reaction of ammonia with perchloric acid and subsequent purification by crystallization, even on a multi-ton scale. Ammonium perchlorate (AP), which is stable at ambient

temperature, decomposes slightly before melting at temperatures above $150\,°C$. At decomposition temperatures below approximately $300\,°C$, an autocatalytic reaction occurs, whereas at temperature above $350\,°C$ the reaction is not autocatalytic anymore and decomposition is complete.[1]

Because of the environmental and health problems of AP (see Chapter 1.3.2), promising candidates as a 'green' replacement are currently under investigation, which are mainly ammonium nitrate (AN), and ammonium dinitramide (ADN).[4,5] However, both provide less available oxygen (AN: $\Omega_{CO_2} = \Omega_{CO} = 20.0\,\%$; ADN: $\Omega_{CO_2} = \Omega_{CO} = 25.8\,\%$) compared to AP ($\Omega_{CO_2} = \Omega_{CO} = 34.0\,\%$). This results in significantly reduced performances. Furthermore, both compounds have additional drawbacks. AN has severe burn rate issues and formulation problems due to its hygroscopicity and several phase transitions. In contrast, ADN has some issues with respect to binder compatibility and thermal stability, because of a relatively low decomposition temperature.[4] To summarize, the advantages of AP are unbeaten so far, therefore essentially all solid propellants rockets are based on this oxidizer.[1]

Usually aluminum serves as the fuel in solid rocket propellants. There exist also attempts to replace aluminum with more efficient compounds. As an example, nano-aluminum and aluminum hydride (AlH_3) are currently discussed. Both would increase the combustion efficiency due to a more quantitative combustion, but are on the other side significantly more sensitive against oxidation, which will also occur by the surrounding air.

1.3. High Energy Dense Oxidizer

A jet engine is using oxygen from the surrounding atmosphere to enable the combustion of its fuel. A rocket engine, which needs more oxygen than the surrounding atmosphere can provide, must carry its own oxidizer. For operating outside the atmosphere, also the addition of an oxidizer is essential. Therefore, the properties regarding performance, toxical and ecological aspects as well as the requirements for the development of new oxidizers should be investigated and discussed. The often used term *High Energy Dense Oxidizer* (HEDO) refers to such an oxidizer with superior chemical, physical and energetic properties, satisfying as much requirements as possible of new advanced energetic oxidizers (see Chapter 1.3.3).[1]

1.3.1. Properties and Performance

The most basic and obvious key-factor of a compound to be a member of the general class of oxidizers, is a positive oxygen balance (Ω). The oxygen balance describes the relative amount of oxygen excess or oxygen deficit of a compounds when it is burned, without

adding or removing external oxygen. [1,5] The procedure for calculating in terms of $100\,\mathrm{g}$ is to determine the number of moles of oxygen that are excess or deficient for $100\,\mathrm{g}$ of a compound. It is calculated from the empirical formula of a compound in percentage of oxygen required for an assumed complete conversion of carbon to carbon dioxide (or carbon monoxide), hydrogen to water and metal/metalloid to metal/metalloid oxide. For simplification, usually only the most stable metal/metalloid oxide is considered during calculation (e. g. $B \rightarrow B_2O_3$). Also elements like nitrogen and fluorine, which will primarily not form oxygen containing combustion products, affect the oxygen balance. Beside their contribution to the overall molecular weight, elements like fluorine form mainly HF during combustion, indirectly interfering with the amount of oxygen needed for forming water. The general oxygen balance of a compound can be calculated according to Equation 1.

$$\Omega_{\mathrm{CO/CO_2}} = \underbrace{\left(\sum O_A - x \sum C_A - \frac{1}{2} \left(\sum H_A - \sum H_P \right) - \sum O_P \right)}_{\text{Number of oxygen atoms per molecule (excess ``+'', deficient ``−'')}} \frac{M_{\mathrm{Ox}}}{M_A} \times 100 \quad (1)$$

$$x = 1 \quad \text{for } \Omega_{\mathrm{CO}} \ \text{ (calculated for CO)}$$
$$x = 2 \quad \text{for } \Omega_{\mathrm{CO_2}} \ \text{ (calculated for CO}_2)$$

$\sum O_A =$ number of oxygen atoms of the compound
$\sum C_A =$ number of carbon atoms of the compound
$\sum H_A =$ number of hydrogen atoms of the compound
$\sum H_P =$ number of hydrogen atoms of all formed decomposition products
except water (mostly hydrogen halogenides)
$\sum O_P =$ number of oxygen atoms of all formed decomposition products
except water and carbon oxides (mostly metal/metalloid oxide(s))
$M_{\mathrm{Ox}} =$ molecular mass of an oxygen atom
$M_A =$ molecular mass of the compound

The first part of Equation 1 refers to the number of oxygen atoms per oxidizer molecule which are left ($\Omega > 0$) or needed ($\Omega < 0$) to achieve a balanced ratio between the oxidizer and an assumed fuel. Furthermore, beside a logically high oxygen and low carbon/hydrogen content, also a low molecular weight favors a higher oxygen balance.

As an example, tris(2-fluoro-2,2-dinitroethyl) borate, $B(OCH_2CF(NO_2)_2)_3$, which is discussed in Chapter 4 of this work, will theoretically decompose according to the following decomposition equation (assuming CO as product):

$$C_6H_6BF_3N_6O_{15} \longrightarrow 6 \text{ CO} + \frac{1}{2} \text{ H}_2\text{O} + \frac{1}{2} \text{ B}_2\text{O}_3 + 3 \text{ HF} + 3 \text{ N}_2 + 3 \text{ O}_2$$
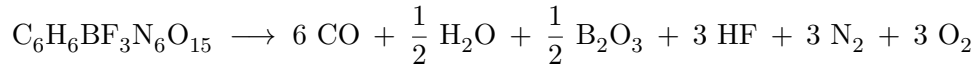
The reaction equation shows, that for this compound under these conditions an excess of 6 atoms of oxygen per molecule is found, which expresses a positive oxygen balance. With the molecular mass of oxygen ($16.00\,\text{g}\,\text{mol}^{-1}$) and that of the borate compound ($469.95\,\text{g}\,\text{mol}^{-1}$), Equation 1 reads:

$$\Omega_{\text{CO}} = \left(15 - 1 \times 6 - \frac{1}{2}(6-3) - \frac{3}{2}\right) \frac{16.00\,\text{g}\,\text{mol}^{-1}}{469.95\,\text{g}\,\text{mol}^{-1}} \times 100 = +\,20.4\,\%$$

Therefore, tris(2-fluoro-2,2-dinitroethyl) borate shows a positive oxygen balance of $\Omega_{\text{CO}} = 20.4\,\%$, if solely the formation of CO is assumed. For a similar calculation assuming the formation of CO_2, the oxygen balance is calculated to $\Omega_{\text{CO}_2} = \pm 0\,\%$. But since the combustions occur at high temperatures, not only CO_2 is formed, but also CO as stated in the *Boudouard equilibrium.*

One of the most important indicators for the efficiency of rocket propellants is the specific impulse I_{sp}, stated in seconds. The higher the number, the "better" the energetic properties of the propellant. The specific impulse I_{sp} is the period in seconds for which a $0.45\,\text{kg}$ ($1\,\text{lb}$) mass of propellant (total of fuel, oxidizer and binder) will produce a thrust of $0.45\,\text{kg}$ ($1\,\text{lb}$) of force. This important performance parameter shows the effective velocity of the combustion gases when leaving the nozzle, and is therefore a measure for the effectiveness of a propellant composition. The specific impulse I_{sp}^* is defined as the time dependent thrust $\text{F}(t)$ divided by the mass of the propellant m (Equation 2).[1,2,5]

$$I_{\text{sp}}^* = \frac{1}{m} \int_0^{t_{\text{b}}} \text{F}(t)\text{d}t \tag{2}$$

$$\text{F}(t) = \text{time dependent thrust}$$
$$t_{\text{b}} = \text{combustion time (in s)}$$
$$m = \text{mass of the propellant (in kg)}$$

As seen from Equation 2, I_{sp}^* has the unit $\text{N}\,\text{s}\,\text{kg}^{-1}$ or $\text{m}\,\text{s}^{-1}$. But usually, the specific impulse I_{sp} is given based on the gravitation of the earth at sea level, thus

$I_{sp} = \frac{I_{sp}^*}{g}$ ($g = 9.81\,\mathrm{m\,s^{-2}}$) with the unit in seconds.[1,2] Equation 3 shows the exact calculation of the specific impulse. Although the specific impulse is a characteristic of the propellant system, its exact value will vary to some extent with the operating conditions and design of the rocket engine. It is for this reason, that different numbers are often quoted for a given propellant or combination of propellants. Nevertheless, typical values for the specific impulse I_{sp} of solid rockets are around $250\,\mathrm{s}$ and that of liquid bipropellants around $450\,\mathrm{s}$.[1] Eliminating all constant values from Equation 3, assuming a given propellant mixture, forms Equation 4.

$$I_{sp} = \frac{1}{g}\sqrt{\frac{2\,\gamma\,R\,T_c}{(\gamma - 1)\,M}} \tag{3}$$

$$I_{sp} \propto \sqrt{\frac{T_c}{M}} \tag{4}$$

$g =$ gravity of the earth ($9.81\,\mathrm{m\,s^{-2}}$)

$R =$ gas constant ($8.3145\,\mathrm{J\,mol^{-1}\,K^{-1}}$)

$T_c =$ temperature in the combustion chamber (in K)

$\gamma =$ ratio of the specific heat capacities of the gas mixtures $\left(\dfrac{C_p}{C_v}\right)$

$M =$ average molecular weight of the combustion gases (in $\mathrm{kg\,mol^{-1}}$)

Equation 4 shows, that the specific impulse I_{sp} is proportional to the square root of the temperature inside the combustion chamber T_c and the reciprocal of the molecular weight of the decomposition products M. Therefore, high combustion temperatures and low molecular mass of the propellant promote a higher specific impulse. It was found empirically, that when the specific impulse is increased by $20\,\mathrm{s}$, the freight carried by the rocket can approximately be doubled.[1]

1.3.2. Toxical and Ecological Aspects

Ecological concerns have become more and more important in the last decades. All hydrazine derivatives, widely used in liquid propellants, are extremely toxic and carcinogenic even in small amounts.[1] Furthermore, they show strong corrosive behavior. In solid propellants, currently the most used oxidizer is ammonium perchlorate (AP), with his great variety of different applications (see Chapter 1.2.2). As a result of these extensive uses and because of the high solubility, chemical stability, persistence, and

also due to the appearance as a contaminant of agricultural fertilizers, AP has become widely distributed in surface and ground water systems. The perchlorate anion has almost the same size and shape as the iodine anion, and therefore competes for the iodine binding site in the thyroid of all vertebrates.[6] Due to its endocrine disrupting property when ingested, it results in thyroid malfunction which impacts both growth and development of the organism. Furthermore, the perchlorate anion is known to affect the normal pigmentation of amphibian embryos, although only few information about general effects on the aquatic life is investigated.[1] Further negative impact on the environment derive from the combustion products, most likely HCl, which gives rise to acidic rain. Furthermore, chlorine containing compounds are potentially hazardous for ozone depletion, if released in the upper atmosphere.

1.3.3. Requirements for the Development

As described above, many oxidizers used today suffer from serious environmental and toxicity problems in various concerns. Therefore, attempts to seek new options in terms of propellants to avoid these drawbacks are an important task. In the area of solid rocket propulsion, replacements for ammonium perchlorate are urgently needed. One option might be overcome by the use of halogen-free oxidizers, containing high amounts of oxygen and nitrogen.[1] These materials gain more and more interest since they mainly decompose into environmentally benign gaseous products. Many factors influence the development of a suitable oxidizer. The primary factors include ease of operation, performance, cost and hazards.

The general requirements for a novel advanced *High Energy Dense Oxidizer* are the following:[1]

- High oxygen content ($\Omega_{\mathrm{CO}} > 25.0\,\%$)
- High density (best: $\rho \approx 2.0\,\mathrm{g\,cm^{-3}}$)
- Melting point higher than $150\,°\mathrm{C}$
- Decomposition temperature higher than $200\,°\mathrm{C}$
- Sensitivities not higher than PETN
  (Impact: $4\,\mathrm{J}$, Friction: $80\,\mathrm{N}$, Electrostatic discharge: $0.1\,\mathrm{J}$)
- Low vapor pressure
- High enthalpy of formation
- Compatibility with fuel and binders
- Facile synthesis with minimum number of synthesis steps
- Economic or bulk starting materials

1.4. Scope of the Dissertation

The objective of this dissertation is to explore chemical compounds which contain a high amount of oxygen and therefore qualify themselves as an oxidizer. Furthermore, these oxidizers should have convincing chemical, physical and energetic properties, providing as much requirements as possible of new advanced *High Energy Dense Oxidizer* (HEDO) (see Chapter 1.3.3). Moreover, the finding of suitable precursors and building blocks for the synthesis of these compounds is of interest, as well as the understanding of their chemistry. Beside the synthesis and characterization of these compounds, also intra- and intermolecular interactions in the molecules, which are often present in highly nitrated compounds, should be investigated due to their general influence on the properties. The general concept of this work is to introduce particularly highly nitrated moieties into various molecules, to gain a higher oxygen content of these compounds. A promising building block is or contains the trinitromethyl moiety $C(NO_2)_3$, as well as the fluoro-dinitromethyl moiety $CF(NO_2)_2$. Both building blocks are mainly used as the corresponding ethylalcohols.

In this context, various compounds were synthesized, characterized and the results discussed. Beside this introduction, the work contains eight further chapters, whereas each is an enclosed research project including their own abstract, introduction, results and discussion, experimental section and conclusion. If available, the corresponding supporting informations are found in the appendix. Foremost, trinitroethyl substituted esters based on a carbon center were investigated (see Chapter 2), as well as trinitroethyl carbamates and their starting material trinitroethyl chloroformate (see Chapter 3). Further studies of substituted esters, here with boron as the central atom, led to the corresponding polynitroethyl and fluorodinitroethyl substituted boron esters (see Chapter 4). In this chapter, also the starting material fluorodinitroethanol and the formation and chemical structure of an unusual dianion are evaluated. The reaction pathway of a promising trinitromethyl transfer agent, silver trinitromethanide, was studied and examples including an acetylene derivative are given (see Chapter 5). Furthermore, the structures of halogenotrinitromethanes in the crystalline and gaseous phase were examined and discussed (see Chapter 6). In the last chapter, the synthesis and structure of an interesting acid chloride was investigated (see Chapter 7).

A side project dealing with organomercury azides (see Chapter 8), led to the unexpected reaction with solvent nitriles to form organomercury tetrazoles. Not only because of general academic interest, but also because of continuing understanding of the formation of tetrazoles, this project from the Master Thesis was extended and these compounds were investigated thoroughly (see Chapter 9).

1.5. References

[1] T. M. Klapötke, *Chemistry of High-Energy Materials*, 2nd ed., Walter de Gruyter: Berlin, **2012**.

[2] N. Kubota, *Propellants and Explosives*, 2nd ed., Wiley-VCH: Weinheim, **2007**.

[3] J. Akhavan, *The Chemistry of Explosives*, 2nd ed., RSC Paperback: Cambridge, **2004**.

[4] A. H. Ghee, G. Santhosh, *Advances in Energetic Dinitramides*, World Scientific Publishing: Singapore, **2007**

[5] J. P. Agrawal, *High Energy Materials*, Wiley-VCH: Weinheim, **2010**

[6] R. E. Tarone, L. Lipworth, J. K. McLaughlin, *J. Occup. Environ. Med.* **2010**, *52*, 653–660.

2. Trinitroethyl Substituted Carbonates

CHNO Based Molecules Containing 2,2,2-Trinitroethoxy Moieties as Possible High Energy Dense Oxidizers

Thomas M. Klapötke,*[a] Burkhard Krumm,[a] Richard Moll,[a] and Sebastian F. Rest [a]

*   Prof. Dr. Thomas M. Klapötke

        E-Mail: tmk@cup.uni-muenchen.de

[a]   Department of Chemistry

        Ludwig-Maximilian University of Munich

        Butenandtstrasse 5–13 (D)

        81377 Munich, Germany

2.1. Abstract

Tetrakis(2,2,2-trinitroethyl) orthocarbonate (**1**) and 2,2,2-trinitroethyl formate (**2**) were synthesized by the reaction of carbon tetrachloride, respectively chloroform, with the corresponding equivalents of 2,2,2-trinitroethanol and catalytic amounts of anhydrous iron(III) chloride. 2,2,2-Trinitroethyl formal (**3**) was prepared by the condensation of paraformaldehyde with 2,2,2-trinitroethanol. The compounds were fully characterized by single-crystal X-ray diffraction, vibrational spectroscopy (IR and Raman), multinuclear NMR spectroscopy, elemental analysis, and multi-temperature DSC measurements. Due to the positive oxygen balance, the suitability of all three compounds mentioned as potential oxidizers in energetic formulations was investigated and discussed. In addition, the heats of formation of the products were determined experimentally using bomb calorimetric methods. With this value and the experimental (X-ray) density, several detonation parameters such as the detonation pressure, velocity, energy, and temperature were computed using the EXPLO5 code. Furthermore, the sensitivity towards impact, friction and electrical discharge was tested using the BAM drop hammer, a friction tester as well as a small-scale electrical discharge device.

2.2. Introduction

Highly nitrated CHNO compounds were found to be useful as high explosives because of their high oxygen content. Especially compounds derived from 2,2,2-trinitroethanol form an entirely new class of oxidizers.[1–3] In the course of our investigations into high energetic dense oxidizers (HEDO), we recently focused our attention on various compounds of 2,2,2-trinitroethanol as possible new oxidizers for high performance, halogen-free propellants. These might overcome the problem of hydrogen chloride formation during the use of ammonium perchlorate as oxidizer in rocket propellant formulations.[2,4] The specific impulse I_s is one of the main parameters specifying the performance of solid rocket boosters. It is proportional to the temperature inside the combustion chamber T_c and the reciprocal of the molecular weight of the decomposition products M (Equation (1)).[5,6]

$$I_s \propto \sqrt{\frac{T_c}{M}} \tag{1}$$

An increase of the value for I_s by 20 s leads empirically to a doubling of the usual payload.[5,6] Therefore, the development of new energetic oxidizers based on CHNO

compounds decomposing into small aerially molecules is a promising way to increase the specific impulse of solid rocket boosters. The chemistry of 2,2,2-trinitroethanol is different to that of other alcohols. The electron-withdrawing inductive effect of the trinitromethyl group ($\sigma^* = 4.54$)[7] decreases the oxygen basicity of the hydroxyl group and therefore turns acidic ($pK_a = 6.1$). At a pH value above 6, the equilibrium is predominated towards the direction of the trinitromethanide anion and formaldehyde.[3,8] A detailed study of the syntheses and characterizations of tetrakis(2,2,2-trinitroethyl) orthocarbonate (**1**), 2,2,2-trinitroethyl formate (**2**) and 2,2,2-trinitroethyl formal (**3**) is presented in this work. These compounds were reported prior to this study, but were only partially characterized.[1,9–11] Especially for **2** and **3** only very few analytical data are known.

2.3. Results and Discussion

Synthesis

The reported route for the preparation of the orthoesters of 2,2,2-trinitroethanol **1** and **2** is the reaction of 2,2,2-trinitroethanol with carbon tetrachloride, respectively chloroform, in the presence of a Lewis acid like anhydrous ferric chloride (ah. FeCl$_3$) in catalytic amounts (Scheme 1).[1] The reaction with carbon tetrachloride led to higher yields than the corresponding reaction with chloroform. The reaction has to take place under careful exclusion of moisture to prevent side reactions introduced by the presence of water leading to 2,2,2-trinitroethyl carbonate (Scheme 2). The disubstituted derivative **3** was prepared by the condensation reaction of 2,2,2-trinitroethanol with paraformaldehyde in concentrated sulfuric acid (Scheme 3).
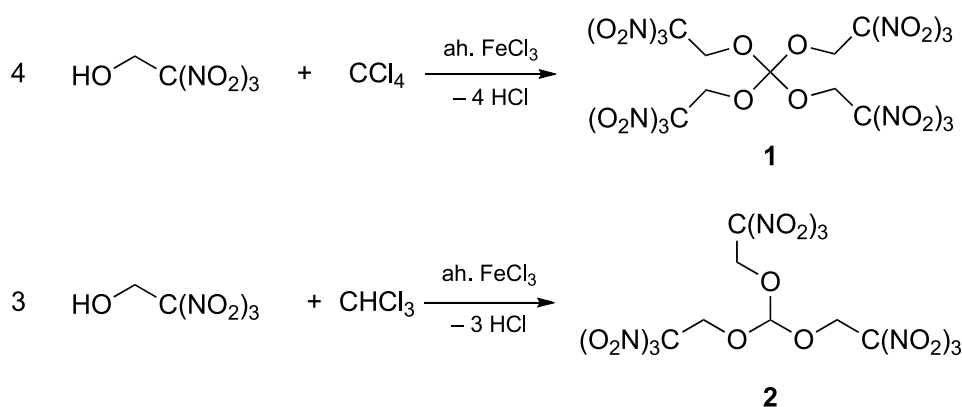
Scheme 1: Synthesis of **1** and **2** with catalytic amounts of FeCl$_3$.

$$2 \ \ HO\diagup C(NO_2)_3 \ + \ CCl_4 \quad \xrightarrow[- \ 4 \ HCl]{FeCl_3 \ / \ H_2O} \quad (O_2N)_3C\diagup O \overset{O}{\underset{}{\diagup}} O \diagdown C(NO_2)_3$$
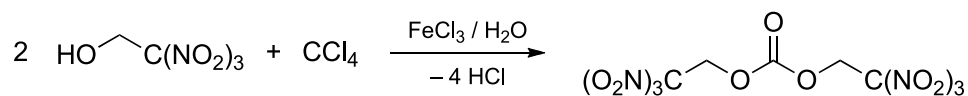
Scheme 2: Possible side reaction leading to 2,2,2-trinitroethyl carbonate during the synthesis of **1** and **2**.

$$HO\diagup C(NO_2)_3 \quad \xrightarrow[- \ 2 \ H_2O]{(CH_2O)_n \ / \ H_2SO_4} \quad (O_2N)_3C\diagup O \diagup O \diagdown C(NO_2)_3$$

3
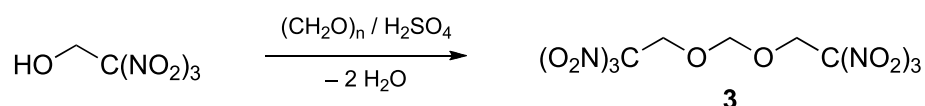
Scheme 3: Synthesis of **3** by the reaction of 2,2,2-trinitroethanol and paraformaldehyde.

Compounds **1**–**3** are soluble in polar organic solvents like acetone, acetonitrile, chloroform, and methanol; insoluble in water and nonpolar solvents like *n*-hexane. The compounds were found to be sensitive towards impact and friction and burn smoke- and residue-less in a Bunsen burner with a yellow flame.

NMR Spectroscopy

All compounds were thoroughly characterized by ^{1}H, ^{13}C, and ^{14}N NMR spectroscopy (Table 1). In the ^{1}H NMR spectra of **1**–**3** the singlet for the $CH_2C(NO_2)_3$ moiety can be observed and determined at $\delta = 5.14 - 5.04$ ppm in [D$_3$]acetonitrile. Compound **2** and **3** show also singlets for the additional CH respectively the CH$_2$ group at $\delta = 5.89$ and 4.96 ppm. In the ^{13}C{^{1}H} NMR spectra the resonances of the carbons of the methylene groups could be observed at 67.3–63.7 (CH_2) and the trinitromethyl groups at 126.0–124.1 ppm [$C(NO_2)_3$] with decreased intensity. The carbon atoms of the orthocarbonate, formate and formal group were identified at 119.1 (**1**), 112.7 (**2**) and 98.1 ppm (**3**). At -35 to -33 ppm in the ^{14}N NMR spectra the nitrogen atoms of $C(NO_2)_3$ group were found. The NMR signals of **1** agree with the literature values. [10]

Vibrational Spectroscopy

The vibrational analysis of **1**–**3** showed the characteristic asymmetric NO$_2$ stretching vibrations in the range of 1610 to 1581 cm^{-1} and the symmetric stretching vibrations at 1308 to 1305 cm^{-1} (Table 2). All vibrations of the nitro groups for **1**–**3** are in a narrow range, explained by the similarity of the functional groups. The C−H stretching vibrations for **1**–**3** were found in the range of 3009–2876 cm^{-1}. The C−N, C−O, and

Table 1.: Multinuclear NMR resonances of **1**–**3** in CD_3CN [ppm].

	1	2	3
^{1}H	5.14 (CH_2)	5.89 [s, 1 H, $HC(OCH_2)_3$] 5.10 [s, 6 H, $CH_2C(NO_2)$]	5.04 [s, 4 H, $CH_2C(NO_2)_3$] 4.96 [s, 2 H, O_2CH_2]
^{13}C	124.1 [br, $C(NO_2)_3$] 119.1 [$C(OCH_2)_4$] 63.8 (OCH_2)	125.0 [br, $C(NO_2)_3$] 112.7 [$C(OCH_2)_3$] 63.7 (OCH_2)	126.0 [br, $C(NO_2)_3$] 98.1 [$C(OCH_2)_2$] 67.3 (OCH_2)
^{14}N	−35 (NO_2)	−34 (NO_2)	−33 (NO_2)

Table 2.: IR and Raman bands of **1**–**3**, characteristic vibrations and their assignments [a].

	1		2		3	
	Raman	IR	Raman	IR	Raman	IR
ν CH	3009 (17) 2960 (35) 2885 (8)	3003 w 2959 w 2888 w	2990 (13) 2955 (30) 2880 (4)	3003 w 2956 w 2884 w	2980 (19) 2950 (17) 2931 (22) 2876 (6)	2987 w 2928 w 2879 w
ν_{as} NO_2	1597 (25)	1594 vs	1610 (18)	1587 vs	1604 (17)	1581 vs
ν_s NO_2	1305 (30)		1308(27)		1307 (27)	
δ CNO_2 / ν chain	859 (100)	856 m	859 (100)	854 w	859 (100)	855 (w)

[a] Vibrational bands in cm^{-1}; Raman intensities in brackets. IR intensities: vs = very strong, s = strong, m = medium, w = weak.

C−C vibrations of **1**–**3** could be observed in the expected ranges and agree with the reported values of **1**.[10,12]

X-ray Diffraction

Suitable single crystals for X-ray diffraction measurements were obtained by slow evaporation of the solvent at 4 °C in chloroform (**1**) or acetone (**3**). DSC measurements (see Figure 5) revealed a phase transition for **1** at reduced temperature. Single crystals of **α-1** could be obtained below −16 °C and are metastable up to 34 °C. Compound **α-1** crystallizes in the monoclinic space group $Fdd2$ with eight formula units per unit cell and a theoretical maximum density of $1.944\,g\,cm^{-3}$. The quite high density of the structure is a result of various inter- and intramolecular H···O interactions. All bond lengths and angles were found in the typical range for polynitro aliphatic CHNO compounds.[3,8]

The density of $\boldsymbol{\beta}$-1 with $1.84\,\mathrm{g\,cm^{-3}}$ is significantly lower than $\boldsymbol{\alpha}$-1. It crystallizes in the tetragonal space group $I\bar{4}2d$ with four formula units per unit cell. Due to the increased symmetry compared to $\boldsymbol{\alpha}$-1, as a result of the different orientations of the nitro groups within the trinitromethyl moiety, less intermolecular H···O interactions could be observed and therefore the density decreased below $1.9\,\mathrm{g\,cm^{-3}}$. The structures of the different modifications of 1 are shown in Figure 1 and Figure 2. The displacement vectors of $\boldsymbol{\beta}$-1 are shown only at $30\,\%$ of probability conditional upon the increased measurement temperature of $258\,\mathrm{K}$. Below this temperature $\boldsymbol{\alpha}$-1 is the preferred conformation of 1.
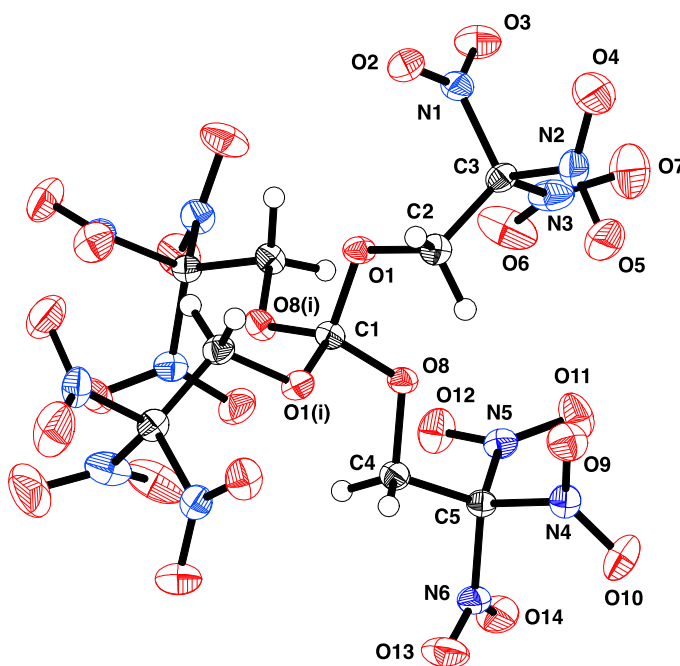
Figure 1.: Molecular structure of $\boldsymbol{\alpha}$-1. Selected distances [Å] and angles [°]: C1−O1 1.388(2), O1−C2 1.425(2), C2−C3 1.513(3), C3−N1 1.519(2), C3−N2 1.528(3), C3−N3 1.513(3), C1−O8 1.376(2), O8−C4 1.425(2), C4−C5 1.513(3), C5−N4 1.533(2), C5−N5 1.517(2), C5−N6 1.521(2), C1−O1−C2 114.7(2), O1−C2−C3 109.7(1), C2−C3−N1 112.7(1), C2−C3−N2 108.2(2), C2−C3−N3 116.5(2), C1−O8−C4 117.6(2), O8−C4−C5 104.7(1), C4−C5−N4 114.5(1), C4−C5−N5 110.9(1), C4−C5−N6 110.2(1), O1−C1−O8 107.7(2), O1(i)−C1−O1 113.1(2), O1−C1−O8(i) 107.7(2), O8(i)−C1−O8 113.7(2).

Previously studied compounds containing this group show a true or approximate C_3 axis in this unit with propeller like twisted NO_2 groups.[12,13] A fundamental structural difference exists by the different orientations of the $C(NO_2)_3$ groups within the two structures of 1. In the solid phase the C−C−N−O dihedral angles unit are in the range of 37.5–47.2° for the C2−C3−$(NO_2)_3$ and −34 to −48.4° for the C4−C5−$(NO_2)_3$ group in $\boldsymbol{\alpha}$-1, with a majority clustering towards ±45°. This propeller like twisting of the
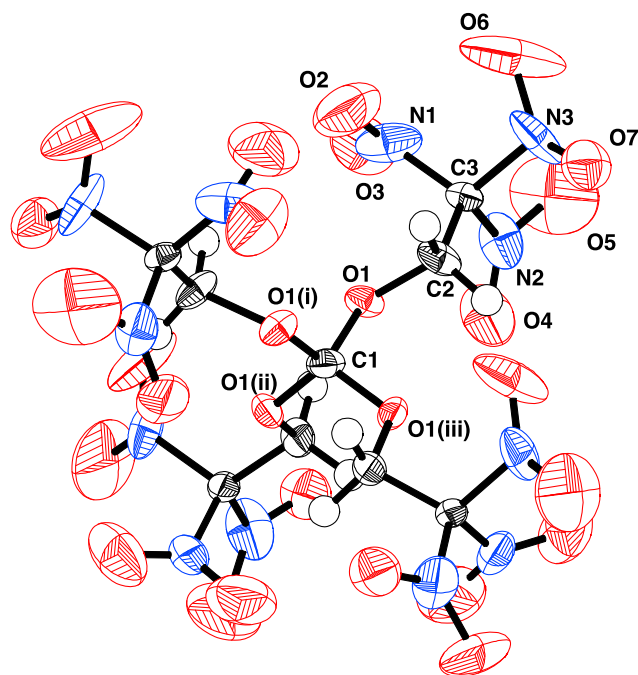
Figure 2.: Molecular structure of **β-1**. Thermal ellipsoids are shown at 30 % probability. Selected distances [Å] and angles [°]: C1−O1 1.397(4), O1−C2 1.421(8), C2−C3 1.47(1), C3−N1 1.50(1), C3−N2 1.52(1), C3−N3 1.50(1), C1−O1−C2 116.5(4), O1−C2−C3 104.2(5), C2−C3−N1 112.6(6), C2−C3−N2 113.9(6), C2−C3−N3 110.6(6), O1(*i*)−C1−O1 114.0(2), O1(*i*)−C1−O1(*ii*) 107.2(2).

trinitromethyl group optimizes the N⋯O nonbonding attractions between two nearby nitro groups, while the corresponding O⋯O repulsions are minimized.[12] These N⋯O contacts were found in the range of 2.53–2.95 Å, some are considerably less than the sum of the van der Waals radii[14] for nitrogen and oxygen (approximately 2.9 Å).[12] The trinitromethyl group of **β-1** basically shows a similar propeller like behavior. The dihedral angle C2−C3−N2−O4 (17°) in contrast is quite small compared to the average array of 23–67°[12] for the twisting of a $C(NO_2)_3$ group. The other dihedral angles are in the expected range. In a similar fashion the N⋯O contacts are slightly shortened (2.477–2.595 Å), which might be a consequence of the higher measurement temperature for **β-1**.

Compound **3** crystallizes in two different modifications side by side. **α-3** crystallizes in the monoclinic space group $P2_1/c$ and **β-3** in the orthorhombic space group *Pbcn*, both with four formula units per unit cell. The theoretical crystal density was calculated to 1.778 g cm^{-3} for **α-3** and 1.844 g cm^{-3} for **β-3**. The distances and angles were in the expected range of organic polynitro compounds such as 2,2,2-trinitroethanol.[15] The higher density of **β-3** is a result of various H⋯O interactions between nearby
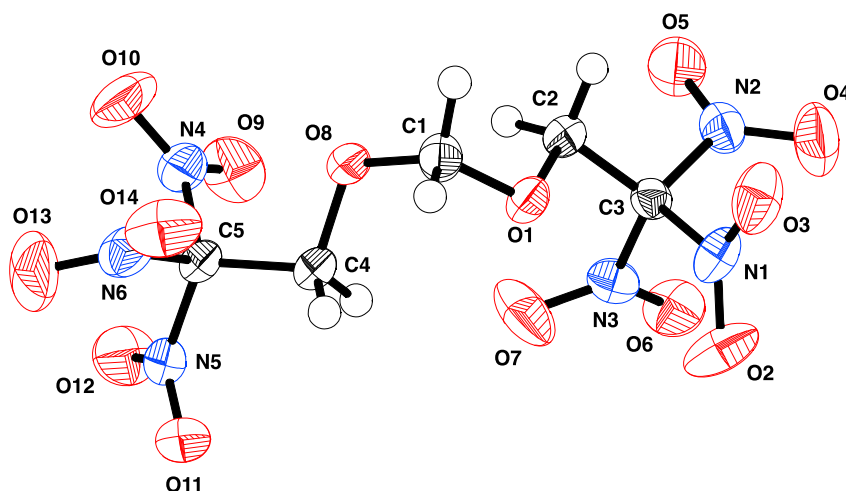
Figure 3.: Molecular structure of **α-3**. Selected distances [Å] and angles [°]: C1−O1 1.406(2), O1−C2 1.409(2), C2−C3 1.510(3), C3−N1 1.519(2), C3−N2 1.512(3), C3−N3 1.517(2), C1−O8 1.400(2), O8−C4 1.416(2), C4−C5 1.500(3), C5−N4 1.517(2), C5−N5 1.515(3), C5−N6 1.515(3), C1−O1−C2 113.7(1), O1−C2−C3 105.8(1), C2−C3−N1 110.0(1), C2−C3−N2 111.2(1), C2−C3−N3 114.7(1), C1−O8−C4 113.3(1), O8−C4−C5 105.9(1), C4−C5−N4 109.9(1), C4−C5−N5 110.5(1), C4−C5−N6 114.8(2), O1−C1−O8 111.9(1).
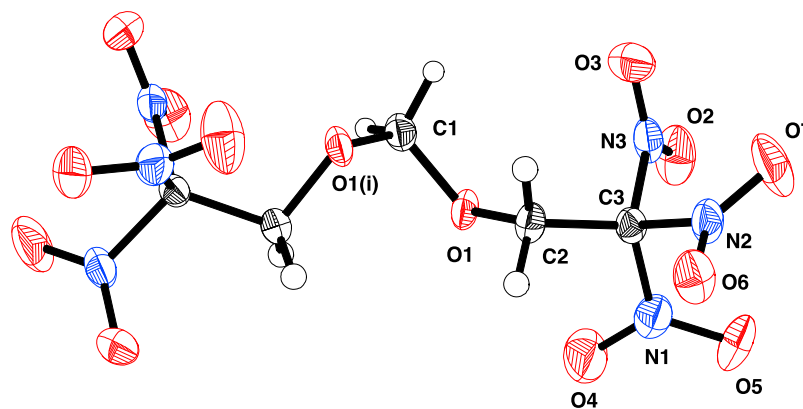
Figure 4.: Molecular structure of **β-3**. Selected distances [Å] and angles [°]: C1−O1 1.407(2), O1−C2 1.417(2), C2−C3 1.514(3), C3−N1 1.514(2), C3−N2 1.515(3), C3−N3 1.526(3), C1−O1−C2 114.5(2), O1−C2−C3 107.4(2), C2−C3−N1 111.0(2), C2−C3−N2 114.1(2), C2−C3−N3 110.9(2), O1(i)−C1−O1 112.1(3).

molecules. The molecular structures of **α-3** and **β-3** are shown in Figure 3 and Figure 4. The two different phases could also be distinguished by different dihedral angles of the trinitromethyl groups. The C−C−N−O dihedral angles are in the range of −58.2 to −23.4° for the C2−C3−(NO$_2$)$_3$ and 15.7–58.4° for the C4−C5−(NO$_2$)$_3$ group in

α-3. The dihedral angle C4−C5−N6−O14 (15.6°) is the smallest angle found for this structure and outside the average array of 23–67° for the twisting of a C(NO$_2$)$_3$ group.[12] The corresponding N⋯O contacts were found in the range of 2.53–2.95 Å, which is considerably less than the sum of the van der Waals radii[14] for nitrogen and oxygen (approximately 2.9 Å).[12] The trinitromethyl group of **β-3** is more likely an ideal propeller. The C−C−N−O dihedral angles are in the range of 28.6–53.3° and are fully integrated in the average array for trinitromethyl groups. Similarly the length of the N⋯O contacts are also in the expected range (2.477–2.595 Å).[12] Detailed information on the structure are given in Table 3 and the discussed dihedral angles of the different trinitromethyl groups for compounds **1** and **3** are listed in the Supporting Information.

In addition, it was also possible to obtain and analyze crystals of **2**, but these ended up only in a poor data set. However, it was possible to find a basic refinement showing clearly the asymmetric unit of 2,2,2-trinitroethyl orthoformate (**2**).

Thermal and Energetic Properties

Despite the fact that **1** has to be synthesized under inert gas conditions, the compound is stable when exposed to air. The exclusion of moisture is necessary to avoid side reactions leading to 2,2,2-trinitroethyl carbonate as by-product (Scheme 2). DSC measurements show that the product melts at a temperature of 159 °C. The decomposition starts at 191 °C (onset).

Single crystal X-ray diffraction experiments showed an interesting behavior at decreased temperatures. The colorless crystals of **1** started to crack, turned yellow, and the observed reflections at ambient temperature disappeared, while chilling the sample to measurement temperature of 173 K. Further DSC measurements at lowered temperatures showed a phase transition state (exothermic peak) between the **α**- and **β**-configuration of **1** starting at −16 °C (onset) during chilling the compound to −80 °C. Reheating the same sample provided an endothermic signal at 34 °C (onset) which indicates reversible phase transition. The rate of heating was ±5 °C. The **α**-configuration of **1** is metastable up to 33 °C. Above this temperature **β-1** could be observed. Between −16 and 34 °C both conformations of **1** are coexistent (Figure 5). FOX-7 shows a comparable behavior between two different phases at a temperature of 116 °C.[16]

The formate **2** was prepared under similar conditions like **1**. It is stable towards air and moisture and it decomposes at 192 °C, measured by DSC experiments. A melting point was observed at 126.5–128 °C. No phase transition could be observed according to similar DSC measurements of **2** compared with **1**.

The thermal stability for **3** was determined by DSC measurements. Thermal stress at 165 °C causes decomposition of the compound. It crystallizes in two different space

groups $P2_1/c$ and *Pbcn* side by side. Compared to **1**, similar DSC measurements of **3** did not show a phase transition in the range of -80 to $220\,°C$.

The sensitivity tests towards impact, friction, and electrostatic discharge provided the following results given in Table 5. All compounds are very sensitive towards impact and sensitive towards friction and electrostatic discharge.

Predictions of the detonation parameters using the EXPLO5 code[17] were performed based on heats of formations calculated *ab initio* using the Gaussian 03 program package[18,19] and verified with bomb calorimetric measurements (Table 4). Energetic parameters are attributed to the density of the corresponding compound. The resulting

Table 3.: Crystal and structure refinement data for $\boldsymbol{\alpha}$**-1**, $\boldsymbol{\beta}$**-1**, $\boldsymbol{\alpha}$**-3**, and $\boldsymbol{\beta}$**-3**.

	$\boldsymbol{\alpha}$**-1**	$\boldsymbol{\beta}$**-1**
Empirical formula	$C_9H_8N_{12}O_{28}$	$C_9H_8N_{12}O_{28}$
Formula mass [$g\,mol^{-1}$]	732.22	732.22
Temperature [K]	200(2)	258(2)
Crystal size [mm]	$0.20 \times 0.20 \times 0.10$	$0.40 \times 0.25 \times 0.02$
Crystal description	colorless block	colorless platelet
Crystal system	orthorhombic	tetragonal
Space group	$Fdd2$	$I\bar{4}2d$
a [Å]	16.6356(9)	13.356(2)
b [Å]	18.7450(8)	13.356(2)
c [Å]	16.0963(8)	15.083(3)
β [°]	90.0	90.0
V [Å^3]	5019.4(4)	2690.5(8)
Z	8	4
ρ_{calc} [$g\,cm^{-3}$]	1.938	1.808
μ [mm^{-1}]	0.200	0.186
$F(000)$	2960	1480
θ range [°]	4.14–32.00	4.31–29.99
Index ranges	$-24 \leq h \leq 24$	$-12 \leq h \leq 17$
	$-27 \leq k \leq 21$	$-18 \leq k \leq 3$
	$-24 \leq l \leq 17$	$-7 \leq l \leq 21$
Reflections collected	9644	3752
Reflections observed	2235	1288
reflections unique	1535	531
$R1$, $wR2$ (2σ data)	0.0326, 0.0474	0.0875, 0.2160
$R1$, $wR2$ (all data)	0.0545, 0.0500	0.1620, 0.2397
max./min. transmission	1.00000/0.88628	1.00000/0.90990
data/restraints/parameters	2235/1/223	1288/0/111
GOOF on F^2	0.808	0.879
Larg. diff. peak/hole [e Å^{-3}]	0.214/-0.171	0.436/-0.280

	α-3	β-3
Empirical formula	$C_5H_6N_6O_{14}$	$C_5H_6N_6O_{14}$
Formula mass [g mol^{-1}]	374.13	374.13
Temperature [K]	200(2)	200(2)
Crystal size [mm]	$0.30 \times 0.25 \times 0.15$	$0.21 \times 0.20 \times 0.02$
Crystal description	colorless block	colorless platelet
Crystal system	monoclinic	orthorhombic
Space group	$P2_1/c$	$Pbcn$
a [Å]	10.4605(5)	9.9980(6)
b [Å]	11.0072(5)	11.8416(7)
c [Å]	12.3025(6)	11.3826(9)
β [°]	99.409(4)	90.0
V [Å^3]	1397.5(1)	1347.6(2)
Z	4	4
ρ_{calc} [g cm^{-3}]	1.778	1.844
μ [mm^{-1}]	0.181	0.188
$F(000)$	760	760
θ range [°]	4.36–25.00	4.38–25.25
Index ranges	$-11 \leq h \leq 12$	$-12 \leq h \leq 10$
	$-6 \leq k \leq 13$	$-14 \leq k \leq 8$
	$-13 \leq l \leq 14$	$-13 \leq l \leq 4$
Reflections collected	5040	3114
Reflections observed	2449	1207
reflections unique	1609	648
$R1$, $wR2$ (2σ data)	0.0347, 0.0747	0.0340, 0.0512
$R1$, $wR2$ (all data)	0.0589, 0.0805	0.0792, 0.0558
max./min. transmission	0.99999/0.93162	1.00000/0.03211
data/restraints/parameters	2449/0/226	1207/1/118
GOOF on F^2	0.894	0.740
Larg. diff. peak/hole [e Å^{-3}]	0.243/$-$0.227	0.148/$-$0.189

heats of detonation (Q_v), detonation temperatures (T), pressures (p) and velocities (D) for **1**–**3** are shown in Table 5, as well as the oxygen balances (Ω). As a result, the detonation velocity of $\boldsymbol{\alpha}$-**1** (8419 m s^{-1}) is slightly greater than the value for PETN (8400 m s^{-1}).[20] Due to the different densities of $\boldsymbol{\alpha}$-**1** and $\boldsymbol{\beta}$-**1** the velocity decreases to 7994 m s^{-1} for $\boldsymbol{\beta}$-**1**. The values for the two different phases of **3** show a similar behavior. The detonation velocity of $\boldsymbol{\alpha}$-**3** is slightly smaller (8340 m s^{-1}) than PETN and due to its increased density $\boldsymbol{\beta}$-**3** has an increased velocity of 8626 m s^{-1}. The predicted velocity of **2** (8148 m s^{-1}) is in the range of nitroguanidine (8200 m s^{-1}).[20] The detonation parameters of **1**–**3** were calculated *ab initio* based on the predicted values, verified with bomb calorimetric measurements and are displayed in Table 5. The densities needed for the estimation of the detonation parameters with the EXPLO5 code[17] were derived
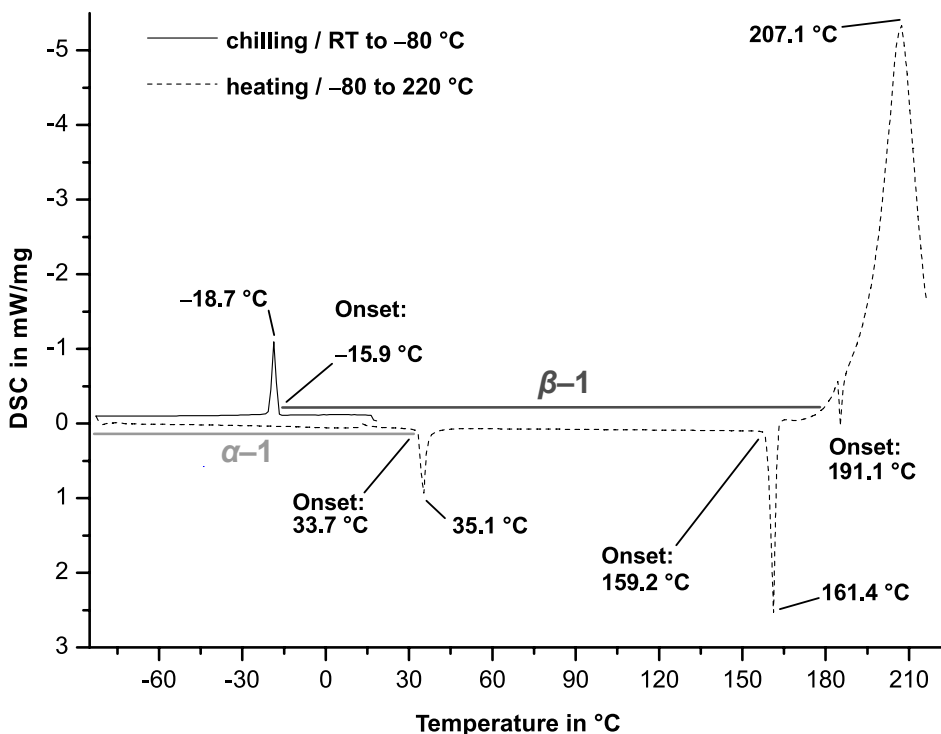
Figure 5.: DSC measurement for **1** from −80 to 220 °C with a chilling/heating rate of ±5 °C min^{-1}.

from the single-crystal X-ray structures for **1** and **3**. The density of **2** was determined experimentally by gas pycnometer measurements.

The specific impulses of compounds **1**–**3** were calculated for compositions of 70 % oxidizer (compound **1**–**3**), 16 % aluminum, 6 % polybutadiene acrylic acid, 6 % polybutadiene acrylonitrile, and 2 % bisphenol-A ether modeled on rocket motor compositions for solid rockets boosters used by the NASA Space Shuttle program.[22,23] These impulses were compared with the calculated impulse of ammonium perchlorate (AP) in an analogous composition. The chosen mixture with AP as oxidizer provides a specific impulse of 258 s. The impulses for **1**–**3** are slightly higher and in the range of 261–262 s. Although, as a consequence of the smaller oxygen balance of the compounds **1**–**3** according to AP, the oxygen balance for the corresponding compositions decreases from −44.78 % for **1** and −46.88 % for **2** to −50.97 % for **3**. A similar composition with AP as oxidizer has an oxygen balance of −30.13 %. Some results of the calculations are shown in Table 5.

Table 4.: Physical and chemical properties of **1**–**3**.

	α-**1**	β-**1**	**2**	α-**3**	β-**3**
Formula	$C_9H_8N_{12}O_{28}$	$C_9H_8N_{12}O_{28}$	$C_7H_7N_9O_{21}$	$C_5H_6N_6O_{14}$	$C_5H_6N_6O_{14}$
Mol mass [g mol^{-1}]	732.22	732.22	553.18	374.13	374.13
T_m [°C] $^{a)}$	–	161	127.5–128	64–65.5	64–65.5
T_d [°C] $^{b)}$	34	191	192	195	195
N [%] $^{c)}$	22.95	22.95	22.79	22.46	22.46
$N + O$ [%] $^{d)}$	84.13	84.13	83.53	82.33	82.33
Ω_{CO} [%] $^{e)}$	+32.8	+32.8	+30.4	+25.7	+25.7
Ω_{CO_2} [%] $^{f)}$	+13.1	+13.1	+10.1	+4.3	+4.3
ρ [g cm^{-3}] $^{g)}$	1.94	1.81	1.81*	1.78	1.84
$-\Delta U_{comb}$ [cal g^{-1}] $^{h)}$	1220.08	1220.08	1315.93	1492.35	1492.35
$-\Delta U_f^\circ$ [kJ kg^{-1}] $^{i)}$	940.28 (1024.92)	940.28 (1024.92)	938.33 (992.33)	994.65 (940.05)	975.99 (940.05)
$-\Delta H_f^\circ$ [kJ kg^{-1}] $^{j)}$	1021.53 (1124.17)	1021.53 (1106.17)	1021.23 (1075.23)	1080.78 (1026.18)	1062.12 (1026.18)

$^{a)}$ Melting point (T_m) from DSC measurement carried out at a heating rate of 5 °C min^{-1}.
$^{b)}$ Decomposition point (T_d) from DSC measurement carried out at a heating rate of 5 °C min^{-1}.
$^{c)}$ Nitrogen content. $^{d)}$ Combined nitrogen and oxygen content. $^{e)}$ Oxygen balance assuming the formation of CO. The oxygen balance of ammonium perchlorate is 34.0 %. $^{f)}$ Oxygen balance assuming the formation of CO_2. $^{g)}$ Calculated density from X-ray measurement. *Experimentally determined density from pycnometer experiments. $^{h)}$ Constant volume energy of combustion measured by bomb calorimetry. $^{i)}$ Energy of formation. $^{j)}$ Heat of formation. Values in brackets are based on the bomb calorimetric measurements.

2.4. Conclusions

Tetrakis(2,2,2-trinitroethyl) orthocarbonate (**1**), 2,2,2-trinitroethyl orthoformate (**2**) and 2,2,2-trinitroethyl formal (**3**) were synthesized and fully characterized by multinuclear NMR, IR and Raman spectroscopy, as well as mass spectrometry, and elemental analysis. The compounds turned out to be very sensitive towards impact. DSC measurements show a phase transition within two solid state configurations of **1** at −16 °C respectively 33 °C. **α-1** is metastable up to 33 °C. Decomposition of compound **1** starts at 191 °C (onset). The crystal structures of both phases of **1** were determined, with densities of 1.94 g cm^{-3} for **α-1** and 1.81 for **β-1**. Interestingly, the formal **3** crystallizes simultaneously in the space groups $P2_1/c$ and $Pbcn$. Compared to **1**, no evidence of a phase transition could be revealed by DSC experiments. The major difference between the phases observed of **1** and **3**, is the differing orientation of the trinitromethyl moieties. This phenomenon of trinitromethyl containing compounds might be of some interest in the case of further

Table 5.: Predicted detonation and combustion parameters (using the EXPLO5 code) and sensitivity data for **1**–**3**.

	α-**1**	β-**1**	**2**	α-**3**	β-**3**
$-Q_\mathrm{v}$ [kJ kg^{-1}]	5092.3 (4995.1)	5074.1 (4994.9)	5418.0	6004.2 (6073.4)	6040.9 (6073.4)
T_ex [K] [a)]	4208.8 (4266.7)	4278.7 (4327.3)	4437.8 (4467.8)	4705.9 (4720.9)	4702.3 (4720.9)
V_0 [L kg^{-1}] [b)]	673.8 (673.9)	674.2 (674.3)	680.1 (680.1)	693.2 (692.7)	692.6 (692.7)
p [kbar] [c)]	316.17 (319.15)	271.95 (274.11)	283.99 (285.32)	295.90 (325.74)	324.85 (325.74)
D [m s^{-1}] [d)]	8419.1 (8450.2)	7993.8 (8018.1)	8147.9 (8162.9)	8339.5 (8635.9)	8626 (8635.9)
Impact [J] [e)]	< 1	< 1	5	1.5	1.5
Friction [N] [e)]	96	96	96	108	108
ESD [J] [f)]	0.20	0.20	0.20	0.18	0.18
Grain size [µm] [g)]	250–500	250–500	500–1000	500–1000	500–1000
Thermal shock [h)]	burns	burns	burns	burns	burns
I_s [s] [i)]	262.6 (261.6)	262.6 (261.7)	262.7 (262.2)	261.9 (262.2)	261.9 (262.2)
Ω_comp [%] [j)]	−44.78	−44.78	−46.88	−50.97	−50.97

[a)] Temperature of the explosion gases. [b)] Volume of the explosion gases (assuming only gaseous products). [c)] Detonation pressure. [d)] Detonation velocity. [e)] Impact and friction sensitivities according to standard BAM methods. [21] [f)] Sensitivity towards electrostatic discharge. [g)] Grain size of the samples used for sensitivity tests. [h)] Response to fast heating in the "flame test". [i)] Specific impulse for compositions with 70 % oxidizer, 16 % aluminum, 6 % polybutadiene acrylic acid, 6 % polybutadiene acrylonitrile, and 2 % bisphenol-A ether at 70.0 bar chamber pressure using the EXPLO5 code [17]. The specific impulse for similar composition with ammonium perchlorate ($I_\mathrm{s\,(AP)} = 258$ s, $\Omega_\mathrm{comp\,(AP)} = -30.13$ %) was calculated. [j)] Oxygen balance for the composition used for combustion calculations. The oxygen balance for comparable composition with ammonium perchlorate: −30.13 %. Values in brackets are based on the bomb calorimetric measurements.

applications and should be investigated for similar molecules. The specific impulse I_s of compositions of **1**–**3** (≈ 262 s) are slightly higher than a comparable calculated composition with ammonium perchlorate (AP) as oxidizer (258 s), although the oxygen balance of the compositions for **1**–**3** are even worse.

2.5. Experimental Section

General Procedures. The synthesis and manipulation of air- and moisture-sensitive materials were performed in an inert atmosphere of dry nitrogen using flame-dried glass vessels and Schlenk techniques.[24] The solvents carbon tetrachloride and chloroform (all Sigma Aldrich) were dried by standard methods and freshly distilled prior to use. Sulfuric acid and paraformaldehyde (all Sigma Aldrich) were used as received. Anhydrous ferric chloride and 2,2,2-trinitroethanol were prepared according to literature known procedures.[15,25–27] Raman spectra were recorded with a Perkin-Elmer 2000 NIR FT spectrometer fitted with a Nd:YAG laser ($\lambda = 1064\,\text{nm}$, 300 mW), infrared spectra were measured with a Perkin-Elmer Spectrum BX-FTIR spectrometer equipped with a Smiths DuraSampl*IR* II ATR device. All spectra were recorded at ambient temperature as neat solids. NMR spectra were recorded with a JEOL Eclipse 400 instrument and chemical shifts were determined with respect to external Me_4Si (^{1}H, 399.8 MHz; ^{13}C, 100.5 MHz) and $MeNO_2$ (^{14}N, 28.9 MHz). Mass spectrometric data were obtained with a JEOL MStation JMS 700 spectrometer (DEI+). Analysis of C,H,N were performed with an Elementar vario EL Analyzer. Melting points were measured with a Perkin-Elmer Pyris6 DSC, using a heating rate of $5\,\text{K}\,\text{min}^{-1}$ and checked by a Büchi Melting Point B-540 apparatus and are not corrected. Bomb Calorimetry was undertaken, using a Parr 1356 Bomb calorimeter with a Parr 1108CL oxygen bomb. The sample pellets were prepared by form pressing a mixture of the energetic material (100–200 mg) and 800–900 mg benzoic acid. The value for $\Delta H_f^{\circ 298}$ was averaged over three measurements. The sensitivity data were performed using a BAM drophammer and a BAM friction tester.[21]

Computational Details. All ab initio calculations were carried out using the program package Gaussian 03 (Revision B.03)[18] and visualized by GaussView 5.08.[19] Structure optimizations and frequency analyses were performed with Becke's B3 three parameter hybrid functional using the LYP correlation functional (B3LYP). For C, H, N, and O a correlation consistent polarized double-zeta basis set was used (cc-pVDZ). The structures were optimized without symmetry constraints and the energy is corrected with the zero point vibrational energy.[28–30]

The enthalpies (H) and free energies (G) were calculated using the complete basis set (CBS) method in order to obtain accurate values.[28] The CBS models use the known asymptotic convergence of pair natural orbital expressions to extrapolate from calculations using a finite basis set to the estimated complete basis set limit. CBS-4 starts with a HF/3-21G(d) geometry optimization, which is the initial guess for the following SCF calculation as a base energy and a final MP2/6-31+G calculation with a CBS extrapolation to correct the energy in second order. The used reparametrized CBS-4M method additionally implements a MP4(SDQ)/6-31+(d,p) calculation to approximate

higher order contributions and also includes some additional empirical corrections.[29,30] The enthalpies of the gas-phase species were estimated according to the atomization energy method.[28,31–33]

All calculations affecting the detonation parameters were carried out using the program package EXPLO5 V5.03.[17] The detonation parameters were calculated at the CJ point with the aid of the steady-state detonation model using a modified Becker-Kistiakowski-Wilson equation of state for modeling the system. The CJ point is found from the Hugoniot curve of the system by its first derivative.[34,35] The specific impulses were also calculated with the EXPLO5 V5.03 program,[17] assuming an isobaric combustion of a composition of **1**–**3** as oxidizer, aluminum as fuel, 6 % polybutadiene acrylic acid, 6 % polybutadiene acrylonitrile as binder and 2 % bisphenol-A as epoxy curing agent. A chamber pressure of 70.0 bar and an ambient pressure of 1.0 bar with frozen expansion conditions were estimated for the calculations. The best ratios of oxidizer and fuel were determined empirically under constant amounts of binder and epoxy curing agent.

X-ray Crystallography. For all compounds, an Oxford Xcalibur3 diffractometer with a CCD area detector was employed for data collection using Mo-K_α radiation ($\lambda = 0.710\,73$ Å). The structures were solved by direct methods (SIR97)[36,37] and refined by full-matrix least-squares on F^2 (SHELXL).[38–41] All non-hydrogen atoms were refined anisotropically. The hydrogen atoms were located in a difference Fourier map and placed with a C−H distance of 0.99 Å for CH_2 groups. ORTEP plots are shown with thermal ellipsoids at the 50 % probability level, respectively 30 % for **β-1**.

Crystallographic data (excluding structure factors) for the structures in this paper have been deposited with the Cambridge Crystallographic Data Centre, CCDC, 12 Union Road, Cambridge CB21EZ, UK. Copies of the data can be obtained free of charge on quoting the depository numbers CCDC-812189, -812190, -812191, and CCDC-812192 (Fax: +44-1223-336-033; E-Mail: deposit@ccdc.cam.ac.uk, http://www.ccdc.cam.ac.uk).

CAUTION! All of the described compounds are energetic with sensitivity towards heat, impact, and friction. Although no hazards occurred during preparation, and manipulation, additional proper protective precautions (face shield, leather coat, earthened equipment and shoes, Kevlar® gloves and ear plugs) should be used when undertaking work with these compounds.

Synthesis of tetrakis(2,2,2-trinitroethyl) orthocarbonate (1)

2,2,2-Trinitroethanol (1.8 g, 10.0 mmol) and anhydrous iron(III) chloride (0.2 g, 1.23 mmol) were diluted in carbon tetrachloride (6.7 mL, 69.4 mmol) in a 25 mL flask under careful exclusion of moisture. The mixture was heated up in an oil bath (85 °C)

and heated to reflux for 24 h. The chilled carbon tetrachloride solution was decanted from the product and iron(III) chloride. The solvent was removed in vacuo. To dissolve the remaining iron(III) chloride the residue was washed with iced dilute hydrochloric acid (20 mL, 6 M). The crude product was dissolved in dichloromethane (30 mL) and washed three times with iced dilute hydrochloric acid (20 mL, 6 M) to remove the last amounts of iron(III) chloride. Removing the solvent gave 1.0 g of crude product. After recrystallization of the crude product from chloroform ($35\,\mathrm{mL\,g^{-1}}$), 0.88 g of **1** (48 % yield) were obtained. DSC (T_{onset}, $5\,\mathrm{K\,min^{-1}}$): 161 °C (melting point), 191 °C (decomposition). IR: $\tilde{\nu}$ = 3008 (w), 2959 (w), 2888 (w), 2356 (vw), 1594 (vs, $\nu_{\mathrm{as}}\,NO_2$), 1449 (w), 1395 (w), 1349 (vw), 1290 (m), 1261 (w), 1191 (m), 1144 (s), 1120 (m), 1091 (m), 1069 (m), 884 (w), 856 (m), 806 (m), 784 (m), 742 (w), 677 (w), 651 (w), 614 (w) cm^{-1}. Raman: $\tilde{\nu}$ = 3009 (17), 2960 (35), 2885 (8), 1597 (25) ($\nu_{\mathrm{as}}\,NO_2$), 1454 (17), 1435 (9), 1389 (16), 1350 (41), 1305 (30) ($\nu_{\mathrm{s}}\,NO_2$), 1261 (16), 1171 (10), 1147 (7), 1094 (12), 1068 (12), 1019 (9), 994 (11), 885 (17), 859 (100), 809 (9), 782 (12), 746 (6), 640 (9), 622 (9), 555 (15), 474 (9), 415 (44), 404 (42), 377 (80), 313 (17), 270 (26), 201 (27) cm^{-1}. ^{1}H NMR ([D$_6$]acetone): δ = 5.60 (CH_2); (CD$_3$CN): δ = 5.14 (CH_2) ppm. ^{13}C{^{1}H} NMR ([D$_6$]acetone): δ = 124.4 [br, $C(NO_2)_3$], 118.2 [$C(OCH_2)_4$], 63.9 (OCH$_2$); (CD$_3$CN): δ = 124.1 [br, $C(NO_2)_3$], 119.1 [$C(OCH_2)_4$], 63.8 (OCH$_2$) ppm. ^{14}N NMR ([D$_6$]acetone): δ = −35 (NO_2); (CD$_3$CN): δ = −35 (NO_2) ppm. MS (DEI+) m/z (%): 552 (100) [M$^+$ −OCH$_2$(CNO$_2$)$_3$], 164 (80) [CH$_2$C(NO$_2$)$_3$$^+$], 118 (39) [CHC(NO$_2$)$_2$$^+$], 46 (80) [NO$_2$$^+$], 30 (44) [NO$^+$]. EA (C$_9H_8N_{12}O_{28}$, 732.22) calcd.: C 14.75, H 1.10, N 22.95 %; found: C 14.75, H 1.23, N 22.58 %. Impact sensitivity: < 1 J; Friction sensitivity: 92 N; ESD: 0.2 J; Grain size: 250–500 µm.

Synthesis of 2,2,2-trinitroethyl formate (2)

2,2,2-Trinitroethanol (2.5 g, 14.0 mmol) and anhydrous iron(III) chloride (0.2 g, 1.23 mmol) were dissolved in dry chloroform (5 mL) under careful exclusion of moisture. The mixture was heated up in an oil bath (85 °C) and heated to reflux for 120 h. Upon cooling, the content of the reaction vessel was poured into diethyl ether (60 mL). The ether solution was washed with water (3 × 60 mL) and dried with sodium sulfate. Removing the solvent left a cream colored crude product, which was recrystallized from dichloromethane/pentane (50:50). 1.9 g (74 % yield) of **2** as colorless crystals were obtained. DSC (T_{onset}, $5\,\mathrm{K\,min^{-1}}$): 126.5–128 °C (melting point), 192 °C (decomposition). IR: $\tilde{\nu}$ = 3003 (w), 2956 (w), 2884 (w), 2346 (vw), 1587 (vs, $\nu_{\mathrm{as}}\,NO_2$), 1446 (w), 1401 (w), 1341 (vw), 1294 (m, $\nu_{\mathrm{s}}\,NO_2$), 1184 (w), 1125 (m), 1104 (w), 1075 (w), 1029 (vw), 1008 (w), 970 (w), 946 (w), 876 (w), 854 (w), 802 (m), 778 (w), 724 (w), 644 (w) cm^{-1}. Raman: $\tilde{\nu}$ = 2990 (13), 2955 (30), 2880 (4), 1610 (18) ($\nu_{\mathrm{as}}\,NO_2$), 1448 (13), 1395 (13), 1350 (30), 1308 (27) ($\nu_{\mathrm{s}}\,NO_2$), 1251 (10), 1162 (4), 1093 (7), 1078 (9),

1033 (8), 882 (9), 859 (100), 805 (6), 781 (8), 728 (5), 649 (6), 543 (12), 515 (7), 402 (34), 374 (46), 309 (14), 268 (19), 204 (23) cm^{-1}. ^{1}H NMR (CD$_3$CN): δ = 5.89 [s, 1 H, HC(OCH$_2$)$_3$], 5.10 [s, 6 H, CH_2C(NO$_2$)$_3$] ppm. ^{13}C\{^{1}H\} NMR (CD$_3$CN): δ = 125.0 [br, C(NO$_2$)$_3$], 112.7 [C(OCH$_2$)$_3$], 63.7 (OCH$_2$) ppm. ^{14}N NMR (CD$_3$CN): δ = -34 (NO$_2$) ppm. MS (DEI+) m/z (%): 552 (1) [M$^+$], 373 (88) [M$^+$ $-$OCH$_2$(CNO$_2$)$_3$], 164 (95) [CH$_2$C(NO$_2$)$_3$$^+$], 118 (41) [CHC(NO$_2$)$_2$$^+$], 46 (100) [NO$_2$$^+$], 30 (59) [NO$^+$]. EA (C$_7H_7N_9O_{21}$, 553.18) calcd.: C 15.20, H 1.28, N 22.79 %; found: C 15.09, H 1.32, N 20.82 %. Impact sensitivity: 5 J; Friction sensitivity: 92 N; ESD: 0.2 J; Grain size: 500–1000 μm.

Synthesis of 2,2,2-trinitroethyl formal (3)

2,2,2-Trinitroethanol (3.6 g, 19.9 mmol) was dissolved in sulfuric acid (98 %, 50 mL) at 50 °C. Upon chilling to room temperature paraformaldehyde (0.3 g, 10 mmol) was added carefully. The temperature was kept below 40 °C. The solution was stirred for 1 h, subsequently quenched with icewater (100 mL), and was allowed to warm up to room temperature. The colorless precipitate was filtered off, washed with water (100 mL) and dried in vacuo. 2.87 g (77 %) of **3** as colorless solid was obtained. DSC (T_onset, 5 K min^{-1}): 64–65.5 °C (melting point), 195 °C (decomposition). IR: $\tilde{\nu}$ = 2987 (w), 2928 (w), 2879 (w), 2607 (vw), 1581 (vs, ν_as NO$_2$), 1479 (vw), 1445 (w), 1414 (vw), 1353 (vw), 1300 (s, ν_s NO$_2$), 1186 (w), 1135 (m), 1096 (s), 1050 (m), 941 (m), 882 (w), 855 (w), 804 (m), 780 (m), 734 (w), 656 (vw), 638 (vw), 607 (vw) cm^{-1}. Raman: $\tilde{\nu}$ = 2980 (19), 2950 (17), 2931 (22), 2876 (6), 1604 (17) (ν_as NO$_2$), 1480 (9), 1449 (13), 1398 (14), 1355 (30), 1307 (27) (ν_s NO$_2$), 1261 (9), 1187 (3), 1156 (5), 1136 (5), 1093 (5), 1029 (14), 944 (7), 886 (12), 859 (100), 806 (8), 782 (6), 743 (5), 656 (6), 524 (13), 423 (34), 393 (37), 373 (55), 340 (13), 322 (13), 302 (13), 277 (15), 204 (22) cm^{-1}. ^{1}H NMR (CD$_3$CN): δ = 5.04 [s, 4 H, CH_2C(NO$_2$)$_3$], 4.96 (s, 2 H, O$_2$CH_2) ppm. ^{13}C\{^{1}H\} NMR (CD$_3$CN): δ = 126.0 [br, C(NO$_2$)$_3$], 98.1 [C(OCH$_2$)$_2$], 67.3 (OCH$_2$) ppm. ^{14}N NMR (CD$_3$CN): δ = -33 (NO$_2$) ppm. MS (DEI+) m/z (%): 373 (0.3) [M$^+$], 194 (100) [M$^+$ $-$OCH$_2$(CNO$_2$)$_3$], 164 (64) [CH$_2$C(NO$_2$)$_3$$^+$], 119 (57) [CH$_2$C(NO$_2$)$_2$$^+$], 46 (70) [NO$_2$$^+$], 30 (33) [NO$^+$]. EA (C$_5H_6N_6O_{14}$, 374.13) calcd.: C 16.05, H 1.62, N 22.46 %; found: C 16.27, H 1.66, N 21.88 %. Impact sensitivity: 1.5 J; **Friction** sensitivity: 108 N; ESD: 0.18 J; Grain size: 500–1000 μm.

2.6. Acknowledgement

Supporting Information

Complete listing of the $C-C-N-O$ torsion angles containing the $C(NO_2)_3$ group of **α-1**, **β-1**, **α-3**, and **β-3**.

2.7. References

[1] M. E. Hill, *US3306939*, **1967**.

[2] T. M. Klapötke, S. F. Rest, *New Trends Res. Energ. Mater., Proc. Semin., 13th* **2010**, Pt, 2, 642–651.

[3] M. Göbel, T. M. Klapötke, *Adv. Funct. Mater.* **2009**, *19*, 347–365.

[4] M. Göbel, T. M. Klapötke, *Z. Anorg. Allg. Chem.* **2007**, *33*, 1006–1017.

[5] T. M. Klapötke, *Chemie der hochenergetischen Materialien*, 1st. ed., de Gruyter, Berlin, 2009.

[6] T. M. Klapötke, Chemistry of High-Energy Materials, 1st. ed., de Gruyter, Berlin, **2011**.

[7] J. Hine, J. W. Bailey, *J. Org. Chem.* **1961**, *26*, 2098–2099.

[8] T. N. Hall, *Tetrahedron* **1963**, *19*, 115–120.

[9] M. E. Hill, K. G. Shipp, *US3526667*, **1970**.

[10] A. B. Sheremetev, I. L. Yudin, *Mendeleev Commun.* **2005**, *15*, 204–205.

[11] K. G. Shipp, M. E. Hill, *J. Org. Chem.* **1966**, *31*, 853–856.

[12] Y. Oyumi, T. B. Brill, A. L. Rheingold, *J. Phys. Chem.* **1985**, *89*, 4824–4828.

[13] S. K. Bhattacharjee, H. L. Ammon, *Acta Crystallogr., Sect. B* **1982**, *38*, 2503–2505.

[14] A. Bondi, *J. Phys. Chem.* **1964**, *68*, 441–451.

[15] M. Göbel, T. M. Klapötke, *Acta Crystallogr., Sect. C* **2007**, *63*, o562–o564.

[16] J. Evers, T. M. Klapötke, P. Mayer, G. Oehlinger, J. Welch, *Inorg. Chem.* **2006**, *45*, 4996–5007.

[17] M. Sućeska, *EXPLO5 V5.03*, Brodarski Institute, Zagreb, Croatia, **2008**.

[18] M. J. Frisch, G. W. Trucks, H. B. Schlegel, G. E. Scuseria, M. A. Robb, J. R. Cheeseman, J. A. Montgomery Jr., T. Vreven, K. N. Kudin, J. C. Burant, J. M. Millam, S. S. Iyengar, J. Tomasi, V. Barone, B. Mennucci, M. Cossi, G. Scalmani, N. Rega, G. A. Petersson, H. Nakatsuji, M. Hada, M. Ehara, K. Toyota, R. Fukuda, J. Hasegawa, M. Ishida, T. Nakajima, Y. Honda, O. Kitao, H. Nakai, M. Klene, X. Li, J. E. Knox, H. P. Hratchian, J. B. Cross, V. Bakken, C. Adamo, J. Jaramillo, R. Gomperts, R. E. Stratmann, O. Yazyev, A. J. Austin, R. Cammi, C. Pomelli, J. W. Ochterski, P. Y. Ayala, K. Morokuma, G. A. Voth, P. Salvador, J. J. Dannenberg, V. G. Zakrzewski, S. Dapprich, A. D. Daniels, M. C. Strain, O. Farkas, D. K. Malick, A. D. Rabuck, K. Raghavachari, J. B. Foresman, J. V. Ortiz, Q. Cui, A. G. Baboul, S. Clifford, J. Cioslowski, B. B. Stefanov, G. Liu, A. Liashenko, P. Piskorz, I. Komaromi, R. L. Martin, D. J. Fox, T. Keith, M. A. Al-Laham, C. Y. Peng, A. Nanayakkara, M. Challacombe, P. M. W. Gill, B. Johnson, W. Chen, M. W. Wong, C. Gonzalez, J. A. Pople, *Gaussian 03*, *Rev. B.03*, Gaussian, Inc., Wallingford CT, **2003**.

[19] T. K. Roy Dennington, John Millam, *GaussView, Version 5*, Semichem Inc., Shawnee Mission KS, **2009**.

[20] P. W. Cooper, *Explosives Engineering*, 1st ed., Wiley VCH, New York, **1996**.

[21] Laying down test methods pursuant to Regulation (EC) No 1907/2006 of the European Parliament and of the Council on the Evaluation, Authorization and Restriction of Chemicals (REACH), ABl·L 142, **2008**.

[22] NASA, *Space Shuttle News Reference*, 2–20–22–21, http://ntrs.nasa.gov/archive/nasa/casi.ntrs.nasa.gov/19810022734_1981022734.pdf.

[23] NASA, *press release: STS-122 The Voyage of Columbus*, **2008**, 82–84, http://www.nasa.gov/pdf/203212main_sts122_presskit2.pdf.

[24] D. F. Shriver, M. A. Drezdzon, *The Manipulation of Air-Sensitive Compounds*, 2nd ed., John Wiley & Sons, New York, **1986**.

[25] A. F. Holleman, N. Wiberg, *Lehrbuch der Anorganischen Chemie*, 102nd ed., de Gruyter, Berlin, **2007**.

[26] G. Jander, E. Blasius, *Einführung in das anorganisch-chemische Praktikum*, 14th ed., Hirzel Verlag, Stuttgart, **1995**.

[27] M. Binnewies, M. Jäckel, H. Willner, G. Rayner-Canham, *Allgemeine und Anorganische Chemie*, 1st ed., Spektrum Akademischer Verlag, München, **2004**.

[28] T. M. Klapötke, J. Stierstorfer, *Phys. Chem. Chem. Phys.* **2008**, *10*, 4340–4346.

[29] J. J. A. Montgomery, M. J. Frisch, J. W. Ochterski, G. A. Petersson, *J. Chem. Phys.* **2000**, *112*, 6532–6542.

[30] J. W. Ochterski, G. A. Petersson, J. A. Montgomery, Jr., *J. Chem. Phys.* **1996**, *104*, 2598–2619.

[31] E. F. C. Byrd, B. M. Rice, *J. Phys. Chem. A* **2005**, *109*, 1005–1013.

[32] L. A. Curtiss, K. Raghavachari, P. C. Redfern, J. A. Pople, *J. Chem. Phys.* **1997**, *106*, 1063–1079.

[33] B. M. Rice, S. V. Pai, J. Hare, *Combust. Flame* **1999**, *118*, 445–458.

[34] T. M. Klapötke, B. Krumm, F. X. Steemann, K. D. Umland, *Z. Anorg. Allg. Chem.* **2010**, *636*, 234–2346.

[35] M. Sućeska, *Propellants Explos. Pyrotech.* **1991**, *16*, 197–202.

[36] A. Altomare, M. C. Burla, M. Camalli, G. L. Cascarano, C. Giacovazzo, A. Guagliardi, A. G. G. Moliterni, G. Polidori, R. Spagna, *J. Appl. Crystallogr.* **1999**, *32*, 115–119.

[37] A. Altomare, G. Cascarano, C. Giacovazzo, A. Guagliardi, A. G. G. Moliterni, M. C. Burla, G. Polidori, M. Camalli, R. Spagna, *SIR97*, **1997**.

[38] G. M. Sheldrick, *SHELX-97*, University of Göttingen, Göttingen, Germany, **1997**.

[39] G. M. Sheldrick, *Acta Crystallogr., Sect. A* **2008**, *64*, 112–122.

[40] L. J. Farrugia, *J. Appl. Crystallogr.* **1999**, *32*, 837–838.

[41] A. L. Spek, *Acta Crystallogr., Sect. D* **2009**, *65*, 148–155.

3. Trinitroethyl Substituted Carbamates

PHOSGENE

$\rightarrow\rightarrow\rightarrow$
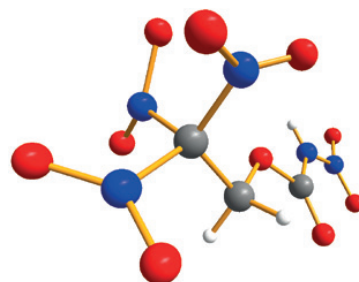
The Energetic Nitrocarbamate O$_2$NN(H)CO[OCH$_2$C(NO$_2$)$_3$] Derived from Phosgene

Quirin J. Axthammer,[a] Thomas M. Klapötke,*[a] Burkhard Krumm,[a] Richard Moll,[a] and Sebastian F. Rest [a]

Keywords: Nitrocarbamate • Explosives • High energetic oxidizer • Crystal structure • Sensitivities

*   Prof. Dr. Thomas M. Klapötke

      E-Mail: tmk@cup.uni-muenchen.de

[a]   Department of Chemistry

      Ludwig-Maximilian University of Munich

      Butenandtstrasse 5–13 (D)

      81377 Munich, Germany

3.1. Abstract

A new simple synthesis route for 2,2,2-trinitroethyl chloroformate (**1**), from easily available starting materials 2,2,2-trinitroethanol and phosgene is presented. 2,2,2-Trinitroethyl carbamate (**2**) was obtained by the reaction of **1** with aqueous ammonia. The nitration of **2** with anhydrous nitric acid and sulfuric acid yields 2,2,2-trinitroethyl nitrocarbamate (**3**), which has potential as a perchlorate free high energetic dense oxidizer with a high oxygen balance of $\Omega(CO_2) = +14.9\,\%$. The thermal stability was studied using differential scanning calorimetry and the energies of formation were calculated on the CBS-4M level of theory, as well as several detonation parameters and propulsion properties were determined. In addition to full spectroscopic characterization, X-ray diffraction studies were performed for **2** and **3**.

3.2. Introduction

The 1,1,1-trinitroethyl moiety is a widely-used building block in the chemistry of high energetic explosives, especially if performing as a high energy dense oxidizer (HEDO).[1,2] Such compounds can be used as high performance, halogen-free propellants. These might overcome the environmental problems of hydrogen chloride formation during the use of ammonium perchlorate as oxidizer in rocket propellant formulations.[3] Furthermore, the perchlorate anion has negative health effects, scientific research indicates that perchlorate contaminated water can disrupt the thyroid's ability to produce hormones needed for normal growth and development.[4] There are three synthesis routes for the chemical transfer of a 1,1,1-trinitroethyl functionality known. The most common way is the nucleophilic substitution of halogen atoms in reactive organic compounds like haloalkanes, acid halides and esters of the formic acid with the easy available alcohol 2,2,2-trinitroethanol.[5–8] An alternative to this is the widespread Mannich reaction, which is a multi-component condensation between a nitroalkane, an aldehyde, and a primary or secondary amine. The mechanism of it starts with the formation of an iminium ion from the amine and formaldehyde. This cationic intermediate can be attacked from the trinitromethanide anion to form the 2,2,2-trinitroethylamine unit.[2,9] The third and less applied route, is the transfer of the 1,1,1-trinitroethyl moiety by a chloroformate.[10]

3.3. Results and Discussion

Synthesis

The standard synthesis of chloroformates is the reaction between alcohols and an excess of phosgene with a base as acid acceptor.[11] Pure 2,2,2-trinitroethyl chloroformate (**1**) was first prepared in 1979 in a three step synthesis via S-ethyl chloroformate as starting material and claimed that a direct chloroformylation of β-nitro alcohols such as 2,2,2-trinitroethanol does not work properly.[10] This was explained by the very fast reaction to the by-product bis(2,2,2-trinitroethyl) carbonate and a reverse Henry reaction with a decomposition of the alcohol to the corresponding aldehyde and nitroalkane introduced by the required base.[7,10] Therefore, for the synthesis of **1** was used the phosgene analogue S-ethyl chlorothioformate with a subsequent replacement of the ethylthio group by chlorine with sulfuryl chloride.[10] In contrast to the literature prediction, the direct chloroformylation with phosgene and 2,2,2-trinitroethanol was successful (Scheme 1). The reaction works best with an excess of phosgene and the aid of one equivalent of non-nucleophilic bases, such as triethylamine. The product can easily be removed from the reaction mixture and was obtained as a colorless liquid in very good yields around 86 %. The described one-pot reaction procedure has several advantages such as a reduced consumption of chemicals and reduced reaction time.
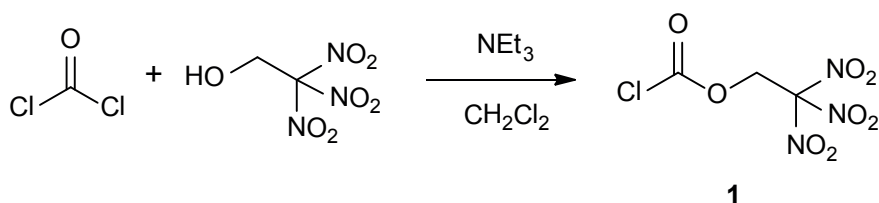
Scheme 1: Synthesis of 2,2,2-trinitroethyl chloroformate (**1**).

In the 1990ies it was briefly mentioned, that 2,2,2-trinitroethyl carbamate (**2**) could be synthesized by the reaction of 2,2,2-trinitroethanol and carbamoyl chloride.[12] However, the synthesis of **2** via the chloroformate **1** and aqueous ammonia in dichloromethane is the more preferred route of choice (Scheme 2). The nitration of the carbamate **2** with a mixture of sulfuric (95 %) and nitric acid (100 %) (1:1) leads to the formation of 2,2,2-trinitroethyl nitrocarbamate (**3**). Recrystallization from tetrachloromethane yielded almost quantitatively pure colorless product **3** as fine needles.
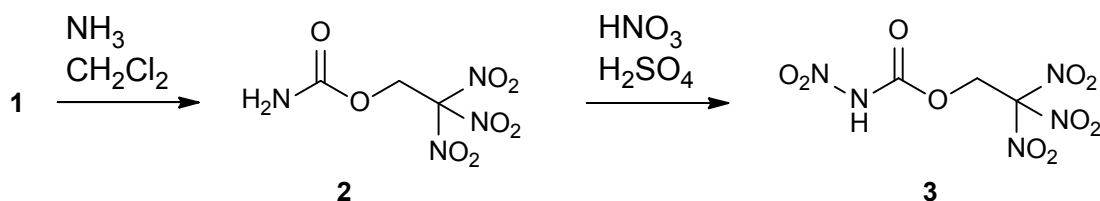
Scheme 2: Synthesis of 2,2,2-trinitroethyl carbamate (**2**) and 2,2,2-trinitroethyl nitrocarbamate (**3**).

NMR Spectroscopy

All compounds were characterized by ^{1}H, ^{13}C and ^{14}N NMR spectroscopy (Table 1). In the ^{1}H NMR spectra of **1**–**3** the CH$_2$ group is observed at 5.68–5.51 ppm. The ^{1}H NMR spectrum of the carbamate **2** shows an interesting temperature dependent dynamic behavior of the NH$_2$ resonance of the amide group, which splits at 25 °C into two different signals. This is due to a restricted rotation along the C$-$NH$_2$ bond of the amide **2**. Temperature-dependent ^{1}H NMR spectra were recorded in [D$_6$]DMSO in the range of 25 to 60 °C (Figure 1). From these measurements, a coalescence temperature T_c of 42.5 °C and the corresponding chemical shift difference $\Delta\nu$ (= 42.5 °C) of 75.2 Hz are determined. With these data, the free enthalpy of activation $\Delta G^{\ddagger}$ (15.3 kcal mol^{-1}) is calculated by applying the Eyring equation.[13,14] This activation barrier of rotation is within the range of other values obtained for amides.[15] Furthermore, a diamagnetic shift of the amine resonance with increasing temperature is observed. This temperature dependence is the result of weakening the hydrogen bond and therefore lessening the electron withdrawing effect of the hydrogen-bond acceptor on the proton. As a result the proton becomes more shielded and its resonance is shifted upfield.[16]

The NH resonance of the nitrocarbamate **3** compared to the NH$_2$ of **2** is shifted downfield to 10.70 ppm. In the ^{13}C{^{1}H} NMR spectra the resonances of the carbon atoms of the methylene groups were observed at 63.3–61.8 ppm, those of the trinitromethyl groups broadened at 125.7–121.4 ppm and the carbonyl groups at 149.5 (**1**), 154.5 (**2**), and 145.2 ppm (**3**). The nitro resonances in the ^{14}N NMR of the trinitromethane moiety were found for **1**–**3** between -33 and -36 ppm and in addition, that of the nitrocarbamate of **3** was observed at -55 ppm. For compounds **2** and **3** a very broad resonance for the amide nitrogen atom was detected at -310 (**2**) and -292 ppm (**3**).

Single Crystal Structural Analysis

Single crystals of **2** and **3** were obtained from tetrachloromethane at ambient temperature (Table 2). Both compounds crystallize in the monoclinic space group $P2_1/c$ with four

Table 1.: Multinuclear NMR resonances [ppm] of **1**–**3** in [D$_6$]acetone.

	1	**2**	**3**
^{1}H	5.51 (CH_2)	6.77 (s, NH)	10.70 (s, NH)
		6.49 (s, NH)	5.53 (CH_2)
		5.68 (CH_2)	
^{13}C	149.5 (CO$_2$Cl)	154.5 (CO$_2$N)	145.2 (CO$_2$N)
	121.4 [C(NO$_2$)$_3$]	125.7 [C(NO$_2$)$_3$]	122.2 [C(NO$_2$)$_3$)]
	63.3 (CH$_2$)	61.8 (CH$_2$)	62.1 (CH$_2$)
^{14}N	−36 (NO$_2$)	−33 (NO$_2$)	−36 (NO$_2$)
		−310 (NH$_2$)	−55 (NNO$_2$)
			−292 (NNO$_2$)

formula units per unit cell. The asymmetric unit with selected bond lengths and angles are shown in Figure 2 (**2**) and Figure 3 (**3**).

The molecular structure of the carbamate **2** shows a large part with nearly planar arrangement. This planar range comprised the carbamate, the C2 carbon of the methylene group and C3 of the trinitromethyl moiety. The conformation of the substituents at C2 and C3 is nearly staggered [N2−C3−C2−H3A 43.3(1)°, N3−C3−C2−H3B 42.6(1)°, N4−C3−C2−O2 42.7(1)°]. The C−N bond lengths of the trinitromethyl moiety are in the range of 1.52 Å, which is significantly longer than a regular C−N bond (1.47 Å).[17] This is typical for molecules with the trinitromethyl moiety and is due to steric repulsion effects.[2,5] The three nitro groups arrange in a propeller-like constitution, which optimize the non-bonded intramolecular attractions [partial charge distribution of nitrogen (δ^+) and oxygen (δ^-) atom in the nitro group] and electrostatic repulsion of two neighboring nitro groups. The N···O attractions (N2···O6, N3···O8, N4···O3) can be found in **2** with distances in the range of 2.55–2.67 Å, which are much shorter than the sum of the van der Waals radii for nitrogen and oxygen (3.07 Å).[18] In addition, another strong attractive intramolecular N···O interaction with 2.60 Å is observed between the nitrogen atom N4 of the trinitro functionality and the oxygen O2. The carbamate group with a short C−NH$_2$ bond (1.333 Å) and shortened N−H bonds (0.87 and 0.91 Å) shows typical values for carbamates.[19]

The molecules of **2** are cross-linked three dimensional by hydrogen bonds. The intermolecular hydrogen-bond lengths and angles are shown in Table 3. In the structure can been found three classical NH···O hydrogen bonds with the carbonyl and the nitro group as acceptors. The two hydrogen interactions with the carbonyl (O1) can be classified as strong, whereas the interaction with the nitro group (O5) is moderate on the basis of the distance and the angle of the hydrogen bond.[20] Also an unusual hydrogen
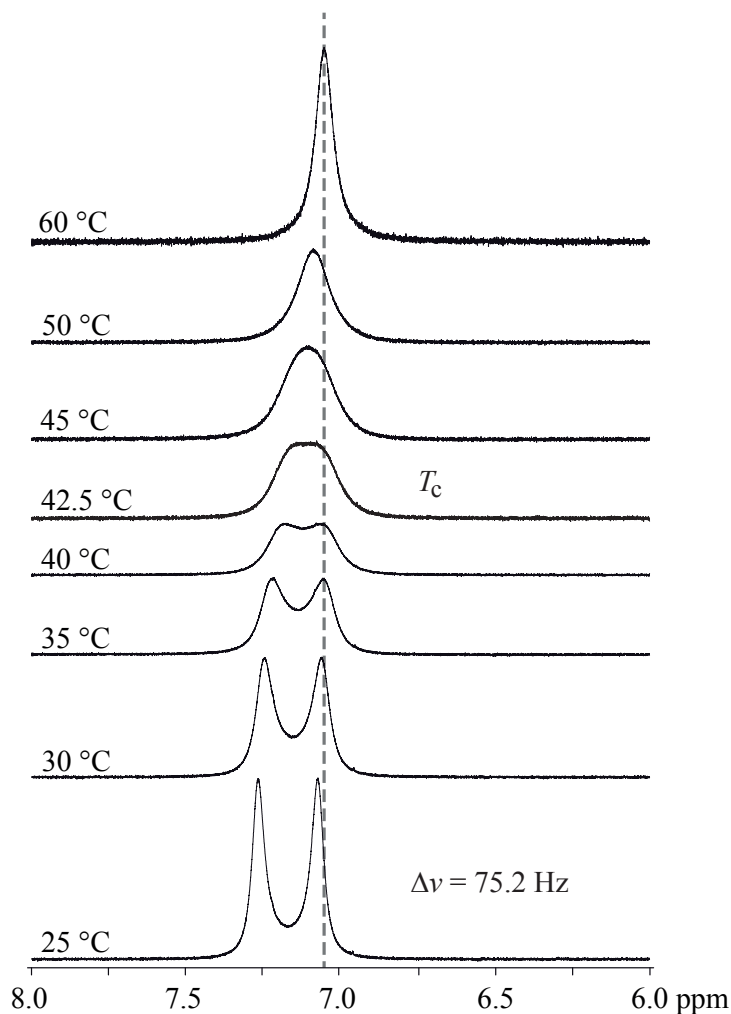
Figure 1.: ^{1}H NMR resonance of the NH_2 group of **2** at variable temperatures in $[D_6]$DMSO.

bond with carbon as donor (CH⋯O) can be observed in **2**, between the methylene (C2−H3A) and one nitro group (O7), which is only weak. [21]

The data collection of **3** had to be performed at higher temperature, because the compound showed a phase transition at about −62 °C. This phase transition leads to microfracture of the single crystal, which made a measurement impossible. Thus, the data collection was carried out at 30 °C, causing much greater thermal vibrations of the atoms, especially of the trinitromethyl group.

In the literature only one single crystal X-ray structure of a nitrocarbamate, alkylated at the carbamate nitrogen, is known. [22] The nitrocarbamate moiety of compound **3** shows a perfect planarity as shown by the sum of the angles around the C1 and the two nitrogen atoms N1/N2, where the angle sum is 360.0° each. The N1−N2 bond of the

Table 2.: X-ray data and parameters of **2** and **3**.

	2	**3**
Formula	$C_3H_4N_4O_8$	$C_3H_3N_5O_{10}$
Formula weight $[\text{g}\,\text{mol}^{-1}]$	224.09	269.08
Temperature [K]	173(2)	243(2)
Crystal size [mm]	$0.28 \times 0.10 \times 0.05$	$0.25 \times 0.02 \times 0.02$
Crystal system	monoclinic	monoclinic
Crystal description	colorless needle	colorless needle
Space group	$P2_1/c$	$P2_1/c$
a [Å]	12.838(1)	10.784(2)
b [Å]	6.572(1)	11.527(2)
c [Å]	9.869(1)	8.752(2)
α [°]	90.0	90.0
β [°]	103.57(1)	108.20(2)
γ [°]	90.0	90.0
V [Å^3]	809.34(1)	1033.5(7)
Z	4	4
$\rho_{\text{calcd.}}$ $[\text{g}\,\text{cm}^{-3}]$	1.839(3)	1.730(2)
μ $[\text{mm}^{-1}]$	0.186	0.178
$F(000)$	456	544
θ range [°]	4.29–25.99	4.30–26.00
Index ranges	$-7 \leq h \leq 15$	$-13 \leq h \leq 13$
	$-8 \leq k \leq 7$	$-13 \leq k \leq 14$
	$-12 \leq l \leq 12$	$-7 \leq l \leq 10$
Reflections collected	3596	5001
Reflections observed	1572	1945
Reflections unique	1082	681
R_{int}	0.0234	0.0526
$R1$, $wR2$ (2σ data)	0.0292, 0.0574	0.0612, 0.1277
$R1$, $wR2$ (all data)	0.0485, 0.0610	0.1759, 0.1633
GOOF on F^2	0.883	0.806
Residual electron density $[\text{e}\,\text{Å}^{-3}]$	$-0.165/0.188$	$-0.198/0.362$

nitramine moiety is 1.373 Å, which indicates a substantial of a double bond character, achieved by delocalization of the nitrogen lone pair. This is also evidenced by a shortened N−H bond (0.82 Å) compared with the carbamate structure of **2**. The carbonyl group, *cis* orientated to the nitro group, shows also a slight shortening (1.182 Å). The trinitroethyl moiety has the same propeller-like configuration compared to **2**, which is stabilized with short strong attractive interactions of N···O atoms (N3···O7, N4···O9, N5···O6). The nitrocarbamate **3** shows two classical hydrogen bonds, which links the hydrogen attached to N1 to two oxygen atoms (O1^i, O4^i), of symmetry related nitrocarbamate
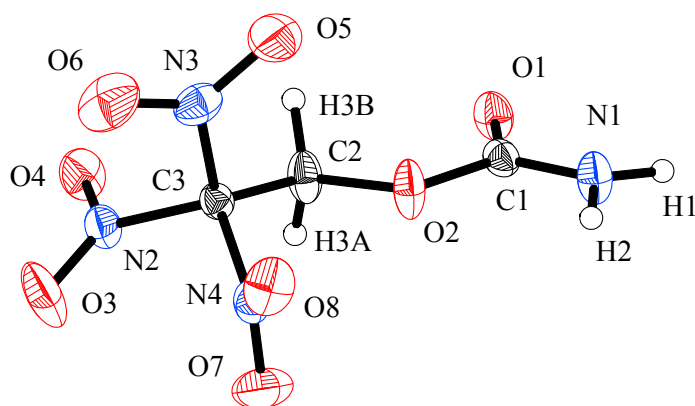
Figure 2.: Molecular structure of 2,2,2-trinitroethyl carbamate (**2**), with thermal ellipsoids at the 50 % probability level. Bond lengths [Å] and angles [°]: O1−C1 1.210(2), O3−N2 1.212(2), O7−N4 1.206(2), O2−C2 1.425(2), O2−C1 1.362(2), O6−N3 1.207(2), O8−N4 1.211(2), N2−O4 1.206(2), N2−C3 1.519(2), C2−C3 1.509(2), N4−C3 1.521(2), N3−O5 1.212(2), N3−C3 1.528(2), N1−C1 1.333(2), N1−H1 0.91(2), N1−H2 0.87(2), C1−O2−C2 114.8(1), C2−C3−N2 111.8(1), N2−C3−N4 108.0(1), C2−C3−N3 113.8(1), N2−C3−N3 106.4(1), C1−N1−H1 118.1(11), C1−N1−H2 119.2(12), H1−N1−H2 119.1(16), O1−C1−N1 127.8(2), O1−C1−O2 122.1(1), N1−C1−O2 110.1(1), N1−C1−O2−C2 176.8(1), O1−C1−O2−C2 −4.7(2), C1−O2−C2−C3 −172.4(1), H1−N1−C1−O1 −170.1(14), H2−N1−C1−O1 169.5(14)

Table 3.: Hydrogen bond lengths [Å] and angles [°] of **2**.

$D-\mathrm{H}\cdots A$	$D-\mathrm{H}$	$\mathrm{H}\cdots A$	$D\cdots A$	$D-\mathrm{H}\cdots A$
N1−H1⋯O1^i	0.91	2.160	3.012	156.0
N1−H2⋯O5^{ii}	0.87	2.709	3.189	116.3
N1−H2⋯O1^{iii}	0.87	2.310	3.152	163.9
C2−H3A⋯O7^{iv}	0.99 $^{a)}$	2.634	3.379	132.1

$^{a)}$ Normalized C−H length 0.99 Å. Symmetry codes of acceptors molecules: $i = -x, 1-y, -z; ii = -x, -\frac{1}{2}+y, \frac{1}{2}-z;$ $iii = x, 1\frac{1}{2}-y, \frac{1}{2}+z; iv = x, 1\frac{1}{2}-y, -\frac{1}{2}+z.$

functionality. Here, the interaction between the carbonyl (O1) and the NH group is significantly the strongest. Also an improper hydrogen bond with carbon as donor (CH⋯O) can be observed, between the methylene (C2−H2A/B) and neighboring nitro groups (Table 4).[21] This extensive hydrogen-bonding may help to explain the good thermal stability.[22]
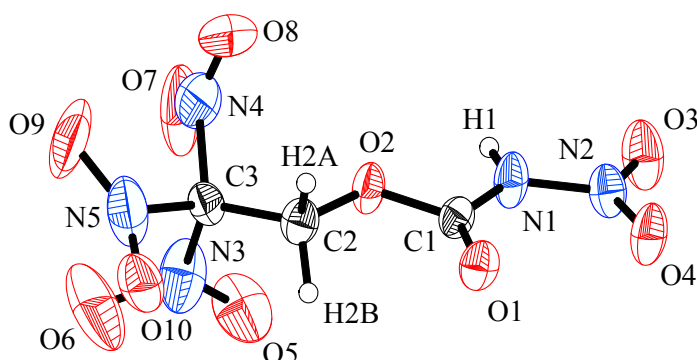
Figure 3.: Molecular structure of 2,2,2-trinitroethyl nitrocarbamate (**3**), with thermal ellipsoids at the 30 % probability level. Bond lengths [Å] and angles [°]: O1−C1 1.182(5), O2−C1 1.333(4), O2−C2 1.437(6), O3−N2 1.201(6), O4−N2 1.213(5), O5−N3 1.15(1), O6−N3 1.31(1), O7−N4 1.40(1), O8−N4 1.16(1), O9−N 5 1.267(7), O10−N5 1.238(8), N1−N2 1.373(5), N1−C1 1.358(6), N1−H1 0.82(5), N3−C3 1.49(1), N4−C3 1.473(8), N5−C3 1.529(8), C2−C3 1.472(6), O3−N2−N1 126.4(4), N1−N2−O4 114.7(4), O4−N2−O3 118.9(4), N2−N1−H1 112(3), H1−N1−C1 123(3), C1−N1−N2 124.6(4), O4−N2−N1−C1 −2.0(6), O4−N2−N1−H1 −177(3), O3−N2−N1−C1 −177.9(4), N2−N1−C1−O2 177.8(4), N2−N1−C1−O1 −1.4(7), N1−C1−O2−C2 −179.8(3), C1−O2−C2−C3 −166.7(3).

Table 4.: Hydrogen bond lengths [Å] and angles [°] of **3**.

D−H$\cdots$A	D−H	H$\cdots$A	$D\cdots$A	D−H$\cdots$A
N1−H1$\cdots$O1^{i}	0.82	2.015	2.797	159.8
N1−H1$\cdots$O4^{i}	0.82	2.634	3.117	119.3
C2−H2B$\cdots$O3^{ii}	0.99 $^{a)}$	2.711	3.635	154.1
C2−H2B$\cdots$O4^{ii}	0.99 $^{a)}$	2.516	3.424	157.2
C2−H2A$\cdots$O10^{iii}	0.99 $^{a)}$	2.607	3.448	143.9

$^{a)}$ Normalized C−H length 0.99 Å. Symmetry codes of acceptors molecules: $i = x, \frac{1}{2}-y, -\frac{1}{2}+z; ii = 1-x, -\frac{1}{2}+y, 1\frac{1}{2}-z; iii = -x, -y, 1-z$.

Vibrational Spectroscopy

The vibrational analysis of **1**–**3** showed the characteristic asymmetric NO$_2$ stretching vibrations in the range of 1615 to 1588 cm^{-1} and the symmetric stretching vibrations at 1304 to 1271 cm^{-1} (Table 5). All vibrations of the nitro groups for **1**–**3** are in a close

range, explained by the similarity of the functional groups. The carbonyl stretching vibration was observed in the typical range between 1785 and 1721 cm^{-1}. The N$-$H stretching vibrations for **2** and **3** were found in the range of 3447–3062 cm^{-1}.

Table 5.: Characteristic IR and Raman vibrations [cm^{-1}] of **1**–**3**. [a]

| | **1** | | **2** | | **3** | |
	Raman	IR	Raman	IR	Raman	IR
νNH			3300 (4)	3447 w	3170 (9)	3168 w
				3352 m		3062 w
				3302 w		
νCO	1785 (14)	1777 m	1721 (17)	1729 m	1768 (49)	1772 m
ν_{as}NO$_2$	1615 (26)	1598 s	1622 (31)	1590 s	1609 (46)	1588 s
ν_sNO$_2$	1301 (32)	1293 m	1304 (31)	1300 m	1303 (55)	1271 w

[a] Raman intensities in brackets. IR intensities: s = strong, m = medium, w = weak.

Thermal Stabilities and Energetic Properties

2,2,2-Trinitroethyl carbamate (**2**) melts at 91 °C (onset) and is thermally stable up to 169 °C (onset) (Table 6). It burns residue-free with a smokeless flame due to a balanced amount of oxygen and shows no sensitivity towards impact, but it is very sensitive to friction. By a low temperature DSC measurement of 2,2,2-trinitroethyl nitrocarbamate (**3**) an endothermic solid phase transformation can be observed at -62 °C (onset). Upon further heating, the compound showed a melting point at 109 °C (onset) and decomposition starts at 153 °C (onset). The sensitivities of **3** are in the range of RDX, and therefore it is sensitive to friction, impact, and electrostatic discharge.

For the calculation of the performance parameters using the EXPLO5 program,[31] the cell parameters of **2** and **3** were determined at 25 °C in order to obtain the density of the substances at standard conditions (Table 7). The performance data of **2** and **3** are summarized in Table 8.

$$I_s = \frac{1}{g} \sqrt{\frac{2\,\gamma\,R\,T_c}{(\gamma - 1)\,M}} \tag{2}$$

$$\gamma = \frac{C_p}{C_v}$$

Table 6.: Physical and chemical properties of **2** and **3**.

	2	**3**
Formula	$C_3H_4N_4O_8$	$C_3H_3N_5O_{10}$
Formula weight $[\mathrm{g\,mol^{-1}}]$	224.09	269.08
T_m [°C] (onset) [a)]	91	109
T_dec [°C] (onset) [b)]	169	153
N [%] [c)]	25.00	26.03
$N+O$ [%] [d)]	82.12	85.49
Ω_CO [%] [e)]	+21.4	+32.7
$\Omega_\mathrm{CO_2}$ [%] [f)]	+0.0	+14.9
$\rho\,[\mathrm{g\,cm^{-3}}]$ [g)]	1.84 (173 K)	1.73 (243 K)
$\Delta U_\mathrm{f}^\circ\,[\mathrm{kJ\,mol^{-1}}]$ [h)]	−459	−366
$\Delta H_\mathrm{f}^\circ\,[\mathrm{kJ\,kg^{-1}}]$ [i)]	−1960	−1278

[a)] Melting (T_m) and [b)] Decomposition (T_dec) point from DSC measurement carried out at a heating rate of $5\,\mathrm{K\,min^{-1}}$. [c)] Nitrogen content. [d)] Combined nitrogen and oxygen content. [e)] Oxygen balance assuming the formation of CO. [f)] Oxygen balance assuming the formation of CO_2. [g)] Calculated density from X-ray measurement. [h)] Energy of formation and [i)] Heat of formation calculated with the CBS-4M method.

Table 7.: Cell parameters of **2** and **3** at 25 °C.

	2	**3**
Temperature [K]	298(1)	298(1)
Crystal system	monoclinic	monoclinic
Space group	$P2_1/c$	$P2_1/c$
a [Å]	12.91(4)	10.79(4)
b [Å]	6.59(2)	11.540(3)
c [Å]	9.88(4)	8.76(4)
α [°]	90.0	90.0
β [°]	103.5(3)	108.2(4)
γ [°]	90.0	90.0
V [Å³]	817(3)	1037(4)
Z	4	4
$\rho_\mathrm{calcd.}\,[\mathrm{g\,cm^{-3}}]$	1.821	1.722

Table 8.: Predicted detonation, combustion parameters (using EXPLO5 V5.05) and sensitivity data for **2** and **3**.

	2	**3**
Q_v [kJ kg^{-1}] [a)]	-5261	-4420
T_{ex} [K] [b)]	4081	3832
V_0 [L kg^{-1}] [c)]	696	687
P_{CJ} [kbar] [d)]	309	242
V_{Det} [m s^{-1}] [e)]	8224	7541
IS [J] [f)]	> 40	10
FS [N] [g)]	64	96
ESD [J] [h)]	0.15	0.10
Grain size [µm] [i)]	< 500	500–1000

[a)] Heat of combustion. [b)] Temperature of the combustion gases. [c)] Volume of the explosion gases. [d)] Detonation pressure. [e)] Detonation velocity. [f)] Impact and [g)] Friction sensitivities. [h)] Sensitivity towards electrostatic discharge. [i)] Grain size of the samples used for sensitivity tests.

The determining parameter for high energy dense oxidizers (HEDO) is the specific impulse I_s. It is used to evaluate the performance of solid rocket propellants and the used high energy dense oxidizers. An expression for I_s is given in Equation 2, were γ is the ratio of specific heats for the combustion gases, R the ideal gas constant, T_c the burning temperature in the combustion chamber and M the molecular weight of the gaseous combustions products at the nozzle. [1] I_s is therefore dependent on the burning temperature proportional and the molecular weight of the combustions products reciprocal. The heat of combustion can be increased by adding a high performing fuel, which has an increased heat of combustion ΔH_c.

$$1\frac{1}{2}\, O_{2\,(g)} + 2\, Al_{(s)} \longrightarrow Al_2O_{3\,(s)} \quad | \; \Delta H_c = -1590\, \text{kJ mol}^{-1} \tag{3}$$

$$3\, CO_{2\,(g)} + 2\, Al_{(s)} \longrightarrow 3\, CO_{(g)} + Al_2O_{3\,(s)} \quad | \; \Delta H_c = -741\, \text{kJ mol}^{-1} \tag{4}$$

$$3\, H_2O_{(g)} + 2\, Al_{(s)} \longrightarrow 3\, H_{2\,(g)} + Al_2O_{3\,(s)} \quad | \; \Delta H_c = -866\, \text{kJ mol}^{-1} \tag{5}$$

$$3\, CO_{(g)} + 2\, Al_{(s)} \longrightarrow 3\, C_{(s)} + Al_2O_{3\,(s)} \quad | \; \Delta H_c = -1251\, \text{kJ mol}^{-1} \tag{6}$$
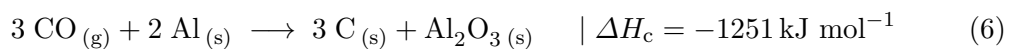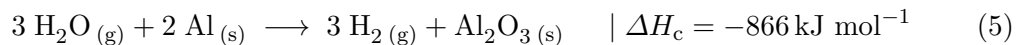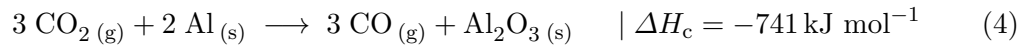
Aluminum has a very high heat of combustion ΔH_c and the combustion products (Al_2O_3) are not harmful to the environment. The oxidation of aluminum with oxygen is highly exothermic and produces a lot of heat [Equation 3][23], which increases T_c. In the case of an oxygen deficit, the aluminum reacts further with the gaseous products water and carbon dioxide, to form hydrogen and carbon monoxide. Also, these two reactions in an oxygen-deficient composition produce a great amount of heat [Equation 4 and Equation 5][23] and no change in the volume of produced gas. However, there is a limit to the amount of aluminum that can be added, because aluminum can also react with carbon monoxide to form carbon and alumina. This reaction also causes an increase of heat but the gas volume decreases radically from 3 to 0 mol for this reaction [Equation 6][23]. An increase of the value for I_s by 20 s leads empirically to a doubling of the usual payload.[1] Therefore, the development of new energetic oxidizers based on CHNO compounds decomposing into small aerialy molecules is a promising way to increase the specific impulse of solid rocket boosters.

The specific impulse of **2** in a mixture of 20 % of aluminum as fuel is 249 s. The specific impulse of **3** achieved with an admixture of 25 % aluminum, is a specific impulse of 247 s and is therefore in the range of the standard mixture of ammonium perchlorate (Table 9).

3.4. Conclusions

The facile synthesis route of choice for 2,2,2-trinitroethyl chloroformate (**1**) is a direct chloroformulation of 2,2,2-trinitroethanol with phosgene. This route has compared to the known route several advantages. The reaction with aqueous ammonia gives 2,2,2-trinitroethyl carbamate (**2**) and nitration furnishes 2,2,2-trinitroethyl nitrocarbamate (**3**). By a low temperature DSC measurement an endothermic solid phase transformation of **3** was observed at $-62\,°C$. On further heating melting occurs at $109\,°C$ and decomposing at $153\,°C$. The nitrocarbamate **3** has a very positive high oxygen balance $\Omega(CO_2)$ of 14.9 %. Thus, the molecule consists of 59.5 % of oxygen and 26.0 % of nitrogen. These examples demonstrate that the 2,2,2-trinitroethylformate group is a very promising energetic moiety, which combines very high oxygen content and relative high stability. The specific impulse I_s of compositions with **3** is comparable with compositions using ammonium perchlorate as oxidizer. Advantageously, the burning of **3** with aluminum produces no toxic substances such as hydrogen chloride.

3.5. Experimental Section

General Procedures. Raman spectra were recorded with a Bruker Multi-RAM Raman Sample Compartment D418 equipped with a Nd-YAG-Laser (1064 nm) and a Ge diode

Table 9.: Predicted specific impulse I_s [s] of mixtures with aluminum (using EXPLO5 V5.05) for **2** and **3**.

	2	**3**	AP
I_s [a]	234	223	153
I_s (30 % Al) [b]	–[d]	244	243
I_s (25 % Al) [b]	249	247	242
I_s (20 % Al) [b]	249	247	232
I_s (15 % Al) [b]	248	247	234
I_s (10 % Al) [b]	245	239	181
I_s (5 % Al) [b]	240	233	178
I_s (15 % Al, 14 % binder) [c]	–[d]	257	257
I_s (10 % Al, 14 % binder) [c]	–[d]	251	253
I_s (5 % Al, 14 % binder) [c]	–[d]	244	247

[a] Specific impulse. [b] Specific impulse for mixtures with the compound **2**, **3** and ammonium perchlorate (AP) as oxidizer with different amounts of aluminum. [c] Specific impulse for mixtures with different amounts of aluminum and binder (6 % polybutadiene acrylic acid, 6 % polybutadiene acrylonitrile and 2 % bisphenol-A ether) at 70.0 bar chamber pressure and isobaric combustion condition (1 bar). [d] Too low oxygen balance of the composition to calculate.

detector. Infrared spectra were measured with a Perkin-Elmer Spectrum BX-FTIR spectrometer equipped with a Smiths DuraSampl*IR* II ATR device. All spectra were recorded at ambient temperature. NMR spectra were recorded with a JEOL Eclipse 400 instrument and chemical shifts were determined with respect to external Me_4Si (^1H, 399.8 MHz; ^{13}C, 100.5 MHz) and $MeNO_2$ (^{14}N, 28.9 MHz). Mass spectrometric data were obtained with a JEOL MStation JMS 700 spectrometer (DCI+, DEI+). Elemental analyses of C/H/N were performed with an Elemental vario EL Analyzer. Melting points were measured with a a Linseis DSC-PT10 instrument, using a heating rate of $5\,°C\,min^{-1}$ and checked by a Büchi Melting Point B-540 apparatus and are not corrected. The sensitivity data (impact, friction, and electrostatic discharge) were performed with a drophammer, friction tester, and electrostatic discharge device conform to the directive of the Federal Institute for Materials Research and Testing (BAM). [2]

Computational Details. All ab initio calculations were carried out using the program package Gaussian 03 (Revision B.03) [24] and visualized by GaussView 5.0.8. [25] Structure optimizations and frequency analyses were performed with Becke's B3 three parameter hybrid functional using the LYP correlation functional (B3LYP). For C, H, N

and O a correlation consistent polarized double-zeta basis set was used (cc-pVDZ). The structures were optimized without symmetry constraints and the energy is corrected with the zero point vibrational energy.[26,27]

The enthalpies (H) and free energies (G) were calculated using the complete basis set (CBS) method in order to obtain accurate values.[26] The CBS models use the known asymptotic convergence of pair natural orbital expressions to extrapolate from calculations using a finite basis set to the estimated complete basis set limit. CBS-4 starts with a HF/3-21G(d) geometry optimization, which is the initial guess for the following SCF calculation as a base energy and a final MP2/6-31+G calculation with a CBS extrapolation to correct the energy in second order. The used reparametrized CBS-4M method additionally implements a MP4(SDQ)/6-31+(d,p) calculation to approximate higher order contributions and also includes some additional empirical corrections.[28] The enthalpies of the gas-phase species were estimated according to the atomization energy method.[29,30]

All calculations affecting the detonation parameters were carried out using the program package EXPLO5 V5.05.[31] The detonation parameters were calculated at the CJ point with the aid of the steady-state detonation model using a modified Becker-Kistiakowski-Wilson equation of state for modeling the system. The CJ point is found from the Hugoniot curve of the system by its first derivative. The specific impulses were also calculated with the EXPLO5 V5.05 program, assuming an isobaric combustion of a composition of **2** and **3** as oxidizer, aluminum as fuel, 6 % polybutadiene acrylic acid, 6 % polybutadiene acrylonitrile as binder and 2 % bisphenol-A as epoxy curing agent. A chamber pressure of 70.0 bar and an ambient pressure of 1.0 bar with frozen expansion conditions were estimated for the calculations.

X-ray Crystallography. For all compounds, an Oxford Xcalibur3 diffractometer with a CCD area detector was employed for data collection using Mo-K_α radiation ($\lambda = 0.71073$ Å). The structures were solved by direct methods (SIR97)[32,33] and refined by full-matrix least-squares on F^2 (SHELXL).[34] All non-hydrogen atoms were refined anisotropically. The hydrogen atom positions were calculated, except for the N-terminal hydrogens which were located in a difference Fourier map and then refined freely.

Crystallographic data (excluding structure factors) for the structures in this paper have been deposited with the Cambridge Crystallographic Data Centre, CCDC, 12 Union Road, Cambridge CB21EZ, UK. Copies of the data can be obtained free of charge on quoting the depository numbers CCDC-923988 (**2**) and CCDC-923989 (**3**) (Fax: +44-1223-336-033; E-Mail: deposit@ccdc.cam.ac.uk, http://www.ccdc.cam.ac.uk).

CAUTION! All of the described compounds are energetic with sensitivities towards heat, impact, and friction. Although no hazards occurred during preparation and manipulation,

additional proper protective precautions (face shield, leather coat, earthened equipment and shoes, Kevlar® gloves and ear plugs) should be used when performing work with these compounds.

CAUTION! Phosgene is a highly toxic, irritating, and corrosive gas. Inhalation can cause fatal respiratory damage. Phosgene reacts violently and decomposes to toxic compounds on contact with moisture, including chlorine and carbon monoxide.

2,2,2-Trinitroethylchloroformate (1)

In a four-necked, 250 mL round-bottomed flask cooled in a dry-ice/ethanol bath and equipped with a magnetic stirrer, gas inlet, septum, dry-ice/ethanol cooled reflux condenser with gas outlet, and a thermometer, phosgene (14.0 g, 13.9 mmol) was condensed at $-70\,°C$. A solution of 2,2,2-trinitroethanol (5.0 g, 27.6 mmol) in dichloromethane (100 mL) was added, while the temperature was maintained below $-50\,°C$. A solution of triethylamine (2.9 g, 4.0 mL, 29.0 mmol) diluted in dichloromethane (50 mL) was added dropwise within 1 h, still maintaining the temperature below $-50\,°C$. Afterwards, the mixture and the reflux condenser were allowed to warm up and were stirred for 12 h at ambient temperature. The organic solvent was removed and the light yellow residue was extracted with diethyl ether (3×50 mL). The insoluble triethylammonium chloride was filtered off and the combined organic phase was washed with ice-cold water (200 mL) and dried with magnesium sulfate. All volatiles were removed in vacuo and the residue was distilled (oil bath 65 °C, 0.03 mbar) yielding 8.9 g of **1** (86 %) as a colorless liquid.

IR: $\tilde{\nu}$ = 3024 (w), 2974 (w), 2893 (w), 1777 (m), 1598 (s), 1438 (w), 1384 (w), 1347 (w), 1293 (m), 1124 (s), 1088 (s), 979 (w), 853 (w), 826 (w), 796 (s), 778 (m), 721 (w), 676 (m) cm^{-1}. Raman (200 mW): $\tilde{\nu}$ = 3020 (16), 2972 (56), 1785 (14), 1615 (26), 1439 (14), 1384 (25), 1349 (42), 1301 (32), 1170 (6), 1091 (8), 1034 (24), 892 (21), 856 (100), 827 (10), 800 (16), 777 (9), 723 (7), 641 (8), 549 (14), 531 (14), 501 (55), 462 (14), 398 (45), 374 (75), 338 (17), 285 (46), 234 (31) cm^{-1}. ^{1}H NMR ([D$_6$]acetone): δ = 5.51 (s, 2 H, CH$_2$) ppm. ^{13}C{^{1}H} NMR ([D$_6$]acetone): δ = 149.5 (CO$_2$Cl), 121.4 [C(NO$_2$)$_3$], 63.3 (CH$_2$) ppm. ^{14}N NMR ([D$_6$]acetone): δ = -36 [C(NO$_2$)$_3$] ppm. EA (C$_3$H$_2$N$_3$O$_8$Cl, 243.52) calcd.: C 14.80, H 0.83, N 17.26, Cl 14.56 %; found: C 15.01, H 0.73, N 17.01, Cl 14.16 %.

2,2,2-Trinitroethyl carbamate (2)

Into a stirring solution of **1** (0.50 g, 2.1 mmol) in dichloromethane (5 mL), chilled to $-30\,°C$, concentrated ammonia (30 %, 0.5 mL, 8.0 mmol) was added dropwise. The mixture was stirred for 1 h at $-30\,°C$. The precipitate formed was filtered off and recrystallized from hot water, to obtain 0.38 g (83 %) colorless needles of the carbamate **2**.

IR: $\tilde{\nu}$ = 3447 (w), 3352 (w), 3302 (w), 2962 (m), 1729 (m), 1590 (s), 1441 (w), 1399 (m), 1367 (w), 1325 (m), 1300 (m), 1248 (w), 1167 (w), 1138 (w), 1105 (m), 1027 (w), 910 (w), 873 (w), 858 (w), 804 (m), 784 (m), 772 (m), 741 (w), 673 (w), 646 (w), 606 (w), 546 (m), 527 (m) cm^{-1}. Raman: (200 mW): $\tilde{\nu}$ = 3300 (4), 3004 (23), 2964 (51), 2828 (3), 1721 (17), 1622 (31), 1608 (28), 1587 (18), 1445 (17), 1404 (8), 1369 (54), 1304 (31), 1250 (15), 1171 (10), 1145 (10), 1112 (9), 1091 (9), 1027 (17), 910 (19), 878 (10), 859 (100), 802 (14), 786 (12), 745 (10), 674 (10), 647 (12), 549 (18), 524 (9), 426 (55), 397 (46), 377 (72), 305 (53), 265 (17), 212 (30) cm^{-1}. ^{1}H NMR ([D$_6$]acetone): δ = 6.77 (s, 1 H, NH$_2$), 6.49 (s, 1 H, NH$_2$), 5.68 (s, 2 H, CH$_2$) ppm. ^{13}C{^{1}H} NMR ([D$_6$]acetone): δ = 154.5 (CO$_2$N), 125.7 [C(NO$_2$)$_3$], 61.8 (CH$_2$) ppm. ^{14}N NMR ([D$_6$]acetone): δ = −33 [C(NO$_2$)$_3$], −310 (NH$_2$) ppm. MS (DEI+) m/z (%): 225 (15) [(M + H)$^+$], 59 (13) [CHNO$_2{}^+$], 46 (59) [NO$_2{}^+$], 44 (100) [(M − OCH$_2$(NO$_2$)$_3$)$^+$, CONH$_2{}^+$], 43 (31) [CHNO$^+$], 30 (71) [NO$^+$]. EA (C$_3$H$_4$N$_4$O$_8$, 224.09): calcd.: C 16.08, H 1.80, N 25.00 %; found: C 15.89, H 1.78, N 24.50 %. BAM drophammer: > 40 J; friction tester: 64 N; ESD: 0.15 J (grain size < 500 μm).

2,2,2-Trinitroethyl nitrocarbamate (3)

Into concentrated sulfuric acid (1 mL) was dropped red fuming nitric acid (> 99.5 %, 1 mL) at 0 °C. To this chilled nitration mixture, 2,2,2-trinitroethyl carbamate (**2**) (0.25 g, 1.1 mmol) was added in small portions. The solution was stirred for 2 h at 0 °C and for 2 h at ambient temperature. The mixture was poured onto ice-water (200 mL), extracted with ethyl acetate (3 × 50 mL) and the combined organic phase was dried with magnesium sulfate. The solvent was removed under reduced pressure and the crude solid product was recrystallized from carbon tetrachloride to obtain 0.30 g (99 %) colorless needles of **3**.

DSC (5 K min^{-1}): 109 °C (onset mp.), 153 °C (onset dec.). IR: $\tilde{\nu}$ = 3168 (w), 3062 (w), 3013 (w), 2900 (w), 1772 (m), 1588 (s), 1466 (m), 1444 (w), 1390 (w), 1351 (w), 1326 (m), 1398 (s), 1271 (w), 1170 (s), 990 (m), 972 (s), 882 (w), 856 (w), 826 (m), 792 (m), 777 (m), 760 (m), 745 (m), 710 (w), 668 (w) cm^{-1}. Raman: (200 mW): $\tilde{\nu}$ = 3170 (9), 3013 (33), 2966 (48), 2868 (9), 1768 (49), 1609 (46), 1468 (23), 1442 (23), 1393 (32), 1353 (46), 1324 (75), 1303 (55), 1272 (26), 1183 (19), 1095 (16), 1050 (51), 998 (62), 883 (21), 859 (100), 794 (17), 781 (18), 761 (19), 657 (18), 542 (25), 461 (58), 377 (72), 407 (85), 376 (92), 271 (69) cm^{-1}. ^{1}H NMR ([D$_6$]acetone): δ = 10.70 (s, 1 H, NH), 5.53 (s, 2 H, CH$_2$) ppm. ^{13}C{^{1}H} NMR ([D$_6$]acetone): δ = 145.2 (CO$_2$N), 122.2 (C(NO$_2$)$_3$), 62.1 (CH$_2$) ppm. ^{14}N NMR ([D$_6$]acetone): δ = −36 (C(NO$_2$)$_3$), −55 (NNO$_2$), −292 (NNO$_2$) ppm. MS (DCI+) m/z (%): 270 (1) [(M + H)$^+$], 225 (2) [(M − NO$_2$)$^+$]. EA (C$_3$H$_3$N$_5$O$_{10}$, 269.08) calcd.: C 13.39, H 1.12, N 26.03 %; found: C 13.54, H 1.09, N 25.70 %. BAM drophammer: 10 J; friction tester: 96 N; ESD: 0.10 J (grain size 500–1000 μm).

3.6. Acknowledgements

3.7. References

[1] T. M. Klapötke, *Chemistry of High-Energy Materials*, 2nd ed., de Gruyter, Berlin, **2012**.

[2] M. Göbel, T. M. Klapötke, *Adv. Funct. Mater.* **2009**, *19*, 347–365.

[3] M. Göbel, T. M. Klapötke, *Z. Anorg. Allg. Chem.* **2007**, *633*, 1006–1017.

[4] C. Hogue, *Chem. Eng. News* **2011**, *89*, 6.

[5] T. M. Klapötke, B. Krumm, R. Moll, S. F. Rest, *Z. Anorg. Allg. Chem.* **2011**, *637*, 2103–2110.

[6] T. M. Klapötke, B. Krumm, R. Moll, *Chem. Eur. J.* **2013**, *19*, 12113–12123.

[7] H. Feuer, T. Kucera, *J. Org. Chem.* **1960**, *25*, 206–2070.

[8] M. Göbel, T. M. Klapötke, *Acta Crystallogr., Sect. C* **2007**, *63*, o562–o564.

[9] S. V. Lieberman, E. C. Wagner, *J. Org. Chem.* **1949**, *14*, 1001–1012.

[10] W. H. Gilligan, S. L. Stafford, *Synthesis* **1979**, 600–602.

[11] L. Cotarca, H. Eckert, in *Phosgenations – A Handbook*, Wiley-VCH, Weinheim, **2005**.

[12] O. A. Luk'yanov, G. V. Pokhvisneva, *Russ. Chem. Bull.* **1992**, *41*, 1286–1288.

[13] M. Oki, *Applications of Dynamic NMR Spectroscopy to Organic Chemistry*, VCH Publishers, Deerfield Beach, FL, **1985**.

[14] T. M. Klapötke, B. Krumm, P. Mayer, K. Polborn, O. P. Ruscitti, *Inorg. Chem.* **2001**, *40*, 5169–5176.

[15] K. B. Wiberg, P. R. Rablen, *J. Am. Chem. Soc.* **1995**, *117*, 2201–2209.

[16] D. S. Raiford, C. L. Fisk, E. D. Becker, *Anal. Chem.* **1979**, *51*, 2050–2051.

[17] A. F. Holleman, E. Wiberg, N. Wiberg, *Lehrbuch der Anorganischen Chemie*, 102nd ed., de Gruyter, Berlin, **2008**.

[18] A. Bondi, *J. Phys. Chem.* **1964**, *68*, 441–451.

[19] B. Sepehrnia, J. R. Ruble, G. A. Jeffrey, *Acta Crystallogr., Sect. C* **1987**, *43*, 249–251.

[20] T. Steiner, *Angew. Chem.* **2002**, *114*, 50–80.

[21] Y. Gu, T. Kar, S. Scheiner, *J. Am. Chem. Soc.* **1999**, *121*, 9411–9422.

[22] R. Butcher, R. Gilardi, C. George, J. Flippen-Anderson, *J. Chem. Crystallogr.* **1996**, *26*, 381–388.

[23] J. Akhavan, *The Chemistry of Explosives*, 2nd ed., The Royal Society of Chemistry, Cambridge, **2004**.

[24] M. J. Frisch, G. W. Trucks, H. B. Schlegel, G. E. Scuseria, M. A. Rob, J. R. Cheeseman, J. A. Montgomery Jr., T. Vreven, K. N. Kudin, J. C. Burant, J. M. Millam, S. S. Iyengar, J. Tomasi, V. Barone, B. Mennucci, M. Cossi, G. Scalmani, N. Rega, G. A. Petersson, H. Nakatsuji, M. Hada, M. Ehara, K. Toyota, R. Fukuda, J. Hasegawa, M. Ishida, T. Nakajima, Y. Honda, O. Kitao, H. Nakai, M. Klene, X. Li, J. E. Knox, H. P. Hratchian, J. B. Cross, V. Bakken, C. Adamo, J. Jaramillo, R. Gomperts, R. E. Stratmann, O. Yazyev, A. J. Austin, R. Cammi, C. Pomelli, J. W. Ochterski, P. Y. Ayala, K. Morokuma, G. A. Voth, P. Salvador, J. J. Dannenberg, V. G. Zakrzewski, S. Dapprich, A. D. Daniels, M. C. Strain, O. Farkas, D. K. Malick, A. D. Rabuck, K. Raghavachari, J. B. Foresman, J. V. Ortiz, Q. Cui, A. G. Baboul, S. Clifford, J. Cioslowski, B. B. Stefanov, G. Liu, A. Liashenko, P. Piskorz, I. Komaromi, R. L. Martin, D. J. Fox, T. Keith, M. A. Al-Laham, C. Y. Peng, A. Nanayakkara, M. Challacombe, P. M. W. Gill, B. Johnson, W. Chen, M. W. Wong, C. Gonzalez, J. A. Pople, *Gaussian 03*, Rev. B.03, Gaussian, Inc., Wallingford CT (USA), **2003**.

[25] R. D. Dennington II, T. A. Keith, J. M. Millam, *GaussView*, Version 5.0.8, Semichem Inc., Shawnee Mission, KS, USA, **2009**.

[26] T. M. Klapötke, J. Stierstorfer, *Phys. Chem. Chem. Phys.* **2008**, *10*, 4340–4346.

[27] J. A. Montgomery Jr., M. J. Frisch, J. W. Ochterski, G. A. Petersson, *J. Chem. Phys.* **2000**, *112*, 6532–6542.

[28] J. W. Ochterski, G. A. Petersson, J. A. Montgomery Jr., *J. Chem. Phys.* **1996**, *104*, 2598–2619.

[29] E. F. C. Byrd, B. M. Rice, *J. Phys. Chem. B* **2005**, *110*, 1005–1013.

[30] L. A. Curtiss, K. Raghavachari, P. C. Redfern, J. A. Pople, *J. Chem. Phys.* **1997**, *106*, 1063–1079.

[31] M. Sućeska, *EXPLO5* V5.05, Brodarski Institut, Zagreb (Croatia), **2011**.

[32] A. Altomare, M. C. Burla, M. Camalli, G. L. Cascarano, C. Giacovazzo, A. Guagliardi, A. G. G. Moliterni, G. Polidori, R. Spagna, *J. Appl. Crystallogr.* **1999**, *32*, 115–119.

[33] A. Altomare, G. Cascarano, C. Giacovazzo, A. Guagliardi, A. G. G. Moliterni, M. C. Burla, G. Polidori, M. Camalli, R. Spagna, *SIR97*, **1997**.

[34] G. M. Sheldrick, *SHELX-97*, University of Göttingen, Göttingen (Germany), **1997**.

4. Polynitroethyl Substituted Boron Esters
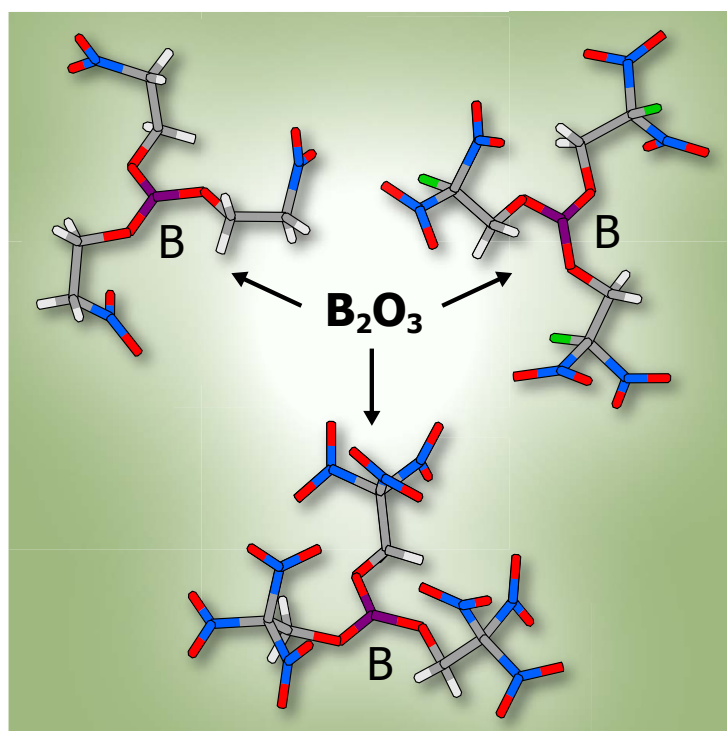
Green burning boron: Various nitroethyl boron esters were prepared and structurally characterized. In addition, the precursor fluorodinitroethanol and the product of a condensation of dinitroethanol to an unusual dianion were also investigated. The boron esters are of interest as potential candidates for smoke-free, green colorants in pyrotechnic applications, and in case of the polynitrated esters, also as promising high-energy oxidizers.

Polynitroethyl- and Fluorodinitroethyl Substituted Boron Esters

Thomas M. Klapötke,*[a] Burkhard Krumm,[a] and Richard Moll[a]

*   Prof. Dr. Thomas M. Klapötke

     E-Mail: tmk@cup.uni-muenchen.de

[a]   Department of Chemistry

     Ludwig-Maximilian University of Munich

     Butenandtstrasse 5–13 (D)

     81377 Munich, Germany

4.1. Abstract

The reaction of boron oxide with various nitro-substituted ethanols (2-nitroethanol, 2-fluoro-2,2-dinitroethanol, 2,2,2-trinitroethanol) furnished the corresponding nitroethyl borates $B(OCH_2CH_2NO_2)_3$ (**1**), $B(OCH_2CF(NO_2)_2)_3$ (**2**), and $B(OCH_2C(NO_2)_3)_3$ (**3**). Fluorination of the anion $[(NO_2)_2CCH_2OH]^-$ (**4**) resulted in 2-fluoro-2,2-dinitroethanol (**5**), a precursor for **2**, and was thoroughly characterized. An interesting condensation was observed with the anion **4** to form the unusual dianion $[(NO_2)_2CCH_2C(NO_2)_2]_2^-$ (**6**). All compounds were fully characterized by multinuclear NMR spectroscopy, vibrational spectroscopy (IR, Raman), mass spectrometry and elemental analysis. The chemical, physical and energetic properties of **1**–**3** and **5** are reported, as well as quantum chemical calculations at the CBS-4M level to predict the enthalpies and energies of formation. X-ray diffraction studies were performed, and the crystal structures for compounds **1**–**6** were determined and discussed thoroughly. The boron esters **1**–**3** are of interest as possible candidates for smoke-free, green colorants in pyrotechnic applications, and in case of **2** and **3** also as promising high energy oxidizers.

4.2. Introduction

Highly nitrated energetic materials based on a carbon backbone are widely known for their potential use as explosives and oxidizers. Especially compounds containing (poly-)nitro methyl and ethyl moieties are promising materials in this class of compounds, and are of general interest in our laboratory.[1,2] In the course of our investigations, we recently focused our attention on boron containing compounds. The interest in boron-based homogeneous explosives or oxidizers for pyrotechnic applications derive from the low atomic weight of boron with a high molar enthalpy of formation and high affinity for both nitrogen and oxygen.[3,4] Furthermore, the application of boron-containing energetic materials to propellant formulations may decrease the effect of the water-gas equilibrium on the specific impulse of propellants caused by competing formation of CO and CO_2.[3,4] Tris(2-nitroethyl) borate (**1**) and tris(2-fluoro-2,2-dinitroethyl) borate (**2**) have been briefly mentioned prior to this study.[5–7] Both boron esters were neither properly described nor sufficiently characterized, in this context only elemental analysis and for **2** some simple NMR results are reported.[5–7] Tris(2,2,2-trinitroethyl) borate (**3**) has, to the best of our knowledge, not been reported in literature, prior to our initial results.[8–10] Aside from the above mentioned literature and a cursory description of the 2,2-dinitropropyl substituted boron ester,[11] no further (poly-)nitroalkyl substituted boron esters are known in the literature. Consequently, herein we present the first thorough investigation of highly energetic boron esters of this under investigated class of compounds.

Various reactions to forming the important starting material, potassium 2-hydroxy-1,1-dinitroethan-1-ide, $K[(NO_2)_2CCH_2OH]$ (**4**), referred to in older literature as potassium 2,2-dinitroethanol, are known.[12–16] 2-Fluoro-2,2-dinitroethanol (**5**) has been prepared prior to our work by fluorination of **4** with elemental fluorine,[17–22] and fluorinations by other less common fluorinating reagents are also reported.[20,23,24] Alternate methods for the synthesis of **5** consist of the reaction of fluorotrinitromethane or (chloro)fluorodinitromethane with formaldehyde in the presence of a reducing agent.[20,25–29] Although some NMR and IR spectroscopic data as well as elemental analyses have been previously reported,[19–21,30,31] full characterization of these materials has yet to be performed. During the preparation of **4**,[12–16] the unusual dianion $[(NO_2)_2CCH_2C(NO_2)_2]_2^-$ (**6**) was detected and isolated as an unexpected by-product.[15,32–40] Our general interest in polynitro compounds prompted us, to re-examine the compounds **4**–**6** by modern analytical methods.

Herein, a detailed study of the synthesis, characterization and energetic properties of tris(2-nitroethyl) borate (**1**), tris(2-fluoro-2,2-dinitroethyl) borate (**2**), and tris(2,2,2-trinitroethyl) borate (**3**) is presented. Furthermore, the fluorination of 2-hydroxy-1,1-dinitroethan-1-ide (**4**) to 2-fluoro-2,2-dinitroethanol (**5**) and the side reaction leading to 1,1,3,3-tetranitropropan-1,3-diide (**6**) are investigated in detail.

4.3. Results and Discussion

Synthesis

The general procedure for the preparation of boron esters involves the reaction of boric acid with the appropriate alcohol.[41] For a high conversion rate the water formed during the reaction should be removed. The syntheses of the boron esters **1**–**3** are conveniently performed with boron oxide, instead of boric acid. An excess of boron oxide is used, which consumes the water in the reaction forming boric acid, which may also react to form the desired boron ester (Scheme 1).
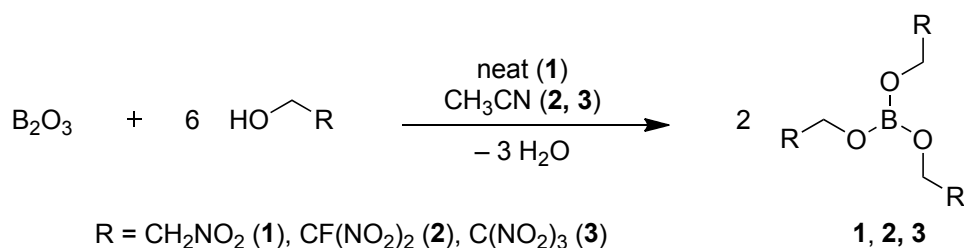
Scheme 1: Synthesis of the nitroethyl borates **1**–**3**.

The preparation of **1**–**3** is performed by slight warming of the reaction mixture for seven hours. In the case of **1**, the highest temperature (60 °C) is required to obtain the product, whereas for **3** room temperature is sufficient for good yields, with reaction times of more than 24 h. Purification of the crude reaction products by re-crystallization furnish pure and crystalline boron esters **1**–**3**. Boron compounds **1**–**3** are moisture sensitive and hydrolyze slowly when exposed to moist air. Nevertheless, they are stable during the preparation, even with the presence of the water formed as a by-product as shown in Scheme 1. Reactions of boron oxide with in situ generated 2,2-dinitroethanol under similar reaction conditions did not result in the corresponding boron ester, due to the instability of 2,2-dinitroethanol at even ambient temperature.[13] Further chemistry of the boron esters **1**–**3** is rather limited, for example, attempts to synthesize tetra-coordinated borates of the type $[B(OCH_2R)_4]^-$ with R = CH_2NO_2, $CF(NO_2)_2$ and $C(NO_2)_3$ failed, probably due to the increased steric requirements of nitro groups, which effectively shield the Lewis-acidic boron center. Treatment with fluoride, azide or trinitroethoxide led either to decomposition of **1**–**3** or failed to react.

The precursor of the boron ester **2**, 2-fluoro-2,2-dinitroethanol (**5**) was prepared by fluorination of the anion $[(NO_2)_2CCH_2OH]^-$ (**4**) with stoichiometric amounts of Selectfluor at ambient temperature. The fluorination of the corresponding salt in aqueous solution is a common method and furnishes **5** as a stable, colorless liquid, which is miscible with water without decomposition (Scheme 2). The use of Selectfluor significantly simplifies experimental efforts compared to the experimental setup required for fluorination with elemental fluorine.
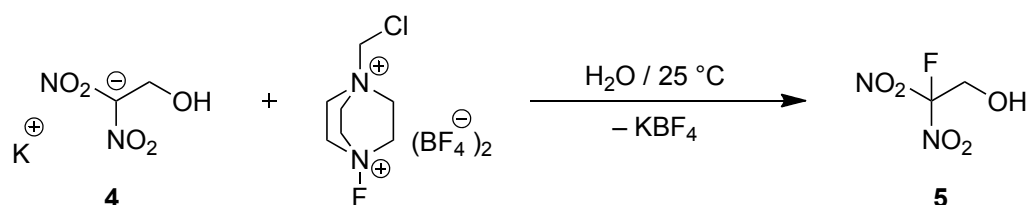
Scheme 2: Synthesis of 2-fluoro-2,2-dinitroethanol (**5**) from 2-hydroxy-1,1-dinitroethane-1-ide (**4**).

The synthesis of **4** from potassium dinitromethanide with formaldehyde[12,14,16] in a mixture of ethanol and water produced small amounts of an interesting by-product, which was identified as the dianion 1,1,3,3-tetranitropropane-1,3-diide $[(NO_2)_2CCH_2C(NO_2)_2]_2^-$ (**6**). The orange-red crystals of **6** were easily distinguishable from the yellow crystals of **4** formed during the crystallization process. This side reaction can be explained by reaction of two molecules of **4** (Scheme 3) under elimination of water, forming the reactive intermediate species 1,1-dinitroethene, and further elimination
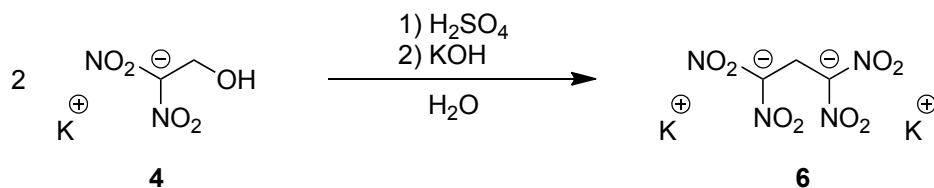
Scheme 3: Formation of 1,1,3,3-tetranitropropane-1,3-diide (**6**) from **4**.

of formaldehyde from the condensation product. The formation of **6** could also be explained by the reaction (condensation) of residual dinitromethanide with **4** followed by elimination of water. However, no direct evidence for the latter pathway is available. Performing both possibilities on lab scale led to the formation of **6**, with or without dinitromethanide. The selective preparation of **6** from **4** is described in literature,[34] whereas reacting **4** with dinitromethanide anion may form **6**, which is always only very briefly mentioned.[35,36,42] Both reaction paths are successfully performed in this work, but it is not possible to precisely distinguish between these two reaction mechanisms.

NMR Spectroscopy

All compounds were thoroughly characterized by multinuclear NMR spectroscopy (Table 1). The low solubility of **2** and **3** in CDCl$_3$ necessitate the use of the more polar CD$_3$OD as a suitable solvent for NMR spectroscopy. In the ^{1}H NMR spectra of **1**–**3** the resonances of the methylenoxy moiety were observed between 4.92–4.04 ppm, and a further resonance at 4.55 ppm was observed for the additional nitromethylene group. For the fluorine containing derivative **2**, the $^3J_{\text{H}-\text{F}}$ coupling was determined to 18.1 Hz. All resonances of the ^{11}B nucleus for **1**–**3** are found at 18.1 ppm in CD$_3$OD, whereas those in CDCl$_3$ are slightly highfield shifted, indicating no influence of the terminal nitro groups on the ^{11}B NMR resonances (Table 1). The ^{13}C NMR spectra of **1**–**3** show resonances for the methylenoxy carbon atoms in the range of 64.0–59.3 ppm. An increasing number of electron-withdrawing groups in the vicinity of a carbon atom leads to a downfield shift. Therefore, the resonance of the trinitromethyl carbon of **3** at 128.3 ppm and that of the fluorodinitromethyl group of **2** at 123.6 ppm is found significantly downfield relative to that of the mononitromethyl carbon of **1** at 78.8 ppm. Both resonances of the carbon atoms in **2** are split into doublets with coupling constants $^1J_{\text{C}-\text{F}}$ of 289.3 Hz for the dinitromethyl and $^2J_{\text{C}-\text{F}}$ of 19.8 Hz for the methyleneoxy carbon atom. The solubility of **1**–**3** in CD$_3$OD is sufficiently high to obtain the ^{15}N NMR spectra. These spectra show the resonances for mononitro (**1**), dinitro (**2**) and trinitro (**3**) moieties in the region of 2.3 to −31.1 ppm (Table 1). For **1** a triplet of triplets with coupling constants $^3J_{\text{N}-\text{H}}$ (4.2 Hz) and $^4J_{\text{N}-\text{H}}$ (1.9 Hz) is observed in the ^{15}N NMR spectrum, whereas the spectrum

of the fluorodinitroethyl derivative, **2**, displays a doublet due to the nitrogen-fluorine coupling with a coupling constant $^2J_{N-F}$ of 15.0 Hz. The corresponding resonance in the ^{19}F NMR spectrum of **2** was found to be similar to the literature value[7] at -114.5 (CD_3OD), respectively -111.8 ppm ($CDCl_3$), as a broadened multiplet due to coupling to ^1H and ^{14}N nuclei. The ^{19}F NMR resonance of the precursor **5** at -111.9 ppm is in agreement with previously reported values,[21] and is similar to that of the boron ester **2** measured $CDCl_3$. Also the carbon atoms in **5** are split into doublets with coupling constants $^1J_{C-F}$ of 290.2 Hz for the dinitromethyl and $^2J_{C-F}$ of 21.3 Hz for the methylenoxy carbon atom. In addition, $^3J_{H-F}$ and $^4J_{H-F}$ couplings are observed in the ^1H NMR spectrum. The ^{15}N nucleus shows coupling to the fluorine ($^2J_{N-F} = 15.0$ Hz) as well as to the hydrogen atom ($^3J_{N-H} = 1.3$ Hz), leading to a doublet of triplets in the ^{15}N NMR spectrum (Figure 1).
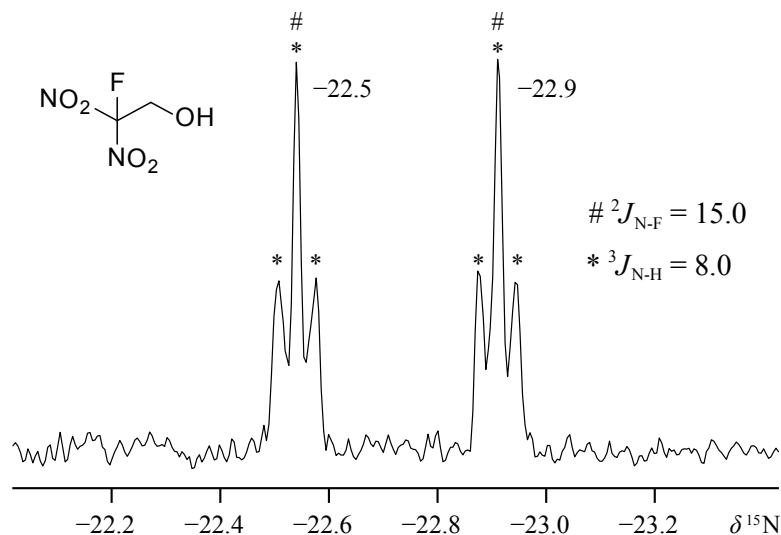
Figure 1.: ^{15}N NMR spectrum of **5** in $CDCl_3$ at 25 °C showing both J_{N-F} and J_{N-H} couplings (δ in ppm, J in Hz).

In the ^1H NMR spectrum of **4**, the resonance of the hydroxy group is found at 4.44 ppm, a resonance for a $HC(NO_2)_2$ group, expected at higher field, is missing. This also supports the concept of a negative charge at the carbon atom of the dinitromethyl moiety in **4**. Furthermore, the successful fluorination of **4** to **5** at the nitrosubstituted carbon also confirms this localization of the negative charge. In older literature, **4** was usually referred to as potassium 2,2-dinitroethanol, which only insufficiently describes the bonding situation. Additional evidence for the structure of **4** is described in the X-ray section.

Table 1.: Multinuclear NMR resonances of **1**–**6** (δ in ppm, J in Hz).

	Solvent	^{1}H	^{11}B	^{13}C	^{14}N/^{15}N	^{19}F
1	CD_3OD	4.55 (CH_2NO_2) 4.04 (OCH_2)	18.1	78.8 (CH_2NO_2) 59.3 (OCH_2)	2.3 (^{15}N) $^2J_{N-H} = 4.2$ $^3J_{N-H} = 1.9$	
	$CDCl_3$	4.47 (CH_2NO_2) 4.25 (OCH_2)	17.1	76.0 (CH_2NO_2) 59.7 (OCH_2)	-0.5 (^{14}N)	
2	CD_3OD	4.63 (OCH_2) $^3J_{H-F} = 18.1$	18.1	123.6 ($C(NO_2)_2F$) $^1J_{C-F} = 289.3$ 62.3 (OCH_2) $^2J_{C-F} = 19.8$	-21.3 (^{15}N) $^2J_{N-F} = 15.0$	-114.5
	$CDCl_3$		17.8		-24 (^{14}N)	-111.8
3	CD_3OD	4.92 (OCH_2)	18.1	128.3 ($C(NO_2)_3$) 64.0 (OCH_2)	-31.1 (^{15}N)	
	$CDCl_3$		17.6		-33 (^{14}N)	
4	$(CD_3)_2SO$	4.70 (OCH_2) 4.44 (HO)		135.9 ($C(NO_2)_2$) 57.0 (OCH_2)	-22 (^{14}N)	
5	$CDCl_3$	4.66 (OCH_2) $^3J_{H-F} = 15.3$ 2.80 (OCH_2) $^4J_{H-F} = 1.6$		120.8 ($C(NO_2)_2F$) $^1J_{C-F} = 290.2$ 61.6 (OCH_2) $^2J_{C-F} = 21.3$	-22.7 (^{15}N) $^2J_{N-F} = 15.0$ $^3J_{N-H} = 1.3$	-111.9
6	$(CD_3)_2SO$	4.57 (CH_2)		131.7 ($C(NO_2)_2$) 29.6 (CH_2)	-24 (^{14}N)	

Vibrational Spectroscopy

The vibrational analysis of **1**–**3** and **5** showed the characteristic asymmetric NO_2 stretching vibration between $\tilde{\nu} = 1599$–$1548\,\mathrm{cm}^{-1}$, in agreement with other nitro group containing compounds.[1,2,43] The symmetric NO_2 stretching vibration is found for these compounds is found in the typical range of $\tilde{\nu} = 1382$–$1297\,\mathrm{cm}^{-1}$. For **1**–**3** the B−O stretching vibration is also observed in this region, making definite assignment difficult.[43,44] It is very likely that the bands observed at $\tilde{\nu} = 1337\,(\mathbf{2})$, $1330\,(\mathbf{3})$ and $1319\,\mathrm{cm}^{-1}\,(\mathbf{1})$ derive from B−O vibrations (which compare well with an authentic IR spectrum of $B(OCH_3)_3$, and therefore the bands at $\tilde{\nu} = 1380/1345\,(\mathbf{1})$, $1310\,(\mathbf{2})$ and $1306/1297\,\mathrm{cm}^{-1}\,(\mathbf{3})$ stem from NO_2 vibrations. The asymmetric NO_2 stretching vibrations in **4** and **6** were found at lower frequencies ($\tilde{\nu} = 1498$–$1470\,\mathrm{cm}^{-1}$) due to

the presence of free electron pairs in the dinitromethyl moieties, best described by mesomeric resonance structures showing partial double-bond character. This increases the C−N bond order as compared to that in **1**–**3**, which is known to lower the asymmetric NO_2 stretching vibration frequency.[39] The frequency of the symmetric NO_2 stretching vibration in **5** and **6** does not differ remarkably from those in **1**–**3**. No confident assignment could be made for the symmetric NO_2 stretching vibration in the IR spectra of **1**–**6**, because of the many bands observed in this region.[39,43] The C−N stretching vibrations of **2**–**6** occur in a narrow range of $\tilde{\nu} = 860$–$845\,\mathrm{cm}^{-1}$, the low-frequency of which is somewhat surprising, but explained by the low C−N bond order,[39,43] as observed crystallographically. The mononitroethyl compound **1** shows this vibration at a slightly higher frequency and with a lower relative Raman intensity than observed for **2**–**6**. The lack of electron-withdrawing groups at the terminal carbon atoms in **1** leads to these slightly different frequencies in the C−N and NO_2 vibrations compared to **2**–**6**.[43]

X-ray Diffraction

Single crystals suitable for X-ray diffraction measurements were obtained by crystallization at $10\,^{\circ}\mathrm{C}$ from tetrachloromethane (**1**) or dichloromethane (**2**, **3**), from neat material (**5**) or from water/methanol (**4**, **6**). A full list of the crystallographic refinement parameters and structure data for **1**–**6** is shown in Table 2. The crystals of **2** are large blocks, but are predominantly crystalline in only one spatial direction, and the crystals of **3** are very thin rods, therefore the X-ray measurements of both compounds were quite challenging. The nitroethyl borates **1**–**3** crystallize in the monoclinic space group $P2_1/c$ (**1**), respectively $P2_1/n$ (**2**, **3**), each with four formula units per unit cell. The molecular structures of **1**–**3** are shown in Figures 2–4.

The boron atoms of **1**–**3** are bound to three oxygen atoms in an undistorted planar array, which is expected from the electronic configuration of boron. The carbon atoms C1, C3 and C5 of **1**–**3**, belonging to the CH_2 groups, are also nearly in a planar arrangement with the BO_3 moieties. The carbon atom C5 of **1** shows the highest deviation $(0.161(2)\,\text{Å})$ from the BO_3 plane. This nearly planar trimethylene borate moiety is also found in the only two comparable, literature known crystal structures of sp²-hybridized (trigonal surrounded) triethyl borates, $B(OC(C_2H_5)_3)_3$[45] and $B(OCH_2C_3H_4CH_2O)_3B$[46]. Although similar alkyl borates often crystallize in the trigonal[45] or hexagonal[46,47] space group, **1**–**3** crystallize in the lower symmetry monoclinic space group and thus do not have a threefold crystallographic axis (C_3 symmetry) through the respective boron atoms. Because none of their ethoxy moieties are equivalent, the rather unsymmetrical monoclinic space group is explained. The B−O bond lengths of **1**–**3** are in the range of $1.340(7)$–$1.374(2)\,\text{Å}$, most of them between a normal B−O single $(1.50\,\text{Å})$[48] and B=O double bond $(1.26\,\text{Å})$[48]. These shortened
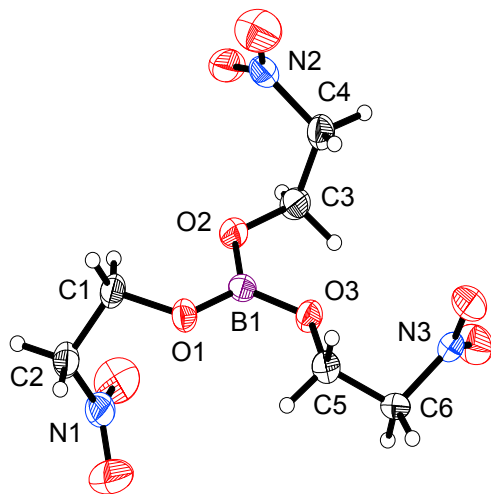
Figure 2.: Molecular structure of **1**. Selected distances [Å] and angles [°]: B1−O1 1.361(2), O1−C1 1.432(2), C1−C2 1.501(2), C2−N1 1.489(2), B1−O2 1.362(2), O2−C3 1.433(2), C3−C4 1.491(2), C4−N2 1.492(2), B1−O3 1.355(2), O3−C5 1.427(2), C5−C6 1.501(2), C6−N3 1.493(2), B1−O1−C1 120.6(2), O1−C1−C2 109.3(2), C1−C2−N1 109.4(2), B1−O2−C3 119.9(2), O2−C3−C4 109.8(2), C3−C4−N2 111.0(2), B1−O3−C5 123.6(2), O3−C5−C6 106.7(2), C5−C6−N3 108.9(2), O1−B1−O2 120.6(2), O2−B1−O3 118.8(2), O3−B1−O1 120.5(2).

bonds are interpreted as the result of π-backbonding to the boron atoms,[46] which is consistent with previous crystal structure results.[45–47,49] The C−N bond lengths of **1** are between 1.489(2) and 1.493(2) Å, only slightly longer than a normal C−N single bond length (1.47 Å)[48,49]. For steric reasons, the C−N bond lengths increase for **2** (1.520(8)–1.552(9) Å) and **3** (1.509(4)–1.530(4) Å) with the introduction of more spatially demanding fluorine atoms or nitro groups. As expected, all nitro groups in **1**–**3** are planar. The N−C−N angles in **2** and **3** are 104.4–108.3° and are therefore smaller than the ideal tetrahedral value of 109.5°[48]. The trinitromethyl moiety in **3** shows an approximate C_3 axis along the C−C bond with the nitro groups adopting a propeller-like conformation (Figure 4). The C−C−N−O dihedral angles, an indicator of the degree of rotation of the nitro groups out of the C C N plane, are in the range of 27.0–55.5°, with the majority clustering towards 49±5°. Similar values are found in other trinitro aliphatic CHNO compounds.[1,2,50–52] The propeller-type twisting of the trinitromethyl moiety optimizes the non-bonding intramolecular N···O interactions (partial charge distribution of the nitrogen (δ^+) and oxygen (δ^-) atom in the nitro groups) between two adjacent nitro groups, as well as minimizing the corresponding O···O repulsion.[1,2,51] These N···O attractions are found for **3** in the range of 2.55–2.61 Å, which is significantly closer than the sum of the van der Waals radii for nitrogen and oxygen (3.07 Å)[53,54]. In contrast, the structure of **2** does not show these attractive intramolecular interactions between
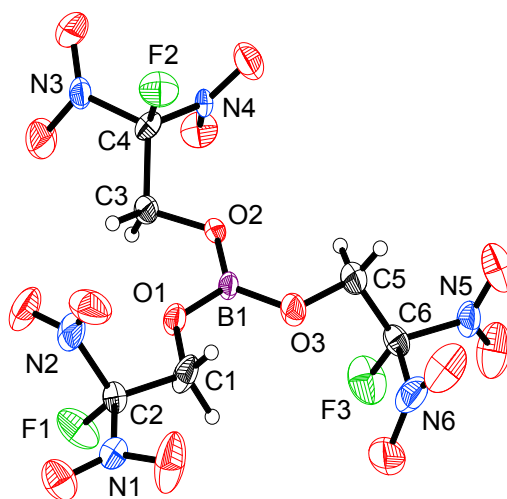
Figure 3.: Molecular structure of **2**. Selected distances [Å] and angles [°]: B1−O1 1.365(8), O1−C1 1.426(7), C1−C2 1.470(8), C2−N1 1.524(7), C2−N2 1.520(8), C2−F1 1.341(6), B1−O2 1.343(7), O2−C3 1.416(6), C3−C4 1.519(8), C4−N3 1.526(7), C4−N4 1.523(7), C4−F2 1.320(6), B1−O3 1.340(7), O3−C5 1.420(7), C5−C6 1.466(9), C6−N5 1.522(8), C6−N6 1.552(9), C6−F3 1.331(6), B1−O1−C1 123.0(4), O1−C1−C2 105.6(5), C1−C2−N1 114.6(5), C1−C2−N2 111.4(5), C1−C2−F1 112.9(5), B1−O2−C3 122.4(4), O2−C3−C4 105.8(4), C3−C4−N3 113.8(5), C3−C4−N4 111.3(4), C3−C4−F2 113.0(5), B1−O3−C5 122.5(5), O3−C5−C6 106.8(5), C5−C6−N5 115.0(5), C5−C6−N6 109.6(5), C5−C6−F3 114.3(5), O1−B1−O2 120.0(5), O2−B1−O3 123.0(5), O3−B1−O1 117.0(5).

the nitro groups. However, the conformation of these groups in **2** is better explained by the intermolecular N···O attractions in the range of 2.96–2.99 Å. The structures of **1** and **3** also show several intermolecular N···O contacts at distances between 2.94–3.07 Å (for **1**) and 2.91–3.03 Å (for **3**) suggesting weak but attractive interactions.

The three 2-nitroethoxy groups in **1** and the three 2-fluoro-2,2-dinitroethoxy groups in **2** point in three different spatial directions, as expected, due to steric interactions (Figure 5). In contrast, the three 2,2,2-trinitroethoxy moieties of **3** point to the same side of the molecule, therefore surprisingly revealing a *cis*-conformation in terms of the trinitromethyl moieties around the boron center. This structural motif seems to be quite uncommon, especially if compared to the structure of **2**. Figure 6 shows the three intramolecular (3.09/3.16/3.31 Å) and two intermolecular (3.28/3.29 Å) B···O contacts in **3**, which provide additional electron density to the normally electron deficient boron atom. These attractive contacts, all considerably shorter than the sum of the van der Waals radii for boron and oxygen (3.52 Å)[53,54], are a possible explanation for the observed conformation. In contrast to another compound with a *cis*-conformation of the trinitromethyl moieties, hexanitrohex-3-yne,[2] in **3** also attractive N···O interactions
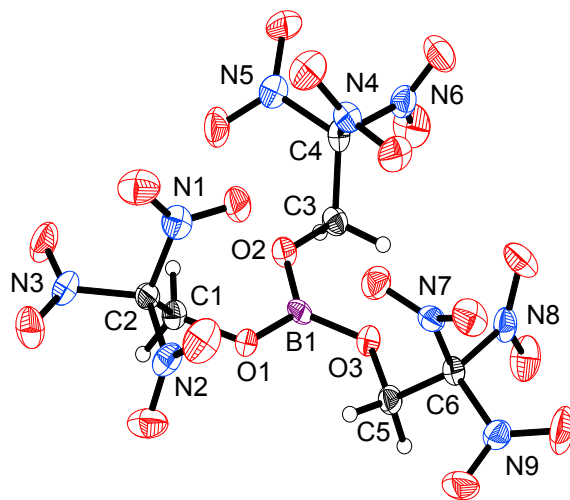
Figure 4.: Molecular structure of **3**. Selected distances [Å] and angles [°]: B1−O1 1.370(4), O1−C1 1.420(4), C1−C2 1.527(4), C2−N1 1.509(4), C2−N2 1.518(4), C2−N3 1.522(4), B1−O2 1.358(4), O2−C3 1.416(4), C3−C4 1.508(5), C4−N4 1.524(4), C4−N5 1.526(4), C4−N6 1.517(4), B1−O3 1.374(4), O3−C5 1.411(4), C5−C6 1.521(4), C6−N7 1.528(4), C6−N8 1.530(4), C6−N9 1.510(4), B1−O1−C1 120.5(3), O1−C1−C2 108.6(2), C1−C2−N1 113.9(3), C1−C2−N2 111.1(3), C1−C2−N3 109.6(2), B1−O2−C3 122.8(3), O2−C3−C4 108.5(3), C3−C4−N4 110.6(3), C3−C4−N5 114.2(3), C3−C4−N6 110.9(3), B1−O3−C5 123.2(2), O3−C5−C6 108.1(3), C5−C6−N7 113.3(3), C5−C6−N8 110.2(3), C5−C6−N9 112.9(3), O1−B1−O2 119.6(3), O2−B1−O3 119.5(3), O3−B1−O1 120.9(3).

between the trinitromethyl moieties support the *cis*-conformation. Besides various intramolecular hydrogen contacts, the oxygen atoms of the nitro groups of **1** are involved in weak intermolecular hydrogen contacts (shortest: 2.53 Å), with in total ten interactions shorter than the sum of the van der Waals radii (2.72 Å)[53,54]. This results in a highly linked network of intermolecular interactions. Applying the same selection criteria, for each **2** and **3**, six hydrogen contacts with the shortest one being 2.46 Å (for **2**) and 2.49 Å (for **3**) were found.

Both compounds **4** and **5** crystallize in the monoclinic space group $P2_1/n$, each with four formula units per unit cell. Due to the trigonal space group $P3_121$, compound **6** crystallizes with three formula units per unit cell. The molecular structures of **4**–**6** are shown in Figures 7–9.

In contrast to the structurally related 2,2,2-trinitroethanol, which crystallizes in the less symmetric monoclinic space group, the molecular structure of **5** does not consist of two crystallographically independent molecules.[55] The C−N bond lengths of **5** are 1.533(2) and 1.544(2) Å, slightly longer than in **2**. The N−C−N angle of **5** is 104.3°, slightly lower than that found in **2**, and substantially less than 109.5°[48]. In
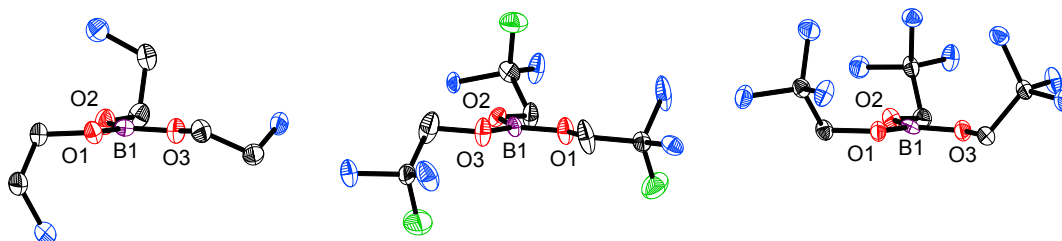
Figure 5.: Orientation of the ethoxy moieties in **1** (left), **2** (center) and **3** (right). Hydrogen atoms and oxygen atoms of the nitro groups not shown and only selected atoms labeled for clarity.

analogy to **2**, no attractive intramolecular interactions are observed, rather intermolecular interactions (2.93–3.01 Å) between the nitro groups are found in **5**. All structural bond lengths and angles in **5** show, that the general structural properties of this starting material and the corresponding boron ester **2** are not dramatically different. The same structural similarity is found between 2,2,2-trinitroethanol[55] and the corresponding borate **3**. The molecular structure of **4** (Figure 7) reveals that the negative charge of the anion is located at the dinitromethyl moiety (C1) and not at the potential ethoxy group (O5). This structure motif is also supported by the ^{1}H NMR spectrum of **4** in solution. The mesomeric stabilization of the negative charge by the two nitro groups favors placing the negative charge in this position rather than in an ethanolate compound. This mesomeric stabilization is also found in **6**. The C−N bond lengths of **4** (1.372(2)/1.380(2) Å) and **6** (1.377(3)/1.378(3) Å) show more double bond character. Due to the sp^2-hybridized carbon atom C1 and the free electron located there (Figures 7 and 9), the short C1−N1/N2 bond lengths in **4** and **6** can be explained. All nitro groups in **4**–**6** are planar. The molecular structures of **4** and **6** also show an almost planar orientation of these nitro groups with respect to the sp^2-hybridized carbon center. Maximal mesomeric resonance interaction requires this coplanarity, but some skewing of the nitro groups due to oxygen-oxygen repulsion is observed with the nitro groups are rotated out of the C C N plane by less than 10° in **4** and **6**. The two dinitromethyl moieties of **6** are twisted with respect to each other, as indicated by the angle between the C1 N1 N2 and C1(i) N1(i) N2(i) planes (72.1°; Figure 9). In addition to several intramolecular hydrogen bonds, intermolecular contacts are also present in the crystal structures of **4**–**6**. The shortest one is found in **5**, similarly to 2,2,2-trinitroethanol,[55] for an interaction between the hydroxyl groups of two adjacent molecules (2.15 Å). All other hydrogen bonds, which are shorter than the sum of the van der Waals radii (2.72 Å)[53,54] are weak and in the range of 2.45–2.69 Å (for **4**), 2.63–2.64 Å (for **5**) and 2.50–2.70 Å (for **6**). The coordination around the potassium atom of **6** is depicted in Figure 10,
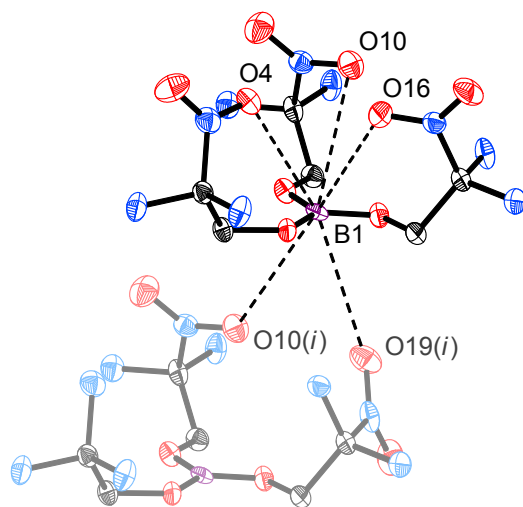
Figure 6.: Intra- and intermolecular attractive B⋯O interactions of **3**. Hydrogen atoms and oxygen atoms of the nitro groups not involved in these interactions not shown and only selected atoms labeled for clarity. Selected distances [Å]: B1⋯O4 3.161(5), B1⋯O10 3.309(5), B1⋯O16 3.090(5), B1⋯O10(i) 3.280(5), B1⋯O19(i) 3.290(5). $i = -1 + x, y, z$.

revealing ten K⋯O contacts, which are significantly shorter (< 3.25 Å) than the sum of the van der Waals radii (4.27 Å)[53,54].

Thermal and Energetic Properties

The density of **1** is $1.524\,\mathrm{g\,cm^{-3}}$ and increases to $1.885\,\mathrm{g\,cm^{-3}}$ for **3** with the addition of nitro groups to the terminal carbon atoms of ethoxy moieties. Compound **2** has, compared to **1** and **3**, the highest density of $1.911\,\mathrm{g\,cm^{-3}}$. The replacement of one nitro group in **3** with a fluorine atom per ethoxy moiety slightly increases the density, because of packing effects. This is also found in the starting materials, in which **5** ($1.899\,\mathrm{g\,cm^{-3}}$) has a slightly higher density than 2,2,2-trinitroethanol ($1.839\,\mathrm{g\,cm^{-3}}$)[55]. DTA measurements for **1**–**3** reveal one exothermic peak each in the measurement range of 25–400 °C, which represent the decomposition points of these compounds (Table 3). Compared to **3**, the decomposition of **2** occurs almost 60 °C higher, and in the range of **1**. Thus, the replacement of one nitro group in **3** with one fluorine atom per ethoxy moiety stabilizes the compound thermally. Beside these decomposition points, the DTA graphs of **2** and **3** show an endothermic peak each, arising from enantiotropic phase transitions at 61 °C (for **2**), respectively 35 °C (for **3**). It has been found that compounds whose molecular shapes are nearly spherical show enantiotropic polymorphism.[2,56] These occur not only in small molecules, but also in larger molecules such as **2** and **3**, and the orthocarbonate $\mathrm{C[OCH_2C(NO_2)_3]_4}$[1]. Compound **1** is too unsymmetrical,
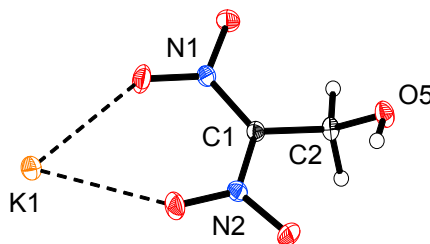
Figure 7.: Molecular structure of **4**. Selected distances [Å] and angles [°]: C1−C2 1.491(2), C2−O5 1.425(2), C1−N1 1.380(2), C1−N2 1.372(2), K1···O1 2.753(2), K1···O3 2.758(2), C1−C2−O5 114.4(2), C2−C1−N1 120.4(2), C2−C1−N2 118.1(2), N1−C1−N2 121.4(2).
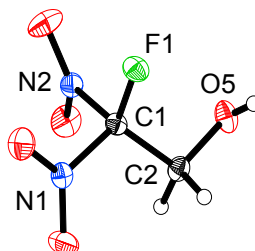
Figure 8.: Molecular structure of **5**. Selected distances [Å] and angles [°]: C1−F1 1.328(2), C1−C2 1.515(2), C2−O5 1.412(2), C1−N1 1.533(2), C1−N2 1.544(2), C1−C2−O5 108.2(1), C2−C1−F1 114.0(1), C2−C1−N1 112.5(1), C2−C1−N2 111.3(1), F1−C1−N1 107.6(1), F1−C1−N2 106.5(1), N1−C1−N2 104.3(1).

which prevents their molecular rotation in the crystal lattice to show polymorphism in that temperature range. Furthermore, high degree of rotational freedom in the solid state leads to unusually high melting points.[56] In the case of **1**–**3** no melting points are found. Due to their potential classification as energetic materials, the sensitivity of these compounds towards impact, friction and electrical discharge was determined (Table 3). According to the UN recommendations[57] **1** is classified as insensitive towards impact, whereas **2**, **3** and **5** are classified as sensitive. Regarding the friction sensitivity, **1** and **2** are classified as insensitive and **3** and **5** as sensitive. Table 3 shows, that in analogy to the thermal stability **2** is less sensitive than **3**, confirming the stabilizing effect of the introduction of a fluorine atom. In the flame of a Bunsen burner, the nitroethyl borates **1**–**3** show similar green flames and a smoke-free combustion, whereas the burn rate increases from **1** to **3**. Therefore, all presented nitroethyl borates may be suitable candidates for smoke-free, green coloring agents in pyrotechnic compositions. The oxygen balances of **2** and **3** show positive values relating to the formation of CO
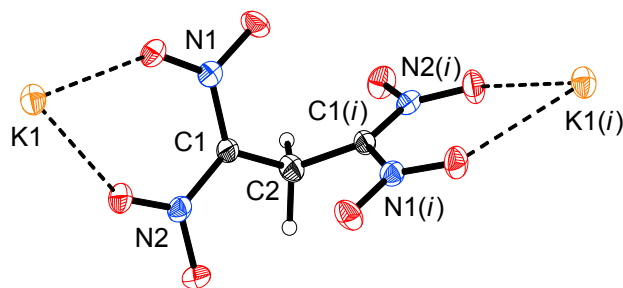
Figure 9.: Molecular structure of **6**. Selected distances [Å] and angles [°]: C1−C2/C1(i)−C2 1.490(3), C1−N1/C1(i)−N1(i) 1.378(3), C1−N2/C1(i)−N2(i) 1.377(3), K1···O1/K1(i)···O1(i) 2.745(2), K1···O3/K1(i)···O3(i) 2.703(2), C1−C2−C1(i) 117.9(2), C2−C1−N1/C2(i)−C1(i)−N1(i) 118.5(2), C2−C1−N2/C2(i)−C1(i)−N2(i) 118.8(2), N1−C1−N2/N1(i)−C1(i)−N2(i) 121.2(2). $i = y, x, 1 - z$.

and CO_2 (Table 3). Compound **3** shows an especially high oxygen balance and is of interest as a potential high energy oxidizer.

4.4. Conclusions

The nitroethyl boron esters tris(2-nitroethyl) borate (**1**), tris(2-fluoro-2,2-dinitroethyl) borate (**2**) and tris(2,2,2-trinitroethyl) borate (**3**) are prepared by reaction of the corresponding nitroethanol with boron oxide. Fluorination of 2-hydroxy-1,1-dinitroethane-1-ide (**4**) with Selectfluor forms the precursor 2-fluoro-2,2-dinitroethanol (**5**). The formation of the dianion 1,1,3,3-tetranitropropan-1,3-diide (**6**) from **4** has been re-investigated. This dianion **6** has a good potential for further chemistry, which is currently explored in our laboratory. The crystal structure of **3** unexpectedly shows a *cis*-conformation with regard to the trinitromethyl moieties due to attractive intra- and intermolecular B···O interactions. The smoke-free combustions of **1**–**3** display a green color, suggesting that they are suitable candidates for coloring agents in green pyrotechnic compositions. Furthermore, the oxygen balances of **2** and **3** show positive values relating to the formation of CO and CO_2, qualifying both compounds as potential high energy oxidizers.

4.5. Experimental Section

General Procedures. All manipulation of air- and moisture-sensitive materials were performed under an inert atmosphere of dry nitrogen using flame-dried glass vessels and Schlenk techniques.[58] The solvents acetonitrile, carbon tetrachloride and dichloromethane were dried by standard methods and freshly distilled prior to use.
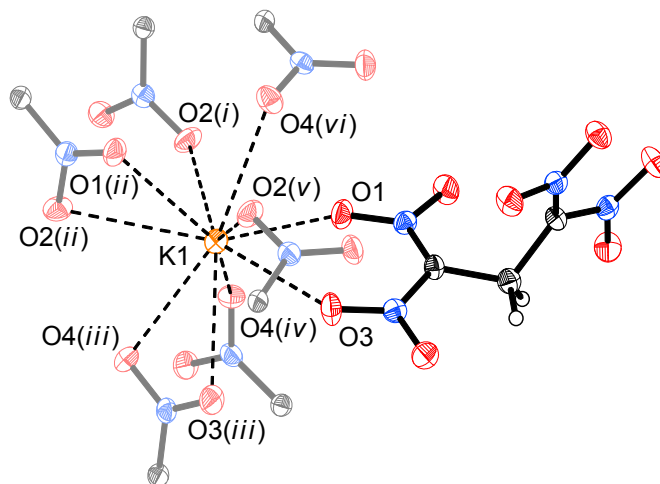
Figure 10.: Coordination around the potassium atom in **6**. Selected distances [Å]: K1···O1 2.745(2), K1···O3 2.703(2), K1···O2(i) 2.904(3), K1···O1(ii) 2.763(2), K1···O2(ii) 3.215(2), K1···O3(iii) 2.937(2), K1···O4(iii) 2.933(2), K1···O4(iv) 3.071(3), K1···O2(v) 3.057(3), K1···O4(vi) 2.901(2). $i = 1 - x + y, 1 - x, -\frac{1}{3} + z; ii = 1 - x, 1 - x + y, \frac{1}{3} - z; iii = -x, -x + y, \frac{2}{3} - z; iv = -x + y, -x, -\frac{1}{3} + z; v = x - y, 1 - y, \frac{2}{3} - z; vi = 1 + x - y, 1 - y, \frac{2}{3} - z$.

Boron oxide, 2-nitroethanol and Selectfluor fluorinating reagent (all Sigma-Aldrich) were used as received. Potassium 2-hydroxy-1,1-dinitroethane-1-ide (**4**) was prepared according to the literature procedure from potassium dinitromethanide with formaldehyde. [14,16] 2,2,2-Trinitroethanol was synthesized by reaction of potassium trinitromethanide with paraformaldehyde in hydrochloric acid at ambient temperature. Similar preparation methods were described, [59–63] whereas for safety reasons a slightly modified and thus a more convenient synthesis route with no heating and no distillation was performed. Furthermore, high purity was achieved by sublimation of the crude product in vacuum. Raman spectra were recorded with a Bruker MultiRAM FT-Raman instrument fitted with a liquid nitrogen cooled germanium detector and a Nd:YAG laser ($\lambda = 1064$ nm, 300 mW). Infrared (IR) spectra were measured with a Perkin-Elmer Spectrum BX-FTIR spectrometer equipped with a Smiths DuraSampl*IR* II ATR device. All spectra were recorded at ambient temperature, the samples were neat solids. NMR spectra were recorded at 25 °C with a JEOL Eclipse 400 ECX instrument, and chemical shifts were determined with respect to external Me$_4$Si (^{1}H, 400.2 MHz; ^{13}C, 100.6 MHz), BF$_3$ · Et$_2$O (^{11}B, 128.4 MHz), MeNO$_2$ (^{14}N, 29.0 MHz; ^{15}N, 40.6 MHz), and CCl$_3$F (^{19}F, 376.5 MHz). Mass spectrometric data were obtained with a JEOL MStation JMS 700 spectrometer (DCI+, CI+, FAB+/−). Boron containing fragments are referred to the isotope with the highest natural abundance, ^{11}B. Elemental analyses (C/H/N) were performed with an Elementar vario EL analyzer. Decomposition and phase transition temperatures were

determined by Differential Thermal Analysis (DTA) measurements with an OZM Research DTA 552-Ex instrument in a range of 25–400 °C, with a heating rate of $5\,°C\,min^{-1}$. Sensitivity data (impact, friction, and electrostatic discharge) were performed using a drophammer, friction tester, and electrostatic discharge device conform to the directive of the Federal Institute for Materials Research and Testing (BAM).[64]

Theoretical Calculations. All quantum chemical calculations were carried out with the program package GAUSSIAN 09 (Revision C.01)[65], visualized with GAUSSVIEW 5

Table 2.: Crystal and structure refinement data for **1**–**6**.

	1	2	3
Chemical formula	$C_6H_{12}BN_3O_9$	$C_6H_6BF_3N_6O_{15}$	$C_6H_6BN_9O_{21}$
Formula weight [$g\,mol^{-1}$]	280.99	469.95	550.97
Crystal dimensions [mm]	$0.58 \times 0.21 \times 0.05$	$0.21 \times 0.19 \times 0.16$	$0.47 \times 0.05 \times 0.04$
Crystal description	colorless platelet	colorless block	colorless rod
Crystal system	monoclinic	monoclinic	monoclinic
Space group (No.)	$P2_1/c$ (14)	$P2_1/n$ (14)	$P2_1/n$ (14)
a [Å]	9.0170(6)	10.3967(18)	6.046(2)
b [Å]	5.3297(3)	8.4998(13)	16.852(2)
c [Å]	25.4885(15)	18.4810(30)	19.105(4)
α [°]	90.0	90.0	90.0
β [°]	91.142(6)	90.339(17)	94.133(19)
γ [°]	90.0	90.0	90.0
V [$Å^3$]	1224.67(14)	1633.1(4)	1941.3(7)
Z	4	4	4
ρ_{calcd} [$g\,mol^{-3}$]	1.524	1.911	1.885
μ [mm^{-1}]	0.142	0.205	0.193
Temperature [K]	200(2)	173(2)	173(2)
$F(000)$	584	944	1112
θ range [°]	3.88–25.25	4.41–26.00	4.16–25.24
Index ranges	$-10 \le h \le 10$	$-12 \le h \le 11$	$-4 \le h \le 7$
	$-6 \le k \le 3$	$-8 \le k \le 10$	$-20 \le k \le 20$
	$-30 \le l \le 30$	$-22 \le l \le 22$	$-22 \le l \le 22$
Reflections measured	5427	6932	9223
Reflections independent	2205	2813	3442
Reflections unique	1480	1546	2207
$R1$, $wR2$ (2σ data)	0.0311, 0.0608	0.0941, 0.2050	0.0556, 0.1124
$R1$, $wR2$ (all data)	0.0582, 0.0653	0.1561, 0.2458	0.0990, 0.1339
Data/restraints/parameters	2205/0/172	2813/0/280	3442/0/334
GOF on F^2	0.874	1.022	0.995
Residual electron density (min/max) [$e\,Å^{-3}$]	$-0.146/0.134$	$-0.376/0.639$	$-0.271/0.286$

	4	5	6
Chemical formula	$C_2H_3KN_2O_5$	$C_2H_3FN_2O_5$	$C_3H_2K_2N_4O_8$
Formula weight [$g\,mol^{-1}$]	174.15	154.05	300.27
Crystal dimensions [mm]	$0.37 \times 0.34 \times 0.27$	$0.42 \times 0.31 \times 0.11$	$0.26 \times 0.19 \times 0.12$
Crystal description	yellow block	colorless block	yellow block
Crystal system	monoclinic	monoclinic	trigonal
Space group (No.)	$P2_1/n$ (14)	$P2_1/n$ (14)	$P3_121$ (152)
a [Å]	6.7743(3)	10.5718(9)	7.5742(4)
b [Å]	6.4378(3)	5.4292(3)	7.5742(4)
c [Å]	12.6160(6)	10.7644(9)	13.3239(7)
α [°]	90.0	90.0	90.0
β [°]	96.279(4)	119.276(12)	90.0
γ [°]	90.0	90.0	120.0
V [Å^3]	546.90(4)	538.92(9)	661.97(8)
Z	4	4	3
ρ_{calcd} [$g\,mol^{-3}$]	2.115	1.899	2.260
μ [mm^{-1}]	0.934	0.206	1.127
Temperature [K]	200(2)	173(2)	200(2)
$F(000)$	352	312	450
θ range [°]	4.54–25.98	4.34–26.00	4.36–26.22
Index ranges	$-8 \leq h \leq 5$	$-12 \leq h \leq 13$	$-9 \leq h \leq 5$
	$-7 \leq k \leq 7$	$-4 \leq k \leq 6$	$-8 \leq k \leq 9$
	$-15 \leq l \leq 15$	$-12 \leq l \leq 13$	$-16 \leq l \leq 16$
Reflections measured	2220	2615	1389
Reflections independent	1059	1049	822
Reflections unique	886	947	730
$R1$, $wR2$ (2σ data)	0.0229/0.0532	0.0246/0.0636	0.0246/0.0416
$R1$, $wR2$ (all data)	0.0293/0.0545	0.0273/0.0654	0.0301/0.0424
Data/restraints/parameters	1059/0/95	1049/0/95	822/0/82
GOF on F^2	1.003	1.052	0.922
Residual electron density (min/max) [e Å^{-3}]	$-0.249/0.292$	$-0.235/0.324$	$-0.186/0.181$

(Version 5.0.8)[66]. The initial geometries of the structures were taken from the corresponding, experimentally determined, crystal structures. The enthalpies (H) and free energies (G) were calculated by the Complete Basis Set (CBS) method in order to obtain very accurate values.[67–70] This method is a complex energy computation involving several pre-defined calculations on the specified system. The method used, CBS-4M ('M' referring to the use of Minimal Population localization), is an updated version of the modified CBS-4 method[71,72] with both the new localization procedure and improved empirical parameters.[72] The solid (**1**–**3**) or liquid (**5**) state enthalpies and energies of formation were calculated from the corresponding enthalpy derived from these quantum

Table 3.: Chemical, physical and energetic properties of **1**–**3** and **5**.

	1	2	3	5
Chemical formula	$C_6H_{12}BN_3O_9$	$C_6H_6BF_3N_6O_{15}$	$C_6H_6BN_9O_{21}$	$C_2H_3FN_2O_5$
Formula weight [g mol^{-1}]	280.99	469.95	550.97	154.05
N [%] [a)	14.95	17.88	22.88	18.18
$N + O$ [%] [b)	66.20	68.95	83.86	70.11
Ω_{CO} [%] [c)	-25.6	$+20.4$	$+30.5$	$+20.8$
Ω_{CO_2} [%] [d)	-59.8	±0.0	$+13.1$	±0.0
T_m [°C] [e)	–	–	–	10
T_p [°C] [f)	–	61	35	–
T_b / T_d [°C] [g)	216 (dec.)	209 (dec.)	150 (dec.)	215 (boil.)
ρ [g cm^{-3}] [h)	1.524 (XRD)	1.911 (XRD)	1.885 (XRD)	1.899 (XRD)
Grain size [µm] [i)	< 100	< 100	< 100	– (liquid)
IS [J] [j)	> 40	18	8	30
FS [N] [k)	> 360	> 360	144	240
ESD [J] [l)	1.5	1.0	0.5	– [p)
$H_{CBS\text{-}4M}$ [H] [m)	-1100.470127	-2010.805654	-2326.136010	-662.543333
ΔH_f° [kJ kg^{-1}] [n)	-4131.8	-3454.4	-1711.7	-2975.7
ΔU_f° [kJ kg^{-1}] [o)	-4026.1	-3375.3	-1630.7	-2886.9

[a) Nitrogen content. [b) Combined nitrogen and oxygen content. [c) Oxygen balance assuming the formation of CO and (if possible) H_2O, N_2, B_2O_3, HF. [d) Oxygen balance assuming the formation of CO_2 and (if possible) H_2O, N_2, B_2O_3, HF. [e) Melting point. [f) Phase transition point. [g) Boiling (boil.) or decomposition (dec.) point. [h) Density calculated from X-ray diffraction (XRD). [i) Grain size of the samples used for sensitivity tests. [j) Impact sensitivity (RDX: 7 J). [k) Friction sensitivity (RDX: 120 N). [l) Sensitivity towards electrostatic discharge (RDX: 0.2 J). [m) Enthalpy derived from quantum chemical CBS-4M calculation. [n) Enthalpy of formation (calculated). [o) Energy of formation (calculated). [p) Not determined (ESD test not measurable for liquids).

chemical CBS-4M calculations ($H_{CBS\text{-}4M}$). Therefore, the enthalpies of formation of the gas-phase species were computed according to the atomization energy method. [73–75] The solid (liquid) state enthalpies of formation (ΔH_f°) were estimated by subtracting the corresponding enthalpy of sublimation (vaporization) obtained by the Trouton's rule from the gas-phase enthalpies computed. [76,77] These enthalpies of formation were used to calculate the energies of formation (ΔU_f°).

X-ray Crystallography. For all compounds, an Oxford Xcalibur3 diffractometer with a CCD area detector was employed for data collection using MoK_α radiation ($\lambda = 0.710\,73$ Å). The structures were solved by direct methods (SIR2004) [78,79] and refined by full-matrix least-squares regression on F^2 (SHELXL) [80,81]. All non-hydrogen

atoms were refined anisotropically. The hydrogen atoms were located in difference Fourier maps and placed with a C−H distance of 0.99 Å for CH_2 groups. ORTEP plots are shown with thermal ellipsoids at the 50 % probability level. CCDC 910729 (**1**), 910730 (**2**), 910731 (**3**), 910732 (**5**), 910733 (**4**), and 910734 (**6**) contain the supplementary crystallographic data for this paper. These data can be obtained free of charge from The Cambridge Crystallographic Data Centre via www.ccdc.cam.ac.uk/data_request/cif.

CAUTION! All nitrogen- and oxygen-rich compounds are potentially explosive energetic materials, although no hazards were observed during preparation and handling these compounds. Nevertheless, this necessitates additional meticulous safety precautions (earthed equipment, Kevlar gloves, Kevlar sleeves, face shield, leather coat, and ear plugs). In addition, 2,2,2-trinitroethanol and especially 2-fluoro-2,2-dinitroethanol show significant degrees of toxicity, [28,82] including our recent results. [83] Particular care should be exercised in handling of those materials and derivatives.

Synthesis of tris(2-nitroethyl) borate (1)

Into 2-nitroethanol (2.27 g, 24.9 mmol) was added B_2O_3 (376 mg, 5.40 mmol) at ambient temperature under careful exclusion of moisture. After stirring the pale yellow mixture for 7 h at 60 °C, the resulting viscous fluid was dissolved in dry acetone (8 mL), and the excess of boron oxide/acid was removed. The colorless mixture was heated under reflux in dry carbon tetrachloride (20 mL). Several washs with carbon tetrachloride, each with subsequent crystallization of the product at lower temperature, yielded **1** (1.47 g, 73 %) as colorless crystals.

Raman: 3036 (14), 2972 (100), 2909 (17), 1556 (10, $\nu_{as}NO_2$), 1472 (10), 1424 (16), 1395 (17), 1370 (42), 1337 (6), 1274 (12), 1222 (7), 1148 (2), 1100 (11), 1070 (7), 992 (8), 921 (3), 898 (8), 876 (60, νCN), 738 (7), 616 (12), 480 (3), 373 (2), 280 (2), 227 (2) cm^{-1}. IR: 3036 (w), 2964 (w), 2917 (w), 1548 (vs, $\nu_{as}NO_2$), 1473 (m), 1413 (s), 1382 (s), 1346 (s), 1319 (vs), 1269 (m), 1216 (m), 1148 (w), 1101 (m), 1064 (s), 991 (w), 894 (m), 874 (m, νCN), 793 (w), 718 (w), 651 (w) cm^{-1}. ^{1}H NMR (CD$_3$OD): δ = 4.55 (m, 6 H, CH_2NO$_2$), 4.04 (m, 6 H, OCH_2) ppm; (CDCl$_3$): δ = 4.47 (m, 6 H, CH_2NO$_2$), 4.25 (m, 6 H, OCH_2) ppm. ^{11}B NMR (CD$_3$OD): δ = 18.1 (br) ppm; (CDCl$_3$): δ = 17.1 (br) ppm. ^{13}C{^{1}H} NMR (CD$_3$OD): δ = 78.8 (s, CH$_2$NO$_2$), 59.3 (s, OCH$_2$) ppm; (CDCl$_3$): δ = 76.0 (s, CH$_2$NO$_2$), 59.7 (s, OCH$_2$) ppm. ^{14}N NMR (CDCl$_3$): δ = −0.5 (s, NO$_2$) ppm. ^{15}N NMR (CD$_3$OD): δ = 2.3 (tt, $^{2}J_{N-H}$ = 4.2 Hz, $^{3}J_{N-H}$ = 1.9 Hz, NO$_2$). MS (DCI+): m/c (%) = 281 (4) [M^{+}], 221 (2) [M^{+} −CH$_2$NO$_2$], 191 (94) [M^{+} −OCH$_2$CH$_2$NO$_2$], 74 (18) [CH$_2$CH$_2$NO$_2$$^{+}$]. C$_6H_{12}BN_3O_9$ (280.99): Anal. calcd C 25.65, H 4.30, N 14.95; found C 24.91, H 4.47, N 14.42. DTA (T_{onset}, 5 °C min^{-1}): 216 °C (decomposition). Sensitivities (grain size: < 100 μm): impact: > 40 J, friction: > 360 N, electrostatic: 1.5 J.

Synthesis of tris(2-fluoro-2,2-dinitroethyl) borate (2)

Into a solution of 2-fluoro-2,2-dinitroethanol (2.30 g, 14.9 mmol) in dry acetonitrile (3 mL) was added B_2O_3 (225 mg, 3.23 mmol) at ambient temperature under careful exclusion of moisture. After stirring the colorless mixture for 7 h at 45 °C, the reaction mixture was decanted to remove unreacted boron oxide/acid. Removing the solvent in vacuo left a colorless solid. Crystallization of the product from dichloromethane yielded **2** (1.66 g, 83 %) as colorless crystals.

Raman: 3017 (11), 2966 (38), 2895 (3), 1612 (12), 1588 (20, $\nu_{as}NO_2$), 1456 (12), 1393 (20), 1359 (33), 1320 (17), 1248 (11), 1180 (3), 1115 (5), 1069 (13), 1019 (6), 1003 (6), 930 (14), 882 (4), 854 (100, νCN), 807 (1), 768 (9), 705 (1), 536 (8), 423 (25), 382 (23), 361 (28), 309 (6), 287 (2), 267 (3), 213 (19), 192 (18) cm^{-1}. IR: 3015 (w), 2963 (w), 2897 (w), 1589 (vs, $\nu_{as}NO_2$), 1457 (s), 1435 (s), 1413 (vs), 1382 (s), 1337 (s), 1310 (vs), 1261 (m), 1243 (s), 1194 (s), 1115 (s), 1068 (s), 1002 (m), 927 (m), 884 (w), 850 (s, νCN), 800 (vs), 760 (s) cm^{-1}. ^{1}H NMR (CD$_3$OD): $\delta = 4.63$ (d, $^3J_{H-F} = 18.1$ Hz, 6 H, OCH_2) ppm. ^{11}B NMR (CD$_3$OD): $\delta = 18.1$ (br) ppm; (CDCl$_3$): $\delta = 17.8$ (br) ppm. ^{13}C{^{1}H} NMR (CD$_3$OD): $\delta = 123.6$ (d, $^1J_{C-F} = 289.3$ Hz, (C(NO$_2$)$_2$F), 62.3 (d, $^2J_{C-F} = 19.8$ Hz, OCH_2) ppm. ^{14}N NMR (CDCl$_3$): $\delta = -24$ (s, NO_2) ppm. ^{15}N NMR (CD$_3$OD): $\delta = -21.3$ (d, $^2J_{N-F} = 15.0$ Hz, NO_2) ppm. ^{19}F NMR (CD$_3$OD): $\delta = -114.5$ (m, br, FC); (CDCl$_3$): $\delta = -111.8$ (m, br, FC) ppm. C$_6$H$_6$BF$_3$N$_6$O$_{15}$ (469.95): Anal. calcd. C 15.33, H 1.29, N 17.88; found C 14.89, H 1.60, N 16.65. DTA (T_{onset}, 5 °C min^{-1}): 209 °C209 ÂřC (decomposition). Sensitivities (grain size: $< 100\,\mu$m): impact: 18 J, friction: > 360 N, electrostatic: 1.0 J.

Synthesis of tris(2,2,2-trinitroethyl) borate (3)

Into a solution of 2,2,2-trinitroethanol (3.45 g, 19.1 mmol) in dry acetonitrile (3 ml) was added B_2O_3 (290 mg, 4.14 mmol) at ambient temperature under careful exclusion of moisture. After stirring the colorless mixture for 7 h at 40 °C, the reaction mixture was decanted to remove unreacted boron oxide/acid. Removing the solvent in vacuo left a colorless solid. Crystallization of the product from dichloromethane yielded **3** (2.65 g, 88 %) as colorless crystals.

Raman: 3009 (18), 2970 (33), 2910 (3), 1612 (19), 1599 (21, $\nu_{as}NO_2$), 1456 (6), 1445 (6), 1426 (3), 1395 (12), 1376 (5), 1355 (36), 1310 (30), 1278 (12), 1180 (1), 1150 (3), 1100 (4), 1075 (7), 1019 (5), 1006 (6), 883 (8), 858 (100, νCN), 824 (2), 809 (5), 782 (6), 762 (3), 722 (3), 652 (5), 566 (2), 542 (15), 418 (37), 402 (44), 378 (62), 340 (4), 306 (10), 261 (10), 233 (7), 205 (19) cm^{-1}. IR: 3009 (w), 2966 (w), 2893 (w), 1586 (vs, $\nu_{as}NO_2$), 1455 (m), 1439 (m), 1419 (m), 1373 (m), 1330 (m), 1306 (m), 1297 (s), 1274 (m), 1259 (m), 1243 (m), 1199 (m), 1148 (m), 1089 (s), 1059 (m), 1005 (m), 941 (w), 881 (m), 856 (m, νCN), 803 (vs), 779 (s), 712 (m) cm^{-1}. ^{1}H NMR (CD$_3$OD): $\delta = 4.92$ (s, 6 H, OCH_2)

ppm. ^{11}B NMR (CD$_3$OD): $\delta = 18.1$ (br) ppm; (CDCl$_3$): $\delta = 17.6$ (br) ppm. $^{13}C\{^1H\}$ NMR (CD$_3$OD): $\delta = 128.3$ (br, $C(NO_2)_3$), 64.0 (s, OCH$_2$) ppm. ^{14}N NMR (CDCl$_3$): $\delta = -33$ (s, NO_2) ppm. ^{15}N NMR (CD$_3$OD): $\delta = -31.1$ (s, NO_2) ppm. C$_6$H$_6$BN$_9$O$_{21}$ (550.97): Anal. calcd. C 13.08, H 1.10, N 22.88; found C 13.18, H 1.41, N 22.01. DTA (T_{onset}, $5\,°C\,min^{-1}$): $150\,°C$ (decomposition). Sensitivities (grain size: $< 100\,\mu m$): impact: 8 J, friction: 144 N, electrostatic: 0.5 J.

Additional analytical data of potassium 2-hydroxy-1,1-dinitroethane-1-ide (4)

Raman: 3032 (13), 2976 (1), 2932 (5), 1498 (4, $\nu_{as}NO_2$), 1465 (2), 1449 (8), 1407 (7), 1387 (22), 1362 (15), 1326 (5), 1311 (9), 1286 (11), 1223 (51), 1133 (14), 1091 (23), 1005 (24), 934 (17), 847 (100, νCN), 778 (2), 766 (5), 745 (1), 738 (1), 675 (3), 662 (1), 484 (50), 455 (12), 434 (14), 363 (5), 292 (15), 218 (2) cm^{-1}. IR: 3510 (w), 3031 (w), 2931 (w), 1470 (s, $\nu_{as}NO_2$), 1410 (m), 1356 (m), 1326 (m), 1288 (m), 1222 (m), 1134 (s), 1122 (vs), 1083 (s), 1006 (vs), 931 (s), 892 (m), 860 (m, νCN), 845 (s), 776 (m), 759 (s), 747 (m), 736 (m), 698 (m), 675 (s) cm^{-1}. ^1H NMR ((CD$_3$)$_2$SO): $\delta = 4.70$ (d, 2 H, OCH$_2$), 4.44 (t, 1 H, HO) ppm. $^{14}C\{^1H\}$ NMR ((CD$_3$)$_2$SO): $\delta = 135.9$ (br, (C(NO$_2$)$_2$), 57.0 (s, OCH$_2$) ppm. ^{14}N NMR ((CD$_3$)$_2$SO): $\delta = -22$ (s, NO_2) ppm. MS (FAB+): m/c (%) $= 39$ (100) [K$^+$]. MS (FAB−): m/c (%) $= 135$ (100) [HOCH$_2$C(NO$_2$)$_2{}^-$]. C$_2$H$_3$KN$_2$O$_5$ (174.15): Anal. calcd. C 13.79, H 1.74, N 16.09; found C 13.70, H 1.66, N 16.17.

Synthesis of 2-fluoro-2,2-dinitroethanol (5)

Into a suspension of **4** (13.4 g, 77.0 mmol) in water (100 mL) was added Selectfluor fluorinating reagent (30.0 g, 84.7 mmol) at $0\,°C$. After stirring the yellow mixture for 2 h at ambient temperature, the reaction mixture had become colorless. The mixture was filtered to remove precipitated reaction residues, extracted with dichloromethane (5×120 mL) and dried over anhydrous magnesium sulfate. After removing the solvent in vacuo, the pale brownish oil is distilled ($41\,°C$ at 6 mbar) yielding **5** (6.02 g, 51 %) as a colorless oil.

Raman: 3006 (5), 2955 (18), 2877 (3), 1591 (13, $\nu_{as}NO_2$), 1448 (11), 1385 (14), 1356 (28), 1326 (10), 1234 (2), 1090 (9), 1001 (4), 916 (4), 852 (100, νCN), 801 (2), 756 (2), 570 (3), 516 (5), 423 (12), 381 (45), 318 (2), 282 (3), 190 (17) cm^{-1}. IR: 3355 (w), 2953 (w), 2908 (w), 1586 (vs, $\nu_{as}NO_2$), 1446 (m), 1381 (w), 1353 (m), 1314 (s), 1231 (m), 1079 (s), 1002 (m), 917 (m), 878 (w), 850 (m, νCN), 798 (vs), 759 (m), 691 (m) cm^{-1}. ^1H NMR (CDCl$_3$): $\delta = 4.66$ (dd, $^3J_{H-F} = 15.3$ Hz, 2 H, OCH$_2$), 2.80 (t, $^4J_{H-F} = 1.6$ Hz, 1 H, HO) ppm. $^{13}C\{^1H\}$ NMR (CDCl$_3$): $\delta = 120.8$ (d, $^1J_{C-F} = 290.2$ Hz, C(NO$_2$)$_2$F), 61.6 (d, $^2J_{C-F} = 21.3$ Hz, OCH$_2$) ppm. ^{15}N NMR (CDCl$_3$): $\delta = -22.7$ (dt, $^2J_{N-F} = 15.0$ Hz, $^3J_{N-H} = 1.3$ Hz, NO_2) ppm. ^{19}F NMR (CDCl$_3$): $\delta = -111.9$ (m, br, FC) ppm. MS (CI+): m/c (%) $= 155$ (100) [M$^+$ + H]. MS (EI+): m/c (%) $= 155$ (0.3) [M$^+$ + H], 62 (100)

$[M^+ - 2 NO_2]$, 46 (89) $[NO_2{}^+]$. $C_2H_3FN_2O_5$ (154.05): Anal. calcd. C 15.59, H 1.96, N 18.18; found C 15.81, H 1.94, N 18.11. DTA (T_{onset}, $5\,°C\,min^{-1}$): 215 degreeCelsius (boiling point). Sensitivities (liquid): impact: 30 J, friction: 240 N.

Additional analytical data of potassium 1,1,3,3-tetranitropropane-1,3-diide (6)

Into a suspension of **4** (1.35 g, 7.75 mmol) in water (6 mL) was added 1 M sulfuric acid until a pH value of 4 was achieved (ca. 2 mL). After stirring the yellow solution for 1 h, the color had changed to red and a saturated potassium hydroxide solution was added at 0 °C. The precipitated product was filtered and washed with cold water and diethylether (each 2×2 mL). Drying on air at room temperature yielded **6** (0.74 g, 63 %) as yellow-orange crystals.

Raman: 3010 (1), 2976 (6), 1520 (1), 1490 (12, $\nu_{as}NO_2$), 1422 (2), 1403 (1), 1380 (8), 1348 (25), 1321 (10), 1220 (51), 1153 (7), 1146 (6), 1111 (6), 1085 (44), 1061 (2), 984 (29), 893 (3), 861 (54), 851 (100, νCN), 778 (14), 743 (3), 721 (1), 704 (1), 661 (4), 627 (2), 620 (4), 484 (49), 455 (5), 436 (5), 376 (18), 286 (4), 271 (6), 245 (6) cm^{-1}. IR: 3007 (w), 2975 (w), 1498 (m, $\nu_{as}NO_2$), 1470 (m), 1380 (m), 1355 (m), 1334 (m), 1321 (m), 1232 (s), 1206 (s), 1195 (s), 1153 (s), 1142 (s), 1103 (vs), 1081 (vs), 1031 (s), 983 (m), 891 (m), 860 (m, νCN), 776 (m), 742 (m), 718 (m), 698 (s) cm^{-1}. ^1H NMR $((CD_3)_2SO)$: $\delta = 4.57$ (d, 2 H, CH_2) ppm. $^{13}C\{^1H\}$ NMR $((CD_3)_2SO)$: $\delta = 131.7$ (br, $C(NO_2)_2$), 29.6 (s, CH$_2$) ppm. ^{14}N NMR $((CD_3)_2SO)$: $\delta = -24$ (s, NO_2) ppm. MS (FAB+): m/c (%) = 39 (100) $[K^+]$. MS (FAB−): m/c (%) = 223 (100) $[^-(NO_2)_2CCH_2C(NO_2)_2{}^- + H^+]$. $C_3H_2K_2N_4O_8$ (300.27): Anal. calcd. C 12.00, H 0.67, N 18.66; found C 12.07, H 0.70, N 18.57.

4.6. Acknowledgment

Supporting Information

CIF files with crystallographic data for all compounds (**1**–**6**). This material is available free of charge via the Internet at http://pubs.acs.org.

4.7. References

[1] T. M. Klapötke, B. Krumm, R. Moll, S. F. Rest, *Z. Anorg. Allg. Chem.* **2011**, *637*, 2103–2110.

[2] T. M. Klapötke, B. Krumm, R. Moll, A. Penger, S. M. Sproll, R. J. F. Berger, S. A. Hayes, N. W. Mitzel, *Z. Naturforsch.* **2013**, *68b*, 719–731.

[3] F. Zwicky, *Astronautics (Easton. 1957–63)* **1957**, *2*, 45–49/95–97.

[4] E.-C. Koch, T. M. Klapötke, *Propellants Explos. Pyrotech.* **2012**, *37*, 335–344.

[5] V. I. Burmistrov, L. M. Kozlov, T. F. Telkova (Chem. Technol. Inst., Kazan), SU154243, **1963**.

[6] L. M. Kozlov, V. I. Burmistrov, T. F. Telkova, *Izv. Vyssh. Uchebn. Zaved. Khim. Khim. Tekhnol.* **1966**, *9*, 63–64.

[7] V. Grakauskas, *J. Org. Chem.* **1970**, *35*, 3030–3036.

[8] T. M. Klapötke, B. Krumm, R. Moll, in *Nitro compounds based on boron esters*, New Trends Res. Energ. Mater., 13th Proc. Semin., Pardubice, Czech Republic, **2010**, pp. 523–527.

[9] T. M. Klapötke, B. Krumm, R. Moll, S. F. Rest, *Spectroscopic and structural studies of nitro substituted fluoro-methanes and ethanes*, 20th International Symposium on Fluorine Chemistry (ISFC), Kyoto, Japan, **2012**.

[10] Less economic route from $B(OCH_2CH_3)_3$ and no yields, see brief notice in Dissertation, M. Göbel, Ludwig-Maximilian University of Munich, Germany, **2009**, pp. 207.

[11] L. W. Kissinger, T. M. Benziger, H. E. Ungnade, R. K. Rohwer, *J. Org. Chem.* **1963**, *28*, 2491–2494.

[12] P. Duden, G. Ponndorf, *Ber. Dtsch. Chem. Ges.* **1905**, *38*, 2031–2036.

[13] M. H. Gold, E. E. Hamel, K. Klager, *J. Org. Chem.* **1957**, *22*, 1665–1667.

[14] V. Grakauskas, A. M. Guest, *J. Org. Chem.* **1978**, *43*, 3485–3488.

[15] A. L. Laikhter, T. I. Cherkasova, L. G. Mel'nikova, B. I. Ugrak, A. A. Fainzil'berg, V. V. Semenov, *Bull. Acad. Sci. USSR, Div. Chem. Sci. (Engl. Transl.)* **1991**, *40*, 1637–1643.

[16] O. A. Ivanova, E. M. Budynina, E. B. Averina, T. S. Kuznetsova, Y. K. Grishin, N. S. Zefirov, *Synthesis* **2007**, 2009–2013.

[17] V. Grakauskas, E. E. Hamel (Aerojet-General Corporation, Azusa), GB1077065, **1967**.

[18] V. Grakauskas, E. E. Hamel (Aerojet-General Corporation, Azusa), US3387044, **1968**.

[19] L. T. Eremenko, F. Y. Natsibullin, *Bull. Acad. Sci. USSR, Div. Chem. Sci. (Engl. Transl.)* **1968**, *17*, 875–876.

[20] M. J. Kamlet, H. G. Adolph, *J. Org. Chem.* **1968**, *33*, 3073–3080.

[21] V. Grakauskas, K. Baum, *J. Org. Chem.* **1968**, *33*, 3080–3082.

[22] G. W. Nauflett, R. E. Farncomb (U. S. Navy), US3652686, **1972**.

[23] V. M. Khutoretskii, L. V. Okhlobystina, A. A. Fainzil'berg, *Bull. Acad. Sci. USSR, Div. Chem. Sci. (Engl. Transl.)* **1970**, *19*, 333–337.

[24] M. J. Kamley (U. S. Navy), US3624129, **1971**.

[25] L. T. Eremenko, F. Y. Natsibullin, *Bull. Acad. Sci. USSR, Div. Chem. Sci. (Engl. Transl.)* **1969**, *18*, 1227–1231.

[26] H. G. Adolph (U. S. Navy), US3446857, **1969**.

[27] H. G. Adolph (U. S. Navy), US3542884, **1970**.

[28] M. B. Frankel, G. L. Bauerle, L. R. Grant, R. L. Kistner, J. V. Lecce, E. R. Wilson, D. O. I. Woolery, *Process studies on nitroform and related compounds: Final report for period 30 January 1984 to 31 March 1987*, UCRL-15908, Rockwell International Corp., Rocketdyne Division, Canoga Park, CA (USA), March **1987**, pp. 1–66.

[29] T. G. Archibald, N. N. Van, K. Baum (U. S. Navy), US1223, **1993**.

[30] L. T. Eremenko, N. G. Zhitomirskaya, G. V. Oreshko, *Bull. Acad. Sci. USSR, Div. Chem. Sci. (Engl. Transl.)* **1969**, *18*, 2514–2519.

[31] L. T. Eremenko, N. G. Zhitomirskaya, G. V. Oreshko, *Bull. Acad. Sci. USSR, Div. Chem. Sci. (Engl. Transl.)* **1969**, *18*, 2520–2525.

[32] S. S. Novikov, A. A. Fainzil'berg, S. A. Shevelev, I. S. Korsakova, K. K. Babievskii, *Dokl. Akad. Nauk SSSR* **1959**, *124*, 589–591.

[33] S. S. Novikov, A. A. Fainzil'berg, S. A. Shevelev, I. S. Korsakova, K. K. Babievskii, *Dokl. Akad. Nauk SSSR* **1960**, *132*, 846–849.

[34] K. Klager, J. P. Kispersky, E. Hamel, *J. Org. Chem.* **1961**, *26*, 4368–4371.

[35] M. J. Kamlet, J. C. Dacons, J. C. Hoffsommer, *J. Org. Chem.* **1961,** *26,* 4881–4886.

[36] R. B. Kaplan, H. Shechter, *J. Am. Chem. Soc.* **1961**, *83*, 3535–3536.

[37] K. Klager (Aerojet-General Corporation, Azusa), US3020317, **1962**.

[38] E. E. Hamel, *Tetrahedron* **1963**, *19*, 85–95.

[39] M. J. Kamlet, R. E. Oesterling, H. G. Adolph, *J. Chem. Soc.* **1965**, 5838–5849.

[40] H. Piotrowska, K. Wejroch, *Liebigs Ann. Chem.* **1992**, 871–875.

[41] H. Steinberg, D. L. Hunter, *Ind. Eng. Chem.* **1957**, *49*, 174–181.

[42] M. J. Kamlet, J. C. Dacons, *J. Org. Chem.* **1961**, *26*, 3005–3008.

[43] G. Socrates, *Infrared and Raman Characteristic Group Frequencies: Tables and Charts*, 3rd ed., John Wiley and Sons, Chichester, **2004**.

[44] L. J. Bellamy, W. Gerrard, M. F. Lappert, R. L. Williams, *J. Chem. Soc.* **1958**, 2412–2415.

[45] V. D. Makhaev, A. S. Antsyshkina, L. A. Petrova, G. G. Sadikov, *Russ. J. Inorg. Chem.* **2004**, *49*, 1154–1157.

[46] V. J. Heintz, W. A. Freeman, T. A. Keiderling, *Inorg. Chem.* **1983**, *22*, 2319–2324.

[47] M. A. Hartl, D. J. Williams, A. I. Acatrinei, A. Stowe, L. L. Daemen, *Z. Anorg. Allg. Chem.* **2007**, *633*, 120–126.

[48] A. F. Holleman, E. Wiberg, N. Wiberg, *Lehrbuch der Anorganischen Chemie*, 102nd ed., Walter de Gruyter, Berlin, **2008**.

[49] F. H. Allen, O. Kennard, D. G. Watson, L. Brammer, A. G. Orpen, R. Taylor, *J. Chem. Soc. Perkin Trans. 2* **1987**, S1–S19.

[50] S. K. Bhattacharjee, H. L. Ammon, *Acta Crystallogr. Sect. B* **1982**, *38*, 2503–2505.

[51] Y. Oyumi, T. B. Brill, A. L. Rheingold, *J. Phys. Chem.* **1985**, *89*, 4824–4828.

[52] H. Schödel, R. Dienelt, H. Bock, *Acta Crystallogr. Sect. C* **1994**, *50*, 1790–1792.

[53] A. Bondi, *J. Phys. Chem.* **1964**, *68*, 441–451.

[54] M. Mantina, A. C. Chamberlin, R. Valero, C. J. Cramer, D. G. Truhlar, *J. Phys. Chem. A* **2009**, *113*, 5806–5812.

[55] M. Göbel, T M. Klapötke, *Acta Crystallogr. Sect. C* **2007**, *63*, o562–o564.

[56] R. W. Crowe, C. P. Smyth, *J. Am. Chem. Soc.* **1950**, *72*, 4009–4015.

[57] T. M. Klapötke, *Chemistry of High-Energy Materials*, 2nd ed., Walter de Gruyter, Berlin, **2012**.

[58] D. F. Shriver, M. A. Drezdzon, *The Manipulation of Air-Sensitive Compounds*, 2nd ed., John Wiley and Sons, New York, **1986**.

[59] N. S. Marans, R. P. Zelinski, *J. Am. Chem. Soc.* **1950**, *72*, 5329–5330.

[60] R. Schenck (Nitroglycerin Aktiebolaget, Gyttorp), SE135832, **1952**.

[61] H. Feuer, T. J. Kucera, *J. Org. Chem.* **1960**, *25*, 2069–2070.

[62] P. F. Hartman (U. S. Rubber company, New York), US3041383, **1962**.

[63] F. G. Borgardt, A. K. Seeler, P. Noble, Jr., *J. Org. Chem.* **1966**, *31*, 2806–2811.

[64] Test procedure *A.14 Explosive Properties* according to Council Regulation (EC) No 440/2008 of 30 May 2008 laying down test methods pursuant to Regulation (EC) No 1907/2006 of the European Parliament and of the Council on the Registration, Evaluation, Authorisation and Restriction of Chemicals (REACH), *OJ L 142*, 93–103, **2008**.

[65] *Gaussian 09*, Rev. C.01, M. J. Frisch, G. W. Trucks, H. B. Schlegel, G. E. Scuseria, M. A. Robb, J. R. Cheeseman, G. Scalmani, V. Barone, B. Mennucci, G. A. Petersson, H. Nakatsuji, M. Caricato, X. Li, H. P. Hratchian, A. F. Izmaylov, J. Bloino, G. Zheng, J. L. Sonnenberg, M. Hada, M. Ehara, K. Toyota, R. Fukuda, J. Hasegawa, M. Ishida, T. Nakajima, Y. Honda, O. Kitao, H. Nakai, T. Vreven, J. A. Montgomery, Jr., J. E. Peralta, F. Ogliaro, M. Bearpark, J. J. Heyd, E. Brothers, K. N. Kudin, V. N. Staroverov, R. Kobayashi, J. Normand, K. Raghavachari, A. Rendell, J. C. Burant, S. S. Iyengar, J. Tomasi, M. Cossi, N. Rega, J. M. Millam, M. Klene, J. E. Knox, J. B. Cross, V. Bakken, C. Adamo, J. Jaramillo, R. Gomperts, R. E. Stratmann, O. Yazyev, A. J. Austin, R. Cammi, C. Pomelli, J. W. Ochterski, R. L. Martin, K. Morokuma, V. G. Zakrzewski, G. A. Voth, P. Salvador, J. J. Dannenberg, S. Dapprich, A. D. Daniels, Ö. Farkas, J. B. Foresman, J. V. Ortiz, J. Cioslowski, D. J. Fox, Gaussian, Inc., Wallingford CT (USA), **2009**.

[66] *GaussView*, R. D. Dennington II, T. A. Keith, J. M. Millam, Version 5.0.8, Semichem Inc., Shawnee Mission KS (USA), **2009**.

[67] M. R. Nyden, G. A. Petersson, *J. Chem. Phys.* **1981**, *75*, 1843–1862.

[68] G. A. Petersson, M. A. Al-Laham, *J. Chem. Phys.* **1991**, *94*, 6081–6090.

[69] G. A. Petersson, T. G. Tensfeldt, J. A. Montgomery, Jr., *J. Chem. Phys.* **1991**, *94*, 6091–6101.

[70] J. A. Montgomery, Jr., J. W. Ochterski, G. A. Petersson, *J. Chem. Phys.* **1994**, *101*, 5900–5909.

[71] J. W. Ochterski, G. A. Petersson, J. A. Montgomery, Jr., *J. Chem. Phys.* **1996**, *104*, 2598–2619.

[72] J. A. Montgomery, Jr., M. J. Frisch, J. W. Ochterski, G. A. Petersson, *J. Chem. Phys.* **2000**, *112*, 6532–6542.

[73] L. A. Curtiss, K. Raghavachari, P. C. Redfern, J. A. Pople, *J. Chem. Phys.* **1997**, *106*, 1063–1079.

[74] B. M. Rice, S. V. Pai, J. Hare, *Combust. Flame* **1999**, *118*, 445–458.

[75] E. F. C. Byrd, B. M. Rice, *J. Phys. Chem. A* **2006**, *110*, 1005–1013.

[76] F. Trouton, *Philos. Mag.* **1884**, *18*, 54–57.

[77] M. S. Westwell, M. S. Searle, D. J. Wales, D. H. Williams, *J. Am. Chem. Soc.* **1995**, *117*, 5013–5015.

[78] *SIR2004*, M. C. Burla, R. Caliandro, M. Camalli, B. Carrozzini, G. L. Cascarano, L. De Caro, C. Giacovazzo, G. Polidori, R. Spagna, Institute of Crystallography, Bari (Italy), **2004**.

[79] M. C. Burla, R. Caliandro, M. Camalli, B. Carrozzini, G. L. Cascarano, L. De Caro, C. Giacovazzo, G. Polidori, R. Spagna, *J. Appl. Crystallogr.* **2005**, *38*, 381–388.

[80] *SHELX-97*, G. M. Sheldrick, University of Göttingen, Göttingen (Germany), **1997**.

[81] G. M. Sheldrick, *Acta Crystallogr. Sect. A* **2008**, *64*, 112–122.

[82] A. L. Fridman, O. B. Kremleva, V. S. Zalesov, Z. V. Platonova, F. A. Gabitov, L. A. Rubinshtein, A. N. Plaksina, *Pharm. Chem. J.* **1977**, *11*, 64–67.

[83] R. Scharf, T. M. Klapötke, *Private communication*, Ludwig-Maximilian University of Munich, Germany, September **2012**.

5. Hexanitrohexyne and Trinitroethane
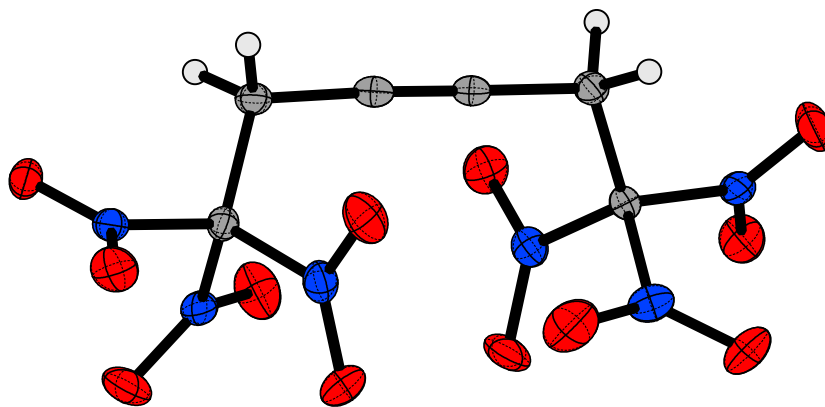
Structures of Energetic Acetylene Derivatives HC≡CCH$_2$ONO$_2$, (NO$_2$)$_3$CCH$_2$CC≡CH$_2$C(NO$_2$)$_3$ and Trinitroethane, (NO$_2$)$_3$CCH$_3$

Thomas M. Klapötke,[a] Burkhard Krumm,[a] Richard Moll,[a] Alexander Penger,[a] Stefan M. Sproll,[a] Raphael J. F. Berger,[b] Stuart A. Hayes,[b] and Norbert W. Mitzel [b]

Dedicated to Professor Heinrich Nöth on the occasion of his 85th birthday

*   Prof. Dr. Thomas M. Klapötke

     E-Mail: tmk@cup.uni-muenchen.de

[a]   Department of Chemistry

     Ludwig-Maximilian University of Munich

     Butenandtstrasse 5–13 (D)

     81377 Munich, Germany

[b]   Inorganic and Structural Chemistry

     Bielefeld University

     Universitätsstraße 25

     33615 Bielefeld, Germany

5.1. Abstract

The molecular structures and relative ratios of the two conformers (*anti* and *gauche*) of $HCCCH_2ONO_2$ detected in the gas phase at room temperature have been determined by electron diffraction. The results are discussed on the basis of quantum chemical calculations. The molecular structures of $(NO_2)_3CCH_2C{\equiv}CCH_2C(NO_2)_3$ and $(NO_2)_3CCH_3$ have been determined by X-ray diffraction. A ^{109}Ag NMR study was performed for silver trinitromethanide $Ag[C(NO_2)_3]$ in various polar solvents.

5.2. Introduction

The research of energetic materials is driven by the goal to obtain materials with superior properties, but it is also highly desirable to generate a better understanding of well described systems. Among the class of energetic nitrate esters, nitroglycerine and nitrocellulose are well established liquid propellant systems and smokeless powders, whereas pentaerythritol tetranitrate is a powerful explosive. Low molecular weight nitrate esters like methyl nitrate, designated as MYROL in WWII, have been widely discussed as components for liquid rocket engines. [1] Unfortunately, all nitrate esters tend to show extreme sensitivities towards shock and impact, which is a result of adiabatic compression and consequently local overheating. [2,3]

The combination of oxidizing groups with an organic backbone as fuel is a common approach for designing new energetic materials. Surprisingly, energetic compounds based on the highly endothermic acetylene are rare in the literature. However, butin-2-diol-1,4-dinitrate has been investigated and shown to be more sensitive than nitroglycerine. [4] Another member of acetylenic energetic materials is propargyl nitramine, which has been discussed due to its high specific impulse of $I_{sp} = 233\,s$ as a liquid monopropellant for rocket motors. [5] The high volatility limits its usage for standard applications drastically, but opens possibilities for structural investigations in the gas phase. The related propargyl azide was investigated by means of gas-phase electron diffraction (GED). Its hydrocarbon skeleton has been found to adopt a *gauche* conformation with respect to the azide group. [6]

Earlier reports have shown that the reaction of acetylenes with HNO_3 can result in the formation of isoxazole heterocycles. [7–12] Propargyl nitrate, $HC{\equiv}CCH_2ONO_2$ (**1**), among other acetylene and diacetylene alcohols, has been prepared by nitration of propargyl alcohol, [13] but only poorly characterized. Hexanitrohex-3-yne, $(NO_2)_3CCH_2C{\equiv}CCH_2C(NO_2)_3$ (**2**), another known energetic acetylene derivative, has also been only insufficiently described and characterized. [14] In addition, for **2** the results of theoretical studies predicting impact sensitivities have been reported. [15–19] 1,1,1-Trinitroethane, $(NO_2)_3CCH_3$ (**3**), was first briefly mentioned in 1886. [20] Further

work on **3** was performed together with the discovery of silver trinitromethanide used as a starting material.[21] Some mechanistic studies on the synthesis of **3** by alkylation reaction using silver trinitromethanide and methyl iodide followed.[22] This synthesis and its kinetics have been further investigated more than half a century later.[23] Various formation reactions of **3** have been reported,[21,24–26] as well as some characterization using NMR spectroscopy,[26–30] vibrational spectroscopy[31,32] and mass spectrometry[33–35]. Apart from some basic theoretical predictions of its molecular geometry,[22,36] structural studies of **3** using X-ray diffraction have not been undertaken so far (*cf.* our initial results displayed in ref. 37).

In this contribution, the results of a detailed study of the synthesis and characterization of propargyl nitrate (**1**), 1,1,1,6,6,6-hexanitrohex-3-yne (**2**), and 1,1,1-trinitroethane (**3**) are presented.

5.3. Results and Discussion

Synthesis and spectroscopic characterizations

Propargyl nitrate (**1**) was synthesized by using the well-established nitration system Ac_2O/HNO_3 (100 %). Due to its high volatility, the gas phase structure could be determined by means of gas electron diffraction (GED) along with quantum chemical calculations.
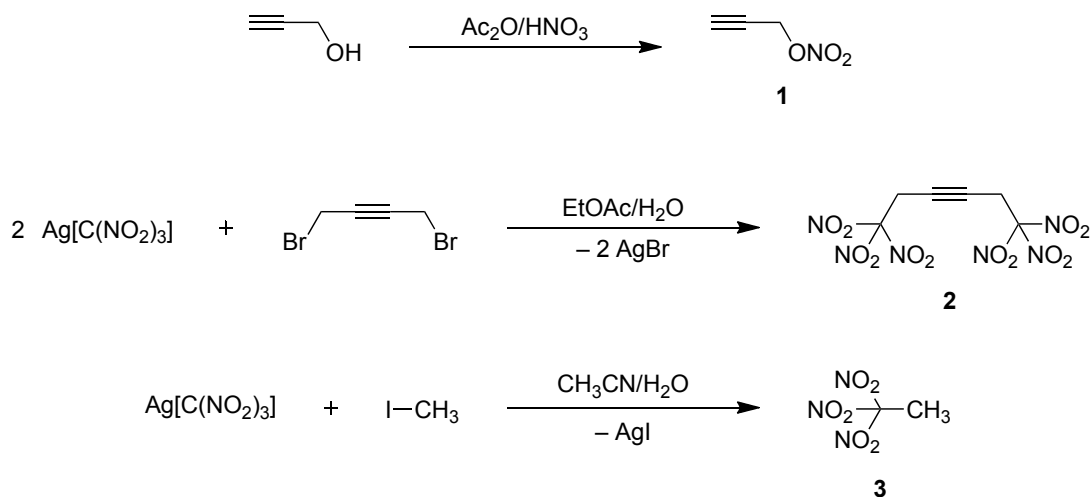
Scheme 1: Synthesis of compounds **1**–**3**.

The synthesis of 1,1,1,6,6,6-hexanitrohex-3-yne (**2**) and 1,1,1-trinitroethane (**3**) was performed by alkylation reactions of silver trinitromethanide with the appropriate aliphatic halides (Scheme 1). The driving force of this reaction, which works even at

ambient temperature, is the affinity of the silver cation to heavier halide ions, *i. e.* the formation of silver bromide for **2** and silver iodide for **3**. By contrast, the reactions of 1,4-dibromobut-2-yne or iodomethane with potassium trinitromethanide did not yield a product, although a very slow reaction of iodomethane with potassium trinitromethanide in acetone has earlier been reported.[38,39] The progress and extent of the formation of **2** and **3** can be conveniently followed by filtering and weighing the precipitated silver halides. Previous kinetic and mechanistic investigations of silver salts with alkyl halides have supported a mechanism which has both S_N1 and S_N2 character.[23,40] The alkylation can proceed in two directions, either by C- or O-alkylation. It was found that the formation of unstable O-alkylated products is predominant for many halides other than primary halides.[23,41–43] The alkylation of silver trinitromethanide to form **2** and **3** leads primarily to the desired C-alkylated products, due to the lack of stabilization of a S_N1-type transition state.[22,42] Solvent effects on alkylation reactions of silver trinitromethanide have earlier been investigated.[23]

To achieve a successful synthesis and a high conversion rate, silver trinitromethanide should be freshly prepared and be used in situ. The presence of water stabilizes silver trinitromethanide against decomposition to silver nitrate and nitrogen oxides. Otherwise, silver nitrate would react more rapidly with alkyl halides than silver trinitromethanide, to form nitrate esters and not the desired trinitromethyl derivatives.[23] In this context it should be noted that only reports on the crystal structure of silver trinitromethanide as a mono- or hemihydrate have been published.[22,44] The decomposition mechanism is analogous to that of the corresponding potassium salt.[21,23] The synthesis of silver trinitromethanide described in the literature uses moist silver oxide and trinitromethane.[21,23,44] It was found in this work that the use of silver carbonate or acetate instead is more convenient due to more facile work-up and increased yields. Both reactions can be performed in water or acetonitrile as solvents.

The solubility of $Ag[C(NO_2)_3]$ in several polar solvents enabled ^{109}Ag and ^{14}N NMR studies and showed that the NMR chemical shift is highly dependent on the nature and polarity of the coordinating solvent (Table 1). This is due to the formation of silver complexes with electron donating solvents,[23,45] which results in significant shifts of the ^{109}Ag and, to some extent, the ^{14}N NMR resonances. Similar large shielding variations have been observed in ^{109}Ag NMR spectra of silver halides in S/N/O-bonded ligands, but not, as in this case, to a complex anion, such as the trinitromethanide anion.[46]

Gas-phase structure analysis

GED structure models. Two conformers of **1** (*gauche* and *anti*, Figure 1) differing with respect to the dihedral angle N6/N16−O5/O15−C4/C14−C3/C13 have been included into the structure refinement model. Based on the results of quantum chemical

Table 1.: ^{109}Ag and ^{14}N NMR data of silver trinitromethanide (in ppm).

Solvent	Ag[C(NO$_2$)$_3$]	
	$\delta\,^{109}$Ag	$\delta\,^{14}$N
D$_2$O	27.5	−33
[D$_4$]Methanol	48.8	−24
[D$_6$]Acetone	108.4	−20
[D$_6$]DMSO	181.1	−30
[D$_3$]Acetonitrile	429.7	−29

calculations the following model assumptions were made: For both conformers planarity of the NO$_3$ moieties, linearity of the HCCC moieties and equal C−H distances; moreover, C_s symmetry was assumed for the *anti*-conformer. The remaining degrees of freedom to describe the molecular structures of both conformers were chosen as the following set of primitive internal coordinates: H1−C2, C2≡C3, C3−C4, C4−H9, C4−H10, C4−O5, O5−N6, N6=O8, N6=O7 (bonded lengths); O8−N6−O5, O8=N6=O7, N6−O5−C4, H9−C4−H10; H9−C4−H10$_{rock}$, H9−C4−H10$_{twist}$ H9−C4−H10$_{wagg}$ (angles; *rock*-, *twist*- and *wag*-angular degrees of freedom are defined according to the nomenclature for vibrational spectroscopy.[47]; the deviations of these angles refer to the fully regular tetrahedral configuration); N6−O5−C4−C3, O8−N6−O5−C4 (torsions); and the respective internal coordinates for the *anti*-conformer. In agreement with the C_s symmetry constraint in the *anti*-conformer, the H19−C14−H20$_{rock}$ and the H19−C14−H20$_{twist}$ angles were fixed to 0°, the N16−O15−C14−C13 dihedral angle was set to 180°, and the O18−N16−O15−C14 dihedral angle was set to 0°.
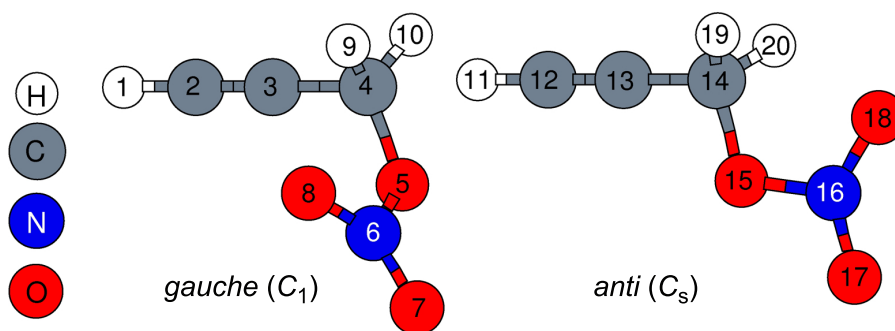
Figure 1.: Molecular structures of *gauche*- and *anti*-HCCCH$_2$ONO$_2$ (**1**), showing the atom-numbering scheme used for the GED structure refinement.

GED structure refinement. Due to the occurrence of two conformations of **1** (Figure 1) in significant amounts and a subset of structure parameters

Table 2.: Independent parameters [a] used in the GED refinement of **1** (refined parameter values, calculated values obtained at the SCS-MP2/TZVPP level of theory, and applied restraints).

	Parameter description	GED r_a	GED $r_{a3,1}$	MP2 r_e	Restraint uncertainty [b]
p_1	d N6−O5−C4−C3	83.8(9)	86(1)	77.3	∞
p_2	d O7−N6−O5−C4	168(1)	168(2)	−175.1	∞
p_3	rXX^s_{m1} average (*gauche, anti*)	1.203(1)	1.2015(9)	1.1943	∞
p_4	rXX^s_{m1} diff. (*gauche, anti*)	0.0013(1)	0.0013(1)	0.0013	0.0001
p_5	rXX^l_{m1} average (*gauche, anti*)	1.447(1)	1.435(1)	1.427	∞
p_6	rXX^l_{m1} diff. (*gauche, anti*)	−0.009(1)	−0.008(8)	−0.003	∞
p_7	rXX^s_{m2} average (*gauche, anti*)	0.005			0
p_8	rXX^s_{m2} diff. (*gauche, anti*)	0.0			0
p_9	rXX^l_{m2} average (*gauche, anti*)	0.023(6)	0.024(6)	0.026	∞
p_{10}	rXX^l_{m2} diff. (*gauche, anti*)	0.0025			0
p_{11}	rXX^s_{m3} average (*gauche, anti*)	−0.03(3)	−0.03(3)	−0.01	∞
p_{12}	rXX^s_{m3} diff. (*gauche, anti*)	−0.008			0
p_{13}	rXX^l_{m3} average (*gauche, anti*)	−0.05(2)	−0.03(2)	0.02	∞
p_{14}	rXX^l_{m3} diff. (*gauche, anti*)	−0.029			0
p_{15}	$[\angle$(O18−N16−O17) $+ \angle$(O8−N6−O7)]/2	132.0(7)	131.3(8)	130.1	∞
p_{16}	$[\angle$(O18−N16−O17) $- \angle$(O8−N6−O7)]/2	−0.3			0
p_{17}	$[\angle$(O15−N16−O17) $+ \angle$(O5−N6−O7)]/2	111.8(8)	112.7(6)	112.6	∞
p_{18}	$[\angle$(O15−N16−O17) $- \angle$(O5−N6−O7)]/2	0.4			0
p_{19}	$[\angle$(N16−O15−C14) $+ \angle$(N6−O5−C4)]/2	114.4(4)	112.4(4)	113.1	∞
p_{20}	$[\angle$(N16−O15−C14) $- \angle$(N6−O5−C4)]/2	0.0			0
p_{21}	$[\angle$(O15−C14−C13) $+ \angle$(O5−C4−C3)]/2	107.7(4)	109.4(5)	108.2	∞
p_{22}	$[\angle$(O15−C14−C13) $- \angle$(O5−C4−C3)]/2	−2.6			0
p_{23}	rCH average (CH$_2$, CH)	1.097(6)	1.095(5)	1.099	0.01
p_{24}	rCH diff. (CH$_2$, CH)	0.0275			0
p_{25}	$\angle$CH$_2$	108.2			0
p_{26}	*rock* (CH$_2$, *gauche*)	2.8			0
p_{27}	*twist* (CH$_2$, *gauche*)	3.9			0
p_{28}	*wagg* (CH$_2$, *gauche*)	−16.8			0
p_{29}	*fraction*(*anti*)	69(2) %	69(2) %	70 % [c]	∞
	R-factor (R_G)	8.08 %	8.72 %	–	–

[a] All distances are in Å, and angles are in degrees. The two sets of parameter values for the GED refinement, r_a and r_e, correspond to different approaches accounting for vibrational motion. The r_a structure is based on harmonic thermal average distances, whilst the $r_{a3,1}$ structure is an approximation to an equilibrium structure r_e based on a computed (DFT, see Experimental Section) cubic molecular force field; [51–53] [b] "0" for unrefined (=fixed) values, "∞" for freely refined (unrestrained); [c] estimated from $k = \exp(-\Delta E/RT)$, $R = 8.314\,\mathrm{J\,mol^{-1}\,K^{-1}}$, $T = 293\,\mathrm{K}$, $\Delta E = -0.55\,\mathrm{kcal\,mol^{-1}}$ (from the SCS-MP2/TZVPP calculation).

corresponding to bonded interatomic distances similar in size, inter-parameter correlation in the least-squares refinement procedure has to be expected. In order to circumvent correlation problems to some extent, problem adapted combinations of internal coordinates were formed. The general strategy for such a procedure has previously been outlined.[48] For example, the three short bonded inter-heavy-atom-distances $C2\equiv C3$, $N6=O8$, and $N6=O7$ (given in increasing size according to the calculated values) were transformed into the three problem adapted linear combinations $rXX^{s}_{m1}{}^{gauche} = (C2\equiv C3 + N6=O8 + N6=O7)/3$, $rXX^{s}_{m2}{}^{gauche} = (C2\equiv C3 - N6=O7)/2$ and $rXX^{s}_{m3}{}^{gauche} = (C2\equiv C3 - 2\times N6=O8 + N6=O7)$. For the *anti*-conformer similar parameters were defined ($rXX^{s}_{m1}{}^{anti}$, $rXX^{s}_{m2}{}^{anti}$, $rXX^{s}_{m3}{}^{anti}$). Moreover, corresponding parameters in the two different conformers of **1** (*anti* and *gauche*) were transformed into a set of average and difference parameters, for example: $p_{15} = (O8=N6=O7 + O18=N16=O7)/2$ and $p_{16} = (O8=N6=O7 - O18=N16=O7)/2$ or $p_{3} = (rXX^{s}_{m1}{}^{gauche} + rXX^{s}_{m1}{}^{anti})/2$ and $p_{4} = (rXX^{s}_{m1}{}^{gauche} - rXX^{s}_{m1}{}^{anti})/2$. The resulting set of independent parameters, together with the refined values and applied restraints and constraints is given in Table 2. The refinement was performed according to the SARACEN method,[49,50] which places flexible restraints on parameters that are not well resolved from the GED experiment, with the value of the restraint and the uncertainty estimated from calculated values. The experimental molecular intensity and radial distribution curves are shown in Figures 2 and 3, with the refined difference curves at the bottom of each figure.

Amplitudes of vibration were also refined for both molecules, but those corresponding to distances under a single peak in the respective radial-distribution curve (RDC, see Figure 3) were grouped together by fixing relative amplitude ratios. Restraints of 10 % of the calculated values were applied to the refined reference amplitudes. The full lists of inter-atomic distances, amplitudes of vibration and distance corrections for the $r_{a3,1}$ refinements, including details of which amplitudes were kept at fixed ratios and which were refined, are provided as Supporting Information.

The refinement of the structure of **1** yielded a good fit of the experimental to the theoretical intensities for both the r_{a} and $r_{a3,1}$ structure types, as can be seen from the low R_{G} factors of 8.1 % and 8.7 %, (Tables 2 and 3) respectively. The quality of the fit can also be judged by the appearance of the molecular intensity and radial distribution curves (Figures 2 and 3).

Discussion of gas-phase geometries. The ratio of the *anti*-conformer to the total amount of compound under the conditions of the GED experiment was refined to 69(2) %, which is in agreement with the calculated *ab initio* total energy difference of 0.6 kcal mol^{-1} (*gauche-anti*, SCS-MP2/TZVPP). A selection of the important geometric parameters from the GED structure refinement and the corresponding values determined

Table 3.: Structure parameters from the GED refinement of *anti-* and *gauche-*HCCCH$_2$ONO$_2$ and calculated values obtained at the HF/ and SCS-MP2/TZVPP level of theory (distances [Å], angles in [deg])

Dependent parameter	GED $r_{a3,1}$	GED r_a	MP2 r_e	HF r_e
N6−O7	1.191(6)	1.194(5)	1.201	1.167
N6−O8	1.211(10)	1.214(9)	1.206	1.176
C2−C3	1.201(6)	1.204(5)	1.212	1.180
N6−O5	1.413(6)	1.427(6)	1.423	1.336
C4−O5	1.445(5)	1.459(5)	1.439	1.424
C3−C4	1.458(11)	1.466(10)	1.463	1.464
C3−C4−O5	110.7(5)	110.3(4)	112.6	112.7
C4−O5−N6	112.4(4)	113.7(3)	112.8	116.7
O5−N6−O7	112.4(9)	111.3(8)	112.1	113.5
O5−N6−O8	116.2(3)	116.8(3)	117.3	118.0
O7−N6−O8	131.5(8)	131.9(7)	130.6	128.5
N16−O17	1.191(6)	1.194(5)	1.201	1.167
N16−O18	1.215(10)	1.218(9)	1.209	1.179
C12−C13	1.201(6)	1.204(5)	1.211	1.197
N16−O15	1.398(7)	1.408(6)	1.414	1.331
C14−O15	1.447(9)	1.456(9)	1.446	1.430
C13−C14	1.448(7)	1.452(6)	1.459	1.460
C13−C14−O15	108.1(5)	107.7(5)	105.8	106.6
C14−O15−N16	112.4(4)	113.7(3)	112.0	115.4
O15−N16−O17	112.8(9)	111.7(8)	112.5	117.8
O15−N16−O18	116.1(3)	116.7(3)	117.3	113.9
O17−N16−O18	131.2(8)	131.6(7)	130.2	128.4

in the *ab initio* calculations are displayed in Table 3. GED parameters are given in terms of both the r_a and $r_{a3,1}$ structure types. The inter-nuclear distance obtained directly from the GED data, r_a, is the harmonic mean and can be converted to the arithmetic mean, r_g, using the root-mean-squared amplitude of vibration, u : $r_g \approx r_a + u^2/r$. Distance corrections, k, are regularly applied in GED refinements to account for the 'shrinkage' effect. When the vibrational motion is considered to be harmonic with curvilinear trajectories, the resulting distances and distance corrections are termed r_{h1} and k_{h1}, respectively. Comparison of the calculated values indicates that the alkyne and methylene groups are well described by HF theory, with only small changes in the values of these parameters as the theoretical treatment is improved by way of MP2 theory. In contrast, the HF model appears to have severe limitations with regard to the treatment of the nitrate group. The terminal N−O bonds are significantly elongated
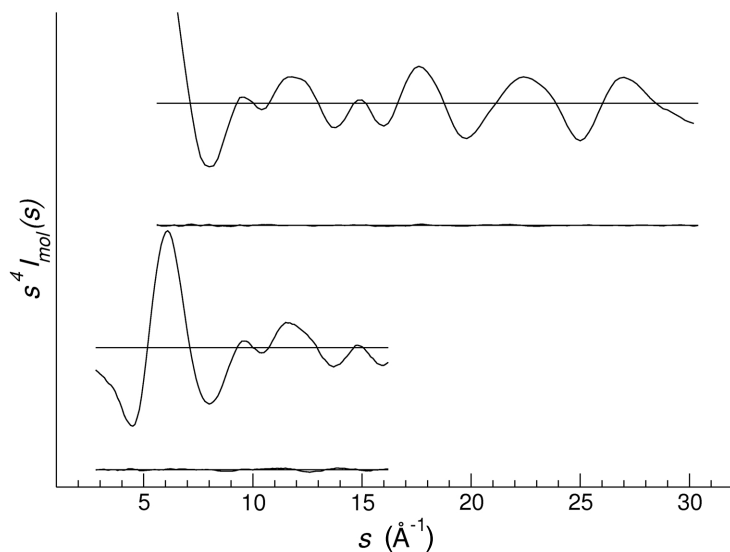
Figure 2.: Experimental and difference (experimental minus theoretical) molecular intensity curves for **1**.

upon introduction of a MP2 correction by about 3 pm when the geometries calculated with identical basis sets are compared. The largest discrepancy between the HF and MP2 geometries is in the length of the N6−O5 bond, which increases by 0.09 Å.
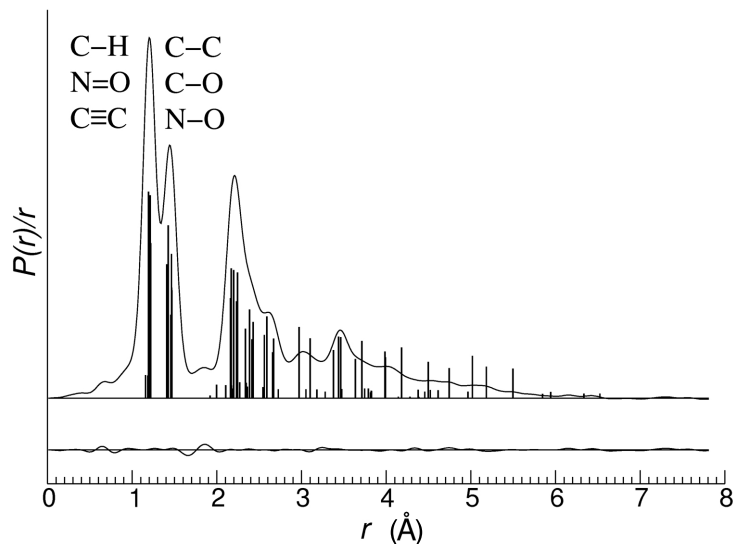
Figure 3.: Experimental and difference (experimental minus theoretical) radial distribution curves for **1**.

X-ray structure determination

Single crystals suitable for X-ray diffraction measurements were obtained by crystallization at lower temperatures ($-25\,^{\circ}\mathrm{C}$) from chloroform (**2**) or from boiling *n*-pentane (**3**). Full lists of crystallographic refinement parameters and structure data for **2** and **3** are shown in Table 4.
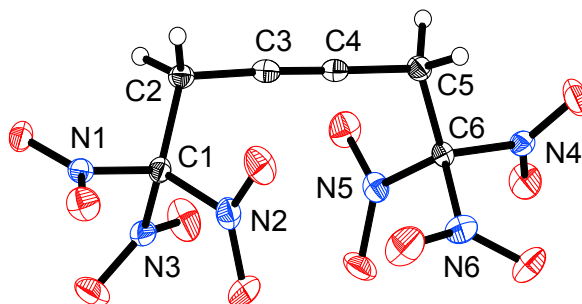
Figure 4.: Molecular structure of **2**. Selected distances [Å] and angles [deg]: C1−N1 1.516(2), C1−N2 1.524(2), C1−N3 1.525(2), C1−C2 1.511(2), C2−C3 1.468(2), C3−C4 1.181(2), C4−C5 1.461(2), C5−C6 1.513(2), C6−N4 1.526(2), C6−N5 1.522(2), C6−N6 1.529(2), N1−C1−C2 111.0(2), N2−C1−C2 113.2(2), N3−C1−C2 113.6(2), C1−C2−C3 112.0(2), C2−C3−C4 176.7(2), C3−C4−C5 178.1(2), C4−C5−C6 112.9(2), C5−C6−N4 111.4(2), C5−C6−N5 112.9(2), C5−C6−N6 112.6(1).

The molecular structures of **2** (Figure 4) and **3** (Figure 5) confirm clearly the preference of C-alkylations vs. O-alkylations, which were predicted many years earlier.[22,36] The C3≡C4 bond length of **2** is 1.181(2) Å, whereas the bond lengths of the single bonds C2−C3 (1.468(2) Å) and C4−C5 (1.461(2) Å) are shorter compared to that of C1−C2 (1.511(2) Å) and C5−C6 (1.513(2) Å). For **3**, the C1−C2 bond length is 1.480(4) Å. All bond lengths in **2** and **3** are shorter than a regular C−C bond length of sp^3-hybridized carbon atoms (1.54 Å). Due to the highly symmetrical cubic space group, the molecular structure of **3** shows a threefold axis along the C1−C2 bond. Hence, only one nitro group is included in the asymmetric unit while the others are symmetry generated, in an analogous manner as in the related structure of trinitromethane.[54] As expected, all nitro groups in **2** and **3** are planar. All bond lengths and angles were found in the range typical for polynitro aliphatic CHNO compounds, especially the elongated C−N bonds.[54–57] The trinitromethyl moieties show an approximate (for **2**) or true (for **3**) C_3 axis with propeller-like twisted nitro groups (Figures 4 and 5).[55–57] The nitro groups of **3** are rotated out of the C C N plane by 39.6°, which is slightly smaller than in trinitromethane.[54] For **2**, these C−C−N−O dihedral angles are in the range
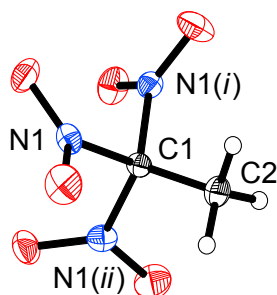
Figure 5.: Molecular structure of **3**. Selected distances [Å] and angles [deg]: C1−C2 1.480(4), C1−N1/N1(*i*)/N1(*ii*) 1.529(2), C2−C1−N1/N1(*i*)/N1(*ii*) 113.4(1), N1−C1−N1(*i*)/N1(*ii*); N1(*i*)−C1−N1(*ii*) 105.3(1). *i* = −*y*, −0.5+*z*, 0.5−*x*; *ii* = 0.5−*z*, −*x*, 0.5+*y*.

between 33.1–56.7°, quite common values for the trinitromethyl moiety without external perturbation.[54–57] This propeller-like twisting of the trinitromethyl moiety optimizes the non-bonded intramolecular N···O attractions between two adjacent nitro groups, while the corresponding O···O repulsions are minimized.[56,57] These attractive N···O contacts were found in the range of 2.54–2.60 Å (for **2**) and 2.56 Å (for **3**), considerably lower than the sum of the van der Waals radii for nitrogen and oxygen (3.07 Å).[58] The N−C−N angles of **2** and **3** are in the range 105.7–107.5° and therefore considerably smaller than the ideal tetrahedral value of 109.5°.[54–57] This is exactly the opposite of what is expected from steric interactions which would result in larger angles, but confirms the existence of N···O attractions within the trinitromethyl moiety.[55]

The molecular structure of **2** reveals surprisingly the *cis*-isomer regarding the trinitromethyl moiety, which seems quite uncommon considering steric effects. The two trinitromethyl moieties are rotated against each other with a small torsion angle of 31.7° between the C1−C2 and C5−C6 bonds (Figure 4), probably also due to attractive N···O interactions between the trinitromethyl moieties. Although these N···O contacts (3.35/3.44 Å) are longer than the sum of the van der Waals radii (3.07 Å),[58] the partial charge distribution in nitro groups could lead to an appreciable Coulomb attraction. This proposal is supported by the fact that the oxygen atoms of one trinitromethyl moiety are pointing exactly towards the nitrogen atoms of the other moiety.

For steric reasons, in **3** the conformation of the hydrogen atoms and the nitro groups is staggered. The H−C1−C2−N1 dihedral angles are 53.8°/66.2°, compared to the ideal value of 60°. Each hydrogen atom of the methyl group in **3** is involved in one H···O interactions with two different adjacent molecules, leading to a total of three

Table 4.: Crystal and structure determination data for **2** and **3**.

	2	**3**
Formula	$C_6H_4N_6O_{12}$	$C_2H_3N_3O_6$
M_r [g mol^{-1}]	352.13	165.06
Cryst. size [mm^3]	$0.41 \times 0.40 \times 0.35$	$0.20 \times 0.19 \times 0.06$
Crystal description	colorless block	colorless block
Crystal system	orthorhombic	cubic
Space group	$Pbca$	$I\bar{4}3d$
a [Å]	12.9956(5)	13.6162(4)
b [Å]	13.0433(4)	13.6162(4)
c [Å]	15.1771(5)	13.6162(4)
V [Å^3]	2572.60(15)	2524.5(2)
Z	8	16
$D_{calcd.}$ [g cm^{-3}]	1.82	1.74
Temperature [K]	100(2)	100(2)
θ range [deg]	3.75–26.00	4.73–25.99
$\mu(MoK_\alpha)$ [mm^{-1}]	0.2	0.2
$F(000)$[e]	1424	1344
hkl range	$-9 \leq h \leq +15$	$-16 \leq h \leq +6$
	$-7 \leq k \leq +16$	$-4 \leq k \leq +16$
	$-18 \leq l \leq +10$	$-11 \leq l \leq +9$
Refl. measured	5183	1018
Refl. independent	2460	387
Refl. "observed" with $I > 2\sigma(I)$	1703	306
R_{int}	0.0209	0.0251
Param. refined	217	38
$R(F)/wR(F^2)$ [a,b] $[I > 2\sigma(I)]$	0.0294 / 0.0575	0.0237 / 0.0337
$R(F)/wR(F^2)$ [a,b] (all refls.)	0.0490 / 0.0599	0.0355 / 0.0347
GoF (F^2) [c]	0.870	0.832
$\Delta\rho_{fin}$ (max/min) [e Å^{-3}]	0.238 / -0.214	0.124 / -0.107

[a] $R1 = \sum ||F_o| - |F_c||/ \sum |F_o|$. [b] $wR2 = \left[\sum w(F_o^2 - F_c^2)^2/ \sum w(F_o^2)^2\right]^{1/2}$, $w = \left[\sigma^2(F_o^2) + (AP)^2 + BP\right]^{-1}$, where $P = (\text{Max}(F_o^2, 0) + 2 F_c^2)/3$ and A and B are constants adjusted by the program. [c] GoF $= S = \left[\sum w(F_o^2 - F_c^2)^2/(n_{obs} - n_{param})\right]^{1/2}$, where n_{obs} is the number of data and n_{param} the number of refined parameters.

hydrogen bonds per molecule. This contact (2.60 Å) is only slightly shorter than the sum of the van der Waals radii (2.62 Å)[58] and consequently a weak interaction. The hydrogen atoms in **2** make a total of four hydrogen bonds to four adjacent molecules. Compared to **3**, these hydrogen bonds in the range 2.46–2.56 Å are slightly shorter.

Energetic properties

The DSC diagram of **3** shows three endothermic signals in the range of 25–400 °C. Beside the melting point at 53 °C and the boiling point at 194 °C (Table 5), an enantiotropic phase transition occurs at 39 °C. This polymorphism of **3** has previously been reported, [59] as an example for the observation that compounds whose molecular shapes are nearly spherical show enantiotropic polymorphism. [57,60] Furthermore, this molecular rotational freedom in the solid state leads to an unusual high melting point. [60]

According to the UN recommendations, [61] **1** and **2** are classified as very sensitive towards impact and friction, whereas **3** is classified as sensitive (*cf.* Table 5). Attempts to adsorb **1** on nitrocellulose to desensitize the material failed. This shows that the vapor pressure is too high for any standard application as double-based propellant.

Predictions of the detonation parameters using the EXPLO5 [62–65] code were made based on the energies of formation, calculated *ab inito* using the GAUSSIAN 09 program package [66]. The energetic properties, calculated detonation parameters as well as further calculated energies and enthalpies of formation of **1**–**3** are shown in Table 5.

5.4. Conclusion

The structures of *anti*- and *gauche*-propargyl nitrate (**1**) in the gas phase have been determined by electron diffraction, and that of hexanitrohex-3-yne (**2**) and 1,1,1-trinitroethane (**3**) in the crystalline state by X-ray diffraction. A vapor composition with 69(2) % *anti*-conformer was found in the GED experiment for **1**, in good agreement with relative conformer energy values from *ab initio* calculations. The structural parameters resulting from the GED date are also in good agreement with computational values. A propeller-type twisting of the trinitromethyl moieties is present in the crystal structures of both **2** and **3** because of N···O interactions. Furthermore, an NMR study (^{109}Ag and ^{14}N) of the important precursor silver trinitromethanide in various solvents was performed and showed significant differences in the corresponding chemical shifts.

5.5. Experimental Section

General procedures. All manipulation of air- and moisture-sensitive materials were performed under an inert atmosphere of dry nitrogen using flame-dried glass vessels and Schlenk techniques. [67] Due to the light sensitivity of silver salts, reactions with silver acetate and silver carbonate were performed under the absence of light. The solvents and silver acetate (Fluka), silver carbonate (ABCR), and iodomethane (Acros Organics) were used as received. The aqueous solution of trinitromethane (Aerospace Propulsion Products B. V.) was extracted and purified by precipitation of its potassium

Table 5.: Energetic properties, calculated values and predicted detonation parameters of **1**–**3**.

	1	**2**	**3**
Chemical formula	$C_3H_3NO_3$	$C_6H_4N_6O_{12}$	$C_2H_3N_3O_6$
Formula weight, $g\,mol^{-1}$	101.06	352.13	165.06
N [%] [a]	13.86	23.87	25.46
$N + O$ [%] [b]	61.35	78.39	83.62
Ω_{CO} [%] [c]	-23.8	$+18.2$	$+24.2$
Ω_{CO_2} [%] [d]	-71.2	-9.1	$+4.9$
Grain size [μm] [e]	(liquid)	500–1000	500–1000
Impact [J] [f]	1	3	8
Friction [N] [g]	72	72	96
ESD [J] [h]	$-$[1]	0.08	0.1
T_m [°C] [i]	$-$	126	53
T_b/T_d, [°C] [j]	132 (dec.)	193 (dec.)	194 (boil.)
ρ [$g\,cm^{-3}$] [k]	1.20 (est.)	1.818 (XRD)	1.737 (XRD)
H_{CBS-4M} [H] [l]	-395.832687 [2] -395.831469 [3]	-1459.864955	-692.516945
ΔH_f° [$kJ\,mol^{-1}$] [m]	114.68 [2]/102.99 [3]	119.65	-120.36
ΔU_f° [$kJ\,kg^{-1}$] [n]	1220.65 [2]/1252.29 [3]	417.23	-639.08
Q_v [$kJ\,kg^{-1}$] [o]	-6990 [2]/-7020 [3]	-7068	-6123
T_{ex} [K] [p]	4661 [2]/4676 [3]	5258	4615
p [kbar] [q]	148 [2]/149 [3]	351	309
D [$m\,s^{-1}$] [r]	6613 [2]/6622 [3]	8535	8306
V_0 [$L\,kg^{-1}$] [s]	679 [2]/679 [3]	625	711
I_s [s^{-1}] [t]	260 [2]/261 [3]	274	262

[a] Nitrogen content. [b] Combined nitrogen and oxygen content. [c] Oxygen balance assuming the formation of CO. [d] Oxygen balance assuming the formation of CO_2. [e] Grain size of the samples used for sensitivity tests. [f] Impact sensitivity. [g] Friction sensitivity. [h] Sensitivity towards electrostatic discharge. [i] Melting point. [j] Boiling (boil.) or decomposition (dec.) point. [k] Density estimated (est.) or calculated from X-ray diffraction (XRD). [l] Enthalpy derived from quantum chemical CBS-4M calculation. [m] Enthalpy of formation (calculated). [n] Energy of formation (calculated). [o] Detonation energy (calculated). [p] Explosion temperature (calculated). [q] Detonation pressure (calculated). [r] Detonation velocity (calculated). [s] Gas volume (calculated, assuming only gaseous products). [t] Specific impulse (calculated isobaric combustion with 100 % **1**, **2** or **3** at 70 bar chamber pressure, equilibrium expansion against 1.0 bar ambient pressure).
[1] Not determined (ESD test not measurable for liquids). [2] *gauche*-Propargyl nitrate. [3] *anti*-Propargyl nitrate.

salt and subsequent acidification. 1,4-Dibromobut-2-yne was synthesized according to the literature procedure.[68] Raman spectra were recorded with a Bruker MultiRAM

FT-Raman instrument fitted with a liquid nitrogen cooled germanium detector and a Nd:YAG laser ($\lambda = 1064\,\text{nm}$, $300\,\text{mW}$). Infrared (IR) spectra were measured with a Perkin-Elmer Spectrum BX FTIR spectrometer equipped with a Smiths DuraSampl*IR* II ATR device. All spectra were recorded at ambient temperature, the samples were neat solids. NMR spectra were recorded at $25\,°\text{C}$ with a JEOL Eclipse 400 instrument, and chemical shifts were determined with respect to external Me_4Si (^{1}H, $400.2\,\text{MHz}$; ^{13}C, $100.6\,\text{MHz}$), $MeNO_2$ (^{14}N, $29.0\,\text{MHz}$; ^{15}N, $40.6\,\text{MHz}$), and $0.5\,\text{M}$ $AgNO_3$ in D_2O (^{109}Ag, $18.6\,\text{MHz}$). Mass spectrometric data were obtained with a JEOL MStation JMS 700 spectrometer (DEI+, DCI+). The fragments are referred to the isotope with the highest natural abundance. Elemental analyses (C/H/N) were performed with a Elementar vario EL analyzer. Melting points and decomposition points were determined by differential scanning calorimetry (DSC) measurements with a Linseis DSC-PT10 apparatus, using a heating rate of $5\,°\text{C}\,\text{min}^{-1}$. Sensitivity data (impact, friction, and electrostatic discharge) were performed using a drophammer, friction tester, and electrostatic discharge device conform to the directive of the Federal Institute for Materials Research and Testing (BAM).[69]

Computational methods. Hartree-Fock (HF) calculations were of the restricted type and the second-order Møller-Plesset (MP2) calculations made use of the resolution-of-the-identity (RI) method and the default frozen-core partitioning as implemented in Turbomole (Version 5.7).[70] The DFT calculation using 6-311++G** type basis sets and the B3LYP functional were performed using the default criteria in Gaussian 03 (Revision C.02),[71] whilst those using the def2-TZVPP (herein shortened to TZVPP) basis set were performed using Turbomole (Version 5.7).

Gas electron diffraction (GED). Electron scattering intensities were recorded at room temperature on a combination of reusable Fuji and Kodak imaging plates using a Balzers KD-G2 Gas-Eldigraph.[72,73] This device was equipped with an electron source built by STAIB Instruments, and was operated at $60\,\text{kV}$ when recording data. The accelerating voltage was stable to within 1 to $2\,\text{V}$ during the course of the experiment. The image plates were scanned using a Fuji BAS 1800 II scanner, yielding digital 16-bit grey-scale image data. Further details about the Bielefeld GED apparatus and the experimental methods are published elsewhere.[48] In preparation for data reduction, the long and short nozzle-to-plate distances were re-measured after recording the short-distance data and before recording the long-distance data. The relative scaling of the two scanning directions was recalibrated using an exposed image plate with two pairs of pin holes, which was scanned in two orientations, approximately perpendicular to one another. The data were reduced to total intensities using Pimag (version 040827)[74] in connection with a sector curve, which was based on experimental xenon scattering data and tabulated scattering factors of xenon. Further data reduction yielding molecular intensity curves

was performed using the ED@ED program (Version 3.0)[75] and scattering factors.[76] For both compounds the ratio of the electron wavelength to the nozzle-to-plate distances was checked using benzene data and the widely accepted r_a value of 1.397 Å for the C−C distance in benzene. The data reduction was performed using indirectly determined nozzle-to-plate distances. The electron wavelengths and nozzle-to-plate distances are provided as Supporting Information, along with other data analysis parameters including the s limits, weighting points, R factors (R_D and R_G), scale factors, data correlation values and the correlation matrix. The amplitudes of vibration, u, used in r_e (by approximated anharmonic corrections implemented as $r_{a3,1}$ in ED@ED) refinement and the anharmonic distance corrections were calculated using the program SHRINK[51,53]. This made use of anharmonic force field calculations at the B3LYP/6-311++G** level of theory (see above for details of computational methods). The SHRINK input files were generated using Q2SHRINK[77].

Energetic properties. All quantum chemical calculations for the prediction of the energetic properties were carried out using the program package Gaussian 09 (Revision C.01),[66] additionally prepared and visualized with GaussView 5 (Version 5.0.8).[78] The initial geometries of the structures were taken from the corresponding, experimentally determined, crystal structures. The enthalpies (H) and free energies (G) were calculated using the complete basis set (CBS) method in order to obtain very accurate values.[79–82] This method is a complex energy computation involving several pre-defined calculations on the specified system. The used method CBS-4M ('M' referring to the use of minimal population localization) is an updated version of the modified CBS-4 method[83,84] with both the new localization procedure and improved empirical parameters.[84] The liquid (**1**) and solid (**2**, **3**) state enthalpies and energies of formation were calculated from the corresponding enthalpy derived from these quantum chemical CBS-4M calculations ($H_{\text{CBS-4M}}$). Therefore, the enthalpies of formation of the gas-phase species were computed according to the atomization energy method.[85–87] The liquid (solid) state energies of formation (ΔH_f°) were estimated by subtracting the gas-phase enthalpies with the corresponding enthalpy of vaporization (sublimation) obtained by Trouton's rule.[88,89] These enthalpies of formation were used to calculate the energies of formation (ΔU_f°). The calculation of the detonation parameters were performed using the program EXPLO5 (Version 5.05).[62–65] The input was made using the sum formula, the liquid respectively solid state energies of formation and the experimentally determined densities, derived from the corresponding single crystal X-ray structures.

X-ray crystallography. For both compounds, an Oxford Xcalibur3 diffractometer with a CCD area detector was employed for data collection using MoK_α radiation ($\lambda = 0.710\,73$ Å). The structures were solved using Direct Methods (SIR2004)[90,91] and refined by full-matrix least-squares on F^2 (SHELXL-97)[92,93]. All non-hydrogen atoms

were refined anisotropically. The hydrogen atoms were located in difference Fourier maps and placed with a C−H distance of 0.99 Å for CH_2 groups, C−H distances for the CH_3 group were refined. ORTEP plots are shown with thermal ellipsoids at the 50 % probability level. CCDC 900037 (**2**), and 900038 (**3**) contain the supplementary crystallographic data for this paper. These data can be obtained free of charge from The Cambridge Crystallographic Data Centre via www.ccdc.cam.ac.uk/data_request/cif.

CAUTION! All compounds with a high nitrogen and oxygen content are potentially explosive energetic materials. Furthermore, many alkyl nitrates are extremely sensitive; therefore they must be handled with care. This necessitates additional meticulous safety precautions (steel-reinforced Kevlar gloves, Kevlar sleeves, face shield, leather coat, and ear plugs). Only earthened and metal-free equipment was used during the synthesis.

Synthesis of propargyl nitrate (1)

A nitration mixture consisting of 10.0 mL of acetic anhydride (91 mmol) and 3.3 mL of nitric acid (79 mmol) is cooled to −10 °C, and 3.7 mL of propargyl alcohol (68 mmol) is added dropwise at such a rate, that the temperature does not exceed −5 °C. Stirring is continued for 1 h and the reaction mixture is allowed to warm to ambient temperature. After pouring on ice the yellowish oil is separated immediately. The oily liquid is dissolved in 20 mL of dichloromethane and treated with a saturated aqueous solution of $NaHCO_3$, until the gas evolution ceases. The organic phase is washed with water (2×25 mL) and a saturated aqueous solution of NaCl and dried over anhydrous $MgSO_4$. Concentration in vacuo afforded 4.0 g (39 mmol) of crude propargyl nitrate (58 %), which was further purified by careful condensation at 25 °C using dry ice cooling. Raman: $\nu = 2961\,(44)$, $2134\,(100, \nu C{\equiv}C)$, $1643\,(5, \nu_{as}NO_2)$, $1427\,(11)$, $1361\,(11)$, $1281\,(34, \nu_s NO_2)$, $921\,(13)$, $848\,(23)$, $613\,(14)$, $474\,(11)$, $431\,(12)$, $296\,(27)$, $221\,(19)$ cm^{-1}. IR: $\nu = 3327\,(m)$, $2952\,(w)$, $2560\,(w)$, $2137\,(w, \nu C{\equiv}C)$, $1776\,(w)$, $1748\,(w)$, $1677\,(vs, \nu_{as}NO_2)$, $1434\,(m)$, $1365\,(m)$, $1284\,(vs, \nu_s NO_2)$, $1230\,(w)$, $1071\,(w)$, $1017\,(s)$, $976\,(m)$, $927\,(m)$, $839\,(s)$, $757\,(w)$, $675\,(m)$, $639\,(m)$, $596\,(w)$, $471\,(w)$ cm^{-1}. ^{1}H NMR (CDCl$_3$): $\delta = 4.96$ (d, $^4J_{H−H} = 2.2$ Hz, 2 H, CH_2), 2.59 (t, CH). ^{13}C{^{1}H} NMR (CDCl$_3$): $\delta = 76.8$ (s, CCH_2), 74.7 (s, CH), 59.9 (s, CH_2). ^{15}N NMR (CDCl$_3$): $\delta = -47.1$ (t, $^3J_{N−H} = 4.4$ Hz, ONO_2). MS (DEI+): m/z (%) $= 100\,(21)$ [M −H$^+$]$^+$. HRMS: m/z (%) $= 101.0113\,(100)$ [M]$^+$. DSC (T_{onset}, 5 K min^{-1}): 132 °C (decomposition). Sensitivities (liquid): impact sensitivity: 1 J, friction sensitivity: 72 N.

Synthesis of 1,1,1,6,6,6-hexanitrohex-3-yne (2)

The synthesis was performed according to the literature procedure.[14] Raman: $\nu = 2972\,(30)$, $2937\,(79)$, $2343\,(9)$, $2305\,(15)$, $2264\,(44, \nu C{\equiv}C)$, $1614\,(17)$, $1598\,(21,$

$\nu_{as}NO_2$), 1407 (25), 1365 (43), 1324 (24), 1307 (36, ν_sNO_2), 1250 (6), 1170 (3), 1142 (4), 1003 (20), 859 (100, νCN), 831 (4), 807 (6), 775 (5), 723 (5), 642 (7), 561 (6), 546 (19), 445 (4), 406 (55), 371 (70), 310 (20), 289 (47), 233 (15), 223 (10), 196 (11) cm^{-1}. IR: ν = 2970 (m), 2936 (m), 2892 (w), 1581 (vs, $\nu_{as}NO_2$), 1404 (m), 1365 (m), 1300 (s, ν_sNO_2), 1262 (m), 1249 (m), 1214 (w), 1169 (w), 1140 (w), 1128 (w), 1021 (w), 863 (m), 857 (m, νCN), 829 (w), 804 (s), 772 (m), 720 (w), 668 (w), 640 (w) cm^{-1}. ^{1}H NMR (CDCl$_3$): δ = 3.99 (s, 4 H, CH$_2$). ^{13}C{^{1}H} NMR (CDCl$_3$): δ = 124.8 (br, C(NO$_2$)$_3$), 74.3 (s, CCH$_2$), 26.8 (s, CH$_2$). ^{15}N NMR (CDCl$_3$): δ = −33.9 (s, NO$_2$). EA for C$_6$H$_4$N$_6$O$_{12}$ (352.13): calcd. C 20.47, H 1.14, N 23.87; found C 20.48, H 1.23, N 22.99 %. DSC (T_{onset}, 5 K min^{-1}): 126 °C (melting point), 193 °C (decomposition). Sensitivities (grain size: 500–1000 µm): impact sensitivity: 3 J, friction sensitivity: 72 N, electrostatic sensitivity: 0.08 J.

Synthesis of 1,1,1-trinitroethane (3)

Into a suspension of silver carbonate (2.12 g, 7.68 mmol) in 5 mL of acetonitrile is added an aqueous solution (30 %) of trinitromethane (2.31 g, 15.3 mmol) at ambient temperature. After stirring the yellow reaction mixture containing the in situ formed silver trinitromethanide for 25 min, iodomethane (2.17 g, 15.3 mmol) is added dropwise, with stirring continued for additional 15 h. The pale yellow precipitate of silver iodide is filtered off. Removing of the solvent in vacuo left a light-yellow solid. Crystallization of the product from *n*-pentane yielded 1.59 g (63 %) of **3** as colorless crystals.

WARNING! If, instead of an aqueous solution of trinitromethane, the trinitromethane is applied in a neat (anhydrous) form, after immediate evaporation of the solvent acetonitrile (5 min), the residue explodes reproducibly and can result in serious damage. Longer reaction times (ca. 30 min) result in significant decomposition of Ag[C(NO$_2$)$_3$] to silver nitrate. Raman: ν = 3032 (35), 2957 (68), 1613 (10), 1600 (37, $\nu_{as}NO_2$), 1436 (13), 1395 (30), 1359 (34), 1313 (24, ν_sNO_2), 1177 (7), 1133 (10), 885 (20), 858 (100, νCN), 784 (14), 713 (5), 643 (14), 530 (34), 412 (62), 383 (73), 319 (28) cm^{-1}. IR: ν = 3032 (m), 2956 (w), 2900 (w), 1587 (vs, $\nu_{as}NO_2$), 1434 (m), 1392 (s), 1307 (s, ν_sNO_2), 1266 (m), 1176 (m), 1131 (s), 881 (s), 858 (m, νCN), 782 (vs), 711 (w) cm^{-1}. ^{1}H NMR (CDCl$_3$): δ = 2.76 (s, 3 H, CH$_3$). ^{13}C{^{1}H} NMR (CDCl$_3$): δ = 128.2 (septet, $^1J_{C-^{14}N}$ = 8.1 Hz, C(NO$_2$)$_3$), 21.1 (s, CH$_3$). ^{15}N NMR (CDCl$_3$): δ = −28.8 (q, $^3J_{N-H}$ = 2.7 Hz, NO$_2$). MS (DCI+): m/z (%) = 166 (5) [M]$^+$, 120 (5) [M −NO$_2$]$^+$, 73 (1) [M −2NO$_2$]$^+$, 46 (52) [NO$_2$]$^+$, 27 (100) [M −3NO$_2$]$^+$. EA for C$_2$H$_3$N$_3$O$_6$ (165.06): calcd. C 14.55, H 1.83, N 25.46; found C 14.51, H 1.88, N 25.04 %. DSC (T_{onset}, 5 K min^{-1}): 38 °C (transition temperature) 53 °C (melting point), 194 °C (boiling point). Sensitivities (grain size:

500–1000 µm): impact sensitivity: 8 J, friction sensitivity: 96 N, electrostatic sensitivity: 0.10 J.

5.6. Acknowledgment

Supporting Information

^{15}N NMR and vibrational (IR and Raman) spectra and further details of the GED determination of **1** are given as Supporting Information available online (DOI: 10.5560/ZNB.2013-2311).

5.7. References

[1] T. Urbanski, *Chemistry and Technology of Explosives*, Vol. 4, Pergamon Press, Oxford, **1984**.

[2] F.P. Bowden, A.D. Yoffe, *Initiation and Growth of Explosion in Liquids and Solids*, Cambridge University Press, Cambridge, **1952**.

[3] F.P. Bowden, A.D. Yoffe, *Fast Reactions in Solids*, Butterworths Scientific Publications, London, **1958**.

[4] T. Urbanski, W. Tarantowicz, *B. Acad. Pol. Sci., Geo. G.* **1958**, *6*, 289–292.

[5] M.S. Cohen, D.D. Perry, P.J. Keenan, US3120566, **1964**.

[6] P. Klaeboe, C.J. Nielsen, H. Priebe, S.H. Schei, C.E. Sjoegren, *J. Mol. Struct.* **1986**, *141*, 161–172.

[7] A. Quilico, M. Freri, *Gazz. Chim. Ital.* **1929**, *59*, 930–941.

[8] A. Quilico, M. Freri, *Gazz. Chim. Ital.* **1930**, *60*, 172–184.

[9] A. Quilico, M. Freri, *Gazz. Chim. Ital.* **1930**, *60*, 721–744.

[10] V. A. Quilico, M. Freri, *Gazz. Chim. Ital.* **1931**, *61*, 484–500.

[11] A. Quilico, M. Simonetta, *Gazz. Chim. Ital.* **1946**, *76*, 200–214.

[12] A. Quilico, M. Simonetta, *Gazz. Chim. Ital.* **1946**, *76*, 255–264.

[13] A. D. Nikolaeva, A. P. Kirsanov, R. G. Kadyrova, *Izv. Vyssh. Uchebn. Zaved., Khim. Khim. Tekhnol.* **1975**, *18*, 1715–1716.

[14] P. O. Tawney, US3040105, **1962**.

[15] S. G. Cho, K. T. No, E. M. Goh, J. K. Kim, J. H. Shin, Y. D. Joo, S. Seong, *Bull. Korean Chem. Soc.* **2005**, *26*, 399–408.

[16] M. H. Keshavarz, H. R. Pouretedal, *J. Hazard. Mater.* **2005**, *124*, 27–33.

[17] N. R. Badders, C. Wei, A. A. Aldeeb, W. J. Rogers, M. S. Mannan, *J. Energ. Mater.* **2006**, *24*, 17–33.

[18] M. H. Keshavarz, *J. Hazard. Mater.* **2007**, *148*, 648–652.

[19] J. A. Morrill, E. F. C. Byrd, *J. Mol. Graphics Modell.* **2008**, *27*, 349–355.

[20] A. P. N. Franchimont, *Rec. Trav. Chim. Pay-Bas.* **1886**, *5*, 281–289.

[21] A. Hantzsch, A. Rinckenberger, *Ber. Dtsch. Chem. Ges.* **1899**, *32*, 628–641.

[22] A. Hantzsch, K. S. Caldwell, *Ber. Dtsch. Chem. Ges.* **1906**, *39*, 2472–2478.

[23] G. S. Hammond, W. D. Emmons, C. O. Parker, B. M. Graybill, J. H. Waters, M. F. Hawthorne, *Tetrahedron* **1963**, *19*, 177–195.

[24] C. W. Plummer, US3049570, **1962**.

[25] F. M. Mukhametshin, V. D. Surkov, A. L. Fridman, F. A. Gabitov, SU515738, **1976**.

[26] N. N. Makhova, I. V. Ovchinnikov, V. G. Dubonos, Y. A. Strelenko, L. I. Khmel'nitsky, *Russ. Chem. Bull.* **1993**, *42*, 131–136.

[27] C. F. Poranski, Jr., W. B. Moniz, *J. Phys. Chem.* **1967**, *71*, 1142–1143.

[28] J. P. Kintzinger, J. M. Lehn, R. L. Williams, *Mol. Phys.* **1969**, *17*, 135–146.

[29] M. Witanowski, Z. Biedrzycka, K. Grela, *Magn. Reson. Chem.* **1998**, *36*, 356–358.

[30] M. Witanowski, Z. Biedrzycka, K. Grela, K. Wejroch, *Magn. Reson. Chem.* **1998**, *36*, S85–S92.

[31] H. Wittek, *Acta Phys. Austriaca* **1948**, *1*, 303–306.

[32] E. M. Popov, *J. Struct. Chem.* **1967**, *8*, 916–918.

[33] J. T. Larkins, F. E. Saalfeld, L. Kaplan, *Org. Mass Spectrom.* **1969**, *2*, 213–221.

[34] J. T. Larkins, J. M. Nicholson, F. E. Saalfeld, *Org. Mass Spectrom.* **1971**, *5*, 265–277.

[35] O. S. Chizhov, V. I. Kadentsev, G. G. Pal'mbakh, K. Y. Burshtein, S. A. Shevelev, A. A. Fainzil'berg, *Org. Mass Spectrom.* **1978**, *13*, 611–617.

[36] K. V. Auwers, L. Harres, *Ber. Dtsch. Chem. Ges.* **1929**, *62B*, 2287–2297.

[37] T. M. Klapötke, B. Krumm, R. Moll, *New Trends Res. Energ. Mater., 14th Proc. Semin.*, Pardubice (Czech Republic), **2011**, Pt. 2, pp. 723–729.

[38] F. S. Holahan, T. C. Castorina, J. R. Autera, S. Helf, *J. Am. Chem. Soc.* **1962**, *84*, 756–759.

[39] V. I. Erashko, V. I. Slovetskii, S. A. Shevelev, A. A. Fainzil'berg, *Russ. Chem. Bull.* **1971**, *20*, 645–649.

[40] N. Kornblum, R. A. Smiley, R. K. Blackwood, D. C. Iffland, *J. Am. Chem. Soc.* **1955**, *77*, 6269–6280.

[41] S. A. Shevelev, V. I. Erashko, A. A. Fainzil'berg, *Russ. Chem. Bull.* **1968**, *17*, 447.

[42] S. A. Shevelev, V. I. Erashko, A. A. Fainzil'berg, *Russ. Chem. Bull.* **1968**, *17*, 2003–2006.

[43] V. I. Erashko, S. A. Shevelev, A. A. Fainzil'berg, *Russ. Chem. Bull.* **1968**, *17*, 2007–2010.

[44] M. Göbel, T. M. Klapötke, P. Mayer, *Z. Anorg. Allg. Chem.* **2006**, *632*, 1043–1050.

[45] A. L. Fridman, T. N. Ivshina, V. P. Ivshin, V. A. Tartakovskii, S. S. Novikov, *Russ. Chem. Bull.* **1969**, *18*, 2193–2194.

[46] R. G. Kidd "Nuclear Shielding of the Transition Metals" in *Annual Reports on NMR Spectroscopy*, Vol. 10A (Ed.: G. A. Webb), Academic Press Inc., London, **1980**, pp. 53–55.

[47] W. W. Simons, *The Sadtler Handbook of Infrared Spectra*, Sadtler Research Laboratories, Philadelphia, **1978**; p. 3.

[48] R. J. F. Berger, M. Hoffmann, S. A. Hayes, N. W. Mitzel, *Z. Naturforsch.* **2009**, *64b*, 1259–1268.

[49] A. J. Blake, P. T. Brain, H. McNab, J. Miller, C. A. Morrison, S. Parsons, D. W. H. Rankin, H. E. Robertson, B. A. Smart, *J. Phys. Chem.* **1996**, *100*, 12280–12287.

[50] N. W. Mitzel, D. W. H. Rankin, *Dalton Trans.* **2003**, 3650–3662.

[51] V. A. Sipachev, *J. Mol. Struct.: THEOCHEM* **1985**, *22*, 143–151.

[52] D. W. H. Rankin in *Stereochemical Applications of Gas-Phase Electron Diffraction*, Vol. 1 (Eds.: I. Hargittai, M. Hargittai), John Wiley & Sons, New York, **1988**, pp. 451–482.

[53] V. P. Novikov, V. A. Sipachev, E. I. Kulikova, L. V. Vilkov, *J. Mol. Struct.* **1993**, *301*, 29–36.

[54] H. Schödel, R. Dienelt, H. Bock, *Acta Crystallogr.* **1994**, *C50*, 1790–1792.

[55] S. K. Bhattacharjee, H. L. Ammon, *Acta Crystallogr.* **1982**, *B38*, 2503–2505.

[56] Y. Oyumi, T. B. Brill, A. L. Rheingold, *J. Phys. Chem.* **1985**, *89*, 4824–4828.

[57] T. M. Klapötke, B. Krumm, R. Moll, S. F. Rest, *Z. Anorg. Allg. Chem.* **2011**, *637*, 2103–2110.

[58] A. Bondi, *J. Phys. Chem.* **1964**, *68*, 441–451.

[59] J. M. Rosen, *Microscope* **1969**, *17*, 141–144.

[60] R. W. Crowe, C. P. Smyth, *J. Am. Chem. Soc.* **1950**, *72*, 4009–4015.

[61] T. M. Klapötke, *Chemistry of High-Energy Materials*, 2nd ed., Walter de Gruyter, Berlin, **2012**.

[62] M. Suceska, *Propellants, Explos., Pyrotech.* **1991**, *16*, 197–202.

[63] M. Suceska, *Propellants, Explos., Pyrotech.* **1999**, *24*, 280–285.

[64] M. Suceska, *Mater. Sci. Forum* **2004**, *465–466*, 325–330.

[65] M. Suceska, EXPLO5 (Version 5.05), Brodarski Institut, Zagreb (Croatia), **2011**.

[66] M. J. Frisch, G. W. Trucks, H. B. Schlegel, G. E. Scuseria, M. A. Robb, J. R. Cheeseman, V. B. G. Scalmani, B. Mennucci, G. A. Petersson, H. Nakatsuji, M. Caricato, X. Li, H. P. Hratchian, A. F. Izmaylov, J. Bloino, G. Zheng, J. L. Sonnenberg, M. Hada, M. Ehara, K. Toyota, R. Fukuda, J. Hasegawa, M. Ishida, T. Nakajima, Y. Honda, O. Kitao, H. Nakai, T. Vreven, J. A. Montgomery, Jr., J. E. Peralta, F. Ogliaro, M. Bearpark, J. J. Heyd, E. Brothers, K. N. Kudin, V. N. Staroverov, R. Kobayashi, J. Normand, K. Raghavachari, A. Rendell, J. C. Burant, S. S. Iyengar,

J. Tomasi, M. Cossi, N. Rega, J. M. Millam, M. Klene, J. E. Knox, J. B. Cross, V. Bakken, C. Adamo, J. Jaramillo, R. Gomperts, R. E. Stratmann, O. Yazyev, A. J. Austin, R. Cammi, C. Pomelli, J. W. Ochterski, R. L. Martin, K. Morokuma, V. G. Zakrzewski, G. A. Voth, P. Salvador, J. J. Dannenberg, S. Dapprich, A. D. Daniels, Ö. Farkas, J. B. Foresman, J. V. Ortiz, J. Cioslowski, D. J. Fox, GAUSSIAN 09 (Rev. C.01), Gaussian, Inc., Wallingford CT (USA), **2009**.

[67] D. F. Shriver, M. A. Drezdzon, *The Manipulation of Air-Sensitive Compounds*, 2nd ed., John Wiley & Sons, New York, **1986**.

[68] M. Saljoughian, H. Morimoto, P. G. Williams, H. Rapoport, *J. Labelled Compd. Radiopharm.* **1988**, *25*, 313–328.

[69] Test procedure *A.14 Explosive Properties* according to Council Regulation (EC) No 440/2008 of 30 May 2008 laying down test methods pursuant to Regulation (EC) No 1907/2006 of the European Parliament and of the Council on the Registration, Evaluation, Authorisation and Restriction of Chemicals (REACH), *OJ L 142*, 93–103, **2008**.

[70] R. Ahlrichs, M. Baer, M. Haeser, H. Horn, C. Koelmel, *Chem. Phys. Lett.* **1989**, *162*, 165–169.

[71] M. J. Frisch, G. W. Trucks, H. B. Schlegel, G. E. Scuseria, M. A. Rob, J. R. Cheeseman, J. A. Montgomery Jr., T. Vreven, K. N. Kudin, J. C. Burant, J. M. Millam, S. S. Iyengar, J. Tomasi, V. Barone, B. Mennucci, M. Cossi, G. Scalmani, N. Rega, G. A. Petersson, H. Nakatsuji, M. Hada, M. Ehara, K. Toyota, R. Fukuda, J. Hasegawa, M. Ishida, T. Nakajima, Y. Honda, O. Kitao, H. Nakai, M. Klene, X. Li, J. E. Knox, H. P. Hratchian, J. B. Cross, V. Bakken, C. Adamo, J. Jaramillo, R. Gomperts, R. E. Stratmann, O. Yazyev, A. J. Austin, R. Cammi, C. Pomelli, J. W. Ochterski, P. Y. Ayala, K. Morokuma, G. A. Voth, P. Salvador, J. J. Dannenberg, V. G. Zakrzewski, S. Dapprich, A. D. Daniels, M. C. Strain, O. Farkas, D. K. Malick, A. D. Rabuck, K. Raghavachari, J. B. Foresman, J. V. Ortiz, Q. Cui, A. G. Baboul, S. Clifford, J. Cioslowski, B. B. Stefanov, G. Liu, A. Liashenko, P. Piskorz, I. Komaromi, R. L. Martin, D. J. Fox, T. Keith, M. A. Al-Laham, C. Y. Peng, A. Nanayakkara, M. Challacombe, P. M. W. Gill, B. Johnson, W. Chen, M. W. Wong, C. Gonzalez, J. A. Pople, GAUSSIAN 03 (Rev. B.03), Gaussian, Inc., Wallingford CT (USA), **2003**.

[72] W. Zeil, J. Haase, L. Wegmann, *Z. Instrumentenkd.* **1966**, *74*, 84–88.

[73] H. Oberhammer, *Mol. Struct. Diffr. Methods* **1976**, *4*, 24–44.

[74] S. Gundersen, S. Samdal, T. G. Strand, H. V. Volden, *J. Mol. Struct.* **2007**, *832*, 164–171.

[75] S. L. Hinchley, H. E. Robertson, K. B. Borisenko, A. R. Turner, B. F. Johnston, D. W. H. Rankin, M. Ahmadian, J. N. Jones, A. H. Cowley, *Dalton Trans.* **2004**, 2469–2476.

[76] A. W. Ross, M. Fink, R. Hilderbrandt in *International Tables for Crystallography*, Vol. C (Ed.: A. J. C. Wilson), Kluwer Academic Publishers, Dordrecht, **1992**, p. 245.

[77] A. V. Zakharov, Y. A. Zhabanov, Q2SHRINK ED Software, http://edsoftware.sourceforge.net.

[78] R. D. Dennington II, T. A. Keith, J. M. Millam, GaussView (Version 5.0.8), Semichem Inc., Shawnee Mission KS (USA), **2009**.

[79] M. R. Nyden, G. A. Petersson, *J. Chem. Phys.* **1981**, *75*, 1843–1862.

[80] G. A. Petersson, M. A. Al-Laham, *J. Chem. Phys.* **1991**, *94*, 6081–6090.

[81] G. A. Petersson, T. G. Tensfeldt, J. A. Montgomery, Jr., *J. Chem. Phys.* **1991**, *94*, 6091–6101.

[82] J. A. Montgomery, Jr., J. W. Ochterski, G. A. Petersson, *J. Chem. Phys.* **1994**, *101*, 5900–5909.

[83] J. W. Ochterski, G. A. Petersson, J. A. Montgomery, Jr., *J. Chem. Phys.* **1996**, *104*, 2598–2619.

[84] J. A. Montgomery, Jr., M. J. Frisch, J. W. Ochterski, G. A. Petersson, *J. Chem. Phys.* **2000**, *112*, 6532–6542.

[85] L. A. Curtiss, K. Raghavachari, P. C. Redfern, J. A. Pople, *J. Chem. Phys.* **1997**, *106*, 1063–1079.

[86] B. M. Rice, S. V. Pai, J. Hare, *Combust. Flame* **1999**, *118*, 445–458.

[87] E. F. C. Byrd, B. M. Rice, *J. Phys. Chem.* **2006**, *110A*, 1005–1013.

[88] F. Trouton, *Philos. Mag.* **1884**, *18*, 54–57.

[89] M. S. Westwell, M. S. Searle, D. J. Wales, D. H. Williams, *J. Am. Chem. Soc.* **1995**, *117*, 5013–5015.

[90] M. C. Burla, R. Caliandro, M. Camalli, B. Carrozzini, G. L. Cascarano, L. De Caro, C. Giacovazzo, G. Polidori, R. Spagna, SIR2004, *An Improved Tool for Crystal Structure Determination and Refinement*, University of Bari, Bari (Italy), **2004**.

[91] M. C. Burla, R. Caliandro, M. Camalli, B. Carrozzini, G. L. Cascarano, L. De Caro, C. Giacovazzo, G. Polidori, R. Spagna, *J. Appl. Crystallogr.* **2005**, *38*, 381–388.

[92] G. M. Sheldrick, SHELXL-97, *Program for the Refinement of Crystal Structures*, University of Göttingen, Göttingen (Germany), **1997**.

[93] G. M. Sheldrick, *Acta Crystallogr.* **2008**, *A64*, 112–122.

6. Halogenotrinitromethanes

As submitted to *Chem. Eur. J.*
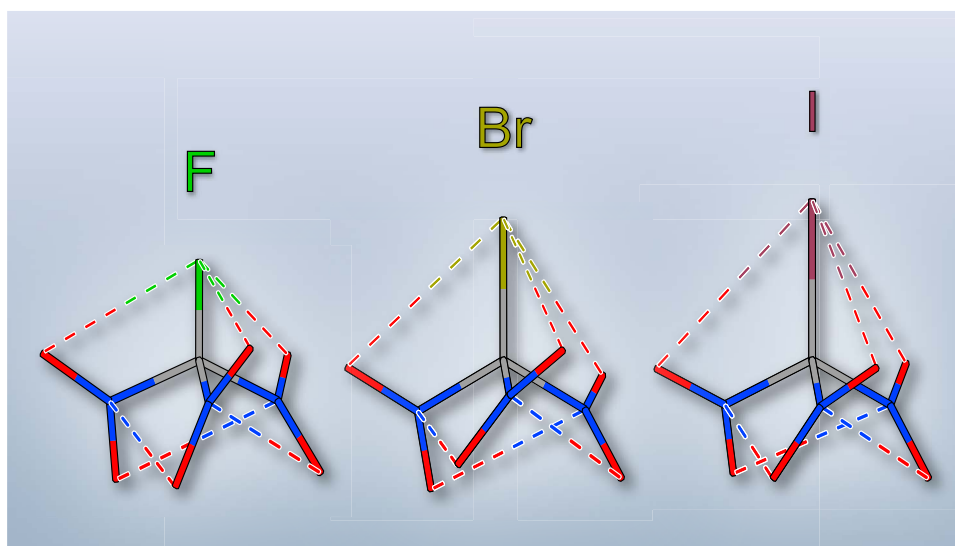
A comprehensive study of spectroscopic and structural properties of the full series of halogenotrinitromethanes (F, Cl, Br, and I) is presented. The molecular structures were determined in the crystalline state by X-ray diffraction, those in the gas phase by electron diffraction. The Hal−C bond lengths were shown to be systematically shorter in the gas phase than those in the crystalline state. The obtained experimental data are interpreted in terms of Natural Bond Orbitals (NBO), Atoms in Molecules (AIM) and Interacting Quantum Atoms (IQA) theories.

Halogenotrinitromethanes –
A Combined Study in the Crystalline and Gaseous Phase and by Quantum Chemical Methods

Thomas M. Klapötke,*[a] Burkhard Krumm,[a] Richard Moll,[a] Sebastian F. Rest,[a] Yury V. Vishnevskiy,[b] Christian Reuter,[b] Hans-Georg Stammler,[b] and Norbert W. Mitzel*[b]

*   Prof. Dr. Thomas M. Klapötke, Prof. Dr. Norbert W. Mitzel
    E-Mail: tmk@cup.uni-muenchen.de, mitzel@uni-bielefeld.de

[a] Department of Chemistry
    Ludwig-Maximilian University of Munich
    Butenandtstrasse 5–13 (D)
    81377 Munich, Germany

[b] Inorganic and Structural Chemistry
    Bielefeld University
    Universitätsstraße 25
    33615 Bielefeld, Germany

6.1. Abstract

The halogenotrinitromethanes $FC(NO_2)_3$ (**1**), $BrC(NO_2)_3$ (**2**) and $IC(NO_2)_3$ (**3**) were synthesized and fully characterized. The molecular structures of **1**–**3** were determined in the crystalline state by X-ray diffraction, gas-phase structures of **1** and **2** were determined by electron diffraction. The $Hal-C$ bond lengths in $F-$, $Cl-$ and $Br-C(NO_2)_3$ are systematically shorter in the gas-phase than those in the crystalline state. The obtained experimental data are interpreted in terms of Natural Bond Orbitals (NBO), Atoms in Molecules (AIM) and Interacting Quantum Atoms (IQA) theories. All halogenotrinitromethanes show various intra- and intermolecular non-bonded interactions. Intramolecular $N\cdots O$ and $Hal\cdots O$ ($Hal = F$ (**1**), Br (**2**), I (**3**)) interactions, both competitors in terms of the orientation of the nitro groups by rotation about the $C-N$ bonds, lead to a propeller-type twisting of these groups favoring the mentioned interactions. The origin of the unusually short $Hal-C$ bonds is discussed in detail. The results of this study are compared to the molecular structure of $ClC(NO_2)_3$ and the respective interactions therein.

6.2. Introduction

Mutual influences of atoms and functional groups in molecules are to a great extent responsible for the chemical and structural properties. Detailed analysis of these influences and the understanding of intra- and intermolecular interactions are of fundamental interest for chemical science. Especially small compounds containing the trinitromethyl moiety, with its strong electron-withdrawing property, may show special and unusual characteristics. A detailed understanding of the nature of bonding within and between these molecules is therefore highly desirable. Although the trinitromethyl moiety consists of C, N and O atoms, its properties are comparable to those of a Group VII element. Early studies of α-halogen derivatives of trinitromethane have demonstrated the pseudo-halogenic nature of the trinitromethyl moiety.[1] Further experimental evidence supporting this behavior as a pseudohalogen are the discoveries of the corresponding strong acid $HC(NO_2)_3$,[2,3] various metal salts like $K[C(NO_2)_3]$ and $Ag[C(NO_2)_3]$,[3] pseudointerhalogen compounds such as $NCC(NO_2)_3$[4,5] and $N_3C(NO_2)_3$,[6,7] as well as its dimer hexanitroethane.[8] Furthermore, the existence of the halogenotrinitromethanes $HalC(NO_2)_3$ ($Hal = F, Cl, Br, I$) confirm this assumption.

Although various syntheses of $HalC(NO_2)_3$ ($Hal = F$ (**1**), Cl, Br (**2**), I (**3**)) by different methods are known,[9] analytical data available in the literature are often fragmentary despite considerable efforts of various researchers. In this context, studies of the NMR spectra[10–12] and vibrational analyses[10,13,14] have been previously

reported. Furthermore, quantum chemical calculations have been performed to predict the molecular structures of the halogenotrinitromethanes.[15,16]

Reliable data of experimental structural investigations of **1**–**3** are rather limited in literature. When it comes to understand the interplay of various types of inter- and intramolecular interactions on the molecular structures, it is generally highly desirable to compare structural data of free molecules in the gas-phase, without distortions from intermolecular forces, with those of molecules embedded in a crystal, the very existence of which depends on the existence of intermolecular forces. So far gas-phase structure determinations exist for $ClC(NO_2)_3$[17–19] and $BrC(NO_2)_3$,[18,19] but the latter are based on a data set of limited quality and is therefore re-investigated in this work. Experimental structure data for both, gas and solid, are completely unknown for $FC(NO_2)_3$. Furthermore, a determination of the crystal structure of $IC(NO_2)_3$ has been previously reported, but using a poor data set of X-ray diffraction data, due to decomposition of upon exposure to Mo-K_α X-ray radiation.[20] This prevented the coordinates of the light atoms carbon, nitrogen and oxygen from being properly determined and the resulting structures show a considerable scatter for bond lengths and made a reinvestigation of the crystal structure desirable.

The molecular structure of $ClC(NO_2)_3$ has previously been investigated in our laboratory, using X-ray diffraction and quantum chemical calculations of the molecular electrostatic potential.[21] Following these studies, we describe here convenient syntheses and full characterization of the halogenotrinitromethanes $FC(NO_2)_3$ (**1**), $BrC(NO_2)_3$ (**2**) and $IC(NO_2)_3$ (**3**) as well as their molecular structures in the crystalline state and in the gas-phase. This completes our detailed investigations of α-halogen derivatives of trinitromethane.

6.3. Results and Discussion

The general and established procedure for the preparation of the halogenotrinitromethanes $HalC(NO_2)_3$ (Hal = F (**1**), Br (**2**), I (**3**)) implies direct halogenation of trinitromethane or its anion (Scheme 1).

Fluorination of trinitromethanide in aqueous solution enables separation of the pure product by evaporation and furnishes **1** as a colorless stable liquid, immiscible with water. The use of Selectfluor (1-chloro-methyl-4-fluoro-1,4-diazoniabicyclo[2.2.2]octane bis(tetrafluoroborate)) as a fluorinating agent significantly simplifies the experimental effort compared to the experimental setup required for elemental fluorine. In case of **2**, the immiscibility with water facilitates the separation of the product. The use of elemental bromine in the synthesis of **2**, cannot be applied to that of **3** by an analogous reaction of trinitromethane or its salt with elemental iodine. Therefore, iodine monochloride, due
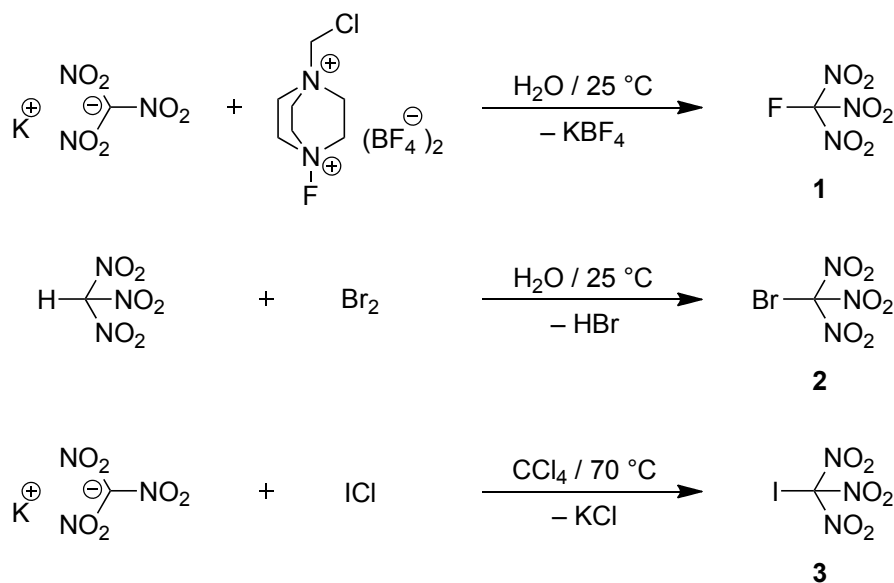
Scheme 1: Synthesis of the halogenotrinitromethanes $FC(NO_2)_3$ (**1**), $BrC(NO_2)_3$ (**2**) and $IC(NO_2)_3$ (**3**).

to its high polarity as a source of I^+, is needed for a successful reaction. At ambient temperature **3** is the only solid halogenotrinitromethane derivative, and in analogy to **1** and **2** not miscible with water. It decomposes slowly at ambient temperature and/or when exposed to daylight, forming elemental iodine.

For comparison of analytic data, an authentic sample of chlorotrinitromethane was also synthesized, according to a procedure in the literature.[9]

NMR Spectroscopy

All compounds were thoroughly characterized by multinuclear NMR spectroscopy (Table 1). The ^{13}C NMR of **1**–**3** and the authentic sample of $ClC(NO_2)_3$ show the resonances for the sole carbon atom between 126.3–106.7 ppm. In general, an increasing number of electron-withdrawing groups in the vicinity of a carbon atom lead to a downfield shift. Therefore, the carbon resonance of $ClC(NO_2)_3$ at 126.3 ppm and that of **2** at 121.9 ppm is found downfield relative to the carbon resonance of **3** at 106.7 ppm (Table 1). The fluorine compound **1** has a special position among this series of halogenotrinitromethanes. The ^{13}C NMR resonance of **1** at 113.7 ppm is surprisingly much more highfield shifted than expected for the electronegative fluorine substituent. All resonances of the carbon atoms of **1**–**3** and $ClC(NO_2)_3$ are split into septets due to coupling with the ^{14}N nuclei, whereas for **1** a doublet of septets is observed due to additional coupling with fluorine. The coupling constants $^{1}J_{C-^{14}N}$ are 12.1 Hz (**1**), 9.3 Hz ($ClC(NO_2)_3$), 8.1 Hz (**2**)

and 6.4 Hz (**3**), a constant decrease along the series of decreasing electronegativity, respectively increasing molecular weight of the halogen atom (Table 1). The $^1J_{C-F}$ coupling constant for **1** at 333.4 Hz is similar to the previously reported value.[12] The ^{15}N NMR resonances are found in the typical range of -30 to -40 ppm for trinitromethyl derivatives.[22–26] In case of **1** the coupling constants $^2J_{F-^{14}N}$ and $^2J_{^{15}N-F}$ are determined with values of 10.2 and 14.2 Hz.

Table 1.: Multinuclear NMR resonances (^{13}C, ^{15}N, ^{19}F) of HalC(NO$_2$)$_3$ **1**–**3** and ClC(NO$_2$)$_3$ in CDCl$_3$ (δ in ppm, J in Hz.)

	1 FC(NO$_2$)$_3$ a)	ClC(NO$_2$)$_3$ b)	**2** BrC(NO$_2$)$_3$	**3** IC(NO$_2$)$_3$
^{13}C	113.7 $^1J_{C-^{14}N} = 12.1$ $^1J_{C-F} = 333.4$	126.3 $^1J_{C-^{14}N} = 9.3$	121.9 $^1J_{C-^{14}N} = 8.1$	106.7 $^1J_{C-^{14}N} = 6.4$
^{15}N	-40.7 $^2J_{^{15}N-F} = 14.2$	-35.7	-34.8	-30.8

a) δ ^{19}F -87.3 (sept, $^2J_{F-^{14}N} = 10.2$ Hz). b) Authentic sample of ClC(NO$_2$)$_3$.

Vibrational Spectroscopy

IR and Raman spectra of **1**, **2**, ClC(NO$_2$)$_3$ in the liquid state and of **3** in the solid state were measured. Vibrational analyses of **1**–**3** and an authentic sample of ClC(NO$_2$)$_3$ show the characteristic asymmetric NO$_2$ stretching vibration at 1622–1583 cm^{-1} (Table 2), in agreement with previously reported values and other nitro group containing compounds.[13,22,23,25–28] The symmetric NO$_2$ stretching vibration is found for these compounds in the typical range of 1298–1272 cm^{-1}. The CN stretching vibrations of **1**–**3** occur at 857–837 cm^{-1}, whereas the frequency decreases with heavier halogens (Table 2). The general low-frequency absorptions of these vibrations are surprising but explainable with the low C−N bond order in the trinitromethyl moiety,[27,29] in agreement with the corresponding elongated C−N bonds observed in the crystal structures (see below). Also the Hal−C stretching vibrations for **1**–**3** could be observed in all vibrational spectra (Table 2).[27] These frequencies of **2**, **3** and ClC(NO$_2$)$_3$ are in agreement with previous investigations,[14] however, there exist also very disputable assignments at much lower frequencies.[13,20] The substantial shift to higher frequencies of the Hal−C stretching vibrations of more than 300 cm^{-1} indicates short Hal−C bonds. Evidence on bond shortening is described in more detail below in the gas and crystal structure section. Very

likely, the C−F stretching vibration of **1** is found at $1011\,cm^{-1}$ (Raman) and $1012\,cm^{-1}$ (IR), respectively. Various frequencies for the C−F stretching vibration are reported, whereas an assignment of a vibration at about $1300\,cm^{-1}$ could not be confirmed.[14]

Table 2.: IR and Raman bands of **1**–**3** and $ClC(NO_2)_3$, characteristic vibrations and their assignments (vibrational bands in cm^{-1}).

	1 $FC(NO_2)_3$		$ClC(NO_2)_3$ [a)]	
	Raman	IR	Raman	IR
$\nu_{as}NO_2$	1622 (16)	1606 (vs)	1620 (18)	1602 (vs)
$\nu_{s}NO_2$	1298 (28)	1288 (s)	1279 (12)	1272 (s)
νCN	857 (100)	856 (m)	845 (100)	843 (s)
$\nu HalC$ [b)]	1011 (8)	1012 (m)	1027 (5)	1024 (s)

	2 $BrC(NO_2)_3$		**3** $IC(NO_2)_3$	
	Raman	IR	Raman	IR
$\nu_{as}NO_2$	1615 (14)	1595 (vs)	1616 (5) / 1597 (35)	1597 (s) / 1583 (vs)
$\nu_{s}NO_2$	1294 (8)	1277 (s)	1298 (7) / 1287 (5)	1290 (s) / 1278 (s)
νCN	840 (88)	838 (s)	839 (97)	837 (s)
$\nu HalC$ [b)]	981 (3)	979 (m)	947 (5)	944 (m)

[a)] Authentic sample of $ClC(NO_2)_3$. [b)] Hal = F (**1**), Cl, Br (**2**), I (**3**).

Gas-phase Structure

Gas electron diffraction (GED) was used to determine the structure of the free molecules of $FC(NO_2)_3$ (**1**) and $BrC(NO_2)_3$ (**2**). The structure including atom labeling is shown in Figure 1. Refined experimental equilibrium structure parameter values along with quantum chemically calculated ones are listed in Table 3. Thermally averaged values for the bond lengths of **1** are: $r_g(F-C) = 1.308(11)$, $r_g(N-C) = 1.532(4)$, $r_g(N1-O1) = r_g(N1-O2) = 1.216(1)$ Å; those of **2** are: $r_g(Br-C) = 1.878(6)$, $r_g(N-C) = 1.548(3)$, $r_g(N1-O1) = 1.215(1)$, $r_g(N1-O2) = 1.218(1)$ Å. The radial distribution curves (Figure 2 and 3), which can be interpreted as spectra of interatomic distances, show that the C−Br bond contribution in **2** is in a separate peak whereas that of the C−F bond in **1** is under the same feature as that of the N−O bonds and therefore correlated. Thus the experimentally determined C−F bond length is considerably less precise than that of C−Br. In addition, the difference curves (Figure 2 and 3) show relative high overall quality of the refined structures. A discussion of structural

parameters will be done in direct comparison with the data obtained from the crystalline state by X-ray diffraction below.
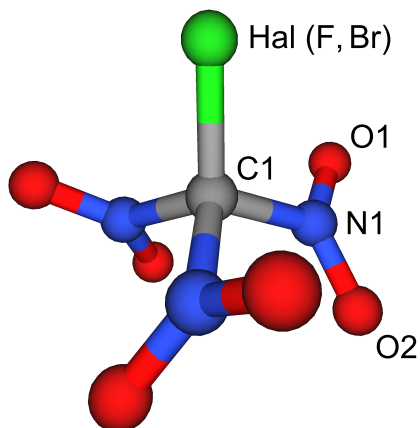
Figure 1.: Molecular structure of $FC(NO_2)_3$ (**1**) and analogously $BrC(NO_2)_3$ (**2**) in the gas-phase.
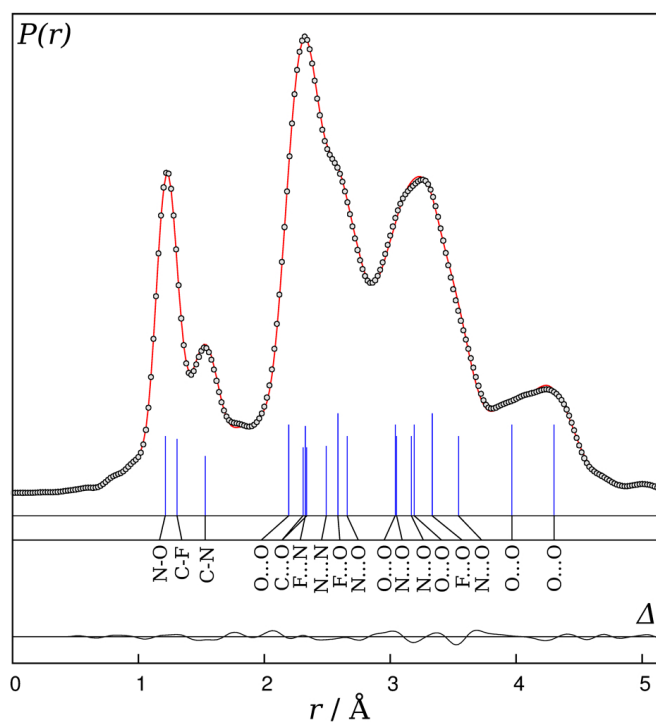
Figure 2.: Experimental (open circles) and model (line) radial distribution functions of $FC(NO_2)_3$ (**1**). The difference curve is shown below. Vertical bars indicate interatomic distances in the model.

Table 3.: Experimental and calculated structural parameters (r_e, $\angle_e$) of $FC(NO_2)_3$ (**1**) and $BrC(NO_2)_3$ (**2**). Levels of theory: **1**: MP2/cc-pVTZ, **2**: MP2/SDB-cc-pVTZ (distances in, angles in deg).

	1 $FC(NO_2)_3$		**2** $BrC(NO_2)_3$	
	GED [a]	MP2	GED [a]	MP2
$r(Hal-C1)$ [b]	1.300(11) [1]	1.304	1.869(6) [1]	1.866
$r(C1-N1)$	1.517(4) [2]	1.517	1.529(3) [2]	1.533
$r(N1-O1)$	1.210(1) [3]	1.220	1.209(1) [3]	1.217
$r(N1-O2)$	1.211(1) [3]	1.221	1.214(1) [3]	1.221
$\alpha(Hal-C1-N1)$ [b]	110.2(6) [4]	110.5	112.5(3) [4]	112.2
$\alpha(C1-N1-O1)$	114.1(3) [5]	114.2	115.7(2) [5]	115.4
$\alpha(C1-N1-O2)$	116.3(3) [5]	116.4	115.9(2) [5]	115.7
$\alpha(O1-N1-O2)$	129.5(6) [d]	129.4	128.3(4) [d]	128.8
$\alpha(N-C1-N)$	108.7(6) [d]	108.4	106.3(3) [d]	106.6
$\varphi(Hal-C1-N1-O1)$ [b]	−37.9(22) [6]	−39.9	−38.3(13) [6]	−44.2
$\varphi(Hal-C1-N1-O2)$ [b]	143.9(31) [d]	141.2	139.6(24) [d]	137.8
$o(O1,C1-N1-O2)$ [c]	−1.6(20) [d]	−1.0	1.9(18) [d]	−1.9
$o(O2,C1-N1-O1)$ [c]	1.5(20) [d]	1.0	−1.9(18) [d]	1.9
R_{str} [%]	6.28	–	5.29	–

[a] Superscript numbers indicate independent groups of parameters in the least-squares (LSQ) analyses. In groups with more than one parameter the differences between parameter values were fixed at theoretical values in order to avoid strong correlations. In those cases the threefold standard deviations given in parentheses correspond to groups and not to parameters independently. [b] Hal = F (**1**), Br (**2**). [c] Out-of-plane angle (A,B−C−D) calculated as the angle between the A−C bond and the B−C−D plane. [d] Dependent parameter.

Crystal Structure Analysis

Single crystals suitable for X-ray diffraction measurements were obtained by crystallization of the neat melt (**1**, **2**) or from solution in *n*-hexane (**3**). Crystals of **1** and **2** were grown in situ in a capillary directly on the X-ray diffractometer. This was achieved by first establishing a solid-liquid equilibrium close to the melting point, then melting all solid but a tiny crystal seed (using a thin copper wire as external heat source) followed by very slowly lowering the temperature until the whole capillary was filled with a single crystalline specimen. In contrast to the literature,[20] crystals of **3** did not show decomposition upon exposure to Mo-K_α radiation and a good data set could be recorded. A full list of the crystallographic refinement parameters and structure data for compounds **1**–**3** is shown in Table 7. All halogenotrinitromethanes **1**–**3** crystallize
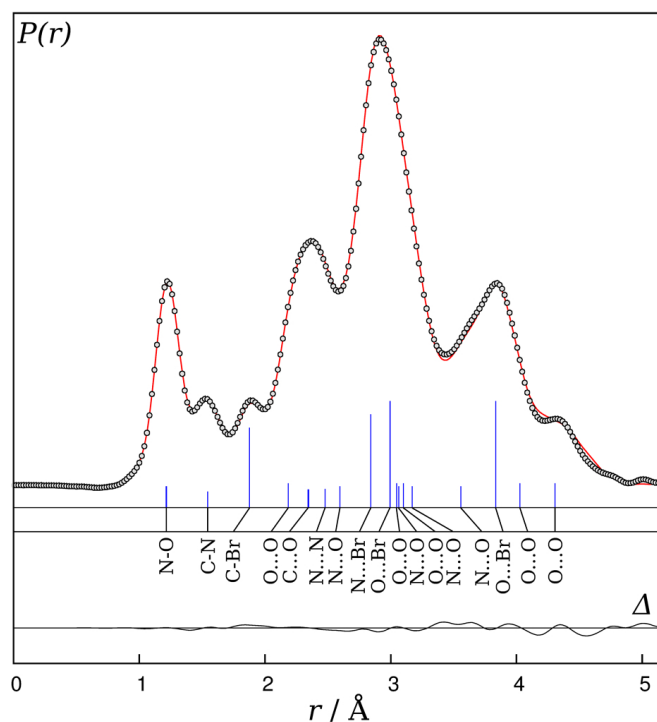
Figure 3.: Experimental (open circles) and model (line) radial distribution functions of $BrC(NO_2)_3$ (**2**). The difference curve is shown below. Vertical bars indicate interatomic distances in the model.

in the monoclinic crystal system, in the space group Cc (**1**), respectively $P2_1/c$ (**2**, **3**), each with four formula units per unit cell. The molecular structures of **1**–**3** are shown in Figure 4–6.
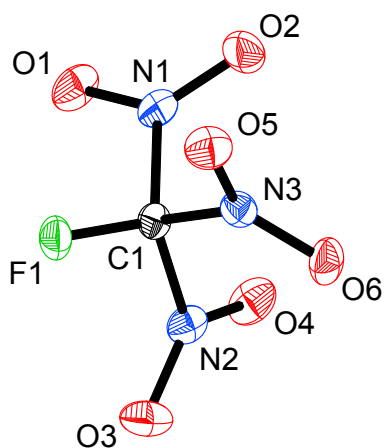
Figure 4.: Molecular structure of **1** in the crystal. Selected distances and angles are listed in Table 5.
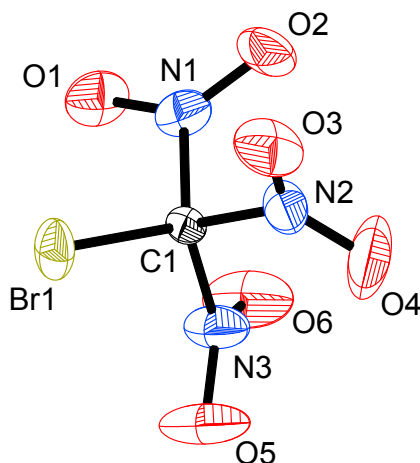
Figure 5.: Molecular structure of **2** in the crystal. Selected distances and angles are listed in Table 5.
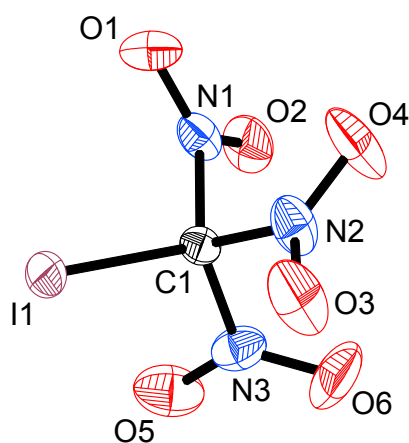
Figure 6.: Molecular structure of **3**. Selected distances and angles are listed in Table 5.

Comparative Discussion of Molecular Structures

In discussion of geometrical parameters below the traditional representations of their experimental errors in parentheses are used: 1σ for values from XRD and 3σ for the values from GED. The quantum chemically optimized structures at the levels MP2/cc-pVTZ for F−, Cl− and MP2/SDB-cc-pVTZ for Br− and I−C(NO$_2$)$_3$ agree well with experimentally determined values. Therefore, the wavefunctions obtained with these approximations were further used in Natural Bond Orbital (NBO)[30] and Atoms in Molecules (AIM)[31] calculations and discussion of various molecular features as supplementary information.

Additionally, Interacting Quantum Atoms (IQA)[32] calculations were performed using RHF/cc-pVTZ (for **1** and $ClC(NO_2)_3$) and RHF/SDB-cc-pVTZ (**2**, **3**) wavefunctions, which were computed for the MP2 geometries obtained with the same basis sets. The IQA theory allows a separation of the molecular energy into terms corresponding to atoms (in the form of the QTAIM atomic basins) and their pairs (Equation 7).

$$E_{mol} = \sum_A E_{(A)} + \sum_A \sum_B E_{(A,B)} \qquad (7)$$

In Equation 7, E_{mol} is the total molecular energy, $E_{(A)}$ is the energy of atom A and $E_{(A,B)}$ is the interaction energy of atoms A and B. The summation is carried out over all atoms and their pairs. Thus, there is possibility to identify stabilizing and destabilizing pairwise atom-atom interactions. The most important results of IQA calculations for the F−, Cl−, Br− and I−$C(NO_2)_3$ molecules are summarized in Table 4 and used in the discussion below.

Relative to the conformation of the gas-phase structures, for which propeller-like C_3 symmetry was assumed in the refinement of the electron diffraction data and confirmed by the good fit of these models to the experimental data, the crystal structures display the lower C_1 symmetry. However, the trinitromethyl moieties of **1**–**3** reveal an approximate threefold axis of symmetry along the Hal−C bond.

The C−N bonds of **1**–**3** in the solid are between 1.501(7) and 1.548(7) Å (Table 5), similar to the equilibrium values obtained from the gas-phase at 1.517(4) Å for **1** and 1.529(3) Å for **2**. All these values are remarkably larger than those for typical C−N bonds (~ 1.47 Å).[33,34] Elongated C−N bonds in trinitromethyl moieties are not unusual and have been reported earlier.[21–26,35–37] In terms of NBO theory this can be explained by orbital interactions of two types. First is the lp(Hal) $\rightarrow \sigma^*$(C−N) interaction, where in the NBO notation lp is one of the lone pairs of electron on a halogen atom and σ^* corresponds to an anti-bonding orbital of a C−N bond. The NBO second order perturbation theory analysis shows that the $E^{(2)}$ energies of such interactions can be as large as 19.7, 17.5, 13.6 and 9.9 kcal mol^{-1} for F−, Cl−, Br− and I−derivatives, respectively. The second type of orbital interactions relevant to the elongation of the C−N bonds is lp(O) $\rightarrow \sigma^*$(C−N) within independent C−NO_2 units. The corresponding $E^{(2)}$ values are even somewhat larger than for those described above of the first type, the largest ones are 26.9, 26.5, 25.5 and 24.9 kcal mol^{-1} along the same series of molecules. Both types of interactions lead to significantly increased occupations (0.22 e in average for all compounds) of anti-bonding σ^*(C−N) orbitals and, as a consequence, to a weakening and elongation of the corresponding C−N bonds.

There is a trend for the N−C−N angles to be slightly smaller for the $HalC(NO_2)_3$ molecules with larger and less electronegative Hal from both the crystal and gas-phase data and the average solid state values nicely match with the gas-phase data (Table 5). As expected, the spatially more demanding bromine and iodine atoms in **2** and **3** lead to wider Hal−C−N and subsequently to narrower N−C−N angles. Due to the small fluorine atom, the conformation of **1** shows the most tetrahedron-like surrounding of the central carbon atom. An argument in the same direction can be derived from the view of the simple VSEPR model. The higher the electronegativity of Hal, the more polarized is the Hal−C bond towards Hal and consequently this bond requires less space at the carbon atom and allows the nitro groups to move further apart.

Table 4.: Results of NBO, AIM and IQA analyses of $HalC(NO_2)_3$ molecules (charges, volumes and energies in atomic units).

	1 $FC(NO_2)_3$	$ClC(NO_2)_3$	**2** $BrC(NO_2)_3$	**3** $IC(NO_2)_3$
$q_{NBO}(Hal)$	−0.29	0.15	0.27	0.42
$q_{NBO}(C)$	0.73	0.29	0.20	0.10
$q_{NBO}(N)$	0.59	0.60	0.59	0.59
$q_{NBO}(O)$ [a]	−0.37	−0.37	−0.37	−0.38
$q_{AIM}(Hal)$	−0.72	0.01	0.17	0.35
$q_{AIM}(C)$	1.70	0.97	0.85	0.74
$q_{AIM}(N)$	0.52	0.54	0.54	0.54
$q_{AIM}(O)$ [a]	−0.43	−0.44	−0.44	−0.45
$Vol(Hal)$ [b]	1789	3962	4613	5205
$Vol(C)$ [b]	23	32	35	40
$E_{(Hal, C1)}$	−0.985	−0.251	−42.212	−63.603
$E_{(Hal, O1)}$	0.054	−0.011	−41.625	−64.932
$E_{(Hal, O2)}$	0.045	−0.003	−32.564	−50.844
$E_{(Hal, N1)}$	−0.088	−0.008	−34.383	−52.733
$E_{(C1, N1)}$	−0.059	−0.134	−0.158	−0.189
$E_{(N, N)}$	0.033	0.037	0.037	0.035
$E_{(O, O)}$ [c]	0.027	0.029	0.030	0.031
$E_{(N, O)}$ [c]	−0.049	−0.054	−0.055	−0.055

[a] Average value. [b] Atomic basin volumes. [c] For the non-bonded pair with shortest interatomic distance.

Expectedly, all C−NO$_2$ groups of **1**–**3** are essentially planar in the solid- and gas-phases. The nitro groups are arranged in a propeller-like twisted array (Figure 1 and 8). In this context, the Hal−C−N−O dihedral angles are indicative for the rotation of the nitro groups out of the Hal C N plane. These dihedral angles are in the range of 27.8–48.8°

in the crystal (for **1**–**3**; $ClC(NO_2)_3$ [21]: 37.0–46.6°) and in a narrow range of 37.9–38.3° in the gas-phase structures (for **1** and **2**; $ClC(NO_2)_3$ [17]: 49.3°), which are all quite common values and comparable to various other trinitromethyl compounds. [17–19,22–26,35,36] The calculated NBO and AIM charges of nitrogen and oxygen atoms for the series F−, Cl−, Br− and I−$C(NO_2)_3$ are collected in Table 4. Both types of charges show high constancy along this series of compounds. In terms of the primitive model of charged atoms, the partial charge distributions of nitrogen (δ^+) and oxygen atoms (δ^-) in the nitro groups optimize propeller-like twisting intramolecular non-bonded N···O attractions while minimizing the corresponding O···O repulsions. This interpretation is supported by results of the IQA calculations since the $E_{(N, O)}$ and $E_{(O, O)}$ values are negative and positive, respectively, in all discussed compounds. These N···O attractive interactions of two adjacent nitro groups in the trinitromethyl moieties are found for **1**–**3** in the range between 2.50 and 2.64 Å (Table 6), which are significantly lower than the sum of the van der Waals radii of nitrogen and oxygen (3.07 Å) [38,39]. Very similar distances have been measured also by GED in the gas-phase. Very strong attractive N···O interactions would be expected to lead to a pyramidalization of nitrogen atoms, but this is neither observed in the gas nor in the solid state. It can thus be concluded that the effect of N···O interactions is of minor influence on the molecular structures. The structure motif of twisted nitro groups with attractive N···O interactions is also found in the crystal structures of the comparable compounds $HC(NO_2)_3$ [37] and $ClC(NO_2)_3$ [21]. Similar to $ClC(NO_2)_3$ [21] the oxygen atoms in **1**–**3** involved in these intramolecular N···O contacts are those most distant to the halogen atom (Figure 8).

The other oxygen atoms in **1**–**3** display short distances to the corresponding halogen atoms in the range of 2.56 to 2.62 Å (crystal) and 2.58 Å (gas-phase) for **1**, 2.99 to 3.01 Å (crystal) and 2.98 Å (gas-phase) for **2** and 3.16 to 3.20 Å (crystal) for **3**. These values are substantially lower than the sum of the van der Waals radii for these atom pairs ($r_{(F+O)} = 2.99$ Å, $r_{(Br+O)} = 3.37$ Å, $r_{(I+O)} = 3.50$ Å), [38,39] but this does not necessarily indicate attractive interactions between the oxygen and halogen atoms. Due to the particularly high electron-withdrawing properties of the trinitromethyl moiety, the C−Hal bonds are shorter than usual and consequently sterically overcrowded structures are observed.

The electron-withdrawing strength can be estimated using the Taft parameter (σ^*), which reflects polar (inductive, field and resonance) effects. [40] The trinitromethyl moiety has a very large value of that polar substituent constant of $\sigma^* = 4.54$, [41] compared to smaller ones for fluorine (3.19), chlorine (2.94), bromine (2.80) and iodine (2.22). [42] Consequently, conventional (electrostatic) properties of the halogen atoms are expected to change under the action of the trinitromethyl moiety, even the strongly electronegative fluorine atom.
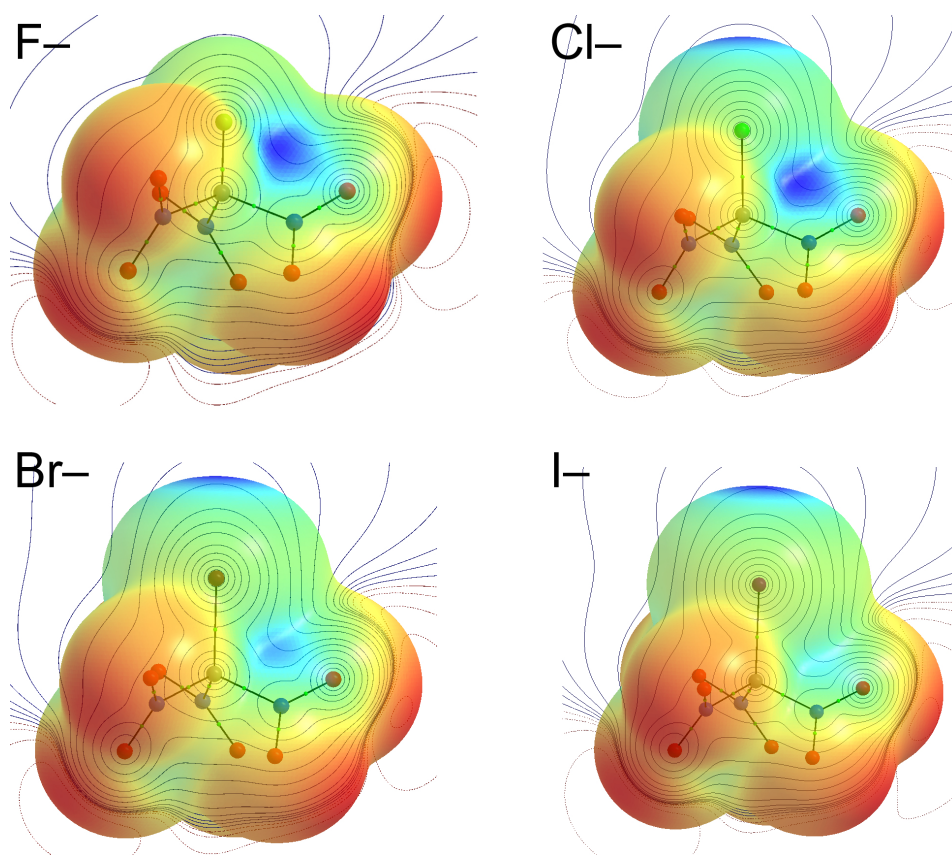
Figure 7.: Total electrostatic potentials of the F−, Cl−, Br− and I−C(NO$_2$)$_3$ molecules mapped on the isosurfaces of electron density (0.001 e Bohr^{-3}). Contour plots are total electrostatic potentials in the planes of three atoms Hal, C1 and O1. Blue color displays positive values, red color displays negative values.

Electronegativity can also be attributed to composition of σ-bonding orbitals. NBO calculations of BrC(NO$_2$)$_3$ have shown that σ(Br−C) can be described as being composed of 0.68(sp$^{6.7}$)$_{Br}$ + 0.73(sp$^{2.8}$)$_C$. The polarization coefficients 0.73 > 0.68 can serve as indicators of electronegativity and show that in **2** bromine is less electronegative than the carbon atom due to the nitro-substituent effect. For comparison we have performed similar calculations for the BrC(CH$_3$)$_3$ molecule. In this case the inverted picture was obtained: the composition of the σ(Br−C) orbital was 0.73(sp$^{6.1}$)$_{Br}$ + 0.68(sp$^{5.7}$)$_C$, indicating a normal situation where bromine is more negative than the carbon atom. The same relationship has been found for σ(Hal−C) orbital composition in the I−, but not for the Cl− and especially for the F−derivatives. Nevertheless, the trend of decreasing halogen electronegativity with respect to that of the carbon atom upon transition from Hal−C(CH$_3$)$_3$ to Hal−C(NO$_2$)$_3$ was observed for all types of halogen atoms. Another observation is the much higher s contribution in the carbon hybrid to the Br−C bond

in $BrC(NO_2)_3$ ($sp^{2.8}$) than in $BrC(CH_3)_3$ ($sp^{5.7}$), again explaining the shorter bond in the first. It may thus be concluded that electronegativity plays an important role in shortening of the Hal−C bonds in the $HalC(NO_2)_3$ molecules.

QTAIM calculations support this view by comparing charges and basin volumes of halogen atoms in $HalC(NO_2)_3$ and $HalC(CH_3)_3$ molecules. The values for $HalC(NO_2)_3$ are given in Table 4. The AIM charges of the halogen atoms in $HalC(CH_3)_3$ molecules are −0.69, −0.31, −0.20 and −0.07 e in the series of F−, Cl−, Br− and I−derivatives, respectively. These results show the systematically smaller values of charges of all halogen atoms in $HalC(CH_3)_3$ compared with those in $HalC(NO_2)_3$. This is consistent with the conclusions on electronegativity made before.

The AIM basin volumes of halogen atoms in $HalC(CH_3)_3$ are 1624, 3486, 4294 and 4937 $Bohr^3$ and in $HalC(NO_2)_3$ the corresponding basin volumes are systematically larger (Table 4). This indicates that in $HalC(NO_2)_3$ the halogen atoms are more diffuse. Also interesting is to compare basin volumes of the central carbon atoms in both series of compounds. Table 4 shows these quantities for the $HalC(NO_2)_3$ molecules. The corresponding values for $HalC(CH_3)_3$ molecules are 36, 44, 44 and 47 $Bohr^3$. Thus, the carbon atoms are more compact in all $HalC(NO_2)_3$ derivatives, in agreement with the concept of electronegativity and explaining the shortening of the Hal−C bonds in these molecules. Therefore, these bonds in **1**–**3**, F−C 1.297(3) Å (crystal), 1.300(11) Å (gas-phase); Br−C 1.853(5) Å (crystal), 1.869(6) Å (gas-phase); I−C 2.097(4) Å (crystal), respectively, are remarkably shorter than average Hal−C_{sp^3} bond lengths (F−C: 1.43 Å, Br−C: 1.97 Å, I−C: 2.16 Å).[33]

Gas-phase equilibrium structures determined by GED allow a direct comparison with theoretically calculated structures. Interestingly, the previously predicted length of the C−F bond in $FC(NO_2)_3$ (1.305 Å on the B3LYP/6-311+G(d,p) level)[16] agrees well with the value measured in this work at 1.300(11) Å. However, the same combination of DFT functional and basis set gives overestimated lengths for the C−Br bond (1.894 Å)[16] versus the experimental value of 1.869(6) Å. The corresponding thermally averaged r_a value found in this work (1.876(6) Å) is also slightly smaller, in fact almost equal, than the r_a values from previous GED measurements (1.885(9) Å and 1.894(9) Å).[17,19]

Concerning the Hal···O contacts in $HalC(NO_2)_3$ according to the simplest model, the calculated AIM charges, predict repulsion for the pair F···O and attraction for the pairs Br···O and I···O. The Cl···O contact is on the border between repulsion and attraction due to almost neutral charge of the chlorine atom (0.01 e). Indeed, the $E_{(Hal, O)}$ energies (Table 4) from the more advanced IQA theory show that the F···O contacts destabilize the molecule, the Cl···O contacts play only a minor role while the Br···O and I···O should stabilize the respective molecules. However, for the last two cases it should be mentioned, that those effects are comparable to the bonded Hal−C and

the non-bonded interactions Hal···N, respectively. Thus, the shortening of the Br−C and I−C bonds cannot be solely due to the stabilizing Br···O and I···O interactions. Interestingly, the already mentioned stabilizing Hal···N terms can also not be predicted on the basis of charges in case of the Cl−, Br− and I−derivatives, since both, halogen and nitrogen atoms, have positive partial charges in these molecules.

Previously performed calculations showed the surfaces of the halogen atoms in F−, Cl− and Br−C(NO$_2$)$_3$ to be entirely positive, with the most positive site on the extension of the C−Hal bond.[21] The presence and magnitude of a positive halogen potential depends upon both, halogen and electron-withdrawing strength of the remainder of the molecule.[43–47] In this work we have calculated the total electrostatic potential (ESP) for the I−derivative and, for consistency, for all other discussed molecules (Figure 7). Since the computed ESP values in the previous work [21] were for points of only one isosurface of electron density (0.001 e Bohr^{-3}) and to extend our knowledge about this property of the molecules, we have also calculated contour plots of ESP for the planes where Hal, C and O atoms reside. Figure 7 clearly shows that the ESPs on the lines (and regions) between halogen and oxygen atoms are entirely positive and cannot serve as indicators of attractive interactions between Hal and O atoms. In fact, the total ESP is positive in areas between all pairs of bonded and non-bonded atoms. However, the bonded atoms, as well as some pairs of non-bonded atoms, demonstrate stabilizing interactions as we already know from the IQA calculations (Table 4). Thus, total ESPs are hardly useful in the discussion of intramolecular properties of these small molecules, but could rather be helpful in the discussion of intermolecular interactions.
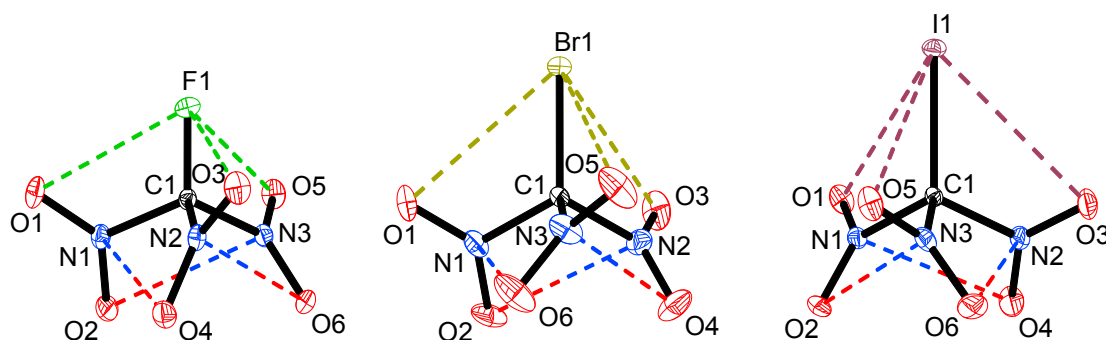
Figure 8.: Intramolecular Hal···O (Hal = F (**1**), Br (**2**), I (**3**)) and N···O interactions of **1** (left), **2** (center) and **3** (right), displayed by dashed lines. Thermal ellipsoids are drawn at the 25 % (**1**), 8 % (**2**) and 12 % (**3**) probability level for clarity. Selected distances [Å]: FC(NO$_2$)$_3$ (**1**): F1···O1 2.609(3), F1···O3 2.563(3), F1···O5 2.616(3), N1···O4 2.637(3), N2···O6 2.615(3), N3···O2 2.604(3); BrC(NO$_2$)$_3$ (**2**): Br1···O1 3.007(5), Br1···O3 2.984(7), Br1···O5 3.002(8), N1···O6 2.518(9), N2···O2 2.539(9), N3···O4 2.504(11); IC(NO$_2$)$_3$ (**3**): I1···O1 3.158(4), I1···O3 3.194(5), I1···O5 3.204(4), N1···O4 2.554(6), N2···O6 2.542(6), N3···O2 2.556(5).

Intermolecular Interactions in the Crystals

Besides intramolecular interactions, various intermolecular interactions determine the arrangement of the molecules within their crystals. Intermolecular $N-O$ contacts with values only slightly lower than the sum of the van der Waals radii for these atoms $(3.07\,\text{Å})$ [38,39] suggest weak, but attractive interactions. The shortest intermolecular $N-O$ contact is found for **1** $(2.92\,\text{Å})$, and even weaker ones for **2** $(3.06\,\text{Å})$ and **3** $(3.05\,\text{Å})$. More important are the intermolecular Hal$-$O contacts in **1**–**3** (Table 6). The unit cell views display these intermolecular interactions for **1**–**3** (Figure 9). Calculations of the electrostatic potential of various molecular environments showed, that covalently bonded halogen atoms may have a localized region of significantly positive electrostatic potential on its outer side, along the extension of that bond [43–49] and this was confirmed in this work as discussed above (Figure 7). It develops when an orbital on the corresponding atom is involved in forming a covalent bond and results in an electron deficiency opposite to that bond. This electron deficiency outer lobe of that orbital and therefore the existence of a positive region is referred to as σ-hole. [43,44,46,47]

Table 5.: Comparison of selected bond lengths and angles of HalC(NO$_2$)$_3$ (Hal = F (**1**), Cl, Br (**2**), I (**3**)) in the crystal and gas-phase structures (distances in Å, angles in deg). [a]

	1 FC(NO$_2$)$_3$		ClC(NO$_2$)$_3$	
	XRD	GED [b]	XRD [21]	GED [17–19] [c]
C1$-$Hal [d]	1.297(3)	1.300(11)	1.694(2)	1.712(12)
C1$-$N1	1.524(3)		1.543(2)	
C1$-$N2	1.530(3)	1.517(4)	1.544(2)	1.513(9)
C1$-$N3	1.520(3)		1.538(2)	
N1$-$O1	1.204(3)		1.214(2)	
N2$-$O3	1.205(3)	1.210(1)	1.205(2)	1.213(3)
N3$-$O5	1.209(3)		1.209(2)	
N1$-$O2	1.218(3)		1.211(2)	
N2$-$O4	1.209(3)	1.211(1)	1.216(2)	1.213(3)
N3$-$O6	1.217(3)		1.215(2)	
Hal$-$C1$-$N1	110.8(2)		112.3(2)	
Hal$-$C1$-$N2	110.2(2)	110.2(6)	112.7(2)	112.1(15)
Hal$-$C1$-$N3	110.3(2)		112.5(2)	
N1$-$C1$-$N2	108.1(2)		106.0(2)	
N2$-$C1$-$N3	109.3(2)	108.7(6)	106.0(2)	106.7(16) [e]
N3$-$C1$-$N1	108.3(2)		106.8(2)	
Hal$-$C1$-$N$-$O	36.3(3) [f]	37.9(22)	42.2(2) [f]	49.3(1)

	2 BrC(NO$_2$)$_3$		**3** IC(NO$_2$)$_3$
	XRD	GED [b)]	XRD
C1−Hal [d)]	1.853(5)	1.869(6)	2.097(4)
C1−N1	1.548(7)	⎫	1.533(5)
C1−N2	1.547(7)	⎬ 1.529(3)	1.540(6)
C1−N3	1.501(7)	⎭	1.531(6)
N1−O1	1.214(7)	⎫	1.211(5)
N2−O3	1.183(8)	⎬ 1.209(1)	1.206(5)
N3−O5	1.198(7)	⎭	1.204(5)
N1−O2	1.219(7)	⎫	1.212(5)
N2−O4	1.208(8)	⎬ 1.214(1)	1.208(5)
N3−O6	1.229(7)	⎭	1.207(5)
Hal−C1−N1	112.8(3)	⎫	112.4(3)
Hal−C1−N2	111.5(3)	⎬ 112.5(3)	112.2(3)
Hal−C1−N3	113.4(3)	⎭	113.8(3)
N1−C1−N2	105.2(4)	⎫	106.3(3)
N2−C1−N3	106.3(5)	⎬ 106.3(3)	105.8(3)
N3−C1−N1	107.0(4)	⎭	105.8(3)
Hal−C1−N−O	42.2(7) [f)]	38.3(13)	44.8(4) [f)]

[a)] Due to the higher symmetry in the gas-phase, parameter values corresponding to groups of parameters in the crystal structures are provided (E.s.d.s quoted are 1σ for XRD and 3σ for GED). [b)] r_e-values. [c)] Presumably r_a-values are given in ref. 19. [d)] For comparison: Average Hal−C$_{sp^3}$ bond lengths: F−C: 1.43 Å, Cl−C: 1.85 Å, Br−C: 1.97 Å, I−C: 2.16 Å. [33] [e)] The value of the parameter and error propagation were calculated from the data given in ref. 19. [f)] Averaged value of Hal−C1−N−O1/3/5.

The positive character of this region increases along the series from the lighter to the heavier, more polarizable and less electronegative halogens, and when the remainder of the molecule becomes more electron-withdrawing. Therefore, the σ-hole is least positive for the fluorine compound **1** and most positive for the iodine compound **3**. The σ-hole bonding R−X⋯B (B = Lewis-base), in this context also commonly called halogen bonding, is the resulting non-covalent interaction that may occur with a negative site.[43–47,50?] The interaction is highly directional, along the extension of the covalent bond, giving rise to the σ-hole.

Table 6.: Distances [Å] and angles [deg] of some intra- and intermolecular interactions of **1**–**3** and $ClC(NO_2)_3$ [21].

	1 $FC(NO_2)_3$		$ClC(NO_2)_3$	**2** $BrC(NO_2)_3$		**3** $IC(NO_2)_3$
	XRD	GED	XRD	XRD	GED	XRD
$N{\cdots}O_{intra}$ [a)]	2.637(3) 2.615(3) 2.604(3)	2.611(7)	2.571(2) 2.547(2) 2.554(2)	2.518(9) 2.539(9) 2.504(11)	2.543(4)	2.554(6) 2.542(6) 2.556(5)
$Hal{\cdots}O_{intra}$ [a)]	2.609(3) 2.563(3) 2.616(3)	2.576(6)	2.939(2) 2.897(2) 2.903(2)	3.007(5) 2.984(7) 3.002(8)	2.980(4)	3.158(4) 3.194(5) 3.204(4)
$Hal{\cdots}O_{inter}$ [a)]	2.782(3)	–	2.950(2)	3.035(5)	–	2.930(3)
$C{-}Hal{\cdots}O_{inter}$	141.0(2)	–	172.8(1)	165.3(2)	–	172.8(2)

[a)] The shortest $Hal{\cdots}O_{intra/inter}$ contacts are given. For comparison: Sum of the van der Waals radii: $r_{(N+O)} = 3.07$ Å, $r_{(F+O)} = 2.99$ Å, $r_{(Cl+O)} = 3.27$ Å, $r_{(Br+O)} = 3.37$ Å, $r_{(I+O)} = 3.50$ Å. [38,39]
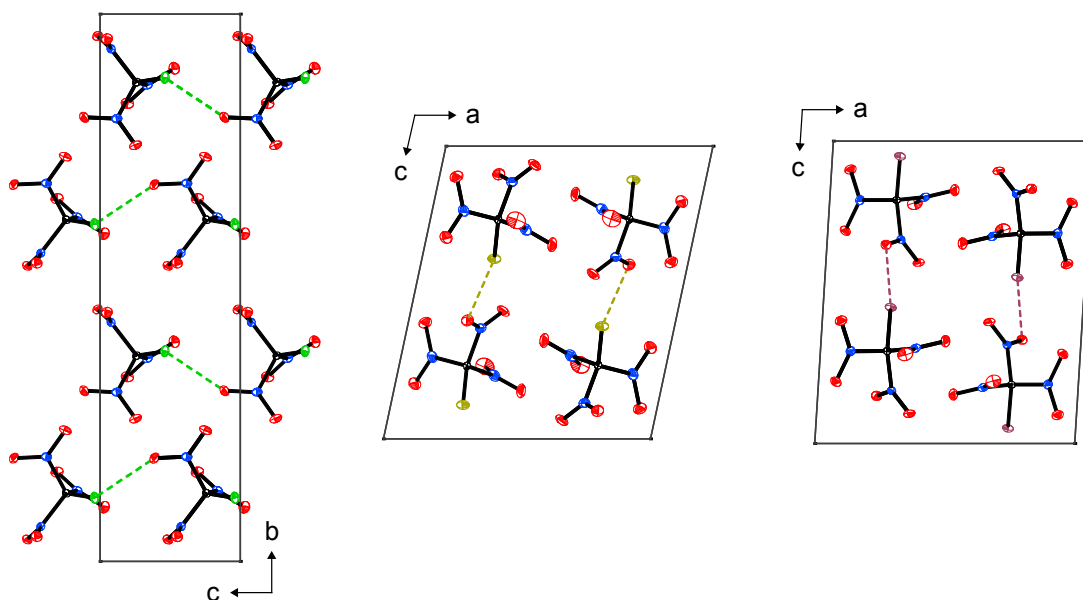
Figure 9.: Intermolecular $Hal{\cdots}O$ (Hal = F (**1**), Br (**2**), I (**3**)) interactions of **1** (left), **2** (center) and **3** (right), displayed by dashed lines. Thermal ellipsoids are drawn at the 25 % (**1**), 8 % (**2**) and 12 % (**3**) probability level for clarity. Selected intermolecular distances [Å]: $FC(NO_2)_3$ (**1**): $F{\cdots}O$ 2.782(3), $BrC(NO_2)_3$ (**2**): $Br{\cdots}O$ 3.035(5), $IC(NO_2)_3$ (**3**): $I{\cdots}O$ 2.930(3).

The strongest halogen bonding of all halogenotrinitromethanes shows the iodine compound **3** due to the most positive σ-hole and the C$-$Hal$\cdots$O angle of 172.8(1)° close to the ideal value of 180°. This leads even to significantly shorter intermolecular than intramolecular Hal$\cdots$O contacts (Table 6, Figure 9). The influence of this interaction on the general bonding situation decreases along the series from the iodine compound (**3**) to the fluorine compound (**1**). Therefore, **1** shows an unfavorable C$-$Hal$\cdots$O angle of 141.0(2)° and much longer intermolecular than intramolecular Hal$\cdots$O contacts (Table 6, Figure 9). Computational investigations predicted that halogen bonding is also likely to affect the Hal$-$C bond length, whereas both longer and shorter ones are possible, depending on the properties of the donor and acceptor.[51] Calculated values for $ClC(NO_2)_3$ revealed no relevant contribution of the halogen bonding to the Cl$-$C bond length.[21]

Table 7.: Crystal and structure refinement data for $FC(NO_2)_3$ (**1**), $BrC(NO_2)_3$ (**2**) and $IC(NO_2)_3$ (**3**).

	1 $FC(NO_2)_3$	**2** $BrC(NO_2)_3$	**3** $IC(NO_2)_3$
Chemical formula	CFN_3O_6	$CBrN_3O_6$	CIN_3O_6
Formula weight [g mol^{-1}]	169.03	229.93	276.93
Crystal dimensions [mm]	$0.30 \times 0.30 \times 0.23$	$0.30 \times 0.30 \times 0.21$	$0.37 \times 0.19 \times 0.03$
Crystal description	colorless block	colorless block	pale yellow block
Crystal system	monoclinic	monoclinic	monoclinic
Space group (No.)	Cc (9)	$P2_1/c$ (14)	$P2_1/c$ (14)
a [Å]	5.4980(3)	9.9590(15)	9.6928(4)
b [Å]	19.1919(11)	6.5930(8)	6.6961(2)
c [Å]	5.4068(3)	10.5270(11)	10.6304(3)
α [°]	90.0	90.0	90.0
β [°]	104.505(3)	102.812(10)	93.782(3)
γ [°]	90.0	90.0	90.0
V [Å^3]	552.33(5)	673.99(15)	688.45(4)
Z	4	4	4
$\rho_{\text{calcd.}}$ [g mol^{-3}]	2.033	2.266	2.672
μ [mm^{-1}]	0.229	6.092	4.645
Temperature [K]	100(2)	270(2)	173(2)
$F(000)$	336	440	512
θ range [°]	3.97–30.00	3.67–24.99	4.50–26.00
Index ranges	$-7 \leq h \leq 7$	$-11 \leq h \leq 11$	$-10 \leq h \leq 11$
	$-26 \leq k \leq 26$	$0 \leq k \leq 7$	$-8 \leq k \leq 8$
	$-7 \leq l \leq 7$	$0 \leq l \leq 12$	$-13 \leq l \leq 12$
Reflections measured	6048	11022	3317
Reflections independent	807	1167	1325
Reflections unique	794	941	1103
$R1$, $wR2$ (2σ data)	0.0350, 0.0902	0.0448, 0.1017	0.0306, 0.0769
$R1$, $wR2$ (all data)	0.0355, 0.0908	0.0583, 0.1088	0.0363, 0.0788
Data/restraints/parameters	807/100/2	1167/100/0	1325/100/0
GOF on F^2	1.095	1.073	0.970
Residual $\rho_{\text{min/max}}$ [e Å^{-3}]	$-0.31/0.43$	$-0.56/0.66$	$-0.92/1.13$

6.4. Conclusions

The molecular structures of the halogenotrinitromethanes $HalC(NO_2)_3$ (Hal = F (**1**), Br (**2**), I (**3**)), have been determined in the crystalline state by X-ray diffraction, as well as for the free molecules in the gas-phase by electron diffraction. The gas-phase structures are qualitatively in agreement with structures in the crystal phase, but the Hal−C bonds are systematically shorter in the crystals in comparison to the values for the gas-phase. All halogenotrinitromethanes **1**–**3**, as well as the previously described $ClC(NO_2)_3$, illustrate various intramolecular non-bonded interactions in the free molecules and intermolecular interactions in the crystal structures. The intramolecular N⋯O, O⋯O and Hal⋯O interactions, both competitors for the degree of rotation of the nitro groups about the C−N bonds, lead to propeller-type conformations favoring these interactions. The Hal⋯O interactions are repulsive in the view of electrostatic potentials between the atoms, while stabilizing in all cases but Hal = F (**1**) in the equilibrium geometries according to Interacting Quantum Atoms (IQA) calculations. The high electronegativity of the halogenotrinitromethyl moiety leads to unusually short Hal−C (Hal = F (**1**), Br (**2**), I (**3**)) bonds. This can be rationalized by different models: (a) a high s contribution to the carbon hybrid involved in the Hal−C bonds and (b) a high contribution of lp(Hal) → σ*(C−N) interactions in terms of the NBO view, as well as (c) a small atomic basin of the carbon atom in the QTAIM view. Intermolecular attractive Hal⋯O interactions in the halogenotrinitromethanes can be explained in terms of the halogen bonding concept based on a positive σ-hole on the far side with respect to the Hal−C bond.

6.5. Experimental Section

General Procedures. The solvents carbon tetrachloride and *n*-hexane were dried by standard methods and freshly distilled prior to use. Bromine (Fluka), iodine monochloride and Selectfluor® fluorinating reagent (both Sigma-Aldrich) were used as received. The aqueous solution of trinitromethane (30 %, stabilized with urea; Aerospace Propulsion Products B.V.) was extracted and purified by precipitation of its potassium salt and subsequent acidification. Potassium trinitromethanide was synthesized by reaction of trinitromethanide with potassium hydroxide in water at ambient temperature. Raman spectra were recorded with a Bruker MultiRAM FT-Raman instrument fitted with a liquid nitrogen cooled germanium detector and a Nd:YAG laser (λ = 1064 nm, 300 mW). Infrared (IR) spectra were measured with a Perkin-Elmer Spectrum BX-FTIR spectrometer equipped with a Smiths DuraSampl*IR* II ATR device. All spectra were recorded at ambient temperature, the samples were neat liquids or solids. NMR spectra were recorded at 25 °C with a JEOL Eclipse 400 ECX instrument, and chemical shifts were

determined with respect to external Me_4Si (^1H, 400.2 MHz; ^{13}C, 100.6 MHz), $MeNO_2$ (^{15}N, 40.6 MHz), and CCl_3F (^{19}F, 376.5 MHz). Mass spectrometric data were obtained with a JEOL MStation JMS 700 spectrometer (EI+). All fragments are referred to the isotope with the highest natural abundance. Elemental analyses (C/N) were performed with an Elementar vario EL analyzer.

Quantum Chemical Calculations. Geometry optimizations using MP2 approximation [52] with cc-pVTZ and SDB-cc-pVTZ have been carried out by using Firefly QC package, [53] which is partially based on the GAMESS (US) source code. [54] Calculations of vibrational frequencies and numeric cubic force fields were done on the same level of theory with the Gaussian 03 program package. [55]

Gas-phase Electron Diffraction Experiment. The electron diffraction patterns were recorded on the heavily improved Balzers Eldigraph KD-G2 gas-phase electron diffractometer [56] at the University of Bielefeld. The experimental details (Table 8) are presented in ref. 56. The electron diffraction patterns were measured on the Fuji BAS-IP MP 2025 imaging plates, which were scanned using a calibrated Fuji BAS-1800II scanner. The intensity curves (Figures A.4 and A.5 of Supporting Information) were obtained by applying the method described earlier. [57] Sector function and electron wavelengths were refined [58] using benzene diffraction patterns, recorded along with the substances under investigation.

Gas-phase Electron Diffraction Structural Analysis. The structural analysis was performed with the UNEX program. [59] All refinements were done using two intensity curves simultaneously (see Figures A.4 and A.5 of Supporting Information), one from short and another from long camera distance, which were obtained by averaging independent intensity curves measured in the experiment. For the definition of independent geometrical parameters and their groups in least-squares refinements see Table 3. An additional dihedral angle $\varphi(O4-C2-N3-O5)$ was used as an independent parameter to define the position of the atom O5 (Figure A.8 of Supporting Information). The structures of $FC(NO_2)_3$ (**1**) and $BrC(NO_2)_3$ (**2**) were assumed to be of C_3 symmetry. The differences between values of parameters in one group were kept fixed at the values taken from MP2/cc-pVTZ and MP2/SDB-cc-pVTZ calculations. Mean square amplitudes were refined in groups (see Tables A.6 and A.7 of Supporting Information). For this purpose the scale factors (one per group) were used as independent parameters. Thus, the ratios between different amplitudes in one group were fixed on the theoretical values, calculated from quadratic and cubic force fields by using the SHRINK program. [60–63] The final determined structural parameters are given in Table 3. Correlation coefficients are provided in the Supporting Information.

X-ray Crystallography. For compound **1** and **2** a Nonius Kappa CCD and for compound **3**, an Oxford Xcalibur3 diffractometer with a CCD area detector was employed

Table 8.: Details of electron diffraction experiment for **1** and **2**.

Parameter	**1** FC(NO$_2$)$_3$		**3** ClC(NO$_2$)$_3$	
$d_{\text{nozzle-detector}}$ [mm]	250.0	500.0	250.0	500.0
$U_{\text{acceleration}}$ [kV]	60	60	60	60
$I_{\text{fast electrons}}$ [μA]	0.95	0.57	1.54	0.51
$\lambda_{\text{electron}}$ [a)] [Å]	0.048901	0.048466	0.048647	0.048511
T_{nozzle} [K]	296	294	353	353
p_{sample} [b)] [mbar]	2×10^{-5}	5×10^{-5}	2×10^{-5}	3×10^{-5}
$p_{\text{residual gas}}$ [c)] [mbar]	5×10^{-7}	6×10^{-7}	5×10^{-7}	7×10^{-7}
t_{exposure} [s]	10	8	4, 5, 6	5, 7, 9
s range [Å^{-1}]	8.6–34.0	2.2–17.4	8.6–32.0	2.2–17.0
inflection points [d)]	5	3	6	5

a) Determined from C$_6$H$_6$ diffraction patterns measured in the same experiment. b) During the measurement. c) Between measurements. d) Number of inflection points on the background lines (see Figure A.4 and A.5 of Supporting Information).

for data collection using Mo-K_α radiation ($\lambda = 0.710\,73$ Å). The structures were solved using direct methods (SHELXS-97[64,65] or SIR2004[66,67]) and refined by full-matrix least-squares on F^2 (SHELXL)[64,65]. All atoms were refined anisotropically. ORTEP plots are shown with thermal ellipsoids at the 50 % (**1**, **3**) or 30 % (**2**) probability level, except for Figures 8 and 9. CCDC 917831 (**1**), 917832 (**2**), and 917833 (**3**) contain the supplementary crystallographic data for this paper. These data can be obtained free of charge from The Cambridge Crystallographic Data Centre via www.ccdc.cam.ac.uk/data_request/cif.

CAUTION! All high nitrogen and oxygen containing compounds are potentially explosive energetic materials, although no hazards were observed during preparation and handling these compounds. Nevertheless, this necessitates additional meticulous safety precautions (earthed equipment, Kevlar® gloves, Kevlar® sleeves, face shield, leather coat, and ear plugs). In addition, especially fluorotrinitromethane shows significant degrees of toxicity. Particular care should be exercised in handling of this material and derivatives.

Synthesis of fluorotrinitromethane (1)

Into a colorless solution of Selectfluor (11.7 g, 33.0 mmol) in water (150 mL) potassium trinitromethanide (5.67 g, 30.0 mmol) was slowly added at 0 °C. After stirring for 12 h at ambient temperature, the reaction mixture turned colorless. Evaporation of the product

out of the reaction mixture into a cooling trap yielded $4.27\,\mathrm{g}$ ($84\,\%$) of **1** as a colorless oil.

M.p.: $-45\,°\mathrm{C}$. Raman: 1622 (16, $\nu_{as}NO_2$), 1358 (30), 1298 (28, $\nu_s NO_2$), 1011 (8), 857 (100, νCN), 800 (6), 641 (2), 523 (9), 407 (22), 365 (66), 326 (12), 223 (8), 184 (19) cm^{-1}. IR: 1606 (vs, $\nu_{as}NO_2$), 1357 (w), 1288 (s, $\nu_s NO_2$), 1012 (m), 856 (m, νCN), 794 (vs) cm^{-1}. ^{13}C$\{^1$H$\}$ NMR (CDCl$_3$): δ = 113.7 (doublet of septets, $^1J_{C-F}$ = 333.4 Hz, $^1J_{C-^{14}N}$ = 12.1 Hz, $C(NO_2)_3$) ppm. ^{15}N NMR (CDCl$_3$): δ = -40.7 (doublet, $^2J_{^{15}N-F}$ = 14.2 Hz, NO_2) ppm. ^{19}F NMR (CDCl$_3$): δ = -87.3 (septet, $^1J_{F-C}$ = 333.4 Hz, $^2J_{F-^{14}N}$ = 10.2 Hz) ppm. MS (EI+): m/z (%) = 169 (1) [M$^+$], 46 (100) [NO$_2^+$]. CFN$_3$O$_6$ (169.03): Anal. calcd. C 7.11, N 24.86; found C 7.27, N 24.95.

Synthesis of bromotrinitromethane (2)

Into an aqueous solution of trinitromethane ($43.8\,\mathrm{g}$ in relation to $30\,\%$ aqueous solution, $87.0\,\mathrm{mmol}$ in relation to pure trinitromethane) was added bromine ($13.9\,\mathrm{g}$, $87.0\,\mathrm{mmol}$) at ambient temperature. After stirring the orange reaction mixture for 30 min, the slightly yellow organic phase was extracted and the product crystallized at $0\,°\mathrm{C}$. The crystals of the crude product were filtered and washed with ice-cold water ($3 \times 10\,\mathrm{mL}$). Warming the product to ambient temperature yielded $15.6\,\mathrm{g}$ ($78\,\%$) of **2** as colorless oil.

M.p.: $10\,°\mathrm{C}$. Raman: 1615 (14, $\nu_{as}NO_2$), 1346 (21), 1294 (8, $\nu_s NO_2$), 981 (3), 919 (11), 840 (88, νCN), 790 (4), 643 (2), 389 (21), 377 (24), 343 (100), 225 (22), 205 (12), 171 (26) cm^{-1}. IR: 1595 (vs, $\nu_{as}NO_2$), 1345 (m), 1277 (s, $\nu_s NO_2$), 979 (m), 918 (w), 838 (s, νCN), 784 (vs) cm^{-1}. ^{13}C$\{^1$H$\}$ NMR (CDCl$_3$): δ = 121.9 (septet, $^1J_{C-^{14}N}$ = 8.1 Hz, $C(NO_2)_3$) ppm. ^{15}N NMR (CDCl$_3$): δ = -34.8 (s, NO_2) ppm. MS (EI+): m/z (%) = 91 (8) [CBr$^+$], 79 (3) [Br$^+$], 46 (100) [NO$_2^+$], 30 (66) [NO$^+$]. CBrN$_3$O$_6$ (229.93): Anal. calcd. C 5.22, N 18.28; found C 5.34, N 18.10.

Synthesis of iodotrinitromethane (3)

Into a yellow suspension of potassium trinitromethanide ($3.40\,\mathrm{g}$, $18.0\,\mathrm{mmol}$) in $40\,\mathrm{mL}$ of dry carbon tetrachloride was added iodine monochloride ($2.92\,\mathrm{g}$, $18.0\,\mathrm{mmol}$) at ambient temperature. After stirring the reaction mixture for 1 h at $70\,°\mathrm{C}$, the dark purple solution was filtered and washed with an ice-cold silver nitrate solution ($40\,\mathrm{mL}$, $20\,\%$ aqueous solution). The organic phase was filtered to remove precipitated silver iodide and dried over anhydrous magnesium sulfate. After removing the solvent under reduced pressure, the yellow solid was washed with ice-cold carbon tetrachloride ($2 \times 10\,\mathrm{mL}$). Crystallization of the product from *n*-hexane yielded $1.0\,\mathrm{g}$ ($20\,\%$) of **3** as pale yellow crystals.

M.p.: $55\,°\mathrm{C}$. Raman: 1616 (5, $\nu_{as}NO_2$), 1597 (35, $\nu_{as}NO_2$), 1348 (37), 1298 (7, $\nu_s NO_2$), 1287 (5, $\nu_s NO_2$), 947 (5), 916 (14), 839 (97, νCN), 789 (5), 649 (5), 607 (2),

400 (31), 371 (39), 309 (100), 224 (31), 183 (61), 159 (33) cm^{-1}. IR: 1597 (s, $\nu_{as}NO_2$), 1583 (vs, $\nu_{as}NO_2$), 1346 (m), 1290 (s, ν_sNO_2), 1278 (s, ν_sNO_2), 944 (m), 913 (m), 837 (s, νCN), 782 (vs) cm^{-1}. $^{13}C\{^1H\}$ NMR (CDCl$_3$): $\delta = 106.7$ (septet, $^1J_{C-^{14}N} = 6.4$ Hz, $C(NO_2)_3$) ppm. ^{15}N NMR (CDCl$_3$): $\delta = -30.8$ (s, NO_2) ppm. MS (EI+): m/z (%) = 277 (2) [M$^+$], 231 (1) [M$^+$ $-NO_2$], 139 (5) [CI$^+$], 127 (100) [I$^+$], 46 (39) [NO$_2^+$], 30 (68) [NO$^+$]. CIN$_3$O$_6$ (276.93): Anal. calcd. C 4.34, N 15.17; found C 4.57, N 15.34.

6.6. Acknowledgment

Supporting Information

GED data of compounds **1** and **2**. CIF files with crystallographic data for all compounds (**1**–**3**). This material is available free of charge via the Internet at http://pubs.acs.org.

6.7. References

[1] L. Birckenbach, K. Huttner, W. Stein, *Ber. Dtsch. Chem. Ges.* **1929**, *62B*, 2065–2075.

[2] L. Schischkoff, *Justus Liebigs Ann. Chem.* **1857**, *103*, 364–366.

[3] A. Hantzsch, A. Rinckenberger, *Ber. Dtsch. Chem. Ges.* **1899**, *32*, 628–641.

[4] L. Schischkoff, *Justus Liebigs Ann. Chem.* **1857**, *101*, 213–217.

[5] C. O. Parker, W. D. Emmons, H. A. Rolewicz, K. S. McCallum, *Tetrahedron* **1962**, *17*, 79–87.

[6] V. I. Pepkin, Y. N. Matyushin, G. K. Khisamutdinov, V. I. Slovetskii, A. A. Fainzil'berg, *Khim. Fiz.* **1993**, *12*, 1399–1403.

[7] G. K. Khisamutdinov, V. I. Slovetsky, Y. M. Golub, S. A. Shevelev, A. A. Fainzil'berg, *Russ. Chem. Bull.* **1997**, *46*, 324–327.

[8] W. Will, *Ber. Dtsch. Chem. Ges.* **1914**, *47*, 961–965.

[9] A. K. Macbeth, D. D. Pratt, *J. Chem. Soc., Trans.* **1921**, *119*, 354–358.

[10] V. Grakauskas, K. Baum, *J. Org. Chem.* **1968**, *33*, 3080–3082.

[11] L. T. Eremenko, A. A. Borisenko, S. I. Petrov, V. F. Andronov, *Russ. Chem. Bull.* **1968**, *17*, 423–424.

[12] M. D. Coburn, C. B. Storm, D. W. Moore, T. G. Archibald, *Magn. Reson. Chem.* **1990**, *28*, 16–20.

[13] V. A. Shlyapochnikov, A. A. Fainzil'berg, S. S. Novikov, *Russ. Chem. Bull.* **1962**, *11*, 478–479.

[14] V. A. Shlyapochnikov, D. V. Levchenkov, A. B. Kharitonkin, *Russ. Chem. Bull.* **2001**, *50*, 1173–1180.

[15] S. G. Vul'fson, A. P. Timosheva, A. N. Vereshchagin, B. A. Arbuzov, V. A. Shlyapochnikov, *J. Mol. Struct.* **1977**, *40*, 225–231.

[16] D. V. Levchenkov, A. B. Kharitonkin, V. A. Shlyapochnikov, *Russ. Chem. Bull.* **2001**, *50*, 385–389.

[17] N. I. Sadova, N. I. Popik, L. V. Vilkov, Y. A. Pankrushev, V. A. Shlyapochnikov, *J. Chem. Soc., Chem. Commun.* **1973**, 708–709.

[18] N. I. Sadova, N. I. Popik, L. V. Vilkov, Y. A. Pankrushev, V. A. Shlyapochnikov, *J. Struct. Chem.* **1974**, *15*, 593–595.

[19] N. I. Sadova, N. I. Popik, L. V. Vilkov, *J. Struct. Chem.* **1976**, *17*, 257–262.

[20] N. I. Golovina, L. O. Atovmyan, *J. Struct. Chem.* **1967**, *7*, 230–233.

[21] M. Göbel, B. H. Tchitchanov, J. S. Murray, P. Politzer, T. M. Klapötke, *Nat. Chem.* **2009**, *1*, 229–235.

[22] T. M. Klapötke, B. Krumm, R. Moll, S. F. Rest, *Z. Anorg. Allg. Chem.* **2011**, *637*, 2103–2110.

[23] T. M. Klapötke, B. Krumm, R. Moll, *Chem. Eur. J.* **2013**, *19*, 12113–12123.

[24] T. M. Klapötke, B. Krumm, R. Moll, A. Penger, S. M. Sproll, R. J. F. Berger, S. A. Hayes, N. W. Mitzel, *Z. Naturforsch.* **2013**, *68b*, 719–731.

[25] T. M. Klapötke, B. Krumm, R. Moll, S. F. Rest, W. Schnick, M. Seibald, *J. Fluorine Chem.* **2013**, *156*, 253–261.

[26] Q. J. Axthammer, T. M. Klapötke, B. Krumm, R. Moll, S. F. Rest, *Z. Anorg. Allg. Chem.* **2014**, *640*, 76–83.

[27] G. Socrates, *Infrared and Raman Characteristic Group Frequencies: Tables and Charts*, 3rd ed., John Wiley & Sons: Chichester, **2004**.

[28] T. M. Klapötke, B. Krumm, R. Moll, S. F. Rest, M. Sućeska, *Z. Naturforsch.* **2014**, *69b*, 8–16.

[29] M. J. Kamlet, R. E. Oesterling, H. G. Adolph, *J. Chem. Soc.* **1965**, 5838–5849.

[30] J. P. Foster, F. Weinhold, *J. Am. Chem. Soc.* **1980**, *102*, 7211–7218.

[31] R. F. W. Bader, *Atoms in Molecules – A Quantum Theory*, Oxford University Press: Oxford, **1990**.

[32] M. A. Blanco, A. M. Pendas, E. Francisco, E. *J. Chem. Theory Comput.* **2005**, *1*, 1096–1109.

[33] F. H. Allen, O. Kennard, D. G. Watson, L. Brammer, A. G. Orpen, R. Taylor, *J. Chem. Soc., Perkin Trans. 2* **1987**, S1–S19.

[34] A. F. Holleman, E. Wiberg, N. Wiberg, *Lehrbuch der Anorganischen Chemie*, 102nd ed., Walter de Gruyter: Berlin, **2008**.

[35] S. K. Bhattacharjee, H. L. Ammon, *Acta Crystallogr.* **1982**, *B38*, 2503–2505.

[36] Y. Oyumi, T. B. Brill, A. L. Rheingold, *J. Phys. Chem.* **1985**, *89*, 4824–4828.

[37] H. Schödel, R. Dienelt, H. Bock, *Acta Crystallogr.* **1994**, *C50*, 1790–1792.

[38] A. Bondi, *J. Phys. Chem.* **1964**, *68*, 441–451.

[39] M. Mantina, A. C. Chamberlin, R. Valero, C. J. Cramer, D. G. Truhlar, *J. Phys. Chem.* **2009**, *A113*, 5806–5812.

[40] R. W. Taft, In *Steric Effects in Organic Chemistry*, M. S. Newman, Ed., John Wiley & Sons: New York, **1956**, Ch. 13.

[41] J. Hine, W. C. Bailey, Jr., *J. Org. Chem.* **1961**, *26*, 2098–2099.

[42] A. Brändström, *J. Chem. Soc., Perkin Trans. 2* **1999**, 1855–1857.

[43] T. Clark, M. Hennemann, J. S. Murray, P. Politzer, *J. Mol. Model.* **2007**, *13*, 291–296.

[44] P. Politzer, P. Lane, M. C. Concha, Y. Ma, J. S. Murray, *J. Mol. Model.* **2007**, *13*, 305–311.

[45] P. Politzer, J. S. Murray, M. C. Concha, *J. Mol. Model.* **2007**, *13*, 643–650.

[46] P. Politzer, J. S. Murray, P. Lane, *Int. J. Quantum Chem.* **2007**, *107*, 3046–3052.

[47] J. S. Murray, P. Lane, P. Politzer, *J. Mol. Model.* **2009**, *15*, 723–729.

[48] P. Auffinger, F. A. Hays, E. Westhof, P. S. Ho, *Proc. Natl. Acad. Sci. USA* **2004**, *101*, 16789–16794.

[49] H.-G. Stammler, Y. V. Vishnevskiy, C. Sicking, N. W. Mitzel, *CrystEngComm* **2013**, *15*, 3536–3546.

[50] P. Metrangolo, H. Neukirch, T. Pilati, G. Resnati, *Acc. Chem. Res.* **2005**, *38*, 386–395.

[51] J. S. Murray, M. C. Concha, P. Lane, P. Hobza, P. Politzer, *J. Mol. Model.* **2008**, *14*, 699–704.

[52] C. Møller, M. S. Plesset, *Phys. Rev.* **1934**, *46*, 618–622.

[53] A. A. Granovsky, Firefly, Version 7.1.G.

[54] M. W. Schmidt, K. K. Baldridge, J. A. Boatz, S. T. Elbert, M. S. Gordon, J. H. Jensen, S. Koseki, N. Matsunaga, K. A. Nguyen, S. Su, T. L. Windus, M. Dupuis, J. A. Montgomery, *J. Comput. Chem.* **1993**, *14*, 1347–1363.

[55] M. J. Frisch, G. W. Trucks, H. B. Schlegel, G. E. Scuseria, M. A. Rob, J. R. Cheeseman, J. A. Montgomery Jr., T. Vreven, K. N. Kudin, J. C. Burant, J. M. Millam, S. S. Iyengar, J. Tomasi, V. Barone, B. Mennucci, M. Cossi, G. Scalmani, N. Rega, G. A. Petersson, H. Nakatsuji, M. Hada, M. Ehara, K. Toyota, R. Fukuda, J. Hasegawa, M. Ishida, T. Nakajima, Y. Honda, O. Kitao, H. Nakai, M. Klene, X. Li, J. E. Knox, H. P. Hratchian, J. B. Cross, V. Bakken, C. Adamo, J. Jaramillo, R. Gomperts, R. E. Stratmann, O. Yazyev, A. J. Austin, R. Cammi, C. Pomelli, J. W. Ochterski, P. Y. Ayala, K. Morokuma, G. A. Voth, P. Salvador, J. J. Dannenberg, V. G. Zakrzewski, S. Dapprich, A. D. Daniels, M. C. Strain, O. Farkas, D. K. Malick, A. D. Rabuck, K. Raghavachari, J. B. Foresman, J. V. Ortiz, Q. Cui, A. G. Baboul, S. Clifford, J. Cioslowski, B. B. Stefanov, G. Liu, A. Liashenko, P. Piskorz, I. Komaromi, R. L. Martin, D. J. Fox, T. Keith, M. A. Al-Laham, C. Y. Peng, A. Nanayakkara, M. Challacombe, P. M. W. Gill, B. Johnson, W. Chen, M. W. Wong, C. Gonzalez, J. A. Pople *GAUSSIAN 03*, Rev. B.03, Gaussian, Inc., Wallingford CT (USA), **2004**.

[56] R. J. F. Berger, M. Hoffmann, S. A. Hayes, N. W. Mitzel, *Z. Naturforsch.* **2009**, *64b*, 1259–1268.

[57] Y. V. Vishnevskiy, *J. Mol. Struct.* **2007**, *833*, 30–41.

[58] Y. V. Vishnevskiy, *J. Mol. Struct.* **2007**, *871*, 24–32.

[59] Y. V. Vishnevskiy, *UNEX*, Version 1.5.7.

[60] V. A. Sipachev, *J. Mol. Struct.: THEOCHEM* **1985**, *22*, 143–151.

[61] V. A. Sipachev, *Struct. Chem.* **2000**, *11*, 167–172.

[62] V. A. Sipachev, *J. Mol. Struct.* **2001**, *567–568*, 67–72.

[63] V. A. Sipachev, *J. Mol. Struct.* **2004**, *693*, 235–240.

[64] G. M. Sheldrick, *SHELX-97*, University of Göttingen, Göttingen (Germany), **1997**.

[65] G. M. Sheldrick, *Acta Crystallogr.* **2008**, *A64*, 112–122.

[66] M. C. Burla, R. Caliandro, M. Camalli, B. Carrozzini, G. L. Cascarano, L. De Caro, C. Giacovazzo, G. Polidori, R. Spagna, *SIR2004*, Institute of Crystallography, Bari (Italy), **2004**.

[67] M. C. Burla, R. Caliandro, M. Camalli, B. Carrozzini, G. L. Cascarano, L. De Caro, C. Giacovazzo, G. Polidori, R. Spagna, *J. Appl. Crystallogr.* **2005**, *38*, 381–388.

7. Nitrilotriacetyl Chloride
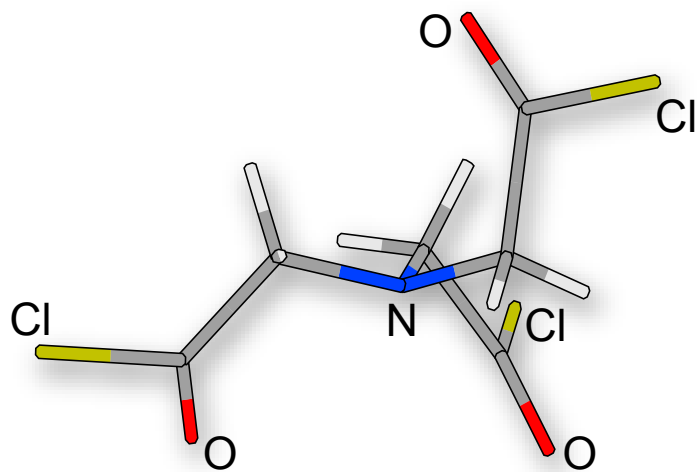
Synthesis and Structure of 2,2,2-Nitrilotriacetyl Chloride with a Flat NC$_3$ Pyramide

Thomas M. Klapötke,*[a] Burkhard Krumm,[a] and Richard Moll[a]

Dedicated to Professor Heinrich Nöth on the occasion of his 85th birthday

Keywords: 2,2,2-Nitrilotriacetic acid • Phosphorus pentachloride • Multinuclear NMR spectroscopy • Vibrational analysis • X-ray diffraction

*   Prof. Dr. Thomas M. Klapötke
     E-Mail: tmk@cup.uni-muenchen.de

[a]   Department of Chemistry
     Ludwig-Maximilian University of Munich
     Butenandtstrasse 5–13 (D)
     81377 Munich, Germany

7.1. Abstract

The reaction of 2,2,2-nitrilotriacetic acid with phosphorus pentachloride furnished 2,2,2-nitrilotriacetyl chloride (**1**), a useful chemical intermediate for various further reactions. The compound has been fully characterized by multinuclear NMR spectroscopy, vibrational analysis (IR and Raman), mass spectrometry and elemental analysis. Furthermore the crystal structure of **1** has been determined and discussed thoroughly, showing a NC_3 unit with an unusual, nearly planar configuration.

7.2. Introduction

The title compound 2,2,2-nitrilotriacetyl chloride (**1**) is useful as a chemical precursor for the preparation of various ester or (carbox-) amide compounds. The former compounds are synthesized using appropriate alcohols and the latter by reaction with suitable amines. This acid chloride **1** is best synthesized from 2,2,2-nitrilotriacetic acid, a very widely used complexant, and has been only briefly described prior to this study. [1–4] Our general interest in these type of compounds, especially containing polynitro groups, [5–7] prompted us to re-investigate 2,2,2-nitrilotriacetyl chloride (**1**). In this contribution, a detailed study of the synthesis, characterization and the crystal structure is presented.

7.3. Results and Discussion

Synthesis

The synthesis of 2,2,2-nitrilotriacetyl chloride (**1**) is performed by a chlorination reaction of 2,2,2-nitrilotriacetic acid with stoichiometric amounts of phosphorus pentachloride (Scheme 1). [1]
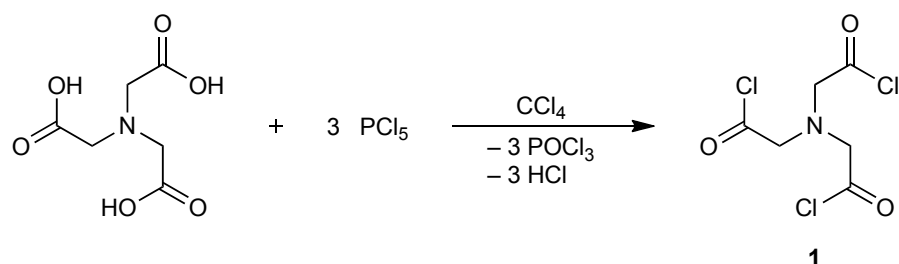
Scheme 1: Synthesis of 2,2,2-nitrilotriacetyl chloride (**1**).

The chlorination reaction starts rapidly upon heating the mixture, and therefore a slow and careful heating is recommended to avoid a fierce reaction. The formation

of gaseous hydrogen chloride is used to clearly monitor the progress and the end of the reaction. To avoid hydrolysis of the product, a work-up at lower temperatures is required. Therefore, in contrast to the previously reported synthesis, [1] the solvent carbon tetrachloride is used instead of benzene, which allows to perform the subsequent work-up at $0\,°C$.

NMR Spectroscopy

Multinuclear NMR spectroscopy of **1** showed in the ^{1}H NMR spectrum the resonance for the methylene group at 4.08 ppm. The resonances of the ^{13}C nuclei are found at 171.9 ppm for the carbonyl carbons and at 64.4 ppm for the methylene carbons. The ^{15}N NMR resonance is observed at -350.6 ppm.

Vibrational Spectroscopy

The vibrational analysis of the acid chloride **1** revealed C=O stretching vibrations between 1801 and 1766 cm^{-1}, in agreement with the typical range and intensities for carboxylic acid chlorides. [8] This stretching vibration shows splitting (in-phase and out-of-phase), both in the Raman (1801 and 1774 cm^{-1}) and IR spectra (1797 and 1766 cm^{-1}). Compared to the starting material 2,2,2-nitrilotriacetic acid (νCO = 1716 cm^{-1}), the C=O stretching vibration of the acid chloride **1** is found at higher frequencies. The C−Cl stretching vibration occurs at 782 cm^{-1} (Raman) and 771 cm^{-1} (IR). The bands with high intensity in the Raman spectrum at 450 and 439 cm^{-1} are assigned to the Cl−C=O in-plane deformation vibration. [8] The C−H stretching vibrations were found in the range of 2973–2850 cm^{-1}.

X-ray Diffraction

A single crystal suitable for X-ray diffraction measurements was obtained by recrystallization of **1** from *n*-hexane (crystallographic refinement parameters and structure data see Experimental Section). Compound **1** crystallizes in the orthorhombic space group *Pbca* with eight formula units per unit cell (Figure 1). While the starting material 2,2,2-nitrilotriacetic acid [9,10] exists in a zwitterionic form in the crystal, this is not possible for **1**. The molecule does not display a crystallographic threefold axis (C_3 symmetry) passing through the amine center, since the acetyl chloride moieties are all inequivalent. The C−N bond lengths are between 1.439(3) and 1.450(3) Å, slightly shorter compared to 2,2,2-nitrilotriacetic acid [10] and to a regular C−N single bond (1.469 Å). [11] This derives from the partial double bond character of the C−N bond, resulting to some extent in an iminium C−N=C resonance structure.
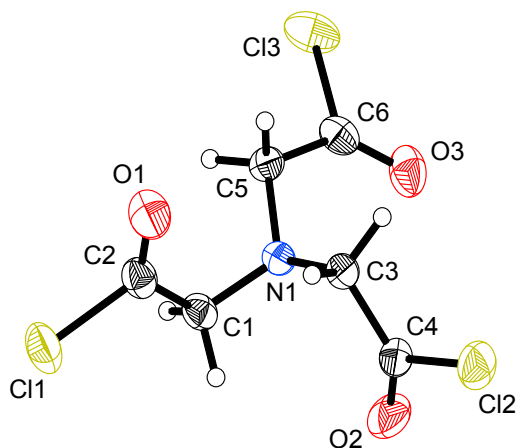
Figure 1.: Molecular structure of **1**. Selected distances [Å] and angles [deg]: N1−C1 1.439(3), C1−C2 1.509(3), C2−O1 1.175(3), C2−Cl1 1.779(2), N1−C3 1.450(3), C3−C4 1.497(3), C4−O2 1.170(3), C4−Cl2 1.792(2), N1−C5 1.446(3), C5−C6 1.500(3), C6−O3 1.174(3), C6−Cl3 1.789(2), N1−C1−C2 114.5(2), C1−C2−O1 127.9(2), C1−C2−Cl1 111.5(2), N1−C3−C4 112.3(2), C3−C4−O2 129.5(2), C3−C4−Cl2 109.5(2), N1−C5−C6 111.1(2), C5−C6−O3 128.2(2), C5−C6−Cl3 111.5(2), C1−N1−C3 114.9(2), C1−N1−C5 115.5(2), C3−N1−C5 116.1(2).

The central nitrogen atom is bound to three carbon atoms, and the C−N−C angles are in the range of 114.9(2)–116.1(2)°. For the sum of these angles a value of 346.5° is obtained. Therefore, this value is between 360° for an ideal planar arrangement and 328.5° for a pyramidal (pseudotetrahedral) arrangement.[12] The nitrogen atom shows a distance of 0.312(2) Å from the C1 C3 C5 plane. For comparison, the C−N bond lengths and the C−N−C angles of selected trimethyleneamine compounds with a similar bonding situation are shown in Table 1. A view of the unit cell view displays intermolecular hydrogen bonding between the molecules of **1** (Figure 2) with contact distances of 2.52 and 2.61 Å, slightly smaller than the sum of the van der Waals radii for hydrogen and oxygen (2.62 Å).[13,14]

7.4. Conclusion

2,2,2-Nitrilotriacetyl chloride (**1**), an interesting precursor for further studies, has been prepared and isolated from the chlorination of 2,2,2-nitrilotriacetic acid with phosphorus pentachloride. In the crystal structure the nitrogen atom approaches a nearly planar configuration.
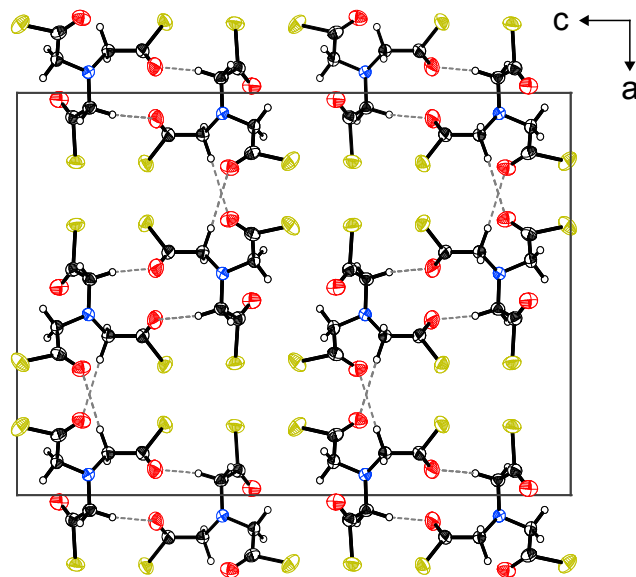
Figure 2.: Unit cell of **1**, viewing direction along the *b* axis. Dashed lines display intermolecular hydrogen bonds along the *a* axis (2.52 Å) and *c* axis (2.61 Å).

7.5. Experimental Section

General procedures. All manipulations of air-and moisture-sensitive materials were performed under an inert atmosphere of dry nitrogen using flame-dried glass vessels and Schlenk techniques.[17] The solvent carbon tetrachloride was dried by standard methods and freshly distilled prior to use. 2,2,2-Nitrilotriacetic acid (Acros Organics) and phosphorus pentachloride (Merck Chemicals) were used as received. Raman spectra were recorded with a Bruker MultiRAM FT-Raman instrument fitted with a liquid nitrogen-cooled germanium detector and a Nd:YAG laser (λ = 1064 nm, 300 mW). Infrared spectra were measured with a Perkin-Elmer Spectrum BX-FTIR spectrometer equipped with a Smiths DuraSampl*IR* II ATR device. All spectra were recorded at ambient temperature, the samples were neat solids. NMR spectra were recorded of solutions in $CDCl_3$ at 25 °C with a JEOL Eclipse 400 ECX instrument, and chemical shifts were determined with respect to external Me_4Si (^{1}H, 400.2 MHz; ^{13}C, 100.6 MHz), and $MeNO_2$ (^{15}N, 40.6 MHz). Mass spectrometric data were obtained with a JEOL MStation JMS 700 spectrometer (DEI+). The fragments are referred to the isotope with the highest natural abundance. Elemental analysis (C/H/N) was performed with an Elementar vario EL analyzer, the halogen (Cl) content was determined by titration using a Metrohm 888 Titrando. The melting point was determined using a Büchi Melting Point B-540 instrument and is uncorrected.

Table 1.: Structural comparison [Å, deg] of the NC_3 units of selected, related trimethyleneamine compounds.

	$N(CH_2COCl)_3$ (**1**)	$N(CH_2COOH)_3$ [10]	$N(CH_2Cl)_3$ [15]	$(CH_2CF_3)_3$ [16]
C−N	1.439(3)	1.499(2)	1.409(4)	1.460(3)
	1.450(3)	1.501(2)	1.411(2)	1.458(3)
	1.446(3)	1.499(1)	1.411(2) [a]	1.442(3)
C−N−C	114.9(2)	113.6(1)	119.5(2)	114.5(2)
	115.5(2)	112.3(1)	119.6(2)	115.3(2)
	116.1(2)	113.2(1)	119.6(2) [a]	115.5(2)
$\sum$C−N−C [b]	346.5	339.1	358.7	345.3

[a] Parameters generated by symmetry; [b] sum of all three C−N−C angles.

Crystal structure determination. An Oxford Xcalibur3 diffractometer with a CCD area detector was employed for the data collection using MoK_α radiation ($\lambda = 0.710\,73$ Å). The structure was solved using Direct Methods (SIR2004) [18,19] and refined by full-matrix least-squares on F^2 (SHELXL-97) [20,21]. All non-hydrogen atoms were refined anisotropically. The hydrogen atoms were located in difference Fourier maps and placed with C−H distances of 0.99 Å for the CH_2 groups. ORTEP plots are drawn with displacement ellipsoids at the 50 % probability level.

Crystal structure data of 2,2,2-nitrilotriacetyl chloride (1): formula: $C_6H_6Cl_3NO_3$; $M_r = 246.48\,\mathrm{g\,mol^{-1}}$; crystal size: $0.53 \times 0.13 \times 0.11\,\mathrm{mm^3}$; crystal description: colorless rod; crystal system: orthorhombic; space group: *Pbca* (no. 61); $a = 15.8495(7)$; $b = 5.3934(3)$; $c = 23.1697(11)$ Å; ti$V = 1980.61(17)$ Å^3; $Z = 8$; $D_{\mathrm{calcd.}} = 1.65\,\mathrm{g\,cm^{-3}}$; temperature: 173(2) K; θ range: 4.36–26.00°; $\mu(MoK_\alpha) = 0.9\,\mathrm{mm^{-1}}$; $F(000) = 992$ e; *hkl* range: $-19 \leq h \leq 19$, $-6 \leq k \leq 6$, $-28 \leq l \leq 25$; refls. measured/independent/R_{int}: 9461/1940/0.0407; refl. "observed" with $I > 2\sigma(I)$: 1341; param. refined: 118; $R(F)/wR(F^2)$ [$I > 2\sigma(I)$]: 0.0348/0.0767; $R(F)/wR(F^2)$ (all refls.): 0.0601/0.0827; GoF (F^2): 0.970; $\Delta\rho_{\mathrm{fin}}$ (max/min): 0.343/−0.267 e Å^{-3}.

CCDC 917352 contains the supplementary crystallographic data for this paper. These data can be obtained free of charge from The Cambridge Crystallographic Data Centre via www.ccdc.cam.ac.uk/data_request/cif.

Synthesis of 2,2,2-nitrilotriacetyl chloride (1)

Into a suspension of 2,2,2-nitrilotriacetic acid (15.0 g, 78.5 mmol) in carbon tetrachloride (65 mL) is slowly added phosphorus pentachloride (49.9 g, 240 mmol) at ambient temperature under exclusion of moisture. After careful and slow heating of the mixture to

50–60 °C and stirring for 2 h at this temperature, additional 100 mL of carbon tetrachloride is added. The reaction mixture is chilled to 0 °C, washed three times with ice-cold 200 mL of water, and dried over anhydrous magnesium sulfate. Removing of the solvent in vacuo left a pale pink solid. Crystallization from *n*-hexane yielded 9.09 g (47 %) of the product as colorless crystalline needles. Melting point: 68 °C (dec.).

Raman: ν = 2973 (39), 2928 (38), 2890 (17), 2850 (21), 1801 (16), 1774 (16), 1431 (12), 1411 (7), 1397 (10), 1365 (11), 1343 (6), 1331 (5), 1298 (2), 1243 (3), 1179 (3), 1166 (1), 993 (4), 974 (3), 933 (3), 868 (12), 782 (8), 744 (55), 509 (26), 490 (22), 467 (34), 450 (100), 439 (70), 362 (5), 297 (5), 265 (5), 226 (33), 205 (11), 188 (21) cm^{-1}. IR: ν = 2972 (m), 2928 (m), 2889 (m), 2853 (m), 1858 (w), 1797 (vs), 1766 (vs), 1735 (s), 1427 (m), 1410 (m), 1395 (m), 1364 (m), 1342 (m), 1329 (m), 1298 (w), 1242 (m), 1199 (m), 1178 (m), 1168 (m), 989 (m), 976 (w), 925 (s), 866 (m), 795 (m), 771 (s), 762 (s), 733 (m) cm^{-1}. ^{1}H NMR (CDCl$_3$): δ = 4.08 (s, CH$_2$). ^{13}C$\{^1$H$\}$ NMR (CDCl$_3$): δ = 171.9 (COCl), 64.4 (CH$_2$). ^{15}N$\{^1$H$\}$ NMR (CDCl$_3$): δ = −350.6 MS (DEI+): m/z (%) = 245 (2) [M]$^+$, 182 (67) [M −COCl]$^+$, 154 (100) [(CH$_2$COCl)$_2$/NCH$_2$(COCl)$_2$]$^+$, 126 (57) [(COCl)$_2$]$^+$. EA for C$_6$H$_6$Cl$_3$NO$_3$ (246.48): calcd. C 29.24, H 2.45, Cl 43.15, N 5.68; found C 29.19, H 2.44, Cl 42.48, N 5.65 %.

7.6. Acknowledgement

7.7. References

[1] G. C. Hopkins, R. R. Hindersinn, *US3709933*, **1973**.

[2] N. Yang, J. Zheng, W. Liu, N. Tang, K. Yu, *J. Mol. Struct.* **2003**, *657*, 177–183.

[3] J. R. Zheng, N. Yang, W. S. Liu, *Pol. J. Chem.* **2004**, *78*, 595–599.

[4] D. Liu, Z. Chen, S. Qin, W. Huang, L. Jiang, F. Liang, *Z. Anorg. Allg. Chem.* **2011**, *637*, 1401–1408.

[5] T. M. Klapötke, B. Krumm, R. Moll, S. F. Rest, *Z. Anorg. Allg. Chem.* **2011**, *637*, 2103–2110.

[6] T. M. Klapötke, B. Krumm, R. Moll, *submitted for publication.*

[7] T. M. Klapötke, B. Krumm, R. Moll, A. Penger, S. M. Sproll, R. J. F. Berger, S. A. Hayes, N. W. Mitzel, *Z. Naturforsch.* **2013**, *68b*, 719–731.

[8] G. Socrates, *Infrared and Raman Characteristic Group Frequencies: Tables and Charts*, 3rd ed., John Wiley & Sons, Chichester, **2004**.

[9] R. H. Stanford, Jr., *Acta Crystallogr.* **1967**, *23*, 825–832.

[10] E. Skrzypczak-Jankun, D. A. Smith, H. Maluszynska, *Acta Crystallogr.* **1994**, *C50*, 1097–1099.

[11] F. H. Allen, O. Kennard, D. G. Watson, L. Brammer, A. G. Orpen, R. Taylor, *J. Chem. Soc., Perkin Trans. 2* **1987**, S1–S19.

[12] A. F. Holleman, E. Wiberg, N. Wiberg, *Lehrbuch der Anorganischen Chemie*, 102nd ed., Walter de Gruyter, Berlin, **2008**.

[13] A. Bondi, *J. Phys. Chem.* **1964**, *68*, 441–451.

[14] M. Mantina, A. C. Chamberlin, R. Valero, C. J. Cramer, D. G. Truhlar, *J. Phys. Chem.* **2009**, *A113*, 5806–5812.

[15] T. M. Klapötke, B. Krumm, M. Scherr, F. X. Steemann, K. Banert, Y.-H. Joo, *Chem. Eur. J.* **2009**, *15*, 11341–11345.

[16] A. Dimitrov, H.-G. Mack, S. Rüdiger, K. Seppelt, H. Oberhammer, *J. Phys. Chem.* **1994**, *98*, 11401–11405.

[17] D. F. Shriver, M. A. Drezdzon, *The Manipulation of Air-Sensitive Compounds*, 2nd ed., John Wiley & Sons, New York, **1986**.

[18] M. C. Burla, R. Caliandro, M. Camalli, B. Carrozzini, G. L. Cascarano, L. De Caro, C. Giacovazzo, G. Polidori, R. Spagna, SIR2004, Institute of Crystallography, Bari (Italy), **2004**.

[19] M. C. Burla, R. Caliandro, M. Camalli, B. Carrozzini, G. L. Cascarano, L. De Caro, C. Giacovazzo, G. Polidori, R. Spagna, *J. Appl. Crystallogr.* **2005**, *38*, 381–388.

[20] G. M. Sheldrick, SHELX-97, University of Göttingen, Göttingen (Germany), **1997**.

[21] G. M. Sheldrick, *Acta Crystallogr.* **2008**, *A64*, 112–122.

8. Organomercury(II) Azides
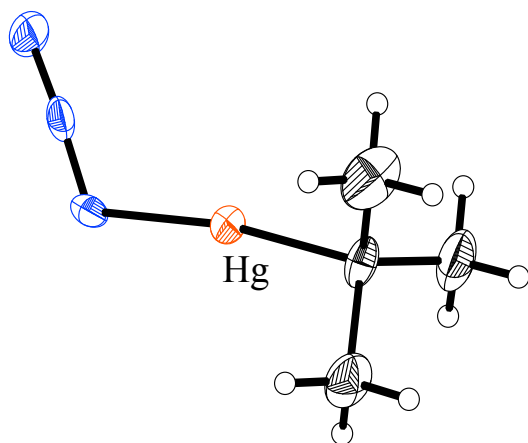
Synthetic and Structural Studies on Methyl-, *tert*-Butyl- and Phenylmercury(II) Azide

Thomas M. Klapötke,*[a] Burkhard Krumm,[a] and Richard Moll[a]

In memory of Professor Kurt Dehnicke

Keywords: Azides • Computational calculations • Mercury • Multinuclear NMR spectroscopy • X-ray diffraction

*   Prof. Dr. Thomas M. Klapötke

        E-Mail: tmk@cup.uni-muenchen.de

[a]   Department of Chemistry

        Ludwig-Maximilian University of Munich

        Butenandtstrasse 5–13 (D)

        81377 Munich, Germany

8.1. Abstract

The reaction of organomercury(II) halogenides (RHgHal, Hal = Cl, I) with silver azide furnished the corresponding covalent organomercury(II) azides RHgN$_3$ (R = Me (**1**), tBu (**2**), Ph (**3**)). In addition to the characterization by multinuclear NMR spectroscopy, IR and Raman spectroscopy as well as mass spectrometry, the mercury content was determined. A dependance on the solvent polarity for the ^{14}N NMR resonances was observed. Furthermore, X-ray diffraction studies were performed and the crystal structures for mercury(II) azides **1**–**3** are reported. A comparison of the bond lengths and angles with data from theoretical calculations is given.

8.2. Introduction

The first organomercury(II) azide of the type RHgN$_3$ is the methyl compound CH$_3$HgN$_3$, which is known for almost 80 years. [1] But the vast majority of the work about organomercury(II) azides was published by *Dehnicke* et al. between 1966 and 1971, with the synthesis of various alkyl- (Me, Et, nPr, iPr, nBu), cycloalkyl- (C$_3$H$_5$, C$_5$H$_9$, C$_6$H$_{11}$) compounds, as well as PhHgN$_3$ and the fluorinated derivative C$_6$F$_5$HgN$_3$. [2–4] Later on, the crystal structure of CH$_3$HgN$_3$ and the preparation of C$_6$H$_5$CH$_2$HgN$_3$ followed. [5,6] The last publication in the field of organomercury(II) azides in 1978 presented the synthesis and structure of the CF$_3$HgN$_3$ molecule. [7,8] Our general interest in metal azides prompted us, to re-examine those compounds with the modern advanced analysis methods.

The methyl- (**1**) [1–3,5,9] and phenylmercury(II) azide (**3**) [3], which had been known prior to this study, were incompletely characterized. Furthermore, the data set of the crystal structure of **1** was poor, in which the hydrogen atoms could not be refined. [5] Therefore, a reinvestigation of the crystal structure seemed to be justified. Also the synthesis routes for the organomercury(II) azides described in literature are not very convenient, because of the high toxicity of the dialkylmercury compounds used as starting materials and the more complex synthesis steps. [1–3,9] The *tert*-butylmercury(II) azide (**2**) has, to the best of our knowledge, not been described at all. In this contribution, a detailed study of the synthesis and characterization of the three organomercury(II) azides with methyl- (**1**), *tert*-butyl- (**2**) and phenyl (**3**) substituents is presented.

8.3. Results and Discussion

The synthesis route for the preparation of the organomercury(II) azides **1**–**3** was the reaction of organomercury(II) halogenides (RHgHal, Hal = Cl, I) with silver azide

to obtain the corresponding covalent organomercury (II) azides $R\mathrm{HgN_3}$ (R = Me (**1**), tBu (**2**), Ph (**3**)) (Scheme 1).

$$R\mathrm{HgHal} \quad + \quad \mathrm{AgN_3} \quad \xrightarrow[- \mathrm{AgHal}]{\text{acetone} / 25\,^{\circ}\mathrm{C}} \quad R\mathrm{HgN_3}$$

$$R = \mathrm{Me}\,(\mathbf{1}),\, t\mathrm{Bu}\,(\mathbf{2}),\, \mathrm{Ph}\,(\mathbf{3})$$
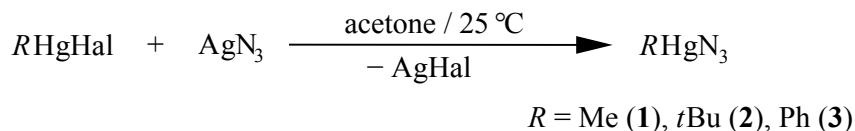
Scheme 1: Synthesis of the organomercury(II) azides **1**–**3**.

The route described here is more convenient than the syntheses reported in literature, because the used organomercury(II) halogenides are less toxic than the diorganomercury compounds and also because of the more straightforward reactions.[1–3,9] For a high conversion rate silver azide was used in excess with a ratio of 2:1 with respect to the organomercury(II) halogenides. The reaction of RHgHal with sodium azide was reported to be effective, but no details given.[9,10] However, we could not confirm a positive reaction with $\mathrm{NaN_3}$. The non-hygroscopic compounds **1**–**3** are soluble in polar organic solvents like acetone, acetonitrile, benzene, chloroform and methanol, whereas the alkyl compounds **1** and **2** are more soluble than the aryl compound **3**. In water and non-polar solvents like hexane all compounds are insoluble. Compounds **1**–**3** were found not sensitive to shock and friction. In a Bunsen burner the compounds deflagrate quite fast, with the alkyl derivatives faster than the phenyl. The explosive combustion of **1** described in literature could not be confirmed.[2,3,10]

NMR Spectroscopy

All compounds were thoroughly characterized by ^{1}H, ^{13}C, ^{14}N and ^{199}Hg NMR spectroscopy. In the ^{1}H NMR spectra of **1** and **2** the ^{1}H–^{199}Hg coupling could be observed and determined to 204 Hz for the $^{2}J_{\mathrm{H-^{199}Hg}}$ (**1**) and 237 Hz for the $^{3}J_{\mathrm{H-^{199}Hg}}$ (**2**) coupling. The ^{1}H NMR spectrum of the phenyl compound **3** shows the expected AA'BB'C spin system of mono-substituted phenyl rings. Beside the expected signals for **1**–**3** in the ^{13}C NMR spectra, also ^{199}Hg satellites could be observed, which verifies clearly the attachment of the alkyl or aryl groups to the mercury atom. The ^{13}C NMR spectrum of **1** shows one signal at -0.8 ppm and a coupling constant for the $^{1}J_{\mathrm{C-^{199}Hg}}$ coupling of 1491 Hz, which is slightly higher than the coupling constant of 1419 Hz for the starting material MeHgI. The $^{1}J_{\mathrm{C-^{199}Hg}}$ coupling for compound **2** was found with a coupling constant of 1663 Hz and the $^{2}J_{\mathrm{C-^{199}Hg}}$ coupling with 14 Hz. Both coupling constants are smaller than the corresponding coupling constants of the starting material $tert$-BuHgCl (1689 Hz and 16 Hz). For **3**, all possible ^{13}C–^{199}Hg couplings of the phenyl carbon atoms

could be observed. The spectrum with the assignment of the signals and the coupling constants is shown in Figure 1.
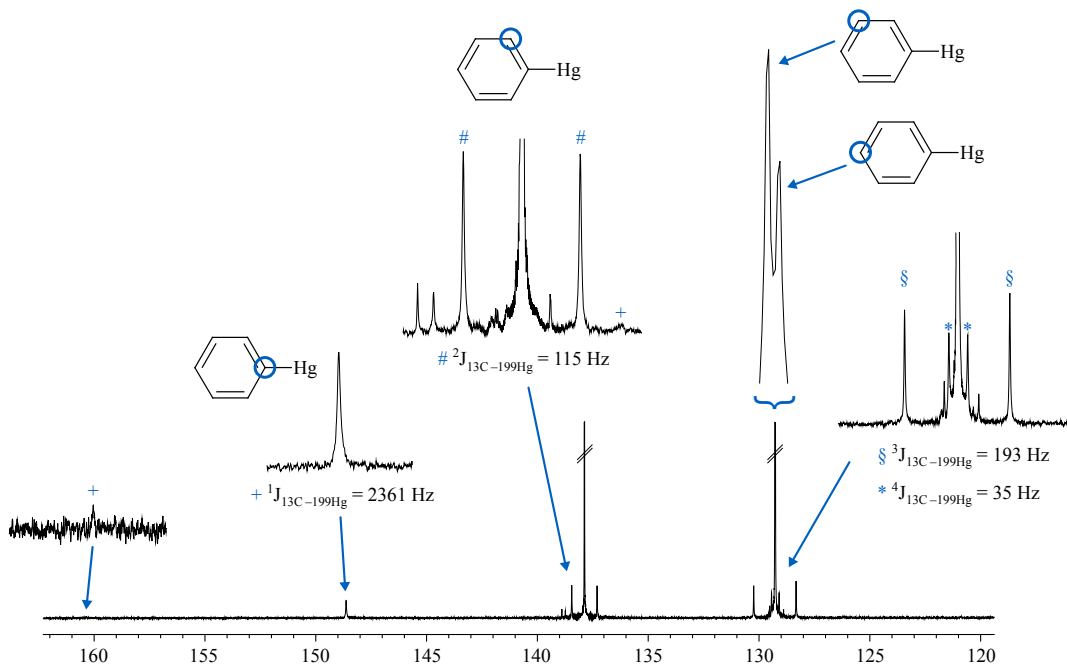
Figure 1.: ^{13}C NMR spectrum of $C_6H_5HgN_3$ (**3**) with ^{199}Hg satellites (δ in ppm).

The coupling constant of 2361 Hz for the $^1J_{C-^{199}Hg}$ coupling is very large due to the sp^2 hybridization and therefore the higher s-character of the phenyl carbon atoms. This is in agreement with the coupling constants of the phenylmercury(II) halogenides.[11,12] The ^2J- (ortho carbon), ^3J- (meta carbon) and ^4J- (para carbon) coupling constants have been determined to 115, 193 and 35 Hz. The assignment of the phenyl carbon atoms in the ^{13}C NMR spectra (Figure 1) was followed as described for phenylmercury(II) chloride.[11] This leads to a smaller coupling constant for the ^2J- in comparison to the $^3J_{C-^{199}Hg}$ coupling.

The ^{199}Hg NMR shift (Table 1) corresponds to the electron density of the substituents, thus a higher electron density leads to a shift to higher field. Therefore the signal in acetone-D$_6$ for **2** at -1357 ppm is shifted to higher field compared to **3** (-1292 ppm) and for the methyl compound **1** the lowest electron density is found (-964 ppm). Furthermore, the resonances of the azide compounds **2** and **3** are shifted to higher field compared to the corresponding chloride compound. However, that of **1** is shifted to lower field compared to the corresponding iodide MeHgI (Table 1). The chemical shift of the ^{199}Hg nucleus significantly depends on the solvent, as found for **1**, resulting in a shift of 84 ppm between benzene-D$_6$ and acetone-D$_6$. The chemical shift

depends basically on the polarity of the solvent, whereas polar solvents induce a shift to higher field compared to non-polar solvents (Table 1). This is also verified by the previously reported dependance on the polarity of the solvent for methylmercury(II) halogenides.[12,13] A somehow unexpected polarity dependance on the solvent could also be found in the ^{14}N NMR spectra of **1**. In the non-polar solvents benzene-D$_6$ and chloroform-D the three expected signals for a covalent bonded azide group could be observed, whereas the spectra in polar solvents like acetone-D$_6$, acetonitrile-D$_3$ and methanol-D$_4$ just showed two signals (Figure 2).

Table 1.: ^{199}Hg and ^{14}N NMR chemical shifts of **1**–**3** (δ in ppm).

Compound	Solvent	^{199}Hg	^{14}N		
			N$_\beta$	N$_\gamma$	N$_\alpha$
CH$_3$HgI	acetone-D$_6$	-1132			
(CH$_3$)$_3$CHgCl	acetone-D$_6$	-1253			
	chloroform-D	-1223			
C$_6$H$_5$HgCl	acetone-D$_6$	-1175			
CH$_3$HgN$_3$ (**1**)	acetone-D$_6$	-964	-134		-258 [a)]
	acetonitrile-D$_3$	-950	-137		-256 [a)]
	benzene-D$_6$	-880	-134	-220	-284
	chloroform-D	-888	-135	-222	-277
	methanol-D$_4$	-959	-135		-251 [a)]
(CH$_3$)$_3$CHgN$_3$ (**2**)	acetone-D$_6$	-1357	-133		-254 [a)]
C$_6$H$_5$HgN$_3$ (**3**)	acetone-D$_6$	-1292	-134	-235	-291

[a)] N$_\gamma$ and N$_\alpha$.

The same is found for **2**, in contrast to **3** where three signals were found in acetone-D$_6$. This phenomenon is likely due to a higher partial charge at the N$_\alpha$ atom in the azide group leading to a more symmetrical charge distribution similar to the charge distribution of ionic azides. Nevertheless, the chemical shifts of the azide nitrogen atoms are in the expected range of covalent and ionic bonded azides.

Vibrational Spectroscopy

The vibrational analysis of **1**–**3** showed the characteristic asymmetric azide stretching vibrations in the range of 2074 to 2027 cm^{-1} (Table 2). All vibrations of the azide ion for **1**–**3** are in a narrow range, explained by the low influence of the substituents to the azide group because of the heavy mercury atom in-between. For compound **2** and **3**, the asymmetric azide stretching vibration is split due to the Fermi resonance

of the phenyl and *tert*-butyl deformation vibrations at larger wave length. The Hg−C stretching vibration for **1** is found at $551 \, \text{cm}^{-1}$ (IR) respectively $553 \, \text{cm}^{-1}$ (Raman), whereas the Hg–N stretching vibration is located at $363 \, \text{cm}^{-1}$ (Raman). The lower energy of the Hg−N vibration can be explained by the higher polarity of this bond compared to the Hg−C bond. This circumstance is also verified by computational frequency calculations with $413 \, \text{cm}^{-1}$ for the Hg−N and $539 \, \text{cm}^{-1}$ for the Hg−C vibration. In contrast to the value of the Hg−N stretching vibration found in this work, *Dehnicke* et al. initially assigned this vibration at $594 \, \text{cm}^{-1}$,[3] but corrected this in a later publication to $392 \, \text{cm}^{-1}$ [4]. The Hg−N vibration of **3** ($372 \, \text{cm}^{-1}$) is also in the same range. The Hg−C vibration ($240 \, \text{cm}^{-1}$) is found at smaller wavenumber, because of the rigidity of the phenyl ring and the more polar Hg−C bond in this mesomer stabilized system. The assignment reported in literature for this vibration was found to be wrong.[3] The H−C and Hg−N vibrations of **2** are quite similar to that of the methyl compound **1**. The full IR and Raman spectrum of **2** is shown in Figure 3. All C−H and C−C vibrations of **1**–**3** could be observed in the expected ranges.
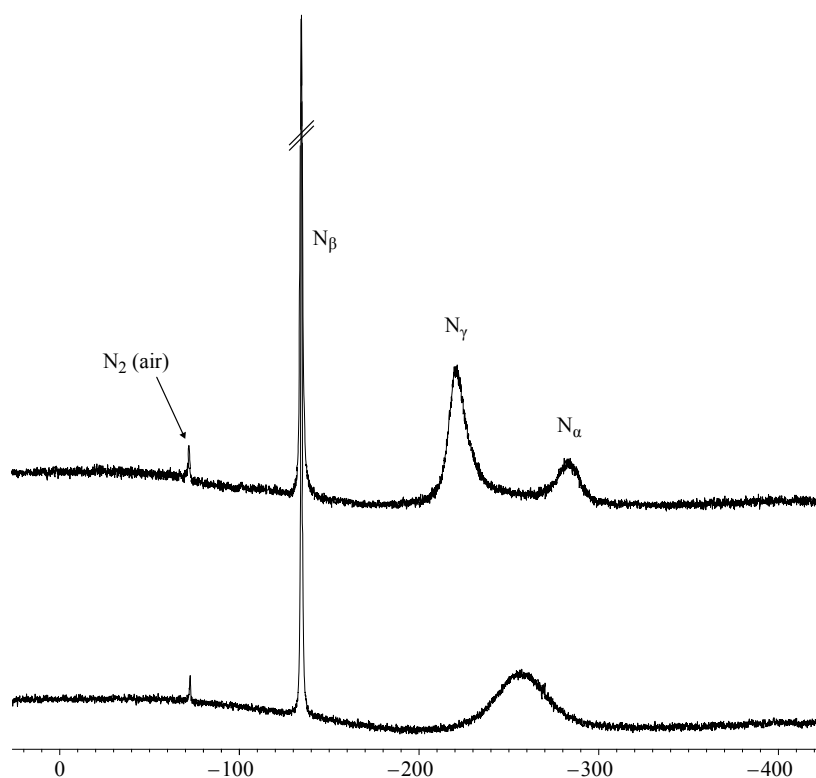
Figure 2.: ^{14}N NMR spectrum of **1** in benzene-D$_6$ (top) and acetone-D$_6$ (bottom) (δ in ppm).

Table 2.: IR and Raman bands of **1**–**3**, characteristic vibrations and their assignments [a)].

Vibrations [b)]	CH_3HgN_3 (**1**)		$(CH_3)_3CHgN_3$ (**2**)		$C_6H_5HgN_3$ (**3**)	
	Raman	IR	Raman	IR	Raman	IR
$\nu_{as}N_3$	2038 (24)	2044 vs 2034 (10)	2074 (7)	2027 vs	2056 (9) 2037 (15)	2048 vs
$\nu_s N_3$	1279 (23)	1278 s	1282 (7)	1282 m	1276 (15)	1278 m
$\delta_\beta N_3$	658 (8)	658 m	656 (6)	654 w	650 (18)	651 w
$\delta_s C_4 H_9$			1161 (100)			
$\delta_\beta C_6 H_5$					994 (100)	
$\delta_\gamma N_3$		592 (m)		597 (w)		594 (w)
νHg–C	553 (100)	551 m	525 (49)	–	240 (78)	–
νHg–N	363 (71)	–	355 (60)	–	372 (27)	–
δ(N–Hg–C)			250 (50)	–	201 (29)	–

[a)] Vibration bands in cm^{-1}; Raman intensities in brackets; IR intensities: vs = very strong, s = strong, m = medium, w = weak. [b)] ν = stretching vibration; ν_{as}, ν_s = antisymmetric and symmetric stretching vibration; δ = deformation vibration; δ_β, δ_γ = "in plane" and "out of plane" deformation vibration.

X-ray Diffraction

Single crystals suitable for X-ray diffraction measurements were obtained by slow evaporation of the solvent at ambient temperature in benzene (**1**, **2**) or acetone (**3**). A full list of the crystallographic refinement parameters and structure data of **1**–**3** is shown in Table 3. Compound **1** crystallizes in the monoclinic space group $P2_1/c$ with four formula units per unit cell. The molecular structure is shown in Figure 4. The Hg−C and Hg−N bond lengths are 2.058(15) respectively 2.117(12) Å and are slightly shorter than the bond lengths of the reported structure. [5] In contrast to the published data, the Hg−C bond is shorter than the Hg−N bond. The calculated bond lengths are 2.081 Å for the Hg−C and 2.063 Å for the Hg−N bond. The discrepancy between the measured and calculated bond lengths is due to the lack of the quantum mechanical calculation to achieve an accurate result for the heavy atom mercury. A comparison of selected measured and calculated bond lengths and angles for compounds **1**–**3** is shown in Table 4. The mercury is as expected double coordinated in an almost linear arrangement. Also the azide group has a linear arrangement with an angle to the Hg−N bond of 118.0°. The free electron pair located at the N_α atom and the resulting sp^2 hybridization is the reason for this angle, theoretical with 120°. Unlike the previous
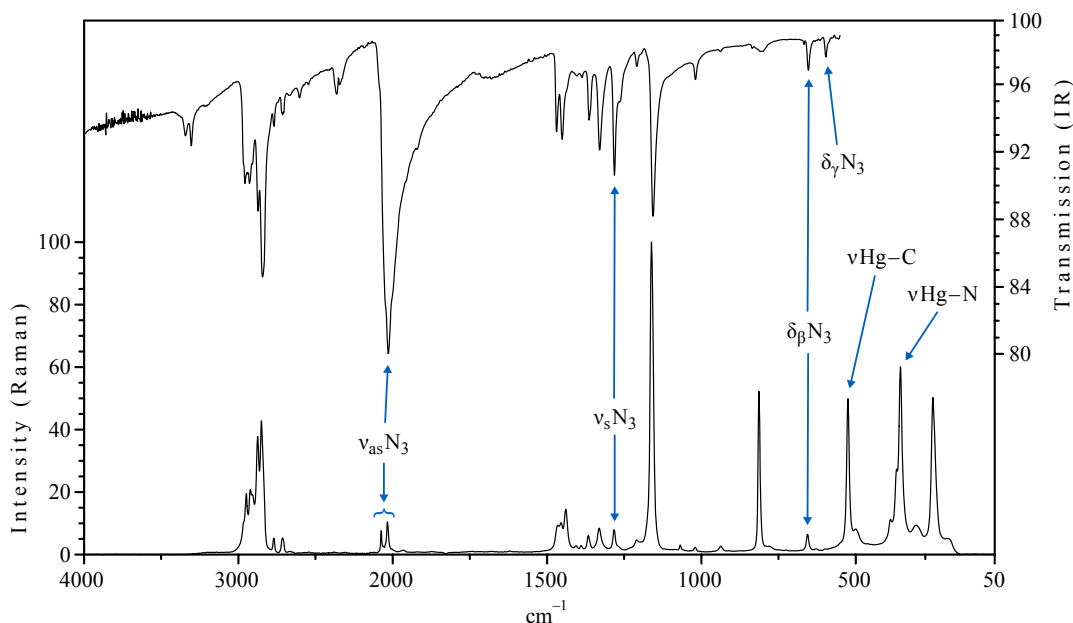
Figure 3.: IR and Raman spectra of $(CH_3)_3CHgN_3$ (**2**).

published crystal structure,[5] the N1−N2 bond is longer than the N2−N3 bond, which can be explained by the typical bonding situation of covalent bonded azides. Each molecule of **1** is surrounded by six further molecules with weak Hg···N contacts between 2.953(13) and 4.800(21) Å (vdWr: 3.1 Å [14]). Due to the absence of strong intermolecular interactions the rather low sensitivity against shock, friction and heat can be explained. In contrast, highly intermolecular coordinated azides such as mercury(II) azide show a quite explosive behavior.[15,16] The missing resonance stabilization of the π-bonding system of the azide group is responsible for the high explosivity of these compounds.

Figure 4.: Molecular structure of **1**. Selected distances [Å] and angles [°]: Hg1−C1 2.058(15), Hg1−N1 2.117(12), N1−N2 1.217(19), N2−N3 1.160(20), C1−Hg1−N1 175.0(7), Hg1−N1−N2 118.0(10), N1−N2−N3 176.6(18).

Table 3.: Crystal and structure refinement data for CH_3HgN_3 (**1**), $(CH_3)_3CHgN_3$ (**2**) and $C_6H_5HgN_3$ (**3**).

	CH_3HgN_3 (**1**)	$(CH_3)_3CHgN_3$ (**2**)	$C_6H_5HgN_3$ (**3**)
empirical formula	CH_3N_3Hg	$C_4H_9N_3Hg$	$C_6H_5N_3Hg$
formula mass $[g\,cm^{-1}]$	257.64	299.72	319.71
temperature [K]	200(2)	173(2)	200(2)
crystal size [mm]	$0.35 \times 0.05 \times 0.03$	$0.40 \times 0.02 \times 0.02$	$0.27 \times 0.24 \times 0.15$
crystal description	colorless platelet	colorless needle	colorless block
crystal system	monoclinic	monoclinic	orthorhombic
space group	$P2_1/c$	$C2/c$	$Pbca$
a [Å]	9.1035(6)	20.1832(9)	6.8777(5)
b [Å]	6.8922(4)	6.4430(2)	7.1423(5)
c [Å]	6.9422(6)	23.6385(11)	29.131(2)
β [°]	107.067(7)	104.191(5)	90.0
V $[Å^3]$	416.39(5)	2980.2(2)	1430.97(18)
Z	4	16	8
ρ_{calc} $[g\,cm^{-3}]$	4.1099(6)	2.6721(2)	2.9681(4)
μ $[mm^{-1}]$	36.765	20.568	21.429
$F(000)$	440	2144	1136
θ range [°]	4.26–28.77	4.10–26.00	4.08–25.99
index ranges	$-12 \leq h \leq 11$	$-24 \leq h \leq 24$	$-8 \leq h \leq 7$
	$-7 \leq k \leq 9$	$-7 \leq k \leq 7$	$-29 \leq k \leq 29$
	$-8 \leq l \leq 8$	$-29 \leq l \leq 29$	$-35 \leq l \leq 24$
reflections collected	2629	13976	4570
reflections observed	944	2906	1405
reflections unique	617	1949	973
	($R_{int} = 0.1435$)	($R_{int} = 0.0691$)	($R_{int} = 0.0381$)
$R1$, $wR2$ (2σ data)	0.0545, 0.1262	0.0340, 0.0543	0.0291, 0.0637
$R1$, $wR2$ (all data)	0.0837, 0.1366	0.0761, 0.0799	0.0483, 0.0676
max./min. transm.	0.4030/0.0407	0.5239/0.0435	0.1925/0.0369
data/restraints/parameters	944/0/47	2906/0/145	1405/0/91
GOOF on F^2	0.957	0.868	1.024
larg. diff. peak/hole $[e\,Å^{-3}]$	$-2.735/2.217$	$-1.698/4.201$	$-0.943/1.570$

The molecules of **1** are oriented in the unit cell approximately in the *ab* plane and are building a pair like structure (Figure 5). The Hg···N1(*i*) and Hg···N3(*ii*) contacts (Figure 6) lying in the *ab* plane (2.953(14) Å and 3.047(15) Å) are shorter than the Hg···N1(*iii*) and Hg···N3(*iv*) contacts (3.072(18) Å and 3.127(20) Å) between these layers. Compound **2** crystallizes in the monoclinic space group $C2/c$ with sixteen formula units per unit cell. The molecular structure shows two molecules in the asymmetric unit

Table 4.: Comparison of selected measured and calculated bond lengths and angles for CH_3HgN_3 (**1**), $(CH_3)_3CHgN_3$ (**2**) and $C_6H_5HgN_3$ (**3**)[a].

	1 CH_3HgN_3	**2** $(CH_3)_3CHgN_3$	**3** $C_6H_5HgN_3$
$d(Hg-C)$	2.058(15)/2.081	2.114(9), 2.097(10)/2.145	2.041(9)/2.065
$d(Hg-N_\alpha)$	2.117(12)/2.063	2.152(8), 2.116(9)/2.085	2.083(8)/2.056
$d(N_\alpha-N_\beta)$	1.217(19)/1.228	1.192(11), 1.215(12)/1.227	1.180(9)/1.229
$d(N_\beta-N_\gamma)$	1.160(20)/1.147	1.142(10), 1.160(12)/1.148	1.160(10)/1.146
$\angle(C-Hg-N_\alpha)$	175.0(7)/175.7	172.2(3), 172.4(4)/175.4	172.4(3)/175.8
$\angle(Hg-N_\alpha-N_\beta)$	118.0(10)/121.5	116.0(6), 118.9(6)/121.0	119.9(6)/121.6
$\angle(N_\alpha-N_\beta-N_\gamma)$	176.6(18)/174.3	175.0(10), 176.6(10)/174.7	175.5(9)/174.1

[a] Measured/calculated; bond lengths in Ångstrom [Å] and angles in degree [°].

(Figure 7), whereas no further symmetry operation could be found between these two molecules. The high number of sixteen formula units per unit cell is not very common, but not impossible in the monoclinic space group. Due to the disorder of one of the two terminal *tert*-butyl groups and their free rotation around the central carbon atom, the ellipsoids are more elongated (see right *t*Bu group in Figure 7). Furthermore, the crystals of **2** are very thin needles, often conglomerated in such a degree that the measurement of the crystals is quite challenging, which explains the elongated thermal ellipsoids and the high residual electron density around the mercury atoms.
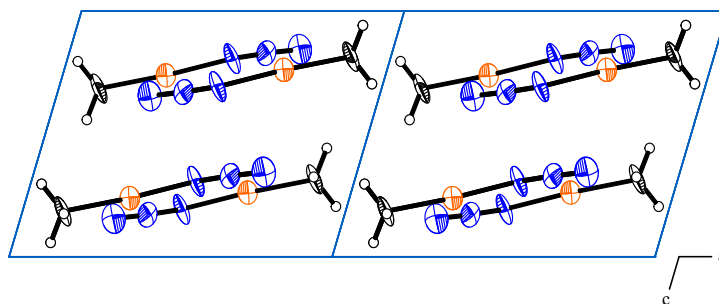
Figure 5.: Unit cell of **1**. Viewing direction along the *b* axis.

The Hg−C bond lengths are 2.114(9) respectively 2.097(10) Å, and the Hg−N bond lengths are 2.152(8) respectively 2.116(9) Å, comparable to that of **1**. Similar as for **1**, the calculated Hg−C bond length is longer than the calculated Hg−N bond length, which is contrary to the measured one (Table 4). As described above, the quantum mechanical calculation for the heavy atom mercury is not very accurate, but
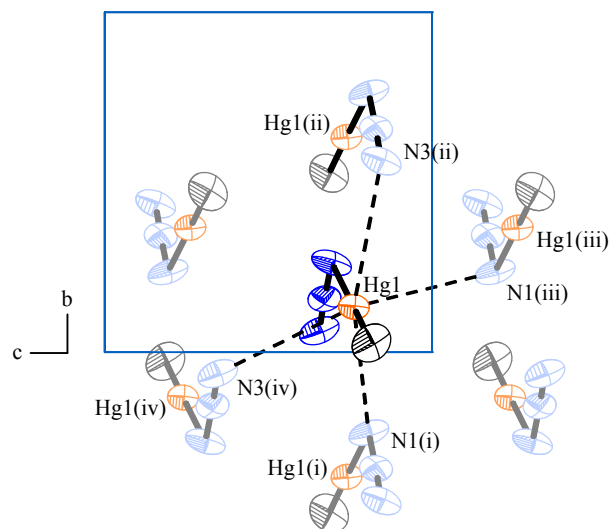
Figure 6.: Molecular structure of **1**. Hydrogen atoms not shown and only selected atoms labeled for clarity. Viewing direction along the a axis. Selected distances [Å] and angles [°]: Hg1···N1(i) 2.953(14), Hg1···N3(ii) 3.047(15), Hg1···N1(iii) 3.072(18), Hg1···N3(iv) 3.127(20). $i = 1-x, -0.5+y, 0.5-z$; $ii = 1-x, 0.5+y, 0.5-z$; $iii = x, 0.5-y, -0.5+z$; $iv = 1-x, -y, 1-z$.
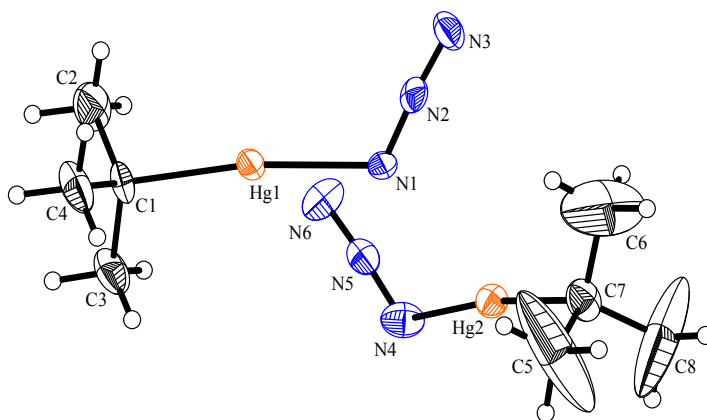
Figure 7.: Molecular structure of **2**. Selected distances [Å] and angles [°]: Hg1−C1 2.114(9), Hg1−N1 2.152(8), N1−N2 1.192(11), N2−N3 1.142(10), Hg2−C5 2.097(10), Hg2−N4 2.116(9), N4−N5 1.215(12), N5−N6 1.160(12), C1−Hg1−N1 172.2(3), Hg1−N1−N2 116.0(6), N1−N2−N3 175.0(10), C5−Hg2−N4 172.4(4), Hg2−N4−N5 118.9(6), N4−N5−N6 176.6(10).

a good indication. The C1−Hg1−N1 angle in **2** is slightly more bent compared to the methyl compound **1**. The almost linear azide group is bent to the Hg−N bond with an angle of 116.0(6) respectively 118.9(6)°, with the N1−N2 bond longer than the N2−N3 bond (Table 4). Some bond lengths and angles of the two molecules in the

asymmetric unit are significantly different, which is somehow surprising for two identical molecules. Each mercury atom of **2** is surrounded by three further molecules (Figure 8) with intermolecular Hg···N distances between 2.847(8) and 3.154(9) Å (vdWr: 3.1 Å[14]). The shortest Hg···N contact is found between the two molecules of the asymmetric unit and is also the shortest one found in this work. Furthermore, all six Hg···N contacts are only between three different molecules, in such fashion that the azide groups are building a cylindric structure with the mercury atoms lying outside (Figure 9). In **2** no strong intermolecular interactions are found, which explains the rather low sensitivity against shock, friction and heat. The molecules of **2** are oriented approximately in the *ac* plane (Figure 9).
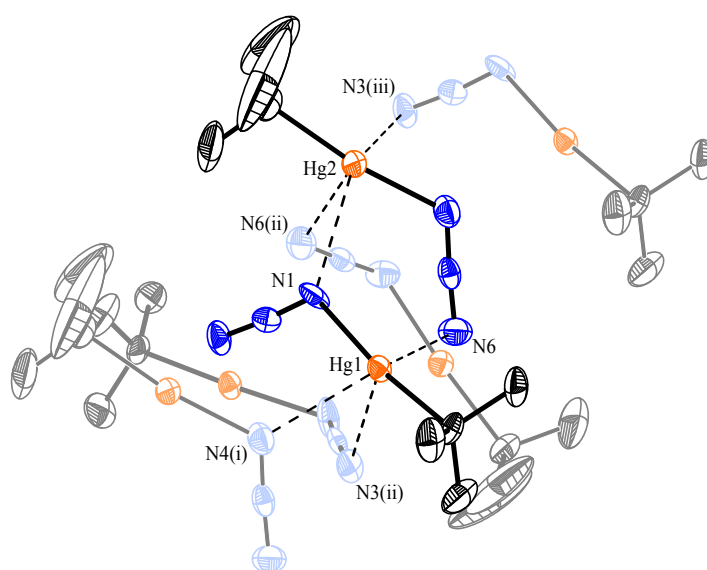
Figure 8.: Molecular structure of **2**. Hydrogen atoms not shown and only selected atoms labeled for clarity. Selected distances [Å] and angles [°]: Hg2···N1 2.847(8), Hg1···N4(*i*) 2.856(9), Hg1···N3(*ii*) 2.900(9), Hg2···N6(*ii*) 2.980(10), Hg1···N6 3.130(9), Hg2···N3(*iii*) 3.154(9). *i* = x, −1+y, z; *ii* = 1−x, y, 0.5−z; *iii* = x, 1+y, z.

Compound **3** crystallizes in the orthorhombic space group *Pbca* with eight formula units per unit cell (Figure 10). Compared to **1** and **2**, the Hg−C bond length (2.041(9) Å) and the Hg−N bond length (2.082(8) Å) of **3** are slightly shorter. The bend of the azide group to the Hg−N bond (119.9(6)°) is very close to the theoretically expected value of 120°. The arrangement of the azide group is similar as with **1** and **2** almost linear with a shorter N2−N3 bond compared to the N1−N2 bond. Each molecule of **3** is surrounded by four further molecules (Figure 11), with Hg···N distances between 2.927(8) and 3.269(8) Å (vdWr: 3.1 Å[14]). As also found with **1** and **2**, there are only weak Hg···N interactions and therefore a low sensitivity against shock, friction and heat is the consequence. Compared to **1**, there is also a pair like structure in **3**, but in contrast the
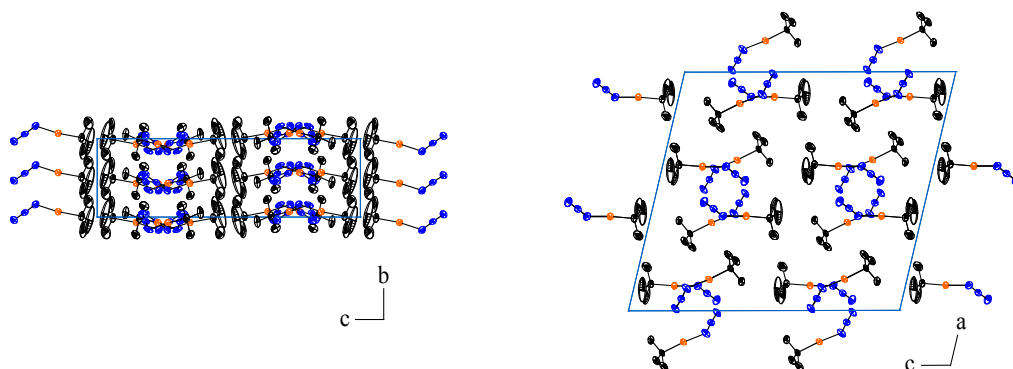
Figure 9.: Unit cell view of **2**. Hydrogen atoms not shown for clarity. Viewing direction along the *a* axis (left) and *b* axis (right).
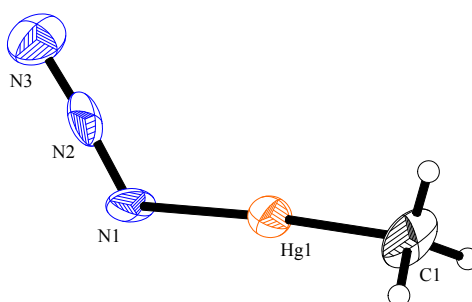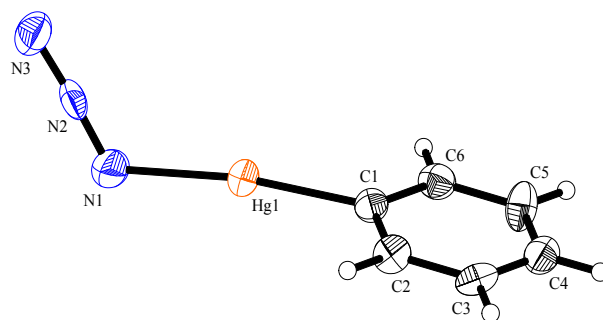

Figure 10.: Molecular structure of **3**. Selected distances [Å] and angles [°]: Hg1−C1 2.041(9), Hg1−N1 2.083(8), N1−N2 1.180(9), N2−N3 1.160(10), C1−Hg1−N1 172.4(3), Hg1−N1−N2 119.9(6), N1−N2−N3 175.5(9).

molecules are not oriented in layers. Because of steric reasons the adjacent phenyl rings lay perpendicular to each other (Figure 11). This structure element is also found in the corresponding phenylmercury(II) chloride and cyanide.[17,18]

The unit cell view (Figure 12) shows a wave like pattern with the smallest Hg···N contact oriented inside the layers and the other three Hg···N contacts between them.

8.4. Conclusions

The covalent organomercury(II) azides $R\mathrm{HgN_3}$ (R = Me (**1**), tBu (**2**), Ph (**3**)) were prepared by reaction of the corresponding organomercury(II) halogenides with silver azide. This synthesis route is more convenient and facile compared to the methods reported in literature. The organomercury(II) azides were fully characterized using multinuclear NMR, IR and Raman spectroscopy as well as mass spectrometry and
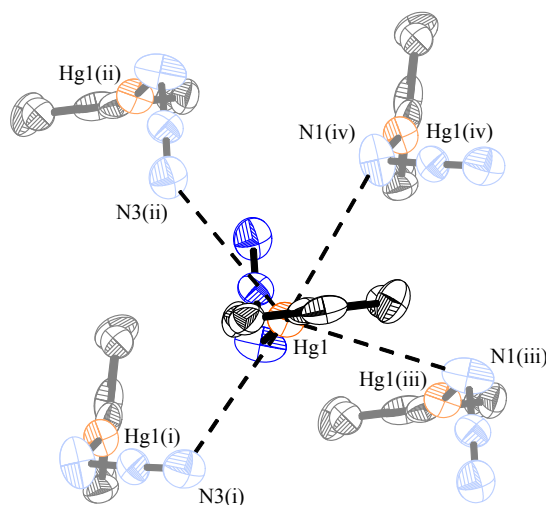
Figure 11.: Molecular structure of **3**. Hydrogen atoms not shown and only selected atoms labeled for clarity. Selected distances [Å] and angles [°]: Hg1···N3(*i*) 2.927(8), Hg1···N3(*ii*) 3.024(8), Hg1···N1(*iii*) 3.135(8), Hg1···N1(*iv*) 3.269(8). $i = -0.5+x$, $0.5-y$, $1-z$; $ii = 1-x$, $1-y$, $1-z$; $iii = 1-x$, $-y$, $1-z$; $iv = 0.5+x$, $0.5-y$, $1-z$.
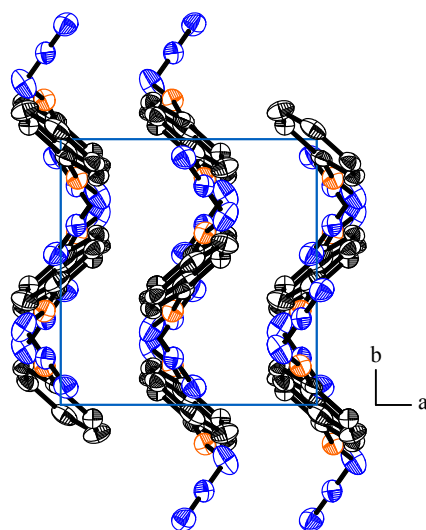
Figure 12.: Unit cell view of **3**. Hydrogen atoms not shown for clarity. Viewing direction along the *c* axis.

mercury analysis. The crystal structures are determined and discussed thoroughly. The relatively small differences in the bond parameters of methyl, *tert*-butyl and phenyl mercury azide can likely be explained by packing effects.

8.5. Experimental Section

General Procedures. All manipulation of air- and moisture-sensitive materials were performed in an inert atmosphere of dry nitrogen using flame-dried glass vessels and Schlenk techniques.[19] The solvents tetrahydrofurane and acetonitrile were dried by standard methods and freshly distilled prior to use. Acetone (Acros Organics, 268310025), *tert*-butylchloride (Fluka), mercury(II) chloride (Acros Organics), methylmercury(II) iodide, phenylmercury(II) chloride and magnesium turnings (all Sigma Aldrich) were used as received. *Tert*-butylmercury(II) chloride was prepared according to the literature procedure.[20] Due to the light sensitivity of silver azide, reactions of RHgHal with AgN_3 were performed under the absence of light.

Raman spectra were recorded with a Perkin-Elmer 2000 NIR FT spectrometer fitted with a Nd:YAG laser ($\lambda = 1064\,\text{nm}$), infrared spectra were measured with a Perkin-Elmer Spectrum BX-FTIR spectrometer equipped with a Smiths DuraSampl*IR* II ATR device. All spectra were recorded at ambient temperature as neat solids. NMR spectra were recorded with a JEOL Eclipse 400 instrument and chemical shifts were determined with respect to external Me_4Si (^1H, 399.8 MHz; ^{13}C, 100.5 MHz), $MeNO_2$ (^{14}N, 28.9 MHz) and Me_2Hg (^{199}Hg, 71.7 MHz). Due to the extreme toxicity of Me_2Hg, $HgCl_2$ (0.5 M in THF) was used as external standard for ^{199}Hg NMR and the shift ($-1517\,\text{ppm}$) was referenced to that of Me_2Hg (0 ppm). Because of the significant temperature dependance on the ^{199}Hg NMR resonances, all samples were measured at 25 °C. Mass spectrometric data were obtained with a JEOL MStation JMS 700 spectrometer (DEI+). Determinations of the mercury content were performed with a Varian Vista RL CCD Simultaneous ICP-AES spectrometer with a mercury ICP standard (CertiPUR®, $Hg(NO_3)_2$ in HNO_3 (10 %), Merck). Analysis of C/H/N contents was not determined because of potential mercury contaminations of the analyzer. Melting points were determined in capillaries using a Büchi B-540 instrument and are uncorrected.

CAUTION! Mercury and most mercury containing compounds are very toxic. Avoiding contact with these compounds is mandatory, especially prevent inhalation of the volatile organomercury compounds. Covalent azides are potentially explosive, although no hazards were observed during preparation and handling. Nevertheless, this necessitates additional meticulous safety precautions (face shield, leather suit, Kevlar gloves and ear plugs), primarily during handling of silver azide.

Computational Details. All calculations were carried out using the program package Gaussian 03 (Revision B.03)[21] and GaussView 3.09[22]. The structure and frequency calculations were performed with Becke's B3 three parameter hybrid functional using the LYP correlation functional (B3LYP).[23,24] For C, H, N and Cl a correlation consistent polarized double-zeta basis set was used (cc-pVDZ). The core electrons of

Hg were treated with a small-core energy-consistent ECP60MWB pseudo-potential (Stuttgart/Dresden),[25] and the valence electrons with a (8s7p6d2f1g)/[6s5p3d2f1g] contracted basis set. The structures were optimized without symmetry constraints and the given energy is corrected with the zero point vibrational energy.

X-ray Crystallography For all compounds, an Oxford Xcalibur3 diffractometer with a CCD area detector was employed for data collection using Mo-K_α radiation ($\lambda = 0.710\,73\,\text{Å}$). The structures were solved by direct methods (SIR97)[26,27] and refined by full-matrix least-squares on F^2 (SHELXL)[28,29]. All non-hydrogen atoms were refined anisotropically. The hydrogen atoms were located in a difference Fourier map and placed with a C−H distance of $0.98\,\text{Å}$ for CH_3 groups and $0.95\,\text{Å}$ for aromatic CH groups. OR-TEP plots are shown with thermal ellipsoids at the 50 % probability level. CCDC 761194, 761195, and 761196 contain the supplementary crystallographic data for this paper. These data can be obtained free of charge via www.ccdc.cam.ac.uk/data_request/cif, or by emailing data_request@ccdc.cam.ac.uk, or by contacting The Cambridge Crystallographic Data Centre, 12, Union Road, Cambridge CB2 1EZ, UK; Fax: +44-1223-336033.

Additional analytic data of *tert*-butylmercury(II) chloride

Raman: 2965 (15), 2951 (20), 2926 (17), 2903 (18), 2874 (39), 2851 (38), 2769 (4), 2710 (6), 1462 (12), 1439 (15), 1405 (2), 1389 (2), 1365 (6), 1210 (4), 1161 (77), 1019 (2), 937 (2), 813 (36), 518 (43, νHgC), 390 (4), 298 (20, νHgCl), 287 (18), 240 (100) cm^{-1}. IR: 2964 s, 2942 s, 2926 m, 2870 s, 2841 vs, 2767 m, 2709 m, 1469 s, 1450 s, 1362 s, 1261 m, 1209 m, 1155 vs, 1019 m, 938 w, 802 m cm^{-1}. MS (DEI+) m/z (%): 294 (0.7) [M$^+$], 279 (4) [M$^+$ −CH$_3$], 237 (7) [M$^+$ −C$_4$H$_9$], 202 (15) [Hg$^+$], 57 (100) [C$_4$H$_9$$^+$]. EA (ICP): Hg 67.8 (calcd. 68.4) %.

General Procedure for the Preparation of RHgN3 (R = Me (1), tBu (2), Ph (3))

Into solutions of MeHgI, tBuHgCl or PhHgCl (0.6 mmol) in acetone (15–55 mL) AgN$_3$ (180 mg, 1.2 mmol) was added at ambient temperature and stirred for 24 h (40 h for tBuHgCl). The precipitation of AgI or AgCl was filtered off and the solvent of the remaining solution was removed in vacuo and yielded colorless, crystalline solids. Yield: 145 mg (**1**) (94 %), 85 mg (**2**) (47 %, after sublimation at 50 °C / 10^{-3} mbar), 185 mg (**3**) (96 %).

Methylmercury(II) azide (1)

M. p. 132 °C. Raman: 3007 (18), 2923 (69), 2799 (10), 2038 (24, ν_{as}N$_3$), 1333 (12), 1279 (23, ν_sN$_3$), 1193 (36), 1066 (7), 658 (8), 553 (100, νHgC), 363 (71, νHgN) cm^{-1}. IR: 3348 w, 3306 m, 2923 m, 2798 w, 2595 w, 2544 w, 2044 vs (ν_{as}N$_3$), 1333 m, 1278 s

(ν_sN$_3$), 1198 m, 792 m, 658 m, 592 m, 551 m (νHgC) cm^{-1}. ^{1}H NMR ((CD$_3$)$_2$CO): $\delta = 0.86$ (s, $^2J_{H-^{199}Hg} = 204$ Hz, CH$_3$Hg). ^{13}C{^{1}H} NMR ((CD$_3$)$_2$CO): $\delta = -0.8$ (s, $^1J_{C-^{199}Hg} = 1491$ Hz, CHg). ^{14}N NMR ((CD$_3$)$_2$CO): $\delta = -134$ (N$_\beta$), -258 (N$_\gamma$/N$_\alpha$, br); (CD$_3$CN): $\delta = -137$ (N$_\beta$), -256 (N$_\gamma$/N$_\alpha$); (C$_6$D$_6$): $\delta = -134$ (N$_\beta$), -220 (N$_\gamma$, br), -284 (N$_\alpha$, br); (CDCl$_3$): $\delta = -135$ (N$_\beta$), -222 (N$_\gamma$, br), -277 (N$_\alpha$, br); (CD$_3$OD): $\delta = -135$ (N$_\beta$), -251 (N$_\gamma$/N$_\alpha$, br). ^{199}Hg{^{1}H} NMR ((CD$_3$)$_2$CO): $\delta = -964$; (CD$_3$CN): $\delta = -950$; (C$_6$D$_6$): $\delta = -880$; (CDCl$_3$): $\delta = -888$; (CD$_3$OD): $\delta = -959$. MS (DEI+) m/z (%): 259 (100) [M$^+$], 244 (11) [M$^+$ $-$CH$_3$], 217 (96) [M$^+$ $-$N$_3$], 202 (76) [Hg$^+$]. EA (ICP): Hg 77.1 (calcd. 77.8) %.

Tert-butylmercury(II) azide (2)

M. p. 97 °C. Raman: 2948 (19), 2922 (20), 2875 (37), 2850 (42), 2770 (5), 2713 (5), 2074 (7)/2034 (10, ν_{as}N$_3$), 1465 (9), 1454 (10), 1439 (14), 1405 (2), 1389 (2), 1366 (6), 1331 (8), 1282 (7, ν_sN$_3$), 1209 (4), 1161 (100), 1020 (2), 937 (2), 813 (52), 656 (6), 525 (49, νHgC), 387 (11), 367 (27), 355 (60, νHgN), 304 (9), 250 (50) cm^{-1}. IR: 3340 w, 3303 w, 2955 m, 2926 m, 2870 m, 2841 s, 2766 w, 2712 w, 2027 vs (ν_{as}N$_3$), 1469 m, 1450 m, 1364 m, 1329 m, 1282 m (ν_sN$_3$), 1261 m, 1209 w, 1156 s, 1019 w, 802 w, 654 w, 597 w cm^{-1}. ^{1}H NMR ((CD$_3$)$_2$CO): $\delta = 1.45$ (s, $^3J_{H-^{199}Hg} = 237$ Hz, (CH$_3$)$_3$C). ^{13}C{^{1}H} NMR ((CD$_3$)$_2$CO): $\delta = 53.7$ (s, $^1J_{C-^{199}Hg} = 1663$ Hz, CHg), 32.5 (s, $^2J_{C-^{199}Hg} = 14$ Hz, (CH$_3$)$_3$C). ^{14}N NMR ((CD$_3$)$_2$CO): $\delta = -133$ (N$_\beta$), -254 (N$_\gamma$/N$_\alpha$, br). ^{199}Hg{^{1}H} NMR ((CD$_3$)$_2$CO): $\delta = -1357$. MS (DEI+) m/z (%) 244 (6) [M$^+$ $-$C$_4$H$_9$], 202 (56) [Hg$^+$], 57 (100) [C$_4$H$_9$$^+$]. EA (ICP): Hg 66.0 (calcd. 66.9) %.

Phenylmercury(II) azide (3)

M. p. 148 °C. Raman: 3137 (9), 3052 (65), 2980 (8), 2946 (7), 2056 (9)/2037 (15, ν_{as}N$_3$), 1569 (27), 1476 (15), 1430 (9), 1385 (8), 1329 (17), 1276 (15, ν_sN$_3$), 1191 (11), 1180 (14), 1156 (14), 1075 (12), 1065 (10), 1018 (25), 994 (100), 908 (6), 844 (7), 661 (16), 650 (18), 613 (9), 593 (5), 372 (27, νHgN), 295 (10), 240 (78, νHgC), 201 (29) cm^{-1}. IR: 3306 w, 3074 w, 3048 w, 2048 vs (ν_{as}N$_3$), 1603 w, 1575 w, 1476 m, 1432 m, 1378 w, 1328 w, 1304 w, 1278 m (ν_sN$_3$), 1018 m, 996 w, 726 m, 694 m, 651 w, 594 w cm^{-1}. ^{1}H NMR ((CD$_3$)$_2$CO): $\delta = 7.46$ (2 H, o-H), 7.33 (2 H, m-H), 7.25 (1 H, p-H). ^{13}C{^{1}H} NMR ((CD$_3$)$_2$CO): $\delta = 148.6$ (s, $^1J_{C-^{199}Hg} = 2361$ Hz, CHg), 137.9 (s, $^2J_{C-^{199}Hg} = 115$ Hz, m-C), 129.28 (s, $^3J_{C-^{199}Hg} = 193$ Hz, o-C), 129.26 (s, $^4J_{C-^{199}Hg} = 35$ Hz, p-C). ^{14}N NMR ((CD$_3$)$_2$CO): $\delta = -134$ (N$_\beta$), -235 (N$_\gamma$, br), -291 (N$_\alpha$, br). ^{199}Hg{^{1}H} NMR ((CD$_3$)$_2$CO): $\delta = -1292$. MS (DEI+) m/z (%) 321 (8) [M$^+$], 279 (12) [M$^+$ $-$N$_3$], 202 (4) [Hg$^+$], 77 (100) [C$_6$H$_5$$^+$]. EA (ICP): Hg 61.9 (calcd. 62.7) %.

8.6. Acknowledgement

Supporting Information

X-ray crystallographic files (CIF) of the crystal data collection and refinement parameters, atomic coordinates, bond lengths and angles, anisotropic displacement parameters for **1**–**3**. Complete listing of the structure calculations and the observed and calculated IR and Raman bands for **1**–**3**.

8.7. References

[1] A. Perret, R. Perrot, *Helv. Chim. Acta* **1933**, *16*, 848–857.

[2] K. Dehnicke, J. Strähle, D. Seybold, J. Müller, *J. Organomet. Chem.* **1966**, *6*, 298–300.

[3] K. Dehnicke, D. Seybold, *J. Organomet. Chem.* **1968**, *11*, 227–241.

[4] A. F. Shihada, K. Dehnicke, *J. Organomet. Chem.* **1971**, *26*, 157–160.

[5] U. Müller, *Z. Naturforsch.* **1973**, *28b*, 426–428.

[6] W. Beck, W. P. Fehlhammer, P. Poellmann, E. Schuierer, K. Feldl, *Chem. Ber.* **1967**, *100*, 2335–2361.

[7] K. H. Flegler, A. Haas, *Z. Anorg. Allg. Chem.* **1976**, *426*, 288–300.

[8] D. J. Brauer, H. Bürger, G. Pawelke, K. H. Flegler, A. Haas, *J. Organomet. Chem.* **1978**, *160*, 389–401.

[9] J. Lorberth, F. Weller, *J. Organomet. Chem.* **1971**, *32*, 145–160.

[10] J. S. Thayer, *Organomet. Chem. Rev.* **1966**, *1*, 157–178.

[11] N. K. Wilson, R. D. Zehr, P. D. Ellis, *J. Magn. Reson.* **1976**, *21*, 437–443.

[12] A. J. Brown, O. W. Howarth, P. Moore, *J. Chem. Soc., Dalton Trans.* **1976**, 1589–1592.

[13] P. L. Goggin, R. J. Goodfellow, N. W. Hurst, *J. Chem. Soc., Dalton Trans.* **1978**, 561–566.

[14] A. Bondi, *J. Phys. Chem.* **1964**, *68*, 441–451.

[15] U. Müller, *Z. Anorg. Allg. Chem.* **1973**, *399*, 183–192.

[16] U. Müller, *Struct. Bonding (Berlin)* **1973**, *14*, 141–172.

[17] G. Gilli, F. H. Cano, S. Garcia-Blanco, *Acta Crystallogr., Sect. B* **1976**, *32*, 2680–2682.

[18] M. Wilhelm, W. Saak, H. Strasdeit, *Z. Naturforsch.* **2000**, *55b*, 35–38.

[19] D. F. Shriver, M. A. Drezdzon, *The Manipulation of Air-Sensitive Compounds*, 2nd ed., John Wiley & Sons: New York, **1986**.

[20] G. A. Russell, P. Ngoviwatchai, H. I. Tashtoush, *Organometallics* **1988**, *7,* 696–702.

[21] M. J. Frisch, G. W. Trucks, H. B. Schlegel, G. E. Scuseria, M. A. Robb, J. R. Cheeseman, J. A. Montgomery Jr., T. Vreven, K. N. Kudin, J. C. Burant, J. M. Millam, S. S. Iyengar, J. Tomasi, V. Barone, B. Mennucci, M. Cossi, G. Scalmani, N. Rega, G. A. Petersson, H. Nakatsuji, M. Hada, M. Ehara, K. Toyota, R. Fukuda, J. Hasegawa, M. Ishida, T. Nakajima, Y. Honda, O. Kitao, H. Nakai, M. Klene, X. Li, J. E. Knox, H. P. Hratchian, J. B. Cross, C. Adamo, J. Jaramillo, R. Gomperts, R. E. Stratmann, O. Yazyev, A. J. Austin, R. Cammi, C. Pomelli, J. W. Ochterski, P. Y. Ayala, K. Morokuma, G. A. Voth, P. Salvador, J. J. Dannenberg, V. G. Zakrzewski, S. Dapprich, A. D. Daniels, M. C. Strain, O. Farkas, D. K. Malick, A. D. Rabuck, K. Raghavachari, J. B. Foresman, J. V. Ortiz, Q. Cui, A. G. Baboul, S. Clifford, J. Cioslowski, B. B. Stefanov, G. Liu, A. Liashenko, P. Piskorz, I. Komaromi, R. L. Martin, D. J. Fox, T. Keith, M. A. Al-Laham, C. Y. Peng, A. Nanayakkara, M. Challacombe, P. M. W. Gill, B. Johnson, W. Chen, M. W. Wong, C. Gonzalez, J. A. Pople, *Gaussian 03*, Rev. B.03; Gaussian, Inc., Pittsburgh PA, **2003**.

[22] R. Dennington II, T. M. Keith, J., K. Eppinnett, W. L. Hovell, R. Gilliland, *GaussView*, Ver. 3.09; Semichem, Inc., Shawnee Mission KS, **2003**.

[23] A. D. Becke, *J. Chem. Phys.* **1993**, *98*, 5648–5652.

[24] T. M. Klapötke, A. Schulz, *Quantum Chemical Methods in Main-Group Chemistry*, John Wiley & Sons, Chichester, **1998**.

[25] D. Andrae, U. Häußermann, M. Dolg, H. Stoll, H. Preuß, *Theor. Chim. Acta* **1990**, *77*, 123–141.

[26] A. Altomare, G. Cascarano, C. Giacovazzo, A. Guagliardi, A. G. G. Moliterni, M. C. Burla, G. Polidori, M. Camalli, R. Spagna, *SIR97*, **1997**.

[27] A. Altomare, M. C. Burla, M. Camalli, G. L. Cascarano, C. Giacovazzo, A. Guagliardi, A. G. G. Moliterni, G. Polidori, R. Spagna, *J. Appl. Crystallogr.* **1999**, *32*, 115–119.

[28] G. M. Sheldrick, *SHELX-97*, University of Göttingen. Göttingen, Germany, **1997**.

[29] G. M. Sheldrick, *Acta Crystallogr., Sect. A* **2008**, *64*, 112–122.

9. Organomercury(II) Tetrazoles
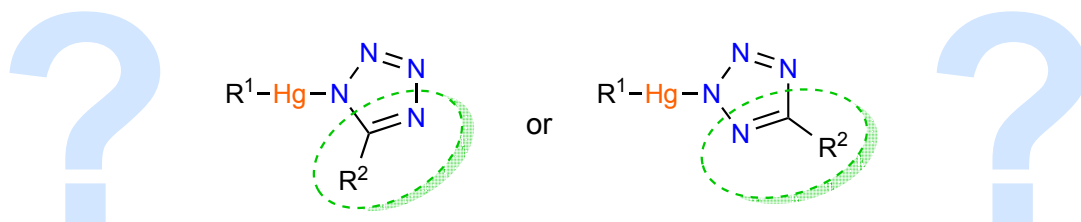
Convenient Room-Temperature, Mercury-Assisted Synthesis of Tetrazoles by 1,3-Dipolar Cycloaddition

Thomas M. Klapötke,*[a] Burkhard Krumm,[a] and Richard Moll [a]

Dedicated to Professor Rolf Huisgen on the occasion of his 90th birthday

*   Prof. Dr. Thomas M. Klapötke
        E-Mail: tmk@cup.uni-muenchen.de

[a]   Department of Chemistry
        Ludwig-Maximilian University of Munich
        Butenandtstrasse 5–13 (D)
        81377 Munich, Germany

9.1. Abstract

The intermolecular 1,3-dipolar cycloaddition of organomercury(II) azides R^1HgN_3 ($R^1 =$ Me, Ph) to organonitriles R^2CN ($R^2 =$ Me, Ph, C_6F_5) forms organomercury(II) tetrazoles $R^1Hg(N_4C)R^2$ [$R^1 =$ Me, $R^2 =$ Me (**1**); $R^1 =$ Me, $R^2 =$ Ph (**2**); $R^1 =$ Ph, $R^2 =$ Me (**3**); $R^1 =$ Ph, $R^2 =$ Ph (**4**); $R^1 =$ Ph, $R^2 =$ C_6F_5 (**5**)]. The reaction is a direct and regioselective formation of the tetrazole moiety, which is easily performed at room temperature or slightly elevated temperature without a catalyst and furnishes quantitatively the pure product. In addition to characterization by multinuclear NMR spectroscopy, IR and Raman spectroscopy, as well as mass spectrometry, the mercury content was determined. Furthermore, X-ray diffraction studies were performed, and the crystal structures for **1**–**3** and **5** are reported.

9.2. Introduction

Cycloaddition reactions with azides and cyanides/nitriles for the synthesis of tetrazoles are known for almost 110 years. In 1901, a method for the synthesis of tetrazoles by the reaction of hydrazoic acid (HN_3) with cyanamide, yielding 5-aminotetrazole, was first reported.[1] In 1932 followed the first reaction with heptanenitrile, benzonitrile, *p*-tolunitrile, and benzylcyanide as representatives of organic cyanides.[2] Although numerous individual examples of cycloaddition to tetrazoles were known, the development of the general synthetic principle has been achieved by *Rolf Huisgen* in 1957–58.[3–6] He first recognized the possibility of varying the 1,3-dipole and dipolarophile and its high value for the synthesis of five-membered heterocycles. His study of the mechanism of addition of diazoalkanes to angularly strained double bonds led to the concept of 1,3-dipolar cycloaddition.[7] This 1,3-dipolar cycloaddition, which is also known as *Huisgen cycloaddition* or *Huisgen reaction*, is an organic chemical reaction belonging to the larger class of [2+3] cycloadditions. *Sharpless* et al. introduced the term "click chemistry" in 2002 as a chemical philosophy that describes chemistry tailored to generate compounds by joining small units together in a practical, quick, and reliable way.[8–11] The authors reported a very easy transformation of *p*-toluenesulfonyl cyanide and acyl cyanides with various aromatic and aliphatic azides under solvent-free conditions to yield exclusively the 1,5-disubstituted 5-acyl and 5-sulfonyltetrazoles, which was the first example of a direct synthesis of a 1,5-substituted tetrazole by an intermolecular [2+3] cycloaddition.[10,12] Comprehensive reviews on 1,3-dipolar cycloaddition chemistry were published in 1984 and 2002.[13,14] In addition, the role of protic and dipolar aprotic solvents in the synthesis of heterocyclic compounds by 1,3-dipolar cycloaddition was investigated and is summarized in a review.[15] Further work on the formation of tetrazoles by the intermolecular condensation of organic azides with nitriles was

performed.[16–24] Dialkylaluminum azide was also used as 1,3-dipole, which gave good yields at low reaction temperature and with a simple work-up procedure.[25] To the best of our knowledge, this work describes the first examples of organomercury(II) tetrazoles prepared by Huisgen 1,3-dipolar cycloaddition. In this context, mercury was only recently used as a catalyst for the synthesis of mercury(II) tetrazolate coordination polymers by an in situ hydrothermal [2+3] cycloaddition.[26] Few compounds with a mercury atom bonded to a tetrazole[27] and the crystal structure of a mercury 5-nitraminotetrazolate were described.[28] Furthermore, mercury was used for the preparation of mercury(II) tetrazolate coordination polymers, but mercury(II) chloride had to be employed to obtain the framework with mercury atoms.[26]

In this contribution, a detailed study of the synthesis and characterization of organomercury(II) tetrazoles with methyl/methyl (**1**), methyl/phenyl (**2**), phenyl/methyl (**3**), phenyl/phenyl (**4**), and phenyl/pentafluorophenyl (**5**) substituents is presented.

9.3. Results and Discussion

Synthesis

The synthesis route for the preparation of the organomercury(II) tetrazoles **1**–**5** is the intermolecular 1,3-dipolar cycloaddition of organomercury(II) azides with various nitriles to obtain the corresponding organomercury(II) tetrazoles $R^1Hg(N_4C)R^2$ [R^1 = Me, R^2 = Me (**1**); R^1 = Me, R^2 = Ph (**2**); R^1 = Ph, R^2 = Me (**3**); R^1 = Ph, R^2 = Ph (**4**); R^1 = Ph, R^2 = C_6F_5 (**5**)] (Scheme 1).
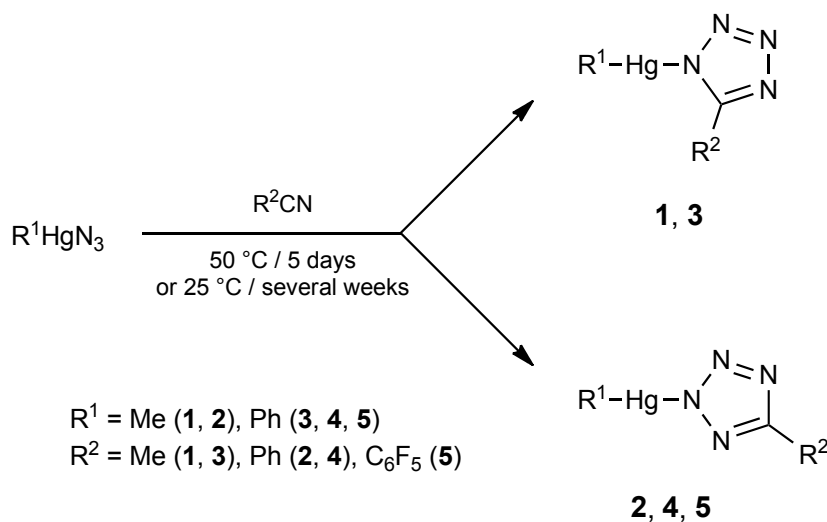
Scheme 1: Dissolution of $RHgN_3$ in nitriles to form organomercury(II) tetrazoles **1**–**5**.

The synthesis of **1**–**5** is performed in a facile fashion by dissolving the corresponding organomercury(II) azides in selected organonitriles at room temperature and slightly warming the reaction mixture. The organonitriles serve in this synthesis as the solvent as well as the reagent, thus a large excess is obvious. After removing the solvent, no other byproducts are observed, and the reaction furnishes the pure products quantitatively, without the need for further purification or isolation. In addition, the reactants are not sensitive to air or water; therefore, no extra precautions need to be taken. The synthesis works at ambient pressure without using a catalyst. The reaction of phenylmercury(II) azide with trimethylsilyl cyanide furnished only crystals of phenylmercury(II) cyanide, which can be explained by the ability of trimethylsilyl cyanide to act as a cyanide transfer agent. It was previously found that the cycloaddition can only be achieved without a catalyst if the nitrile is sufficiently activated by strong electron-withdrawing groups.[4,9,10,15,17,18,29] Electron-withdrawing groups tend to lower the LUMO of the nitriles and thus increase the interaction with the HOMO of the azide.[29,30] It is reported that the reaction of various organic azides with various nitriles failed with nitriles that were not activated, even with the use of various catalysts.[17] Despite the fact that electron-donating acetonitrile was used for the preparation of **1** and **3**, the reaction gave the desired compounds in quantitative yields. The solubilities of nonhygroscopic compounds **1**–**5** are very low in common solvents, whereas the compounds are more soluble in polar solvents than in nonpolar solvents. None of the compounds are soluble in water. In particular, aryl-substituted compounds **2**–**5** are rather insoluble, and compounds **4** and **5** are most insoluble because they contain two aryl groups.

The 1,3-dipolar cycloaddition of **1**–**5** only gave one of the two possible isomeric tetrazole products. For **1** and **3**, the 1,5-disubstituted tetrazole products, whereas for **2**, **4**, and **5**, the 2,5-disubstituted tetrazole products were obtained. This preferred orientation in the cycloaddition seems to be a general phenomenon of 1,3-dipolar cycloaddition,[7,17,31] which is also verified by computational calculations,[30] and was observed in the cycloaddition of organic azides and nitrile groups bound to a sulfur atom, as well.[10] *Huisgen* described that dipolarophiles with multiple bonds including a heteroatom usually add to the dipole in only one of the two possible directions and explained this observation by the smaller σ-bond energy of one of the two possible directions as well as by steric effects.[7] Thus, the interaction of electronic and steric effects is responsible for the orientation of the cyanide moiety inside the tetrazole ring. The electron-donating methyl group (+I effect) leads to the formation of 1,5-disubstituted tetrazoles, whereas the slightly electron-withdrawing phenyl group and the stronger electron-withdrawing pentafluorophenyl group (−I effect) lead to 2,5-disubstituted tetrazoles. Furthermore, even more important for the regioselectivity of the addition are steric effects.[7] The steric demands of benzonitrile and pentafluorobenzonitrile are larger than that of acetonitrile,

which results in the different orientation of the dipolarophile in **1** and **3** relative to that in **2**, **4**, and **5**.

Furthermore, it is possible to obtain tetrazoles **1**–**5** at ambient temperature. After several weeks in a saturated solution of methylmercury(II) azide or phenylmercury(II) azide in acetonitrile, benzonitrile, or pentafluorobenzonitrile, crystals of **1**–**5** are formed. The formation of the tetrazole compounds even at room temperature without any catalyst is due to the strongly polarized and activated azide bond in phenylmercury(II) azide and especially in methylmercury(II) azide.[32] This reactivity even at room temperature is quite unusual, because 1,3-dipolar cycloadditions usually require a catalyst or heating to reflux for a reaction to occur or reach completion.[4,9,19,21,25,26] Similar reactivity at ambient temperature was found with dialkylaluminum compounds, in which the aluminum center acts as a Lewis acid and thereby activates the nitrile.[25] Furthermore, even the electron-donating acetonitrile reacts at ambient temperature to yield **1** and **3**, which is quite uncommon for 1,3-dipolar cycloadditions.[4,9–12,15–25,29,31] Even the use of mercury(II) chloride as catalyst for the hydrothermal cycloaddition of pyrazinecarbonitriles with sodium azide needs elevated temperatures ($> 110\,°C$) and a Teflon-lined reactor.[11] In contrast to the results described by *Sharpless* et al.,[12] the reaction of a fluorinated aromatic nitrile (pentafluorobenzonitrile) with an azide [phenylmercury(II) azide] furnished the corresponding tetrazole compound **5**, primarily even without heating.

NMR Spectroscopy

All compounds were thoroughly characterized by ^{1}H, ^{13}C and ^{199}Hg NMR spectroscopy. In the ^{1}H NMR spectra of **1** and **2**, the $^2J_{\text{H}-^{199}\text{Hg}}$ couplings were determined to be 217 Hz for **1** and 220 Hz for **2**, values which are slightly higher than that for the corresponding methylmercury(II) azide.[32] The ^{1}H NMR spectra of **2**–**5** show the expected AA'BB'C spin system of monosubstituted phenyl rings, whereas the resonances of the phenyl hydrogen atoms attached to the tetrazole ring are shifted to higher frequency relative to those of the phenyl hydrogen atoms directly attached to the mercury atom. In the ^{13}C NMR spectra, the shifts of the carbon atom in the tetrazole ring (carbon C1) are 159.0/159.4 ppm for **1/3** and 163.3/163.5 ppm for **2/4**. It is well established that, for 2,5-disubstituted tetrazoles such as **2** and **4**, the C1 resonances are shifted to higher frequency relative to those in 1,5-disubstituted tetrazoles **1** and **3**.[27] For the other resonances in the ^{13}C NMR spectra of **1**–**4**, ^{199}Hg satellites could also be observed, which verify clearly the attachment of the corresponding methyl or phenyl group to the mercury atom. The ^{13}C NMR spectra of **1** and **2** show the resonances for the methyl group attached to the mercury atom at -2.0 ppm for **1** and -2.6 ppm for **2** with coupling constants $^1J_{\text{C}-^{199}\text{Hg}}$ of 1633 Hz for **1** and 1638 Hz for **2**. Both coupling constants are higher than that of the starting material, methylmercury(II) azide (1491 Hz). For **3**,

all possible ^{13}C–^{199}Hg couplings of the phenyl carbon atoms could be observed. The coupling constant of 2561 Hz for the $^1J_{C-^{199}Hg}$ coupling is very large because of the sp^2 hybridization and therefore the higher s character of the C–Hg hybrid orbital. The $^2J_{ortho\text{-}C}$, $^3J_{meta\text{-}C}$, and $^4J_{para\text{-}C}$ coupling constants were determined to be 117, 204, and 35 Hz, respectively. Because of the low solubility of **4**, only the $^2J_{ortho\text{-}C}$ and $^3J_{meta\text{-}C}$ couplings could be detected, with coupling constants of 119 ($^2J_{C-^{199}Hg}$) and 207 Hz ($^3J_{C-^{199}Hg}$), which matches quite well the values for **3**. These coupling constants are in agreement with the values for other phenylmercury(II) compounds.[33,34] The assignment of the phenyl carbon atoms attached to the mercury atom in the ^{13}C NMR spectra was performed as described for phenylmercury(II) azide and phenylmercury(II) chloride.[32,34] This leads to a smaller coupling constant for the ^2J in comparison to the $^3J_{C-^{199}Hg}$ coupling. Because of the low solubility of **5** and the fluorine substituents on one of the two phenyl rings, only the ortho-, meta-, and para-carbon atoms of the phenyl ring attached to the mercury atom could be observed, without any ^{199}Hg satellites. The ^{199}Hg NMR shifts correspond to the electron density of the substituents, thus a higher electron density leads to a shift to lower frequency. Therefore, the signal for **3** at −1324 ppm is shifted to lower frequency relative to those for **1** (980 ppm) and **2** (−1007 ppm). Since there are methyl groups attached at Hg in both **1** and **2**, the ^{199}Hg NMR shifts are very close for these compounds. Furthermore, the resonances for tetrazole compounds **1**–**3** are slightly shifted to lower frequency relative to those for the corresponding azide compounds,[32] which were used as starting material. All ^{199}Hg NMR spectra were recorded in the same solvent, because the chemical shift of the ^{199}Hg nucleus significantly depends on the polarity of the solvent.[35–38] Because of the very low solubility of the doubly aryl-substituted compounds **4** and **5**, no signal could be observed in the ^{199}Hg NMR spectra, even with extended scan rates. The sufficient solubility of **1** permitted the recording of a ^{15}N NMR spectrum. The ^{15}N NMR spectrum of **1** shows two resonances at −2.5 and −80.4 ppm instead of the four expected signals of the tetrazole ring (Figure 1).

This phenomenon can be explained by the anionic nature of the tetrazole moiety when dissolved in polar solvents, due to the high stability of MeHg$^+$, which results in an anionic and symmetrical 5-methyltetrazolate (Figure 1). Comparison with an authentic sample of potassium 5-methyltetrazolate (CD$_3$OD: ^{15}N $\delta = -4.7, -75.6$ ppm), synthesized according to a procedure in the literature,[39] confirms the ^{15}N NMR resonances and the assumption of the more ionic nature of **1** in polar solvents. A similar behavior of the MeHg group was also observed for methylmercury(II) azide, where this also appears only in polar solvents.[32] Further investigations on the polarity dependence on the solvent were not possible because of the low solubility of **1** in other solvents, especially in nonpolar solvents. Furthermore, the solubilities of **2**–**5** in general are even
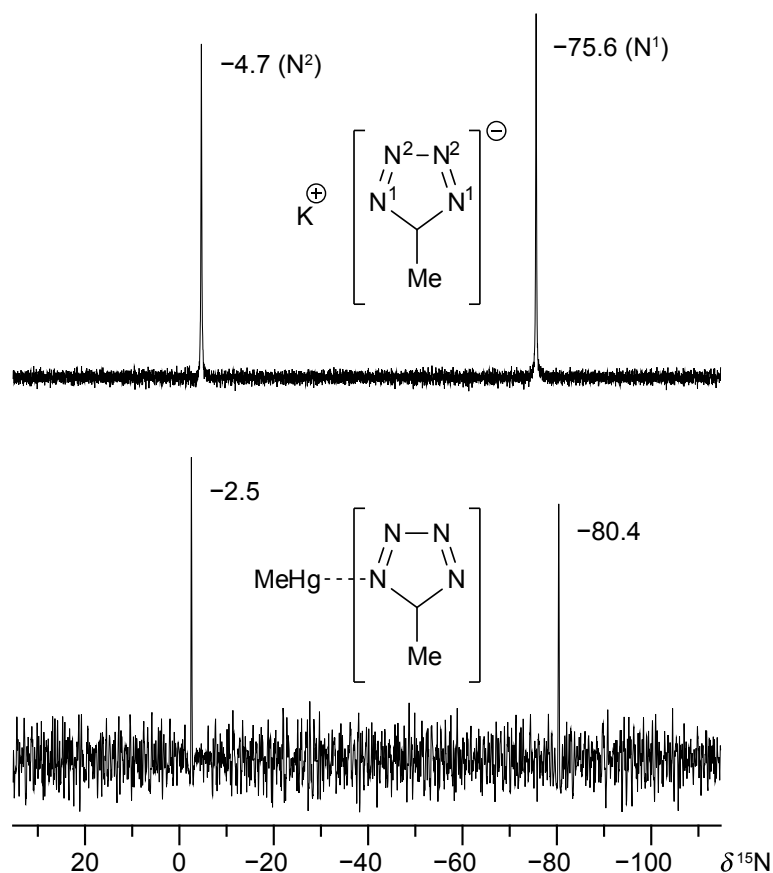
Figure 1.: ^{15}N NMR spectrum of $CH_3Hg(N_4C)CH_3$ (**1**) (bottom) and $K[(N_4C)CH_3]$ (top) in CD_3OD at 25 °C (δ in ppm).

worse; therefore, no resonances in the ^{15}N NMR spectra, independent of the solvent, were observed.

Vibrational Spectroscopy

The Raman spectra of **1**–**5** show the Hg−C stretching vibrations for **1** and **2** at 555 and 565 cm^{-1}, respectively. The corresponding Hg−C stretching vibrations for **3**–**5** are found at smaller wavenumber (all at 240 cm^{-1}) because of the rigidness of the phenyl ring and the more polar Hg−C bond. All Hg−C stretching vibrations are in very good agreement with the stretching vibrations found in similar methyl- and phenylmercury(II) moieties.[32,40–42]

X-ray Diffraction

Single crystals suitable for X-ray diffraction measurements were obtained by slow evaporation of the solvent at ambient temperatures in acetonitrile (for **1**, **3**), benzonitrile (for **2**), or pentafluorobenzonitrile (for **5**). A full list of the crystallographic refinement parameters and structure data for **1**–**3** and **5** is shown in Table 2. Compound **1** crystallizes in the monoclinic space group $C2/c$ with eight formula units per unit cell. The molecular structure is shown in Figure 2.
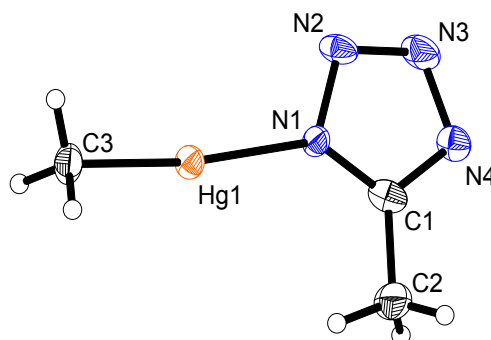
Figure 2.: Molecular structure of **1**. Selected distances [Å] and angles [°]: Hg1−N1 2.113(7), Hg1−C3 2.062(9), N1−N2 1.368(9), N2−N3 1.294(10), N3−N4 1.354(10), N1−C1 1.327(11), N4−C1 1.317(11), C1−C2 1.481(11), C3−Hg1−N1 172.2(3), Hg1−N1−N2 117.7(5), Hg1−N1−C1 135.4(5).

The Hg−C and Hg−N bond lengths are 2.062(9) and 2.113(7) Å, respectively, and are comparable to those in similar organomercury(II) compounds.[26,28,32,43] In agreement with the bond lengths of the corresponding methylmercury(II) azide,[32] the Hg−C bond of **1** is shorter than the Hg−N bond. The mercury atom is, as expected, doubly coordinated in an almost linear fashion, with an C3−Hg−N1 angle of 172.2(3)°. A comparison of selected bond lengths and angles for **1**–**3** and **5** is summarized in Table 1. Each mercury atom is surrounded by three further molecules with weak Hg⋯N contacts of 2.876(8), 2.922(9), and 3.138(9) Å (with a van der Waals radius, r_{vdW}, of 3.1 Å).[44] Compound **2** crystallizes in the monoclinic space group $C2/c$ with eight formula units per unit cell (Figure 3).

Compared to **1**, the Hg−C bond length [2.042(4) Å] and the Hg−N bond length [2.094(3) Å] are shorter, whereas the C8−Hg−N1 angle of 173.1(2)° also shows a slightly nonlinear arrangement (Table 1). Each mercury atom in **2** is surrounded by two molecules with intermolecular Hg⋯N distances of 2.743(4) and 3.097(4) Å (r_{vdW} = 3.1 Å).[44] Compound **3** crystallizes in the monoclinic space group $P2_1/c$ with four formula units per unit cell (Figure 4).
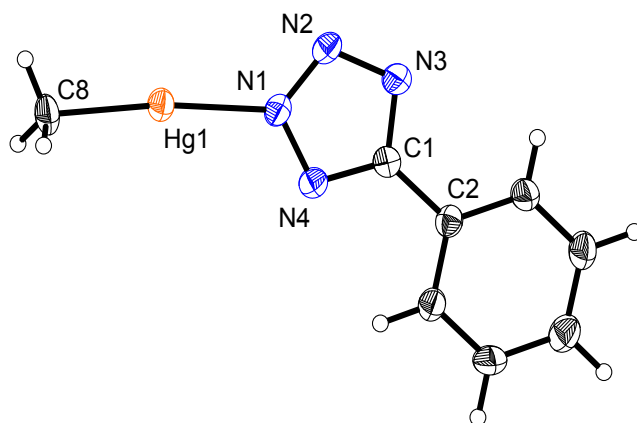
Figure 3.: Molecular structure of **2**. Selected distances [Å] and angles [°]: Hg1−N1 2.094(3), Hg1−C8 2.042(4), N1−N2 1.317(5), N2−N3 1.323(4), N3−C1 1.350(5), C1−N4 1.330(5), N1−N4 1.334(5), C1−C2 1.473(5), C8−Hg1−N1 173.1(2), Hg1−N1−N2 127.0(3), Hg1−N1−N4 120.6(2).
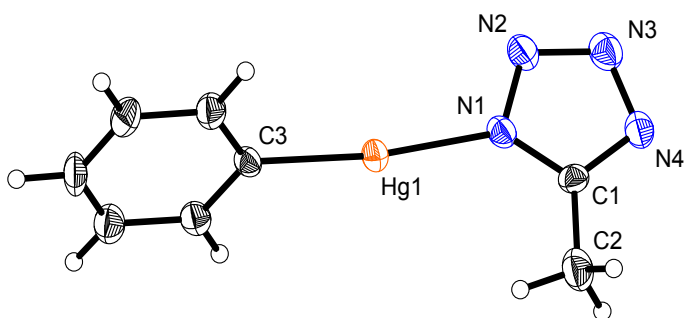
Figure 4.: Molecular structure of **3**. Selected distances [Å] and angles [°]: Hg1−N1 2.090(4), Hg1−C3 2.046(5), N1−N2 1.343(7), N2−N3 1.305(6), N3−N4 1.355(7), N1−C1 1.339(7), N4−C1 1.327(7), C1−C2 1.463(9), C3−Hg1−N1 172.3(2), Hg1−N1−N2 119.4(4), Hg1−N1−C1 132.6(4).

The Hg−C [2.046(5) Å] and Hg−N [2.090(4) Å] bond lengths in **3** are shorter than those in **1** but are very close to those in **2**. The C3−Hg−N1 angle of 172.3(2)° has the same size as the structures described above (Table 1). The values for the Hg1−N1−N2 and the Hg1−N1−C1 angles are quite the same as those for **1**. Each mercury atom in **3** is surrounded by two molecules with intermolecular Hg···N distances of 2.815(6) and 2.906(6) Å (r_{vdW} = 3.1 Å)[44]. In contrast to **1**–**3**, compound **5** crystallizes in the triclinic space group $P\bar{1}$ with two formula units per unit cell. The molecular structure is shown in Figure 5.

The Hg−N bond of 2.115(5) Å is the longest found in this work, whereas the Hg−C bond length of 2.049(6) Å is between the corresponding bond lengths for **1** and
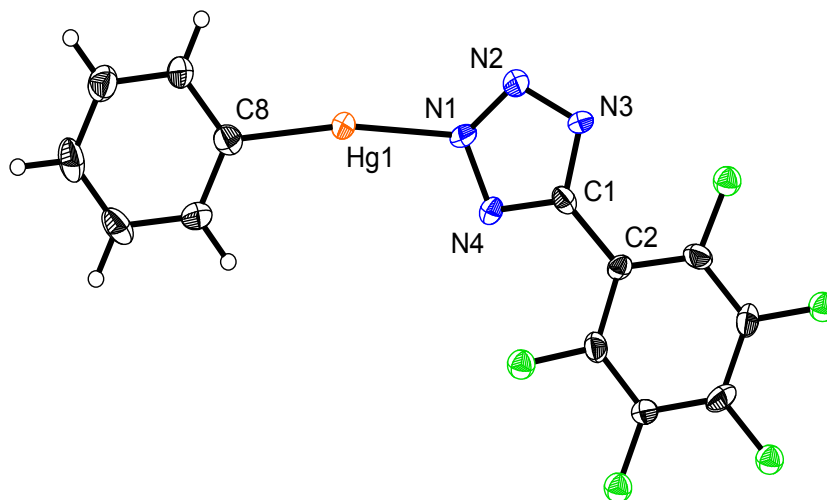
Figure 5.: Molecular structure of **5**. Selected distances [Å] and angles [°]: Hg1−N1 2.115(5), Hg1−C8 2.049(6), N1−N2 1.313(7), N2−N3 1.309(7), N3−C1 1.338(8), C1−N4 1.324(8), N1−N4 1.331(7), C1−C2 1.478(8), C8−Hg1−N1 168.5(2), Hg1−N1−N2 129.0(4), Hg1−N1−N4 116.3(4).

Table 1.: Selected bond lengths [Å] and angles [°] for $CH_3Hg(N_4C)CH_3$ (**1**), $CH_3Hg(N_4C)C_6H_5$ (**2**), $C_6H_5Hg(N_4C)CH_3$ (**3**), and $C_6H_5Hg(N_4C)C_6F_5$ (**5**).

	1	**2**	**3**	**5**
Hg1−C3/C8	2.062(9)	2.042(4)	2.046(5)	2.049(6)
Hg1−N1	2.113(7)	2.094(3)	2.090(4)	2.115(5)
C3/C8−Hg1−N1	172.2(3)	173.1(2)	172.3(2)	168.5(2)
Hg1−N1−N2	117.7(5)	127.0(3)	119.4(4)	129.0(4)
Hg1−N1−C1/N4	135.4(5)	120.6(2)	132.6(4)	116.3(4)

3. Also the C8−Hg−N1 angle of 168.5(2)° is more bent relative to the other reported crystal structures. In contrast to those in **1** and **3**, the Hg1−N1−N2 angle is about 10° larger and the Hg1−N1−N4 angle is, in agreement with this, more than 15° smaller (Table 1). This leads to a general rotation of the tetrazole moiety related to the mercury atom. This bigger bend is also found in **2** and is due to the 2,5-disubstitution of the tetrazole ring. Each mercury atom in **5** is surrounded by two molecules with Hg···N contacts of 2.716(5) Å, which are the shortest ones found in this work, and 2.957(6) Å ($r_{vdW} = 3.1$ Å)[44]. Furthermore, it was also possible to obtain and analyze crystals of compound **4**, but these crystals led only to a poor data set. However, it was possible to find a basic refinement, which clearly shows a 2,5-disubstituted tetrazole and verifies the ^{13}C NMR spectroscopic data described above.

9.4. Conclusions

In summary, the covalent organomercury(II) tetrazoles $R^1Hg(N_4C)R^2$ [R^1 = Me, R^2 = Me (**1**); R^1 = Me, R^2 = Ph (**2**); R^1 = Ph, R^2 = Me (**3**); R^1 = Ph, R^2 = Ph (**4**); R^1 = Ph, R^2 = C_6F_5 (**5**)] were prepared by reaction of the corresponding organomercury(II) azides with organonitriles. Thereby, the direct and regioselective formation of tetrazole rings by 1,3-dipolar cycloaddition of organomercury(II) azides with organonitriles was observed. This intermolecular [2+3] cycloaddition involved simple stirring of the organomercury(II) azides in neat organonitriles at moderate temperatures (starting at 25 °C) without the need of using a catalyst. The reaction gave the product in quantitative yields, and no

Table 2.: Crystal and structure data for $CH_3Hg(N_4C)CH_3$ (**1**), $CH_3Hg(N_4C)C_6H_5$ (**2**), $C_6H_5Hg(N_4C)CH_3$ (**3**), and $C_6H_5Hg(N_4C)C_6F_5$ (**5**).

	1	**2**
Refined formula	$C_3H_6HgN_4$	$C_8H_8HgN_4$
Formula weight	298.69	360.76
Crystal dimensions [mm]	$0.24 \times 0.13 \times 0.04$	$0.42 \times 0.04 \times 0.02$
Crystal description	Colorless platelets	Colorless platelets
Crystal system	Monoclinic	Monoclinic
Space group	$C2/c$	$C2/c$
a [Å]	13.0734(6)	23.5388(11)
b [Å]	8.2417(4)	4.3982(2)
c [Å]	11.4459(5)	19.2321(10)
α [°]	90.0	90.0
β [°]	101.638(5)	111.678(8)
γ [°]	90.0	90.0
V [Å^3]	1207.91(10)	1850.25(19)
Z	8	8
$\rho_{calcd.}$ [g cm^{-3}]	3.2850(5)	2.5902(2)
μ [mm^{-1}]	25.377	16.593
Temperature [K]	100(3)	173(2)
θ range [°]	4.32–25.99	4.24–25.99
Reflections measured	2689	8682
Reflections independent	1185	1815
Reflections unique	841 (R_{int} = 0.0436)	1495 (R_{int} = 0.0529)
$R1$, $wR2$ (2σ data)	0.0287, 0.0624	0.0178, 0.0373
$R1$, $wR2$ (all data)	0.0418, 0.0643	0.0233, 0.0379
Data/restraints/parameters	1185/0/74	1815/0/119
GOF on F^2	0.908	0.926
Residual electron density	−2.036/1.148	−0.590/0.874

	3	5
Refined formula	$C_8H_8HgN_4$	$C_{13}H_5F_5HgN_4$
Formula weight	360.76	512.78
Crystal dimensions [mm]	$0.20 \times 0.10 \times 0.05$	$0.45 \times 0.40 \times 0.20$
Crystal description	Colorless platelets	Colorless blocks
Crystal system	Monoclinic	Triclinic
Space group	$P2_1/c$	$P\bar{1}$
a [Å]	10.6192(9)	6.4318(4)
b [Å]	8.8615(4)	8.5654(4)
c [Å]	10.5311(9)	13.0661(7)
α [°]	90.0	82.186(4)
β [°]	112.681(10)	84.896(5)
γ [°]	90.0	69.442(5)
V [Å^3]	914.36(14)	667.07(7)
Z	4	2
$\rho_{calcd.}$ [g cm^{-3}]	2.6207(3)	2.5530(2)
μ [mm^{-1}]	16.788	11.600
Temperature [K]	200(3)	200(3)
θ range [°]	3.90–26.00	4.28–25.99
Reflections measured	7903	5360
Reflections independent	1786	2607
Reflections unique	1377 ($R_{int} = 0.0506$)	2306 ($R_{int} = 0.0531$)
$R1$, $wR2$ (2σ data)	0.0239, 0.0423	0.0312, 0.0694
$R1$, $wR2$ (all data)	0.0425, 0.0442	0.0356, 0.0703
Data/restraints/parameters	1786/0/118	2607/0/208
GOF on F^2	0.942	1.007
Residual electron density	$-0.795/0.963$	$-2.080/1.293$

further purification was necessary. The reactions presented in this study are therefore a perfect example of the ideal "click chemistry".

9.5. Experimental Section

The solvents acetonitrile and benzonitrile were dried by standard methods and freshly distilled prior to use. Pentafluorobenzonitrile (Acros Organics) was used as received. Methylmercury(II) azide and phenylmercury(II) azide were prepared according to the literature procedure.[32]

Raman spectra were recorded with a Bruker MultiRAM FT-Raman instrument fitted with a liquid nitrogen-cooled germanium detector and a Nd:YAG laser ($\lambda = 1064\,nm$), infrared spectra were measured with a Perkin-Elmer Spectrum BX FTIR spectrometer equipped with a Smiths DuraSampl*IR* II ATR device. All spectra were

recorded at ambient temperature; the samples were neat solids. NMR spectra were recorded with a JEOL Eclipse 400 ECX instrument, and chemical shifts were determined with respect to external Me_4Si (^1H: 399.8 MHz; ^{13}C: 100.5 MHz), $MeNO_2$ (^{14}N: 28.9 MHz; ^{15}N: 40.6 MHz), and Me_2Hg (^{199}Hg: 71.7 MHz). $HgCl_2$ (0.5 M in THF) was used as external standard for ^{199}Hg NMR spectroscopy, and the shift ($\lambda = -1517$ ppm) was referenced to that of Me_2Hg ($\delta = 0$ ppm). Because of the significant temperature dependence of the ^{199}Hg NMR resonances, all samples were measured at 25 °C. Mass spectrometric data were obtained with a JEOL MStation JMS 700 spectrometer (DCI+). Hg-containing fragments are referred to the isotope with the highest natural abundance, ^{202}Hg. Determinations of the mercury content were performed with a Varian Vista RL CCD Simultaneous ICP-AES spectrometer with a mercury ICP standard [CertiPUR®, $Hg(NO_3)_2$ in HNO_3 (10 %), Merck]. C/H/N analysis was not performed because of potential mercury contamination of the analyzer. Melting points were determined in capillaries with a Büchi Melting Point B-540 instrument. For all compounds, an Oxford Xcalibur3 diffractometer with a CCD area detector was employed for data collection using Mo-K_α radiation ($\lambda = 0.710\,73$ Å). The structures were solved by direct methods (SIR97[45,46], SHELXS-97[47,48] and refined by full-matrix least-squares on F^2 (SHELXL).[47,48] All non-hydrogen atoms were refined anisotropically. The hydrogen atoms were located in a difference Fourier map and placed with a C−H distance of 0.98 Å for CH_3 groups and 0.95 Å for aromatic CH groups (see Table 2). ORTEP plots are shown with thermal ellipsoids at the 50 % probability level.

CCDC-793779, -793780, -793781, and -793782 contain the supplementary crystallographic data for this paper. These data can be obtained free of charge via www.ccdc.cam.ac.uk/data_request/cif.

CAUTION! Mercury and most mercury-containing compounds are very toxic. Avoiding contact with these compounds is mandatory, especially avoid inhalation of the volatile organomercury compounds.

General Procedure for the Preparation of $R^1Hg(N_4C)R^2$ [R^1 = Me, R^2 = Me (1); R^1 = Me, R^2 = Ph (2); R^1 = Ph, R^2 = Me (3); R^1 = Ph, R^2 = Ph (4); R^1 = Ph, R^2 = C_6F_5 (5)]

R^1HgN_3 [0.39 mmol (**1, 2**), 0.31 mmol (**3–5**)] was dissolved in R^2CN [5 mL (**1–4**), 15 mL (**5**)] at ambient temperature and stirred for 5 d at 50 °C. The solvent was removed in vacuo and yielded colorless solids.

Methyl (5-Methyl-1H-tetrazol-1-yl)mercury (1)

M. p. 189 °C. Raman: $\tilde{\nu}$ = 3015 (10), 2930 (48), 2861 (3), 2811 (2), 2812 (2), 2736 (1), 1495 (18), 1450 (4), 1421 (4), 1401 (2), 1390 (2), 1375 (4), 1241 (25), 1198 (40), 1131 (6), 1108 (9), 1085 (3), 1041 (1), 1011 (7), 805 (1), 697 (32), 555 (100, νHgC$_{\mathrm{Methyl}}$), 394 (11), 296 (6), 233 (15), 220 (20), 202 (22) cm^{-1}. IR: $\tilde{\nu}$ = 2997 (w), 2927 (m), 2806 (w), 1494 (s), 1425 (m), 1371 (vs), 1261 (w), 1238 (m), 1192 (m), 1129 (w), 1106 (s), 1081 (s), 1042 (w), 1010 (m), 990 (w), 804 (m), 791 (s), 724 (w), 694 (m) cm^{-1}. ^{1}H NMR (CD$_3$OD): δ = 2.55 (s, 3 H, CH_3-C$_{\mathrm{Tetr}}$), 1.04 (s, $^{2}J_{\mathrm{H}-^{199}\mathrm{Hg}}$ = 217 Hz, 3 H, CH_3Hg) ppm. ^{13}C{^{1}H} NMR (CD$_3$OD): δ = 159.0 (s, C_{Tetr}), 9.8 (s, CH_3-C$_{\mathrm{Tetr}}$), -2.0 (s, $^{1}J_{\mathrm{C}-^{199}\mathrm{Hg}}$ = 1633 Hz, CHg) ppm. ^{15}N NMR (CD$_3$OD): δ = -2.5 (s), -80.4 (s) ppm. ^{199}Hg{^{1}H} NMR (CD$_3$OD) δ = -980 ppm. MS (DCI+): m/z (%) = 301 (100) [M$^+$], 273 (7) [M$^+$ $-$CCH$_3$], 259 (4) [M$^+$ $-$CH$_3$CN], 217 (7) [CH$_3$Hg]. C$_3$H$_6$HgN$_4$ (298.69): calcd. Hg 67.2; found Hg 66.6.

Methyl (5-Phenyl-2H-tetrazol-2-yl)mercury (2)

M. p. 161 °C. Raman: $\tilde{\nu}$ = 3064 (20), 3044 (11), 3007 (2), 2961 (2), 2923 (28), 1693 (2), 1609 (100), 1585 (4), 1525 (53), 1492 (3), 1444 (49), 1357 (4), 1243 (3), 1200 (14), 1172 (17), 1154 (11), 1139 (3), 1114 (5), 1043 (9), 1026 (3), 1014 (9), 1007 (13), 998 (68), 789 (7), 695 (5), 618 (6), 565 (59, νHgC$_{\mathrm{Methyl}}$), 509 (3), 466 (3), 381 (5), 325 (14), 234 (16) cm^{-1}. IR: $\tilde{\nu}$ = 3071 (w), 3061 (w), 3042 (w), 3006 (w), 2921 (m), 2805 (w), 1584 (w), 1524 (w), 1456 (m), 1443 (vs), 1428 (m), 1384 (w), 1356 (m), 1279 (w), 1262 (w), 1240 (m), 1200 (w), 1170 (m), 1139 (s), 1113 (w), 1099 (w), 1071 (m), 1045 (m), 1027 (m), 1006 (m), 997 (w), 918 (w), 842 (w), 807 (m), 786 (m), 727 (vs), 709 (m), 694 (s), 686 (s) cm^{-1}. ^{1}H NMR (CD$_3$OD): δ = 8.02/7.51 (2 H/3 H, PhC$_{\mathrm{Tetr}}$), 1.06 (s, $^{2}J_{\mathrm{H}-^{199}\mathrm{Hg}}$ = 220 Hz, 3 H, CH_3Hg) ppm. ^{13}C{^{1}H} NMR (CD$_3$OD): δ = 163.3 (s, C_{Tetr}), 131.3 (s, p-C), 130.2 (s, m-C), 129.1 (s, C-C$_{\mathrm{Tetr}}$), 128.3 (s, o-C), -2.6 (s, CHg, $^{1}J_{\mathrm{C}-^{199}\mathrm{Hg}}$ = 1638 Hz) ppm. ^{199}Hg{^{1}H} NMR (CD$_3$OD): δ = -1007 ppm. MS (DCI+): m/z (%) = 363 (59) [M$^+$], 273 (16) [M$^+$ $-$CC$_6$H$_5$], 259 (8) [M$^+$ $-$C$_6$H$_5$CN], 217 (10) [CH$_3$Hg]. C$_8$H$_8$HgN$_4$ (360.76): calcd. Hg 55.6; found Hg 54.7.

(5-Methyl-1H-tetrazol-1-yl)phenylmercury (3)

M. p. 166 °C. Raman: $\tilde{\nu}$ = 3142 (5), 3061 (31), 3049 (40), 2983 (6), 2941 (16), 2895 (6), 2874 (5), 2861 (5), 1602 (4), 1573 (20), 1499 (10), 1482 (10), 1459 (5), 1448 (5), 1434 (5), 1370 (5), 1331 (6), 1264 (4), 1245 (16), 1195 (8), 1185 (5), 1165 (8), 1153 (5), 1133 (5), 1105 (5), 1083 (6), 1043 (4), 1022 (19), 998 (100), 987 (6), 702 (10), 694 (10), 664 (30), 617 (7), 397 (7), 315 (14), 296 (7), 264 (9), 240 (57, νHgC$_{\mathrm{Phenyl}}$), 225 (27) cm^{-1}. IR: $\tilde{\nu}$ = 3068 (m), 3047 (w), 3030 (w), 3017 (w), 2958 (m), 2929 (m), 2872 (m), 2858 (m), 1726 (s), 1599 (w), 1576 (m), 1498 (s), 1479 (m), 1459 (w), 1431 (vs), 1388 (m), 1379 (s), 1369 (vs),

1329 (w), 1287 (m), 1273 (m), 1244 (s), 1130 (m), 1121 (m), 1103 (s), 1084 (m), 1073 (s), 1041 (w), 1022 (m), 1018 (m), 1003 (w), 998 (m), 907 (w), 852 (w), 733 (vs), 727 (s), 723 (s), 700 (s), 696 (vs), 692 (vs), 664 (w) cm^{-1}. ^{1}H NMR (CD$_3$OD): δ = 7.48/7.37/7.29 (2 H/2 H/1 H, PhHg), 2.63 (s, 3 H, CH_3Tetr) ppm. ^{13}C{^{1}H} NMR (CD$_3$OD): δ = 159.4 (s, C_{Tetr}), 145.8 (s, $^1J_{\text{C}-^{199}\text{Hg}}$ = 2561 Hz, CHg), 138.4 (s, $^2J_{\text{C}-^{199}\text{Hg}}$ = 117 Hz, o-C), 129.9 (s, $^4J_{\text{C}-^{199}\text{Hg}}$ = 35 Hz, p-C), 129.7 (s, $^3J_{\text{C}-^{199}\text{Hg}}$ = 204 Hz, m-C), 9.9 (s, CH_3-C$_{\text{Tetr}}$) ppm. ^{199}Hg{^{1}H} NMR (CD$_3$OD): δ = -1324 ppm. MS (DCI+): m/z (%) = 363 (60) [M$^+$], 335 (36) [M$^+$ $-$CCH$_3$], 321 (48) [M$^+$ $-$CH$_3$CN], 279 (68) [C$_6$H$_5$Hg]. C$_8$H$_8$HgN$_4$ (360.76): calcd. Hg 55.6; found Hg 55.3.

Phenyl (5-Phenyl-2H-tetrazol-2-yl)mercury (4)

M. p. 194 °C. Raman: $\tilde{\nu}$ = 3140 (3), 3063 (28), 3050 (31), 1608 (76), 1571 (16), 1524 (39), 1480 (3), 1444 (28), 1359 (5), 1307 (4), 1237 (3), 1195 (2), 1182 (5), 1173 (12), 1157 (7), 1131 (2), 1110 (6), 1077 (3), 1067 (2), 1042 (13), 1022 (14), 998 (100), 789 (4), 694 (5), 664 (20), 618 (8), 379 (3), 317 (11), 258 (6), 240 (25, νHgC$_{\text{Phenyl}}$), 212 (16) cm^{-1}. IR: $\tilde{\nu}$ = 3047 (w), 1571 (m), 1523 (w), 1477 (m), 1458 (m), 1443 (s), 1431 (m), 1427 (m), 1396 (w), 1377 (w), 1357 (m), 1329 (w), 1305 (w), 1278 (m), 1262 (w), 1236 (m), 1171 (m), 1157 (w), 1130 (m), 1108 (m), 1071 (m), 1064 (m), 1041 (m), 1029 (m), 1021 (m), 1006 (m), 997 (m), 929 (w), 866 (w), 788 (m), 745 (m), 731 (vs), 723 (m), 711 (w), 695 (vs), 692 (vs), 663 (w) cm^{-1}. ^{1}H NMR (CD$_3$OD): δ = 8.08/7.53 (2 H/3 H, PhC$_{\text{Tetr}}$), 7.42/7.35/7.27 (2 H/2 H/1 H, PhHg) ppm. ^{13}C{^{1}H} NMR (CD$_3$OD): δ = 163.5 (s, C_{Tetr}), 146.6 (s, CHg), 138.2 [s, $^2J_{\text{C}-^{199}\text{Hg}}$ = 119 Hz, $(o$-$C)_{\text{Ph(Hg)}}$], 131.3 [s, $(p$-$C)_{\text{Ph(Tetr)}}$], 130.3 [s, $(m$-$C)_{\text{Ph(Tetr)}}$], 129.9 [s, $(p$-$C)_{\text{Ph(Hg)}}$], 129.8 [s, $^3J_{\text{C}-^{199}\text{Hg}}$ = 207 Hz, $(m$-$C)_{\text{Ph(Hg)}}$], 129.2 (s, C-C$_{\text{Tetr}}$), 128.3 [s, $(o$-$C)_{\text{Ph(Tetr)}}$] ppm. ^{199}Hg{^{1}H} NMR (CD$_3$OD): not detected. MS (DCI+): m/z (%) = 425 (92) [M$^+$], 335 (25) [M$^+$ $-$CC$_6$H$_5$], 321 (29) [M$^+$ $-$C$_6$H$_5$CN], 279 (60) [C$_6$H$_5$Hg]. C$_{13}$H$_{10}$HgN$_4$ (422.83): calcd. Hg 47.4; found Hg 48.1.

(5-Pentafluorophenyl-2H-tetrazol-2-yl)phenylmercury (5)

M. p. 173 °C. Raman: $\tilde{\nu}$ = 3146 (6), 3060 (49), 3051 (31), 3021 (5), 2996 (5), 2982 (5), 2967 (5), 2954 (5), 1674 (20), 1660 (37), 1632 (18), 1574 (27), 1535 (71), 1486 (100), 1435 (8), 1389 (12), 1341 (6), 1334 (8), 1285 (9), 1265 (8), 1232 (7), 1194 (12), 1185 (17), 1165 (11), 1115 (22), 1098 (11), 1079 (10), 1053 (11), 1041 (8), 1030 (39), 1000 (79), 988 (12), 913 (5), 838 (25), 769 (12), 715 (6), 693 (5), 665 (41), 616 (12), 585 (32), 505 (29), 446 (23), 432 (30), 389 (18), 377 (12), 364 (10), 315 (18), 287 (10), 278 (9), 255 (27), 240 (75, νHgC$_{\text{Phenyl}}$), 223 (19), 202 (29) cm^{-1}. IR: $\tilde{\nu}$ = 3076 (w), 3058 (w), 2963 (m), 1674 (w), 1650 (m), 1633 (m), 1576 (w), 1535 (s), 1511 (vs), 1481 (vs), 1433 (m), 1388 (m), 1374 (m), 1359 (m), 1341 (m), 1262 (m), 1230 (m), 1183 (m), 1143 (w), 1098 (s), 1064 (m), 1052 (m), 1030 (m), 996 (vs), 910 (w), 873 (w), 835 (s), 802 (m), 768 (m), 727 (s), 690 (m),

664 (w), 616 (w), 584 (w) cm^{-1}. ^{1}H NMR (CD$_3$OD): $\delta = 7.43/7.35/7.28$ (2 H/2 H/1 H, *Ph*Hg) ppm. ^{13}C$\{^1$H$\}$ NMR (CD$_3$OD): $\delta = 138.2$ [s, (*o-C*)$_{Ph(Hg)}$], 129.9 [s, (*p-C*)$_{Ph(Hg)}$], 129.8 [s, (*m-C*)$_{Ph(Hg)}$] ppm; other carbon atoms not detected due to low solubility. ^{19}F NMR (CD$_3$OD): $\delta = -141.4$ (m, *o-F*), -155.1 (m, *p-F*), -164.8 (m, *m-F*) ppm. ^{199}Hg$\{^1$H$\}$ NMR (CD$_3$OD): not detected. MS (DCI+): m/z (%) = 515 (100) [M$^+$], 335 (6) [M$^+$ $-$CC$_6$F$_5$], 321 (8) [M$^+$ $-$C$_6$F$_5$CN], 279 (27) [C$_6$H$_5$Hg]. C$_{13}$H$_5$F$_5$HgN$_4$ (512.78): calcd. Hg 39.1; Hg 37.8.

9.6. Acknowledgments

9.7. References

[1] A. Hantzsch, A. Vagt, *Liebig's Ann.* **1901**, *314*, 339–369.

[2] J. v. Braun, W. Keller, *Ber. Dtsch. Chem. Ges.* **1932**, *65*, 1677–1680.

[3] R. Huisgen, *Proc. Chem. Soc. London* **1961**, 357–396;

[4] R. Huisgen, *Angew. Chem.* **1963**, *75*, 604–637; *Angew. Chem. Int. Ed. Engl.* **1963**, *2*, 565–598.

[5] R. Huisgen, *The Adventure Playground of Mechanisms and Novel Reactions (Profiles, Pathways, and Dreams. Autobiographies of Eminent Chemists)*, American Chemical Society, Washington, D. C., **1994**.

[6] J. I. Seeman, *Helv. Chim. Acta* **2005**, *88*, 1145–1153.

[7] R. Huisgen, *Angew. Chem.* **1963**, *75*, 742–754; *Angew. Chem. Int. Ed. Engl.* **1963**, *2*, 633–645.

[8] H. C. Kolb, M. G. Finn, K. B. Sharpless, *Angew. Chem.* **2001**, *113*, 2056–2075; *Angew. Chem. Int. Ed.* **2001**, *40*, 2004–2021.

[9] Z. P. Demko, K. B. Sharpless, *J. Org. Chem.* **2001**, *66*, 7945–7950.

[10] Z. P. Demko, K. B. Sharpless, *Angew. Chem.* **2002**, *114*, 2214–2217; *Angew. Chem. Int. Ed.* **2002**, *41*, 2110–2113.

[11] F. Himo, Z. P. Demko, L. Noodleman, K. B. Sharpless, *J. Am. Chem. Soc.* **2003**, *125*, 9983–9987.

[12] Z. P. Demko, K. B. Sharpless, *Angew. Chem.* **2002**, *114*, 2217–2220; *Angew. Chem. Int. Ed.* **2002**, *41*, 2113–2116.

[13] A. Padwa, "1,3-Dipolar Cycloaddition Chemistry" in *General Heterocyclic Chemistry Series* (Eds.: E. C. Taylor, A. Weissberger), John Wiley & Sons, Inc., New York, **1984**.

[14] A. Padwa, W. H. Pearson, "Synthetic Applications of 1,3-Dipolar Cycloaddition Chemistry Toward Heterocycles and Natural Products" in *The Chemistry of Heterocyclic Compounds* (Eds.: E. C. Taylor, P. Wipf, A. Weissberger), John Wiley & Sons, Inc., New York, **2002**.

[15] P. K. Kadaba, *Synthesis* **1973**, 71–84.

[16] W. G. Finnegan, R. A. Henry, R. Lofquist, *J. Am. Chem. Soc.* **1958**, *80*, 3908–3911.

[17] W. R. Carpenter, *J. Org. Chem.* **1962**, *27*, 2085–2088.

[18] W. P. Norris, *J. Org. Chem.* **1962**, *27*, 3248–3251.

[19] Z. P. Demko, K. B. Sharpless, *Org. Lett.* **2002**, *4*, 2525–2527.

[20] S. Kamijo, T. Jin, Y. Yamamoto, *J. Org. Chem.* **2002**, *67*, 7413–7417.

[21] I. F. Clemencon, B. Ganem, *Tetrahedron* **2007**, *63*, 8665–8669.

[22] M. Aldhoun, A. Massi, A. Dondoni, *J. Org. Chem.* **2008**, *73*, 9565–9575.

[23] T. Jin, F. Kitahara, S. Kamijo, Y. Yamamoto, *Chem. Asian J.* **2008**, *3*, 1575–1580.

[24] T. Jin, F. Kitahara, S. Kamijo, Y. Yamamoto, *Tetrahedron Lett.* **2008**, *49*, 2824–2827.

[25] V. Aureggi, G. Sedelmeier, *Angew. Chem.* **2007**, *119*, 8592–8596; *Angew. Chem. Int. Ed.* **2007**, *46*, 8440–8444.

[26] Y. Qiu, B. Liu, G. Peng, J. Cai, H. Deng, M. Zeller, *Inorg. Chem. Commun.* **2010**, *13*, 749–752.

[27] R. N. Butler, D. P. Shelly, *J. Chem. Soc. Perkin Trans. 1* **1986**, 1101–1105.

[28] S. N. Semenov, A. Y. Rogachev, S. V. Eliseeva, Y. A. Belousov, A. A. Drozdov, S. I. Troyanov, *Polyhedron* **2007**, *26*, 4899–4907.

[29] C. Schilling, N. Jung, S. Bräse, *Cycloaddition Reactions with Azides: An Overview in Organic Azides – Syntheses and Applications* (Eds.: S. Bräse, K. Banert), John Wiley & Sons, Ltd., Chichester, **2010**, pp. 269–284.

[30] D. H. Ess, G. O. Jones, K. N. Houk, *Adv. Synth. Catal.* **2006**, *348*, 2337–2361.

[31] F. Himo, Z. P. Demko, L. Noodleman, K. B. Sharpless, *J. Am. Chem. Soc.* **2002**, *124*, 12210–12216.

[32] T. M. Klapötke, B. Krumm, R. Moll, *Z. Anorg. Allg. Chem.* **2011**, DOI: 10.1002/zaac.201000036.

[33] A. J. Brown, O. W. Howarth, P. Moore, *J. Chem. Soc., Dalton Trans.* **1976**, 1589–1592.

[34] N. K. Wilson, R. D. Zehr, P. D. Ellis, *J. Magn. Reson.* **1976**, *21*, 437–443.

[35] G. E. Maciel, M. Borzo, *J. Magn. Reson.* **1973**, *10*, 388–390.

[36] M. A. Sens, N. K. Wilson, P. D. Ellis, J. D. Odom, *J. Magn. Reson.* **1975**, *19*, 323–336.

[37] E. Michel, J. Perie, A. Lattes, *J. Organomet. Chem.* **1981**, *204*, 1–12.

[38] G. A. Webb, *Annual Reports on NMR Spectroscopy*, Academic Press Inc., London, **1992**.

[39] S. Poturovic, D. Lu, M. J. Heeg, C. H. Winter, *Polyhedron* **2008**, *27*, 3280–3286.

[40] K. Dehnicke, D. Seybold, *J. Organomet. Chem.* **1968**, *11*, 227–241.

[41] J. Lorberth, F. Weller, *J. Organomet. Chem.* **1971**, *32*, 145–160.

[42] P. L. Goggin, D. M. McEwan, *J. Chem. Res. (S)* **1978**, 171.

[43] D. Grdenić, *Quart. Rev.* **1965**, *19*, 303–328.

[44] A. Bondi, *J. Phys. Chem.* **1964**, *68*, 441–451.

[45] A. Altomare, G. Cascarano, C. Giacovazzo, A. Guagliardi, A. G. G. Moliterni, M. C. Burla, G. Polidori, M. Camalli, R. Spagna, *SIR97*, **1997**.

[46] A. Altomare, M. C. Burla, M. Camalli, G. L. Cascarano, C. Giacovazzo, A. Guagliardi, A. G. G. Moliterni, G. Polidori, R. Spagna, *J. Appl. Crystallogr.* **1999**, *32*, 115–119.

[47] G. M. Sheldrick, *SHELX-97*, University of Göttingen, Göttingen, Germany, **1997**.

[48] G. M. Sheldrick, *Acta Crystallogr., Sect. A* **2008**, *64*, 112–122.

10. Summary

In the course of this work, various polynitro containing compounds were synthesized and examined, often with a positive oxygen balance and thus belonging to the general class of *oxidizers*. Furthermore, work on an earlier project about various organomercury(II) azides and tetrazoles was finished.
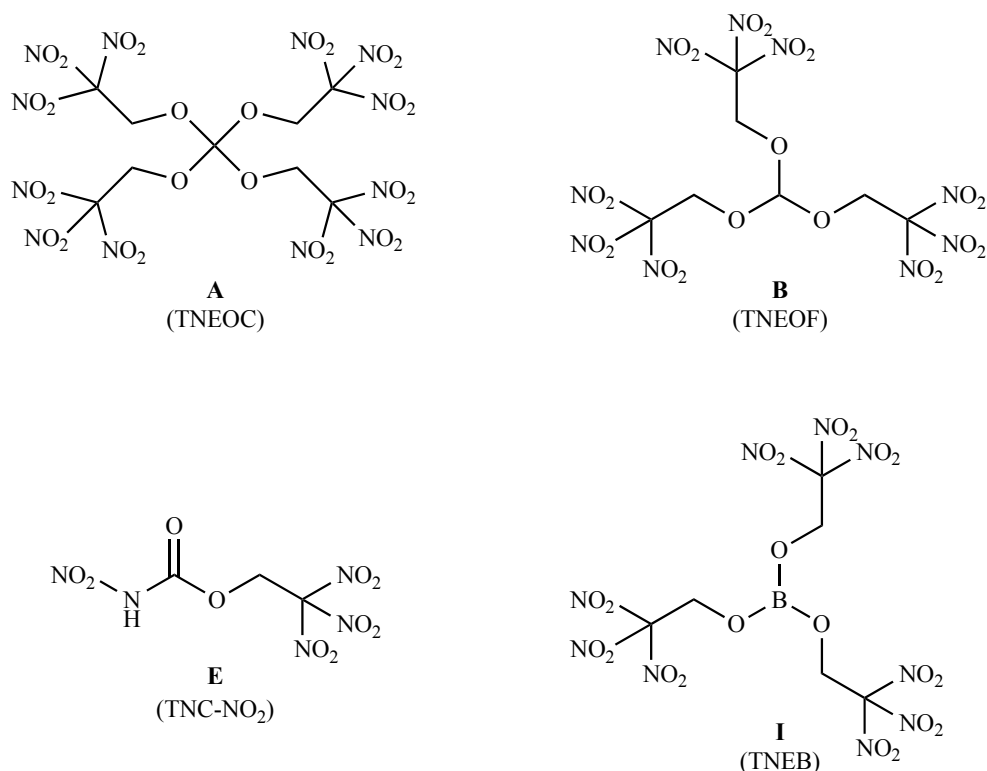
Scheme 1: Selected polynitro compounds.

Starting from the precursor 2,2,2-trinitroethanol, Chapter 2 describes the reaction with chloroform, carbon tetrachloride and paraformaldehyde, yielding the substituted carbonates *tetrakis(2,2,2-trinitroethyl) orthocarbonate* (**A**), *2,2,2-trinitroethyl orthoformate* (**B**) and *2,2,2-trinitroethyl formal* (**C**). Compounds **A**–**C** show a positive oxygen balance, assuming formation of both CO and CO_2 (Table 1). **A** reveales a phase transition at lower temperatures, whereas both structures were determined showing different orientations of

the $C(NO_2)_3$ moieties. Despite this phase transition and the high sensitivities, **A** is a good candidate regarding the requirements for an advanced oxidizer (see Chapter 1.3.3). In contrast, **B** shows no phase transition, lower sensitivities and an only slightly decreased oxygen balance, but also a lower melting point (Table 1). Interestingly, **C** co-crystallizes in two different modifications simultaneously, also showing different conformations of the $C(NO_2)_3$ moieties.

Apart from the trinitroethyl substituted carbonates, also the substituted carbamates *2,2,2-trinitroethyl carbamate* (**D**) and *2,2,2-trinitroethyl nitrocarbamate* (**E**), described in Chapter 3, were synthesized with a different approach and fully characterized. The starting material *2,2,2-trinitroethyl chloroformate* (**F**) was prepared by a challenging new synthesis method via chloroformylation of 2,2,2-trinitroethanol with phosgene. Reacting this ester with ammonia yields **D** and subsequent nitration **E**, a compound with a good oxygen balance (Table 1). Further benefit of **E** displays low sensitivities, but also a low density and a low melting point.
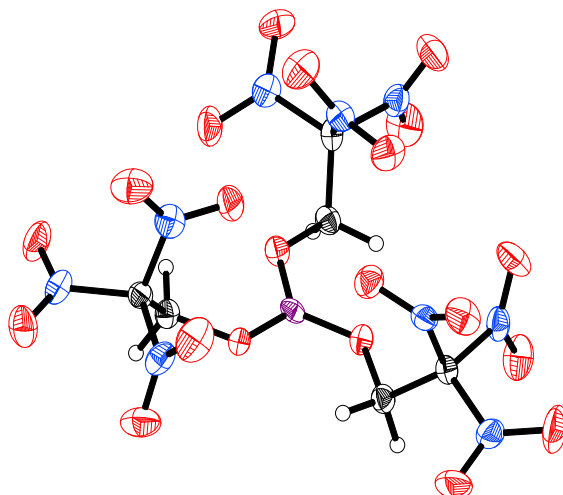
Figure 1.: Molecular structure of **I** (TNEB).

Chapter 4 deals with polynitro substituted boron esters. These are green burning compounds and of potential interest for pyrotechnic applications. Only few nitroalkyl derivatives have been known before, therefore this chapter presents the first thoroughly investigated high energetic boron esters. The compounds *tris(2-nitroethyl) borate* (**G**), *tris(2-fluoro-2,2-dinitroethyl) borate* (**H**), and *tris(2,2,2-trinitroethyl) borate* (**I**) were synthesized in a facile fashion using boron oxide with the corresponding nitro substituted ethanols. The fluorination of the anion *2-hydroxy-1,1-dinitroethane-1-ide* (**J**) yields the starting material *2-fluoro-2,2-dinitroethanol* (**K**). Furthermore, the condensation of **J** to

Table 1.: Chemical, physical and energetic properties of selected polynitro compounds.

	A TNEOC [1]	**B** TNEOF [1]	**E** TNC-NO$_2$ [1]	**I** TNEB [1]
Formula	C$_9$H$_8$N$_{12}$O$_{28}$	C$_7$H$_7$N$_9$O$_{21}$	C$_3$H$_3$N$_5$O$_{10}$	C$_6$H$_6$BN$_9$O$_{21}$
M_r [g mol^{-1}] [a]	732.22	553.18	269.08	550.97
N [%] [b]	22.95	22.79	26.03	22.88
$N + O$ [%] [c]	84.13	83.53	85.49	83.86
Ω_{CO} [%] [d]	+32.8	+30.4	+32.7	+30.5
Ω_{CO_2} [%] [e]	+13.1	+10.1	+14.9	+13.1
T_m [°C] [f]	161	128	109	–
T_d [°C] [g]	191	192	153	150
ρ [g cm^{-3}] [h]	1.94 (200 K)	1.81 (298 K)	1.73 (243 K)	1.89 (173 K)
Grain size [μm] [i]	250–500	500–1000	500–1000	< 100
IS [J] [j]	< 1	5	10	8
FS [N] [k]	96	96	96	144
ESD [J] [l]	0.2	0.2	0.1	0.5

[a] Formula weight. [b] Nitrogen content. [c] Combined nitrogen and oxygen content. [d] Oxygen balance assuming formation of CO and (if possible) H$_2$O, N$_2$, B$_2$O$_3$. [e] Oxygen balance assuming formation of CO$_2$ and (if possible) H$_2$O, N$_2$, B$_2$O$_3$. [f] Melting point. [g] Decomposition point. [h] Density calculated from X-ray diffraction. [i] Grain size of the samples used for sensitivity tests. [j] Impact sensitivity. [k] Friction sensitivity. [l] Sensitivity towards electrostatic discharge.

[1] Inofficial abbreviations.

the unusual dianion *1,1,3,3-tetranitropropan-1,3-diide* (**L**) was investigated. The crystal structures of **G**–**L** were obtained. Due to attractive intra- and intermolecular B···O interactions, **I** occurs in the conformation of the *cis*-isomer (Figure 1). This compound is also the best candidate according to the requirements for an advanced oxidizer (see Chapter 1.3.3), showing a high oxygen balance, no melting point and low sensitivities.

Silver trinitromethanide was prepared and investigated concerning its potential as a transfer agent for the C(NO$_2$)$_3$ moiety. Chapter 5 describes the preparation and characterization of *1,1,1,6,6,6-hexanitrohex-3-yne* (**M**) and *1,1,1-trinitroethane* (**N**). Of special interest is **M** due to the combination of trinitromethyl and alkyne moieties in one compound. Similar to **I**, the crystal structure of **M** occurs in the *cis*-conformation.

An important characteristic of all trinitromethyl moieties is the existence of intra- and intermolecular interactions between the three dipolar nitro groups. These interactions, as well as intra- and intermolecular Hal···O contacts, are described in detail in Chapter 6, by means of the molecular structures of the *halogenotrinitromethanes* HalC(NO$_2$)$_3$ (Hal = F (**O**), Br (**P**), I (**Q**)) in the crystalline and gaseous phase. The

intramolecular N···O and Hal···O interactions in **O**–**Q**, both competitors in terms of the orientation of the nitro groups by rotation about the C−N bonds, lead to a propeller-type twisting of these groups. Beside intermolecular attractive Hal···O interactions, which can be explained in terms of the halogen bonding concept based on a positive σ-hole, the high electronegativity of the halogenotrinitromethyl moiety leads to unusually short Hal−C bonds.

In addition, the synthesis of the promising starting material *2,2,2-nitrilotriacetyl chloride* (**R**) by chlorination of the corresponding triacetic acid was performed. The crystal structure reveals an unusual, nearly planar configuration of the tertiary amine center.

Chapters 8 and 9 describe the side project of this work, in which various organomercury(II) azides and tetrazoles were examined. The *organomercury(II) azides* R^1HgN_3 ($R^1 = CH_3$ (**S**), $(CH_3)_3C$ (**T**), C_6H_5 (**U**) were synthesized by reacting the corresponding halogenides with silver azide. Interestingly, the organomercury(II) azides show an intermolecular 1,3-dipolar cycloaddition with various organonitriles, R^2CN, forming the corresponding *organomercury(II) tetrazoles* $R^1Hg(N_4C)R^2$ ($R^2 = CH_3$ (**U**, **V**), C_6H_5 (**W**, **X**), C_6F_5 (**Y**). Thereby, a simple, direct and regioselective formation of the tetrazole moiety without the need of a catalyst was observed, which either gave explicitly the 1,5-disubstituted or the 2,5-disubstituted tetrazole. This chapter describes the first example of organomercury(II) tetrazoles prepared by Huisgen 1,3-dipolar cycloaddition and displays a perfect model for the chemical philosophy of the term "click chemistry".

A. Appendix

A.1. Supporting Information for Trinitroethyl Substituted Carbonates

CHNO Based Molecules Containing 2,2,2-Trinitroethoxy Moieties as Possible High Energy Dense Oxidizers

Thomas M. Klapötke, Burkhard Krumm, Richard Moll, and Sebastian F. Rest
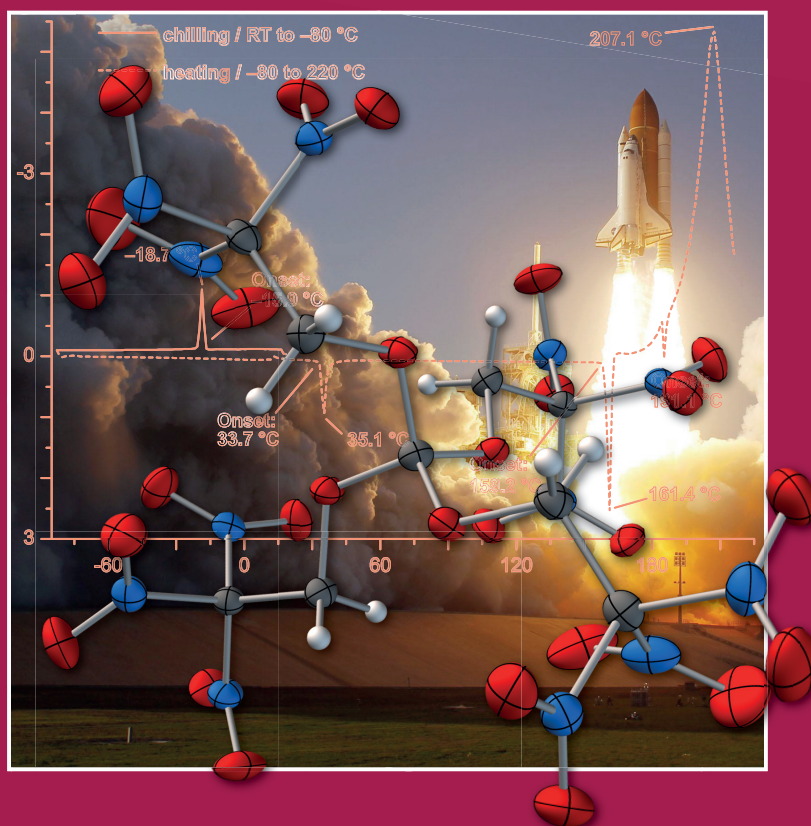
Figure A.1.: Cover picture for *Z. Anorg. Allg. Chem.* **2011**, *637*, 2103–2110.

Table A.1.: Dihedral angles C−C−N−O [°] containing the $C(NO_2)_3$ group for **α-1**

C2−C3−N1−O2	47.2(2)
C2−C3−N1−O3	−133.2(2)
C2−C3−N2−O4	43.9(2)
C2−C3−N2−O5	−136.8(2)
C2−C3−N3−O6	40.9(2)
C2−C3−N3−O7	−142.5(2)
C4−C5−N4−O9	−46.1(2)
C4−C5−N4−O10	134.8(2)
C4−C5−N5−O11	−48.4(2)
C4−C5−N5−O12	132.1(2)
C4−C5−N6−O13	145.9(2)
C4−C5−N6−O14	−34.8(2)

Table A.2.: Dihedral angles C−C−N−O [°] containing the $C(NO_2)_3$ group for **α-3**

C2−C3−N1−O2	120.1(2)
C2−C3−N1−O3	−58.2(2)
C2−C3−N2−O4	135.3(2)
C2−C3−N2−O5	−47.2(2)
C2−C3−N3−O6	156.3(2)
C2−C3−N3−O7	−23.4(2)
C4−C5−N4−O9	58.4(2)
C4−C5−N4−O10	−119.3(2)
C4−C5−N5−O11	54.6(2)
C4−C5−N5−O12	−124.3(2)
C4−C5−N6−O13	−163.0(2)
C4−C5−N6−O14	15.7(3)

Table A.3.: Dihedral angles C−C−N−O [°] containing the $C(NO_2)_3$ group for **β-1**

C2−C3−N1−O2	49(1)
C2−C3−N1−O3	−118(1)
C2−C3−N2−O4	17(1)
C2−C3−N2−O5	−150.1(9)
C2−C3−N3−O6	−131.7(8)
C2−C3−N3−O7	29(1)

Table A.4.: Dihedral angles C−C−N−O [°] containing the $C(NO_2)_3$ group for β-**3**

C2−C3−N1−O4	28.6(3)
C2−C3−N1−O5	−151.6(2)
C2−C3−N2−O6	48.3(2)
C2−C3−N2−O7	−131.9(2)
C2−C3−N3−O2	−126.1(2)
C2−C3−N3−O3	53.3(2)

A.2. Supporting Information for Hexanitrohexyne and Trinitroethane

Structures of Energetic Acetylene Derivatives HC≡CCH$_2$ONO$_2$, (NO$_2$)$_3$CCH$_2$CC≡CH$_2$C(NO$_2$)$_3$ and Trinitroethane, (NO$_2$)$_3$CCH$_3$
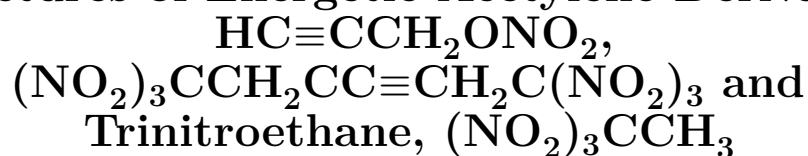
Thomas M. Klapötke, Burkhard Krumm, Richard Moll, Alexander Penger, Stefan M. Sproll, Raphael J. F. Berger, Stuart A. Hayes, and Norbert W. Mitzel

Figure A.2.: ^{15}N NMR (CDCl$_3$) spectrum of propargyl nitrate (**1**).

Figure A.3.: IR and Raman spectrum of propargyl nitrate (**1**).

Table A.5.: Full lists of inter-atomic distances, amplitudes of vibration and distance corrections for the $r_{a3,1}$ refinements, including details of which amplitudes were kept at fixed ratios and which were refined.

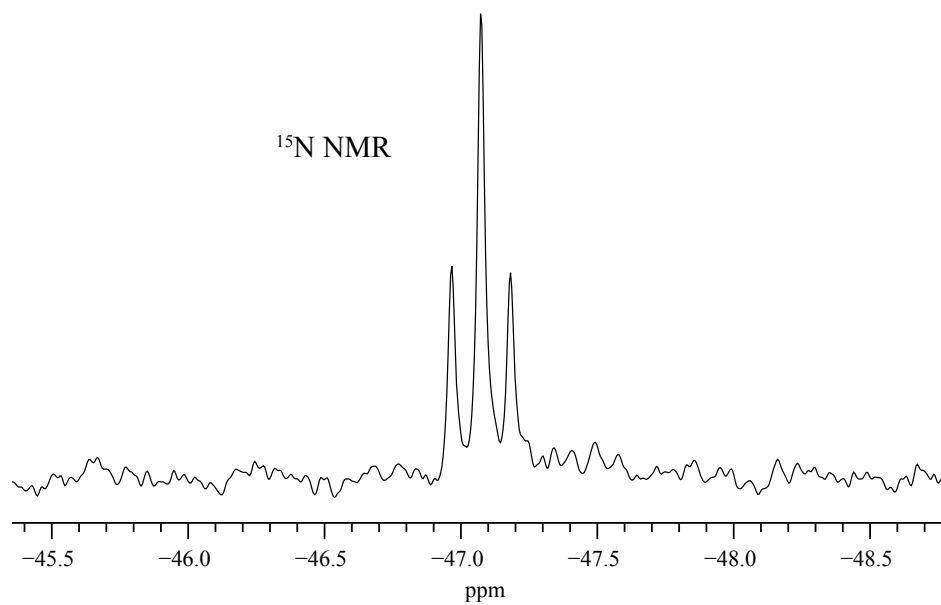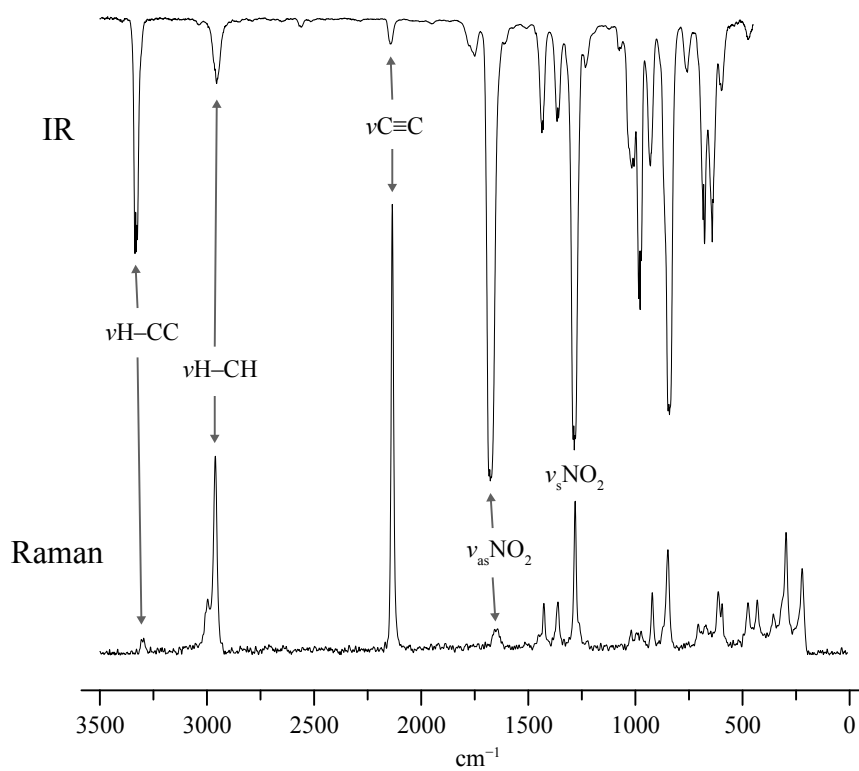| Name	Amplitude	(r_a)	e.s.d.	(r_e)	e.s.d.	u-Value	e.s.d.	Mult.	k-Value	An-harm.	Area	Orig. u-Value
u[1]	H(1)−C(2)	10.943	0.0060	10.808	0.0060	0.0724	Tied to u[46]	0.69	0.0135	20.000	11. Jul	0.0723
u[46]	H(11)−C(12)	10.943	0.0060	0.0060	0.0060	0.0724	0.0066	0.62	0.0135	20.000	10. Jun	0.0723
u[51]	C(14)−H(20)	11.217	0.0060	11.083	0.0060	0.0761	Tied to u[46]	0.62	0.0134	20.000	10. Mrz	0.0760
u[5]	C(4)−H(9)	11.217	0.0060	11.083	0.0060	0.0761	Tied to u[46]	0.69	0.0134	20.000	11. Apr	0.0760
u[6]	C(4)−H(10)	11.217	0.0060	11.083	0.0060	0.0761	Tied to u[46]	0.69	0.0134	20.000	11. Apr	0.0760
u[50]	C(14)−H(19)	11.217	0.0060	11.083	0.0060	0.0761	Tied to u[46]	0.62	0.0134	20.000	10. Mrz	0.0760
u[53]	N(16)−O(17)	11.945	0.0058	0.0058	0.0058	0.0304	0.0021	0.62	0.0036	20.000	90.6	0.0369
u[8]	N(6)−O(7)	11.945	0.0058	11.909	0.0058	0.0304	Tied to u[53]	0.69	0.0036	20.000	100.0	0.0369
u[47]	C(12)−C(13)	12.057	0.0058	12.009	0.0058	0.0286	Tied to u[53]	0.62	0.0048	20.000	57.7	0.0347
u[2]	C(2)−C(3)	12.057	0.0058	12.009	0.0058	0.0286	Tied to u[53]	0.69	0.0048	20.000	63.7	0.0347
u[9]	N(6)−O(8)	12.130	0.0096	12.108	0.0096	0.0311	Tied to u[53]	0.69	0.0022	20.000	98.5	0.0377
u[54]	N(16)−O(18)	12.170	0.0096	12.148	0.0096	0.0311	Tied to u[53]	0.62	0.0022	20.000	88.9	0.0377
u[52]	O(15)−N(16)	14.128	0.0067	0.0067	0.0067	0.0420	0.0022	0.62	0.0148	20.000	76.6	0.0492
u[7]	O(5)−N(6)	14.279	0.0060	14.131	0.0060	0.0420	Tied to u[52]	0.69	0.0148	20.000	83.7	0.0492
u[4]	C(4)−O(5)	14.547	0.0051	14.451	0.0051	0.0420	Tied to u[52]	0.69	0.0096	20.000	70.4	0.0493
u[48]	C(13)−C(14)	14.551	0.0071	14.480	0.0071	0.0396	Tied to u[52]	0.62	0.0071	20.000	47.8	0.0464
u[49]	C(14)−O(15)	14.566	0.0088	14.470	0.0088	0.0420	Tied to u[52]	0.62	0.0096	20.000	63.7	0.0493
u[3]	C(3)−C(4)	14.652	0.0106	14.581	0.0106	0.0396	Tied to u[52]	0.69	0.0071	20.000	52.4	0.0464
u[90]	H(19)···H(20)	18.194	0.0097	0.0097	0.0097	0.1256	0.0080	0.62	0.0238	0.0000	01. Jan	0.1214
u[45]	H(9)···H(10)	18.194	0.0097	17.956	0.0097	0.1256	Tied to u[90]	0.69	0.0238	0.0000	01. Feb	0.1214
u[30]	C(3)···H(10)	19.336	0.0098	19.309	0.0098	0.1072	Tied to u[90]	0.69	0.0027	0.0000	06. Jun	0.1036
u[29]	C(3)···H(9)	20.377	0.0103	20.350	0.0103	0.1072	Tied to u[90]	0.69	0.0027	0.0000	06. Mrz	0.1036
u[82]	O(15)···H(20)	21.121	0.0100	20.952	0.0100	0.1042	Tied to u[90]	0.62	0.0169	0.0000	07. Mrz	0.1007
u[81]	O(15)···H(19)	21.121	0.0100	20.952	0.0100	0.1042	Tied to u[90]	0.62	0.0169	0.0000	07. Mrz	0.1007
u[75]	C(13)···H(20)	21.161	0.0084	21.134	0.0084	0.1072	Tied to u[90]	0.62	0.0027	0.0000	05. Mai	0.1036
u[74]	C(13)···H(19)	21.161	0.0084	21.134	0.0084	0.1072	Tied to u[90]	0.62	0.0027	0.0000	05. Mai	0.1036
u[79]	O(15)···O(17)	21.677	0.0072	0.0072	0.0072	0.0513	0.0019	0.62	0.0087	0.0000	57.1	0.0520
u[34]	O(5)···O(7)	21.757	0.0077	21.670	0.0077	0.0513	Tied to u[79]	0.69	0.0087	0.0000	62.7	0.0520
u[40]	O(7)···O(8)	21.933	0.0059	21.895	0.0059	0.0450	Tied to u[79]	0.69	0.0038	0.0000	62.2	0.0456
u[85]	O(17)···O(18)	21.943	0.0059	21.905	0.0059	0.0450	Tied to u[79]	0.62	0.0038	0.0000	56.4	0.0456
u[36]	O(5)···H(9)	22.032	0.0074	21.863	0.0074	0.0993	Tied to u[79]	0.69	0.0169	0.0000	07. Jul	0.1007
u[37]	O(5)···H(10)	22.050	0.0072	21.881	0.0072	0.0993	Tied to u[79]	0.69	0.0169	0.0000	07. Jul	0.1007
u[80]	O(15)···O(18)	22.382	0.0040	22.188	0.0040	0.0515	Tied to u[79]	0.62	0.0194	0.0000	55.3	0.0522
u[35]	O(5)···O(8)	22.493	0.0064	22.299	0.0064	0.0515	Tied to u[79]	0.69	0.0194	0.0000	60.7	0.0522
u[55]	H(11)···C(13)	22.865	0.0086	22.817	0.0086	0.0765	Tied to u[79]	0.62	0.0048	0.0000	05. Jan	0.0776
u[10]	H(1)···C(3)	22.865	0.0086	22.817	0.0086	0.0765	Tied to u[79]	0.69	0.0048	0.0000	05. Jun	0.0776
u[44]	O(8)···H(10)	23.216	0.0123	22.446	0.0123	0.2218	Tied to u[79]	0.69	0.0770	0.0000	07. Apr	0.2248
u[70]	C(13)···O(15)	23.575	0.0059	23.433	0.0059	0.0663	Tied to u[79]	0.62	0.0142	0.0000	39.3	0.0672
u[76]	C(14)···N(16)	24.012	0.0104	23.643	0.0104	0.0595	Tied to u[79]	0.62	0.0369	0.0000	33.8	0.0603
u[25]	C(3)···O(5)	24.022	0.0098	23.880	0.0098	0.0663	Tied to u[79]	0.69	0.0142	0.0000	42.6	0.0672
u[31]	C(4)···N(6)	24.120	0.0067	23.751	0.0067	0.0595	Tied to u[79]	0.69	0.0369	0.0000	37.1	0.0603
u[88]	O(18)···H(19)	25.197	0.0106	0.0106	0.0106	0.2304	0.0121	0.62	0.0770	0.0000	06. Jan	0.2248
u[89]	O(18)···H(20)	25.197	0.0106	24.427	0.0106	0.2304	Tied to u[88]	0.62	0.0770	0.0000	06. Jan	0.2248
u[78]	C(14)···O(18)	25.611	0.0084	24.956	0.0084	0.0836	Tied to u[88]	0.62	0.0655	0.0000	36.2	0.0816
u[33]	C(4)···O(8)	25.886	0.0080	25.231	0.0080	0.0836	Tied to u[88]	0.69	0.0655	0.0000	39.6	0.0816
u[39]	N(6)···H(10)	26.066	0.0115	25.573	0.0115	0.1629	Tied to u[88]	0.69	0.0493	0.0000	05. Jul	0.1589
u[63]	C(12)···C(14)	26.503	0.0062	26.489	0.0062	0.0524	Tied to u[88]	0.62	0.0014	0.0000	26. Feb	0.0511
u[18]	C(2)···C(4)	26.604	0.0088	26.590	0.0088	0.0524	Tied to u[88]	0.69	0.0014	0.0000	28. Sep	0.0511
u[83]	N(16)···H(19)	26.754	0.0126	26.261	0.0126	0.1629	Tied to u[88]	0.62	0.0493	0.0000	05. Jan	0.1589
u[84]	N(16)···H(20)	26.754	0.0126	26.261	0.0126	0.1629	Tied to u[88]	0.62	0.0493	0.0000	05. Jan	0.1589
u[24]	C(2)···H(10)	29.847	0.0084	29.968	0.0084	0.1328	Tied to u[88]	0.69	−0.0121	0.0000	04. Mrz	0.1296
u[28]	C(3)···O(8)	29.858	0.0066	29.395	0.0066	0.0768	Tied to u[26]	0.69	0.0463	0.0000	34.3	0.0818
u[23]	C(2)···H(9)	31.077	0.0087	31.198	0.0087	0.1215	Tied to u[26]	0.69	−0.0121	0.0000	04. Jan	0.1293
u[26]	C(3)···N(6)	31.093	0.0048	0.0048	0.0048	0.0627	0.0022	0.69	0.0222	0.0000	28. Aug	0.0668
u[69]	C(12)···H(20)	32.024	0.0074	32.145	0.0074	0.1217	Tied to u[26]	0.62	−0.0121	0.0000	03. Jun	0.1296
u[68]	C(12)···H(19)	32.024	0.0074	32.145	0.0074	0.1215	Tied to u[26]	0.62	−0.0121	0.0000	03. Jun	0.1293
u[38]	N(6)···H(9)	33.990	0.0101	33.497	0.0101	0.1493	Tied to u[26]	0.69	0.0493	0.0000	04. Apr	0.1589

Name	Amplitude	(r_a)	e.s.d.	(r_e)	e.s.d.	u-Value	e.s.d.		Mult.	k-Value	An-harm.	Area	Orig. u-Value
u[64]	C(12)···O(15)	34.044	0.0095	33.896	0.0095	0.1124	Tied to u[26]		0.62	0.0148	0.0000	27. Feb	0.1197
u[32]	C(4)···O(7)	34.444	0.0063	34.230	0.0063	0.0560	Tied to u[26]		0.69	0.0214	0.0000	29. Jul	0.0596
u[77]	C(14)···O(17)	34.482	0.0100	34.268	0.0100	0.0560	Tied to u[26]		0.62	0.0214	0.0000	26. Sep	0.0596
u[19]	C(2)···O(5)	34.604	0.0119	34.456	0.0119	0.1124	Tied to u[26]		0.69	0.0148	0.0000	29. Jun	0.1197
u[71]	C(13)···N(16)	36.312	0.0084	0.0084	0.0084	0.0816	0.0039		0.62	0.0222	0.0000	22. Apr	0.0668
u[43]	O(8)···H(9)	36.763	0.0112	35.993	0.0112	0.2745	Tied to u[71]		0.69	0.0770	0.0000	04. Jun	0.2248
u[42]	O(7)···H(10)	37.254	0.0116	36.883	0.0116	0.1944	Tied to u[71]		0.69	0.0371	0.0000	04. Jun	0.1592
u[56]	H(11)···C(14)	37.273	0.0088	37.297	0.0088	0.1054	Tied to u[71]		0.62	−0.0024	0.0000	03. Jan	0.0863
u[22]	C(2)···O(8)	37.308	0.0110	37.023	0.0110	0.1062	Tied to u[71]		0.69	0.0285	0.0000	27. Apr	0.0870
u[11]	H(1)···C(4)	37.374	0.0106	37.398	0.0106	0.1054	Tied to u[71]		0.69	−0.0024	0.0000	03. Apr	0.0863
u[86]	O(17)···H(19)	37.680	0.0120	37.309	0.0120	0.1944	Tied to u[71]		0.62	0.0371	0.0000	04. Jan	0.1592
u[87]	O(17)···H(20)	37.680	0.0120	37.309	0.0120	0.1944	Tied to u[71]		0.62	0.0371	0.0000	04. Jan	0.1592
u[73]	C(13)···O(18)	39.760	0.0078	39.297	0.0078	0.0879	Tied to u[20]		0.62	0.0463	0.0000	23. Mrz	0.0818
u[17]	H(1)···H(10)	39.994	0.0116	40.217	0.0116	0.1749	Tied to u[20]		0.69	−0.0223	0.0000	0.5	0.1627
u[20]	C(2)···N(6)	40.020	0.0089	0.0089	0.0089	0.1132	0.0065		0.69	0.0112	0.0000	22. Apr	0.1053
u[16]	H(1)···H(9)	41.289	0.0121	0.0121	0.0121	0.1710	0.0157		0.69	−0.0223	0.0000	0.5	0.1621
u[27]	C(3)···O(7)	41.756	0.0085	41.755	0.0085	0.0854	Tied to u[20]		0.69	0.0001	0.0000	24. Mai	0.0794
u[62]	H(11)···H(20)	42.296	0.0116	42.519	0.0116	0.1716	Tied to u[16]		0.62	−0.0223	0.0000	0.5	0.1627
u[61]	H(11)···H(19)	42.296	0.0116	42.519	0.0116	0.1710	Tied to u[16]		0.62	−0.0223	0.0000	0.5	0.1621
u[41]	O(7)···H(9)	43.155	0.0123	42.784	0.0123	0.1679	Tied to u[16]		0.69	0.0371	0.0000	4.0	0.1592
u[57]	H(11)···O(15)	44.172	0.0113	43.994	0.0113	0.1760	Tied to u[16]		0.62	0.0178	0.0000	03. Mai	0.1669
u[12]	H(1)···O(5)	44.778	0.0136	44.600	0.0136	0.1760	Tied to u[16]		0.69	0.0178	0.0000	03. Aug	0.1669
u[72]	C(13)···O(17)	45.022	0.0109	0.0109	0.0109	0.0902	0.0056		0.62	0.0001	0.0000	20. Jun	0.0794
u[15]	H(1)···O(8)	45.697	0.0137	45.534	0.0137	0.1317	Tied to u[72]		0.69	0.0163	0.0000	03. Jul	0.1159
u[65]	C(12)···N(16)	47.410	0.0124	47.298	0.0124	0.1197	Tied to u[72]		0.62	0.0112	0.0000	17. Jan	0.1053
u[13]	H(1)···N(6)	49.203	0.0120	49.142	0.0120	0.1746	Tied to u[72]		0.69	0.0061	0.0000	3.0	0.1536
u[21]	C(2)···O(7)	50.212	0.0175	50.337	0.0175	0.1707	Tied to u[72]		0.69	−0.0125	0.0000	20. Apr	0.1502
u[67]	C(12)···O(18)	51.535	0.0075	0.0075	0.0075	0.0954	0.0065		0.62	0.0285	0.0000	18.0	0.0870
u[66]	C(12)···O(17)	55.121	0.0149	55.246	0.0149	0.1648	Tied to u[67]		0.62	−0.0125	0.0000	16. Aug	0.1502
u[58]	H(11)···N(16)	57.724	0.0145	57.663	0.0145	0.1685	Tied to u[67]		0.62	0.0061	0.0000	02. Mrz	0.1536
u[14]	H(1)···O(7)	58.917	0.0229	59.090	0.0229	0.2418	Tied to u[67]		0.69	−0.0173	0.0000	02. Sep	0.2205
u[60]	H(11)···O(18)	62.189	0.0096	62.026	0.0096	0.1271	Tied to u[67]		0.62	0.0163	0.0000	02. Mai	0.1159
u[59]	H(11)···O(17)	64.799	0.0173	64.972	0.0173	0.2418	Tied to u[67]		0.62	−0.0173	0.0000	02. Apr	0.2200

Name	Type	Value	Calculated	Difference	Uncertainty
u46	Amplitude	0.07230	0.07239	−0.00009	0.01000
u53	Amplitude	0.03690	0.03043	0.00647	0.00400
u52	Amplitude	0.04920	0.04196	0.00724	0.00500
u90	Amplitude	0.12140	0.12558	−0.00418	0.01000
u79	Amplitude	0.05200	0.05130	0.00070	0.00500
u88	Amplitude	0.22480	0.23040	−0.00560	0.02000
u26	Amplitude	0.06680	0.06275	0.00405	0.00700
u71	Amplitude	0.06680	0.08157	−0.01477	0.00700
u16	Amplitude	0.16210	0.17098	−0.00888	0.02000
u72	Amplitude	0.07940	0.09024	−0.01084	0.00800
u67	Amplitude	0.08700	0.09543	−0.00843	0.01000
u20	Amplitude	0.10530	0.11321	−0.00791	0.01000

A.3. Supporting Information for Halogenotrinitromethanes

Halogenotrinitromethanes –
A Combined Study in the Crystalline and
Gaseous Phase and by Quantum Chemical
Methods

Thomas M. Klapötke, Burkhard Krumm, Richard Moll, Sebastian F. Rest, Yury V. Vishnevskiy, Christian Reuter, Hans-Georg Stammler and Norbert W. Mitzel
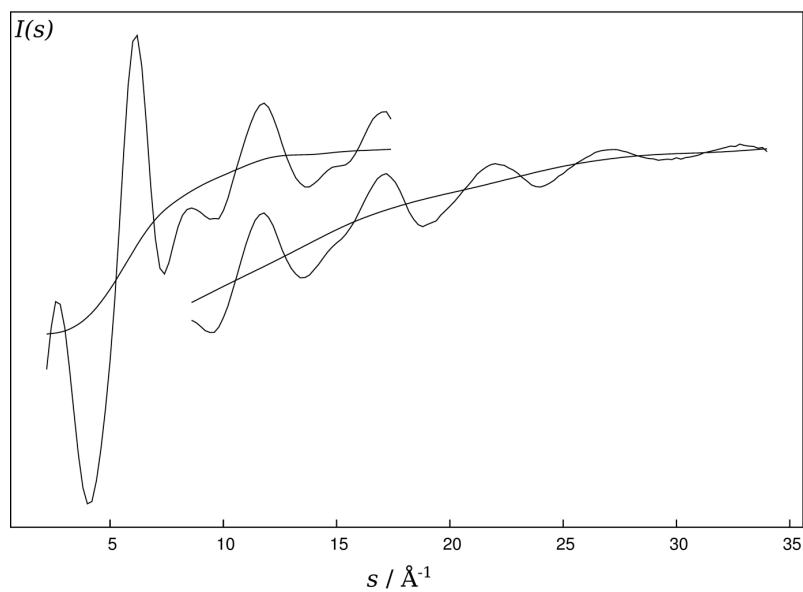
Figure A.4.: Total electron diffraction intensity curves and background lines of $FC(NO_2)_3$ **(1)**.
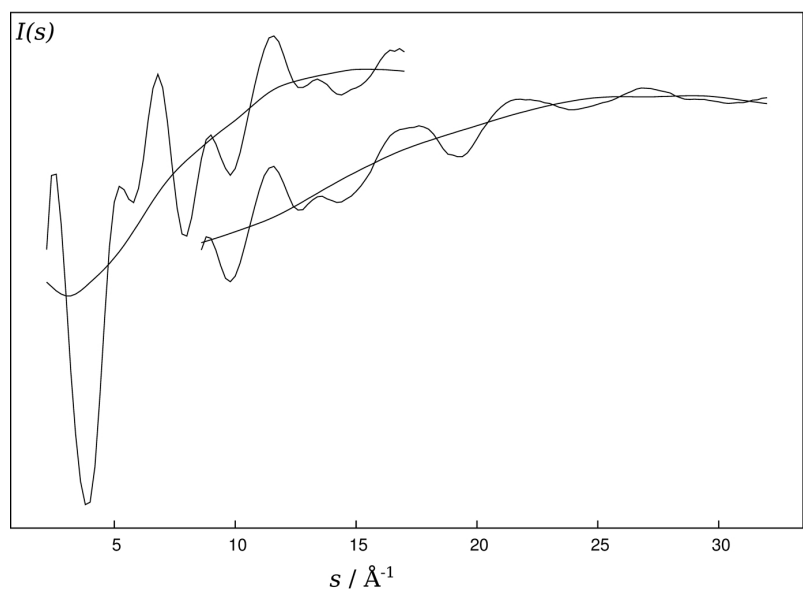
Figure A.5.: Total electron diffraction intensity curves and background lines of $BrC(NO_2)_3$ **(2)**.
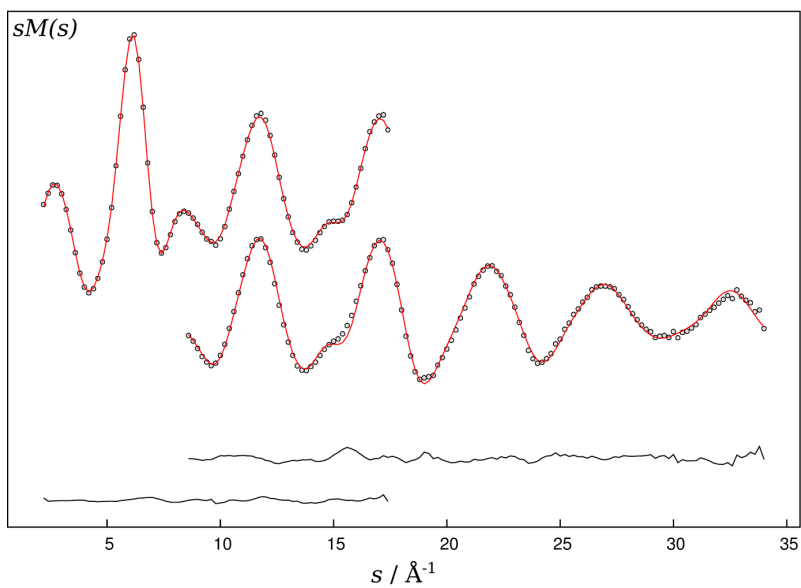
Figure A.6.: Experimental (open circles) and model (line) molecular electron diffraction curves of $FC(NO_2)_3$ **(1)**. The difference curves are shown in the bottom.
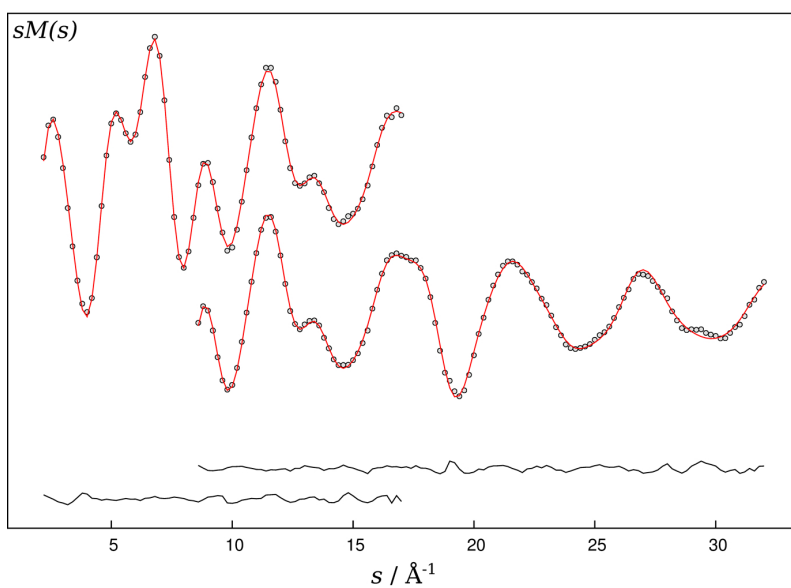
Figure A.7.: Experimental (open circles) and model (line) molecular electron diffraction curves of $BrC(NO_2)_3$ **(2)**. The difference curves are shown in the bottom.
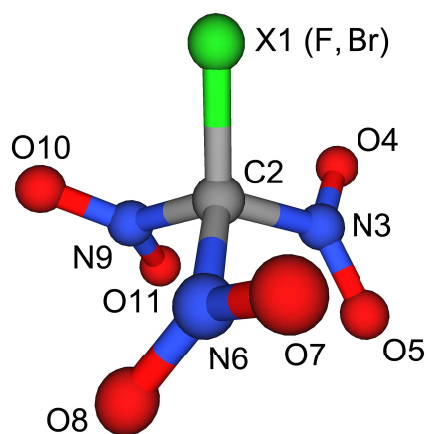
Figure A.8.: Internal atom numbering in the models of $FC(NO_2)_3$ **(1)** and $BrC(NO_2)_3$ **(2)** in GED structural analyses.

Table A.6.: Experimental interatomic distances, mean square amplitudes and vibrational corrections to equilibrium geometry of $FC(NO_2)_3$ **(1)**. All values in [Å]; corrections were calculated using SHRINK program from MP2(full)/cc-pVTZ harmonic and cubic force fields; threefold mean standard deviations for the amplitudes in groups 100, 110, 120, 125, 130, 135, 140 and 145 are 0.002, 0.005, 0.004, 0.008, 0.015, 0.022, 0.042 and 0.033 Å, respectively.

At1	At2	r_a	l_{exp}	$r_e - r_a$	G
N9	O10	1.213987	0.043362	−0.004400	100
N3	O4	1.213987	0.043362	−0.004400	100
N6	O7	1.213987	0.043362	−0.004400	100
N3	O5	1.214371	0.043479	−0.003700	100
N9	O11	1.214371	0.043479	−0.003700	100
N6	O8	1.214371	0.043479	−0.003700	100
F1	C2	1.306614	0.048943	−0.006200	100
C2	N9	1.530224	0.057353	−0.013500	110
C2	N3	1.530224	0.057353	−0.013500	110
C2	N6	1.530224	0.057353	−0.013500	110
O4	O5	2.193983	0.053775	−0.004700	120
O7	O8	2.193983	0.053775	−0.004700	120
O10	O11	2.193983	0.053775	−0.004700	120
C2	O10	2.307898	0.070347	−0.013900	120
C2	O4	2.307998	0.070347	−0.013900	120
C2	O7	2.307998	0.070347	−0.013900	120
F1	N3	2.324978	0.070460	−0.010500	120
F1	N6	2.324978	0.070460	−0.010500	120
F1	N9	2.324978	0.070460	−0.010500	120
C2	O11	2.336061	0.070122	−0.013400	120
C2	O8	2.336061	0.070122	−0.013400	120
C2	O5	2.336061	0.070122	−0.013400	120
N3	N9	2.490383	0.079519	−0.025700	125
N3	N6	2.490383	0.079519	−0.025700	125
N6	N9	2.490383	0.079519	−0.025700	125
F1	O10	2.584552	0.117977	−0.008300	125
F1	O4	2.584552	0.117977	−0.008300	125
F1	O7	2.584552	0.117977	−0.008300	125
N3	O11	2.658091	0.114522	−0.046800	125

At1	At2	r_a	l_{exp}	r_e-r_a	G
O5	N6	2.658091	0.114522	−0.046800	125
O8	N9	2.658091	0.114522	−0.046800	125
O8	O11	3.040572	0.206037	−0.018400	130
O5	O8	3.040572	0.206037	−0.018400	130
O5	O11	3.040572	0.206037	−0.018400	130
N3	O7	3.049731	0.158053	−0.027200	130
N6	O10	3.049731	0.158053	−0.027200	130
O4	N9	3.049731	0.158053	−0.027200	130
N6	O11	3.167823	0.137894	−0.009900	130
O5	N9	3.167823	0.137894	−0.009900	130
N3	O8	3.167823	0.137894	−0.009900	130
O5	O7	3.189590	0.212188	−0.055800	130
O8	O10	3.189590	0.212188	−0.055800	130
O4	O11	3.189590	0.212188	−0.055800	130
F1	O8	3.333716	0.102465	−0.006100	135
F1	O11	3.333716	0.102465	−0.006100	135
F1	O5	3.333716	0.102465	−0.006100	135
N3	O10	3.541891	0.091848	−0.009900	135
O7	N9	3.541891	0.091848	−0.009900	135
O4	N6	3.541891	0.091848	−0.009900	135
O4	O10	3.965985	0.184097	0.001900	140
O7	O10	3.965985	0.184097	0.001900	140
O4	O7	3.965985	0.184097	0.001900	140
O5	O10	4.300241	0.143322	−0.001400	145
O7	O11	4.300241	0.143322	−0.001400	145
O4	O8	4.300241	0.143322	−0.001400	145

Table A.7.: Experimental interatomic distances, mean square amplitudes and vibrational corrections to equilibrium geometry of $BrC(NO_2)_3$ **(2)**. All values in [Å]; corrections were calculated using SHRINK program from MP2/SDB-cc-pVTZ harmonic and cubic force fields; threefold mean standard deviations for the amplitudes in groups 100, 120, 130, 140, 150, 160, 165 and 170 are 0.001, 0.008, 0.010, 0.007, 0.013, 0.007, 0.197 and 0.046 Å0.046 ÃĚ, respectively.

At1	At2	r_a	l_{exp}	$r_e - r_a$	G
N3	O4	1.214086	0.038791	−0.004600	100
N9	O10	1.214086	0.038791	−0.004600	100
N6	O7	1.214086	0.038791	−0.004600	100
N3	O5	1.217114	0.039102	−0.003600	100
N9	O11	1.217114	0.039102	−0.003600	100
N6	O8	1.217114	0.039102	−0.003600	100
C2	N6	1.545149	0.060365	−0.015700	100
C2	N3	1.545149	0.060365	−0.015700	100
C2	N9	1.545149	0.060365	−0.015700	100
Br1	C2	1.876228	0.056129	−0.007100	120
O4	O5	2.185267	0.054579	−0.004700	130
O7	O8	2.185267	0.054579	−0.004700	130
O10	O11	2.185267	0.054579	−0.004700	130
C2	O7	2.341002	0.075415	−0.015600	130
C2	O10	2.341002	0.075415	−0.015600	130
C2	O4	2.341002	0.075415	−0.015600	130
C2	O5	2.347065	0.073490	−0.015600	130
C2	O8	2.347065	0.073490	−0.015600	130
C2	O11	2.347065	0.073490	−0.015600	130
N3	N6	2.478411	0.083681	−0.030300	130
N3	N9	2.478411	0.083681	−0.030300	130
N6	N9	2.478411	0.083681	−0.030300	130
O5	N6	2.596388	0.117199	−0.053100	130
N3	O11	2.596388	0.117199	−0.053100	130
O8	N9	2.596388	0.117199	−0.053100	130
Br1	N6	2.841984	0.080672	−0.010500	140
Br1	N9	2.841984	0.080672	−0.010500	140
Br1	N3	2.841984	0.080672	−0.010500	140
Br1	O10	2.995204	0.130983	−0.014800	140

At1	At2	r_a	l_exp	$r_\mathrm{e}-r_\mathrm{a}$	G
Br1	O4	2.995204	0.130983	−0.014800	140
Br1	O7	2.995204	0.130983	−0.014800	140
O5	O11	3.046740	0.268255	−0.038000	140
O5	O8	3.046740	0.268255	−0.038000	140
O8	O11	3.046740	0.268255	−0.038000	140
N3	O7	3.063596	0.189644	−0.023500	140
O4	N9	3.063596	0.189644	−0.023500	140
N6	O10	3.063596	0.189644	−0.023500	140
O5	O7	3.100436	0.238979	−0.046500	140
O4	O11	3.100436	0.238979	−0.046500	140
O8	O10	3.100436	0.238979	−0.046500	140
O5	N9	3.171159	0.179017	−0.019700	140
N3	O8	3.171159	0.179017	−0.019700	140
N6	O11	3.171159	0.179017	−0.019700	140
N3	O10	3.557919	0.081766	−0.015000	150
O4	N6	3.557919	0.081766	−0.015000	150
O7	N9	3.557919	0.081766	−0.015000	150
Br1	O5	3.834809	0.127729	0.004800	160
Br1	O11	3.834809	0.127729	0.004800	160
Br1	O8	3.834809	0.127729	0.004800	160
O4	O10	4.028006	0.354386	−0.000300	165
O4	O7	4.028006	0.354386	−0.000300	165
O7	O10	4.028006	0.354386	−0.000300	165
O5	O10	4.306568	0.198753	−0.006100	170
O4	O8	4.306568	0.198753	−0.006100	170
O7	O11	4.306568	0.198753	−0.006100	170

Table A.8.: Experimental cartesian coordinates of $FC(NO_2)_3$ (**1**) [Å].

N	At	An	Mass	X	Y	Z
1	F	9	18.99840320	0.000000000000	0.000000000000	−1.685455090782
2	C	6	12.00000000	0.000000000000	0.000000000000	−0.385040888542
3	N	7	14.00307401	−1.006202819407	1.006202819407	0.139899574177
4	O	8	15.99491462	−1.068429240123	2.026449428610	−0.506881519565
5	O	8	15.99491462	−1.600251840223	0.695487106176	1.148009747048
6	N	7	14.00307401	−0.368295793263	−1.374498612670	0.139899574177
7	O	8	15.99491462	−1.220742064599	−1.938511578398	−0.506881519565
8	O	8	15.99491462	0.197816418158	−1.733602299174	1.148009747048
9	N	7	14.00307401	1.374498612670	0.368295793263	0.139899574177
10	O	8	15.99491462	2.289171304722	−0.087937850212	−0.506881519565
11	O	8	15.99491462	1.402435422065	1.038115192997	1.148009747048

Table A.9.: Experimental cartesian coordinates of $BrC(NO_2)_3$ **(2)** [Å].

N	At	An	Mass	X	Y	Z
1	Br	35	78.91833760	1.656908792345	0.000000000000	0.000000000000
2	C	6	12.00000000	−0.212218812089	0.000000000000	0.000000000000
3	N	7	14.00307401	−0.796568442192	−0.109826701780	−1.409144040424
4	O	8	15.99491462	−0.207316242191	0.501121707662	−2.270759529730
5	O	8	15.99491462	−1.767283047678	−0.828498468366	−1.526792922672
6	N	7	14.00307401	−0.796568442192	−1.165441185709	0.799684733967
7	O	8	15.99491462	−0.207316242191	−2.217096292463	0.701395635642
8	O	8	15.99491462	−1.767283047678	−0.907992223169	1.480897181938
9	N	7	14.00307401	−0.796568442192	1.275267887489	0.609459306457
10	O	8	15.99491462	−0.207316242191	1.715974584801	1.569363894088
11	O	8	15.99491462	−1.767283047678	1.736490691536	0.045895740734

Table A.10.: Matrix of correlation factors for parameters of $FC(NO_2)_3$ **(1)** refined in GED structural analysis. First seven columns and rows correspond to independent structural parameters (see Figure A.8 for numeration of atoms): [1] $r(F1{-}C2)$, [2] $r(C2{-}N3)$, [3] $r(N3{-}O4)$ and $r(N3{-}O5)$ in one group, [4] $\alpha(F1{-}C2{-}N3)$, [5] $\alpha(C2{-}N3{-}O4)$ and $\alpha(C2{-}N3{-}O5)$ in one group, [6] $\varphi(F1{-}C2{-}N3{-}O4)$, [7] $\varphi(O4{-}C2{-}N3{-}O5)$. Last eight columns and rows correspond to the groups of amplitudes as described in Table A.7.

1.0000							
0.0810	1.0000						
0.1355	0.0080	1.0000					
−0.5837	−0.3523	−0.2035	1.0000				
−0.3959	−0.5252	0.1366	0.1461	1.0000			
−0.1587	0.2091	0.0011	−0.3088	0.1577	1.0000		
0.2428	0.3405	0.1952	−0.5531	−0.0901	−0.0258	1.0000	
−0.7143	0.0125	−0.0509	0.4024	0.2713	0.1359	−0.1513	1.0000
−0.3597	−0.0431	−0.0995	0.2248	0.1684	0.0582	−0.0846	0.3197
0.1862	0.1895	0.0422	−0.1904	−0.4780	−0.0785	0.0552	−0.1515
0.0958	0.1748	−0.0809	−0.1393	−0.2908	−0.0430	−0.1268	−0.0749
−0.2639	−0.2816	−0.1526	0.4544	0.0503	−0.2689	−0.5995	0.1646
−0.0297	−0.0609	−0.0153	−0.0503	0.0953	0.1270	−0.2922	0.0194
−0.0779	−0.1549	−0.0494	0.1833	0.0517	−0.0687	−0.0699	0.0443
−0.0527	−0.0916	−0.0237	0.1143	0.0344	−0.0389	−0.0339	0.0361

1.0000						
−0.1390	1.0000					
−0.0651	0.6055	1.0000				
0.0979	−0.0041	0.0717	1.0000			
0.0171	0.0405	0.1310	0.5406	1.0000		
0.0441	−0.0372	−0.0629	−0.0092	−0.1754	1.0000	
0.0340	−0.0155	−0.0165	−0.0135	−0.0631	0.6129	1.0000

Table A.11.: Matrix of correlation factors for parameters of $BrC(NO_2)_3$ **(2)** refined in GED structural analysis. First seven columns and rows correspond to independent structural parameters (see Figure A.8 for numeration of atoms): [1] $r(Br1-C2)$, [2] $r(C2-N3)$, [3] $r(N3-O4)$ and $r(N3-O5)$ in one group, [4] $\alpha(Br1-C2-N3)$, [5] $\alpha(C2-N3-O4)$ and $\alpha(C2-N3-O5)$ in one group, [6] $\varphi(Br1-C2-N3-O4)$, [7] $\varphi(O4-C2-N3-O5)$. Last eight columns and rows correspond to the groups of amplitudes as described in Table A.7.

1.0000							
−0.1125	1.0000						
0.0725	0.0061	1.0000					
−0.6918	−0.0916	−0.1376	1.0000				
−0.1611	−0.5148	0.1507	0.0646	1.0000			
−0.2055	0.2448	0.0855	0.2279	0.1212	1.0000		
0.0229	−0.0667	−0.0929	−0.0875	−0.0794	−0.6975	1.0000	
0.0188	0.0064	−0.0190	0.0136	−0.0103	−0.0173	0.0126	1.0000
0.0502	−0.1175	0.0695	−0.0603	−0.0311	−0.0824	0.0824	−0.0098
−0.2748	0.0139	−0.0269	0.5224	−0.0120	−0.0193	−0.0606	0.0734
−0.0653	0.0317	−0.1346	0.5695	−0.2536	−0.0325	0.0900	0.0424
−0.0240	−0.0748	−0.0323	0.0690	−0.0172	−0.1142	0.1456	−0.0162
−0.0069	−0.0473	−0.0153	−0.0029	−0.0071	−0.0943	−0.0091	−0.0229
−0.0769	−0.0153	−0.0626	0.1484	−0.0590	−0.1403	0.5342	0.0069
−0.0349	−0.0752	−0.0130	−0.0301	0.0093	−0.0335	−0.1808	−0.0085
1.0000							
−0.2154	1.0000						
−0.0426	0.4411	1.0000					
0.0259	0.0050	0.0649	1.0000				
−0.0010	−0.0209	−0.0214	0.4740	1.0000			
0.0414	0.0014	0.1730	0.1275	−0.1064	1.0000		
0.0114	−0.0091	−0.1308	0.0050	0.1488	−0.2044	1.0000	

A.4. Supporting Information for Organomercury(II) Azides

Synthetic and Structural Studies on Methyl-, *tert*-Butyl- and Phenylmercury(II) Azide

Thomas M. Klapötke, Burkhard Krumm, and Richard Moll

Table A.12.: IR and Raman spectral data of **1**–**3**. [a]

Vibrations [b]	1 CH$_3$HgN$_3$		2 (CH$_3$)$_3$CHgN$_3$		3 C$_6$H$_5$HgN$_3$	
	Raman	IR	Raman	IR	Raman	IR
ν_{as}CH, ν_sCH					3137 (9)	3306 w
					3052 (65)	3074,w
					2980 (8)	3048 w
					2946 (7)	
ν_{as}CH$_3$, ν_sCH$_3$	3007 (18)	3348 w	2948 (19)	3340 w		
	2923 (69)	3306 m	2922 (20)	3303 w		
	2799 (10)	2923 m	2875 (37)	2955 m		
		2798 w	2850 (42)	2926 m		
		2595 w	2770 (5)	2870 m		
		2544 w	2713 (5)	2841 s		
				2766 w		
				2712 w		
ν_{as}N$_3$	2038 (24)	2044 vs	2074 (7)	2027 vs	2056 (9)	2048 vs
			2034 (10)		2037 (15)	
δ_{as}CH$_3$	1333 (12)	1333 m	1465 (9)	1469 m		
ν_sN$_3$	1279 (23)	1278 s	1282 (7)	1282 m	1276 (15)	1278 m
δ_sCH$_3$	1193 (36)	1198 m	1405 (2)	1364 m		
			1389 (2)	1329 m		
			1366 (6)			
			1331 (8)			
ρC$_4$H$_9$			1020 (2)	1019 w		
δ_sC$_4$H$_9$			1161 (100)	1156 s		
			813 (52)	802 w		

Vibrations [b)	1 CH_3HgN_3		2 $(CH_3)_3CHgN_3$		3 $C_6H_5HgN_3$	
	Raman	IR	Raman	IR	Raman	IR
$\delta_\beta C_6H_5$					1569 (27) 1476 (15) 1430 (9) 1385 (8) 1329 (17) 1191 (11) 1180 (14) 1156 (14) 1075 (12) 1065 (10) 1018 (25) 994 (100) 661 (16) 613 (9)	1603 w 1575 w 1476 m 1432 m 1378 w 1328 w 1304 w 1018 m 996 w 726 m 694 m
$\delta_\beta N_3$	658 (8)	658 m	656 (6)	654 w	650 (18)	651 w
$\delta_\gamma N_3$		592 m		597 w		594 w
$\nu Hg-C$	553 (100)	551 m	525 (49)		240 (78)	
$\nu Hg-N$	363 (71)		355 (60)		372 (27)	
$\delta_\gamma C_6H_5$					908 (6) 844 (7) 593 (5) 295 (10)	
$\delta_{as} C_4H_9$			1209 (4) 937 (2) 387 (11) 367 (27)	1261 m 1209 w		
$\delta(N-Hg-C)$			250 (50)		201 (29)	
τCH_3		792 m	1454 (10) 1439 (14) 304 (9)	1450 m		

[a) Vibrational bands in cm^{-1}; Raman intensities in brackets; IR intensities: vs = very strong, s = strong, m = medium, w = weak. [b) δ = Deformation vibration; δ_{as}, δ_s = antisymmetric and symmetric deformation vibration; δ_β, δ_γ = "in plane" and "out of plane" deformation vibration; ν = valence vibration; ν_{as}, ν_s = antisymmetric and symmetric valence vibration; ρ, τ = "rocking" and "twisting" deformation vibration.

Table A.13.: Quantum mechanical calculations of CH_3HgN_3 (**1**), $(CH_3)_3CHgN_3$ (**2**) and $C_6H_5HgN_3$ (**3**): Summary of some values, bond lengths and angles. [a]

	1 CH_3HgN_3	**2** $(CH_3)_3CHgN_3$	**3** $C_6H_5HgN_3$
energy	357.657716	475.594060	549.402699
point group	C_1	C_1	C_1
NIMAG	0	1	0
zpe	30.3	83.0	64.3
dipol momentum	4.3	5.1	4.5
$d(Hg-C)$	2.081	2.145	2.065
$d(Hg-Cl/N_\alpha)$	2.063	2.085	2.056
$d(N_\alpha-N_\beta)$	1.228	1.227	1.229
$d(N_\beta-N_\gamma)$	1.147	1.148	1.146
$\angle(C-Hg-Cl/N_\alpha)$	175.7	175.4	175.8
$\angle(Hg-N_\alpha-N_\beta)$	121.5	121.0	121.6
$\angle(N_\alpha-N_\beta-N_\gamma)$	174.3	174.7	174.1

[a] Energy in atomic units [a.u.], *zpe* in $kcal\,mol^{-1}$, dipol momentum in Debye [D], bond lengths in Ångstrom [Å], angles in degree [°].

Table A.14.: Quantum mechanical calculations of CH_3HgN_3 (**1**), $(CH_3)_3CHgN_3$ (**2**) and $C_6H_5HgN_3$ (**3**): vibration bands, IR intensities and Raman activities and their assignments. [a)]

Vibration [b)]	**1** CH_3HgN_3	**2** $(CH_3)_3CHgN_3$	**3** $C_6H_5HgN_3$
$\nu_s CH$			3200 (23/402)
$\nu_{as} CH$			3190 (26/68) 3182 (1/135) 3173 (0/81) 3168 (1/1)
$\nu_{as} CH_3$	3152 (3/101) 3150 (3/116)	3104 (29/72) 3104 (29/81) 3102 (1/3)	
$\nu_s CH_3$	3050 (10/184)	3073 (35/238) 3069 (10/12) 3068 (10/16) 2992 (16/39) 2990 (19/74)	
$\nu_{as} N_3$	2223 (880/82)	2212 (1036/127)	2223 (1023/127)
$\delta_{as} CH_3$	1433 (2/8) 1431 (2/8)	1482 (5/0) 1472 (7/17) 1472 (8/14) 1447 (0/0)	
$\nu_s N_3$	1342 (2/8)	1338 (168/12)	1339 (194/9)
$\delta_s CH_3$	1218 (29/24)	1411 (2/4) 1386 (5/11) 1385 (5/10)	
ρC_4H_9		1028 (1/2) 1027 (1/2)	
τC_4H_9		953 (0/0)	
$\delta_s C_4H_9$		1170 (113/155) 810 (0/55)	
ρCH_3	798 (20/1)		

Vibration [b)]	1 CH$_3$HgN$_3$	2 (CH$_3$)$_3$CHgN$_3$	3 C$_6$H$_5$HgN$_3$
δ_βC$_6$H$_5$			1628 (4/10)
			1621 (1/11)
			1503 (4/8)
			1457 (9/3)
			1347 (6/1)
			1319 (1/0)
			1200 (1/6)
			1174 (0/5)
			1094 (3/0)
			1092 (0/6)
			1042 (3/18)
			1009 (16/46)
			675 (2/6)
			626 (0/3)
δ_βN$_3$	660 (7/4)	658 (7/12)	656 (9/23)
δ_γN$_3$	588 (8/2)	590 (7/2)	587 (7/2)
νHgC	539 (14/50)	513 (0/51)	236 (5/15)
νHgN	413 (34/31)	394 (75/65)	420 (65/28)
δ_γC$_6$H$_5$			1014 (0/0)
			986 (0/0)
			930 (1/0)
			862 (0/2)
			747 (27/5)
			712 (21/1)
			465 (7/1)
			404 (0/0)
δ_{as}C$_4$H$_9$		1227 (3/1)	
		1226 (2/1)	
		942 (0/3)	
		941 (0/3)	
		384 (0/0)	
		380 (3/2)	
δ(Hg N1 N2)	90 (0/6)	146 (3/5)	133 (1/7)

Vibration [b)]	**1** CH$_3$HgN$_3$	**2** (CH$_3$)$_3$CHgN$_3$	**3** C$_6$H$_5$HgN$_3$
δ(N Hg C)	179 (5/2)	236 (2/8)	226 (2/0)
	143 (1/2)	232 (1/13)	200 (7/7)
		232 (1/1)	86 (2/1)
		90 (1/1)	44 (0/4)
		53 (0/3)	
τC$_6$H$_5$			14 (0/10)
τCH$_3$	795 (18/0)	1453 (0/22)	
	12 (0/0)	1452 (0/19)	
		297 (0/1)	
		294 (0/1)	
		250 (0/0)	
		−8 (0/3)	

[a)] Vibrational bands in cm^{-1}; IR intensities and Raman activities in brackets (IR/Raman); IR intensities in km cm^{-1}; Raman activities in A^4 a.m.u^{-1}.
[b)] δ = Deformation vibration; δ_{as}, δ_s = antisymmetric and symmetric deformation vibration; δ_β, δ_γ = "in plane" and "out of plane" deformation vibration; ν = valence vibration; ν_{as}, ν_s = antisymmetric and symmetric valence vibration; ρ, τ = "rocking" and "twisting" deformation vibration.